From glycosidase activity profiling to inhibitor discovery in the plant pathogen *Pseudomonas syringae*

Dissertation

zur
Erlangung des Doktorgrades (Dr. rer. nat.)
der
Mathematisch-Naturwissenschaftlichen Fakultät
der
Rheinischen Friedrich-Wilhelms-Universität Bonn

vorgelegt von

Balakumaran Chandrasekar

aus
Virudhunagar, India

Bonn, March 2017

Angefertigt mit Genehmigung der Mathematisch-Naturwissenschaftlichen

Fakultät der Rheinischen Friedrich-Wilhelms-Universität Bonn

1. Gutachter: Prof. Dr. Renier van der Hoorn

2. Gutachter: Prof. Dr. Dorothea Bartels

Tag der Promotion: 22. Juni 2017
Erscheinungsjahr: 2018

Table of contents

Figures and tables

Abbreviations and symbols

ABP	activity-based probe
ABPP	activity-based protein profiling
AFU	alpha-arabinofuranosidase
ALP	aleurain-like protein
AMDIS	automated mass spectral deconvolution and identification System
amiRNA	artificial microRNA
ATP	adenosine triphosphate
Avg	average
BGAL	beta-galactosidase
BGLU	beta-glucosidase
bim	BGAL inhibitor mutant
bp	base pair
BXLU	Beta-xylosidase
CAZy	carbohydrate active enzyme
CBB	coomassie brilliant blue
cDNA	complementary DNA
CFU	colony forming units
cm	centimeter
CTB	cathepsin B
Ctr	control
Cys	cysteine
DMSO	dimethyl sulfoxide
DNA	deoxyribonucleic acid
DNJ	1-deoxynojirimycin
dpi	day-post-infection
DTT	dithiothreitol
E.coli	*Escherichia coli*
EIC	extracted ion chromatogram
E-64	(L-3-trans-Carboxyoxiran-2-Carbonyl)-L-Leucyl-Admat
FDR	false discovery rate
g	gram
g	gravity constant
GABA	gamma-4-aminobutyrate
GC-MS	gas chromatography mass spectrometry
GFP	green fluorescent protein
GHs	glycosyl hydrolases
GLB	gel loading buffer
IAM	iodoacetamide
Inc	incompatibility
IPTG	isopropyl beta-D-thiogalactopyranoside
kDa	kilodalton
l	litre
LB	Luria-Bertani
LC	liquid chromatography
M	Molar (mol/litre)
MES	4-morpholineethansulfonic acid
mg	milligram
$MgCl_2$	magnesium chloride
MGDG	monogalactosyldiacylglycerol
min	minutes
ml	millilitre
mM	millimolar

MOPS	3-Morpholinopropanesulfonic acid
MS	mass spectrometry
MSTFA	n-methyl-n-trimethylsilyl-trifluoroacetamide
MW	molecular weight
m/z	mass/charge
NaCl	sodium chloride
NH_4OH	ammonium hydroxide
NMR	Nuclear Magnetic Resonance spectroscopy
h	hour (s)
HR	hypersensitive response
hrcC	outer-membrane type III secretion protein
HRMS	high resolution mass spectrometry
HRP	horseradish peroxidase
OD	optical density
PAGE	polyacrylamide gel electrophoresis
PCR	polymerase chain reaction
PGS	putative *N*-glycosylation sites
PLCP	papain-like cysteine protease
PR	pathogenesis-related
*Pto*DC3000	*Pseudomonas syringae* pv. *tomato*
PVDF	polyvinylidene difluoride
pv.	pathovar
RBS	ribosome binding site
RD	response to desiccation
RT-PCR	reverse transcription polymerase chain reaction
RuBisCO	ribulose-1,5-bisphosphate carboxylase/oxygenase
s	second (s)
SDS	sodium dodecyl sulphate
SEM	standard error mean
SP	signal peptide
TAIL PCR	thermal asymmetric interlaced polymerase chain reaction
THP	trihydroxy piperidine
TIC	total ion chromatogram
TMS	trimethylsilane
TMV	tobacco mosaic virus
V	volts
VIGS	virus-induced gene silencing
WT	wild-type
X-gal	5-bromo-4-chloro-3-indolyl-β-D-galactopyranoside
XCP	xylem cysteine protease
XBCP	xylem and bark cysteine protease
µM	micromolar
µg	microgram
µl	microlitre
35S	promoter of cauliflower mosaic virus
5’	five prime end of a DNA
3’	three prime end of a DNA
Å	Angstorm
∆	delta
%	percentage
<	less than
>	greater than
°C	degree celcius

Abstract

Retaining glycosidases are important in plants for various biological processes. Plant genomes encode for more than 200 retaining glycosidases but the physiological roles and activities of many remain poorly understood. We established glycosidase activity profiling in plants using activity-based probes based on cyclophellitol-aziridine. These probes targeted a diversity of glycosidases belonging to different GH families in leaf extracts of *Arabidopsis thaliana* and in the cell wall proteome of *Nicotiana benthamiana*. When applied to plants infected with the bacterial pathogen *Pseudomonas syringae*, we discovered that the activity of a cell wall associated beta-galactosidase (BGAL) is suppressed during infection. We also introduce convolution ABPP, a novel inhibitor discovery approach that revealed that the suppression of BGAL is caused by a small, heat-stable inhibitor that is produced by the pathogen. Bacterial genetics together with biochemical approaches indicate that trihydroxy piperidine (THP), an imino sugar might be the BGAL inhibitor produced by the pathogen. Trihydroxy piperidine (THP) was detected during infection and in bacterial cultures using GC-MS and HRMS. Pathogen growth assays using the BGAL inhibitor mutants indicate that BGAL inhibitor production is important for the virulence of *Pto*DC3000, whereas depletion of BGAL using virus-induced gene silencing (VIGS) increased bacterial growth, indicating the discovery of an important immune enzyme that is suppressed by pathogenic bacteria. Furthermore, two candidate PLCPs that might be required for processing the BGAL enzyme in *Nicotiana benthamiana* were identified using VIGS. In addition, a new tool for functional classification of JJB-labeled glycosidases has been introduced based on product inhibition of glycosidases. Moreover, two interesting observations during my PhD program are also documented. First, increased glycosidases activities observed in the growth medium of a *Pto*DC3000 mutant is due to the disruption of a gene encoding for an ABC transporter. Second, unexpected inhibitory effects of commonly used antibiotics on plant glycosidases were discovered.

Chapter 1: Introduction

(Part of this chapter has been published as: Chandrasekar, B and Van der Hoorn, R.A.L. (2016). Beta galactosidases in Arabidopsis and tomato - a mini review. *Biochemical society transactions* 44(1), 150-158)

Carbohydrates are present in all kingdoms of life and are particularly prominent in plants (Sturgeon, 2001). Plants produce carbohydrates as one of their major constituents through their photosynthetic activity. The simplest synthesized forms of carbohydrates are the monosaccharide sugars such as glucose, which provides energy for various cellular activities. Carbohydrates also exist in very complex forms. Monosaccharide sugars are attached to one another through covalent glycosidic linkage, which generates di-, oligo-, and polysaccharides. Carbohydrates are also found attached to a non-carbohydrates species (lipids, proteins, hormones) through a glycosidic linkage to form glycoconjugates (Cheeke, 2001).

1.1 Plant glycosidases or glycoside hydrolases

Glycosidic bonds in carbohydrates are hydrolyzed by class of carbohydrate-active enzymes called glycosyl hydrolases (GHs) or glycosidases (Kötzler et al., 2001). Mechanistically glycosidases are classified as retaining and inverting enzymes (Vuong and Wilson, 2010). To hydrolyze the glycosidic bond, both the retaining and inverting enzymes carry two catalytic glutamate or/and aspartate residues (McCarter and Stephen Withers, 1994). Of these two catalytic residues, one acts as a proton donor and other as a nucleophile/base. The distance between these catalytic residues in the active site of the glycosidases dictates the retaining or inverting mechanism of hydrolysis. Retaining enzymes have two catalytic residues separated by a distance of ~ 5.5 Å and their hydrolysis mechanism retains the net anomeric configuration of the C1 atom in the sugar molecule (Figure 1). By contrast, inverting enzymes have catalytic residues that are ~ 10 Å apart and these enzymes invert the overall anomeric configuration of C1 carbon atom in the released sugar (Davies and Henrissat, 1995). Both retaining and inverting glycosidases are present abundantly in plants. Over 400 genes encoding glycosidases are present in the genome of *Arabidopsis thaliana*, of which 260 are putative retaining enzymes and 140 are putative inverting enzymes (http://www.cazy.org/).

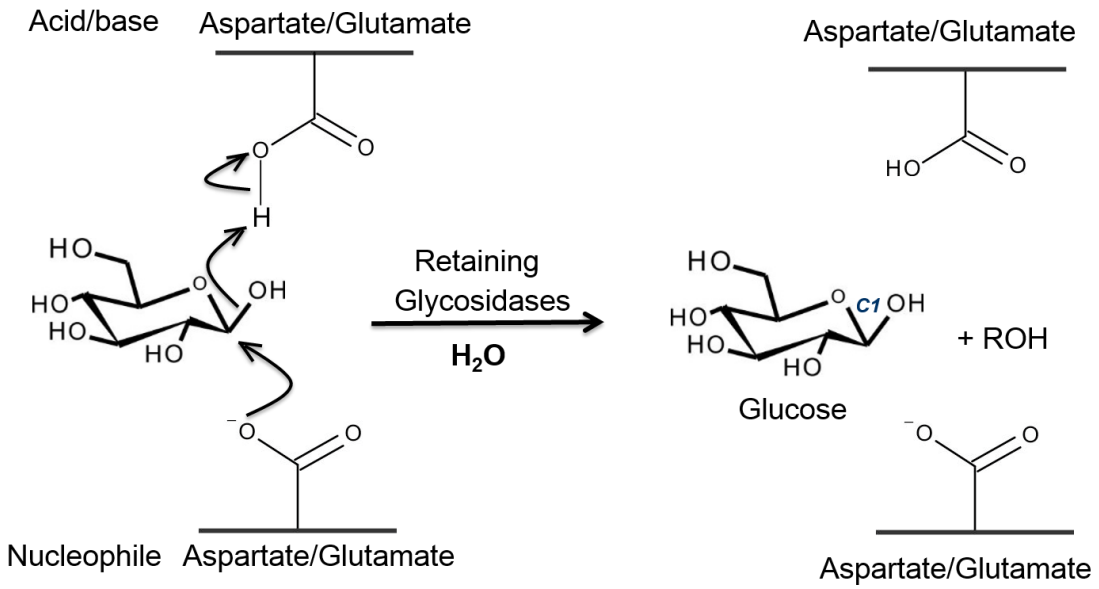

Figure 1.1 Mechanism of glycosidic bond hydrolysis by retaining glycosidases

Retaining glycosidases hydrolyse the glycosidic bond in carbohydrates without the changing the stereochemistry of the released sugar. Hydrolysis of a beta-D-glucoside is shown as an example.

Due to the large carbohydrate diversity in plants, they have a vast variety of glycosidases. Based on the preferred glycoside substrates for hydrolysis, the glycosidases are classified as glucosidases, xylosidases, galactosidases, fucosidases, etc. Based on protein sequence similarities, glycosidases are classified into different GH families and the members from the same GH family share a common mechanism of glycosidic bond cleavage (Henrissat, 1991). *Arabidopsis thaliana*, for example, has 24 retaining and 11 inverting GH families which each consists of several glycosidases. In general, the number of glycosidase related genes in plants (for instance, Arabidopsis) are relatively high when compared to other sequenced organisms (for instance, human) (Coutinho et al., 2003). This signifies the unique importance of glycosidases in plants compared to other organisms. Genetic, molecular and biochemical approaches revealed that glycosidases are localized in different cellular compartments like endoplasmic reticulum, Golgi apparatus and cell walls. The majority of plant glycosidases are predicted to reside in cell walls and these enzymes may play a major role in cell-associated process like cell wall remodelling, fruit ripening and biosynthesis reactions (Minic, 2008). Other characterized glycosidases reside in other compartments to regulate various biological processes like glycosylation of proteins, hormones signalling, lipid metabolism and plant defense.

In my PhD studies, a cell wall-associated beta galactosidase has been characterized for their role during bacterial infections. Beta-galactosidases (BGAL) are glycosyl hydrolases that remove terminal β-D-galactosyl residues from β-D-galactosides and belong to GH35

family. The physiological roles of beta-galactosidases in *Arabidopsis thaliana* and tomato are reviewed here.

1.2 Beta galactosidases

β-D-Galactose is found in many organisms and can be coupled to carbohydrates or non-carbohydrates via an O-glycosidic bond. Beta galactosidases (BGALs, EC 3.2.1.23) are glycosyl hydrolases (GHs) that remove the terminal β-D-galactosyl residues from the non-reducing end of these β-D-galactosides. BGALs performing this hydrolytic activity are found in GH families GH1, GH2, GH3, GH35, GH42, GH50 and GH59 (Lombard et al., 2014). BGALs from these GH families play major roles in different organisms. For instance, a GH35 enzyme *GLB1* in humans are involved in removing terminal galactose residues from GM1 gangliosides in the lysosome (Ohto et al., 2012). Furthermore, deficiency of *GLB1* in humans causes Gangliosidosis due to the accumulation of toxic GM1 gangliosides. *GALC* is a GH59 beta galactosidase which removes galactose from galactocerebrosides and its deficiency causes Krabbe disease in humans (Deane et al., 2011). Finally, the frequently used bacterial *LacZ* gene encodes a GH2 family BGAL in *Escherichia coli* (*E.coli*) that is essential for lactose metabolism during glucose starvation *LacZ* encodes a GH2 family BGAL in *Escherichia coli* (*E.coli*) that is essential for lactose metabolism during glucose limitation (Jacob and Monod, 1961; Juers et al., 2012).

Microbial BGALs are applied in diary industry for the hydrolysis of lactose. These BGALs are known for their thermo stability or activity at low temperatures. BGALs having optimal hydrolytic activity at low temperatures (e.g. 0°C) have been identified in psychrophilic microbes like *Arthobacter sp*, yeast, *Pseudoalteromonas* sp and *Paracoccus* sp (Hoyoux et al., 2001; Nakagawa et al., 2006, 2007; Wierzbicka-Woś et al., 2011). These cold-adapted BGALs have applications in the food industry to remove lactose contaminations from heat sensitive milk products. By contrast, BGALs having optimal hydrolytic activity at higher temperatures (e.g. 70°C) has been identified in microbes like Bacillus *stearothermophilus* (Chen et al., 2008; Hirata et al., 1985) and are used in industry for producing lactose-free milk [12]. Thermostable BGALs are also used in diary industry to remove lactose contaminations from whey, a major by-product from cheese (Bansal et al., 2008; Panesar et al., 2010; Regenhardt et al., 2013; Szczodrak, 2000). In addition to hydrolytic activities, some microbial BGALs also have transgalactosylation activity. Transgalactosylation is the process where BGAL transfers the released galactose to another carbohydrate instead of water. For example, microbial BGALs from different GH families have been used to synthesize β-galacto-oligosaccharides (GOS), an important human prebiotic diet. These BGALs transfer the

hydrolyzed galactose residue to acceptor lactose to build GOS (Hsu et al., 2007; Liu et al., 2011; Torres et al., 2010, 2010).

Notably, all plant beta galactosidases (BGALs) belong to family GH35. Typically, they follow the Koshland retaining mechanism, releasing galactose in their retained, β-anomeric conformation (Zhang et al., 1994). GH35 enzymes belongs to clan GH-A in the CAZy database and fold as a $(\alpha/\beta)_8$ (TIM) barrel domain with the two catalytic glutamate residues (Rojas et al., 2004). One catalytic Glu residue acts as the proton donor and the other as a nucleophile during catalysis. In plants, β-D-linked galactosyl residues are found in glycolipids (e.g. monogalactosyldiacylglycerol, MGDG (Dörmann, 2001)), proteoglycans (e.g. arabinogalactan proteins (Showalter, 2001)), and cell wall polysaccharides (e.g. xyloglucans and Rhamnogalacturonan I, RGI (Yapo, 2011)). A biologically relevant substrate for BGALs during fruit ripening of tomato is galactan, a polymer of β-(1-4) D-galactose attached to RGI (Ali et al., 1995; Gorshkova et al., 1997; Redgwell et al., 1997; Smith and Gross, 2000; Trainotti et al., 2001). In this mini review, we have discuss the BGALs from *Arabidopsis thaliana* and *Solanum lycopersicum* (tomato). We will discuss the phylogeny, domain architecture and expression patterns and summarize the biochemical and physiological functions.

1.3 Arabidopsis BGALs: diversity and functions

The genome of *Arabidopsis thaliana* contains 17 genes encoding putative beta galactosidases, designated as *BGAL1-17* (Figure 1.2A). At2g04060 is not included because although it shares similarities to known BGAL sequences at its C-terminus, this protein does not have a GH35 domain and is probably a truncated duplicate of *BGAL15* (Ahn et al., 2007). Phylogenetic analysis of the 17 BGAL Arabidopsis proteins has divided these proteins into seven different groups: group I (*BGAL17*), II (*BGAL8-9*), III (*BGAL1-5*, *BGAL12*), IV (*BGAL10*), V (*BGAL7, 15*), VI (*BGAL11, 13, 14*) and VII (*BGAL6, 16*) (Perez Almeida, 2004). A second classification based on phylogenetic analysis of BGALs from various plant species, has divided the 17 BGALs into eight sub families: subfamily a1 (*BGAL1-4, BGAL5, BGAL12*), a2 (*BGAL9*), a4 (*BGAL8*), a5 (*BGAL10*), b (*BGAL7, BGAL15*), c1 (*BGAL11, BGAL13, BGAL14*), c2 (*BGAL6, BGAL16*) and d (*BGAL17*) (Ahn et al., 2007).

Of the 17 Arabidopsis BGAL proteins, 13 are predicted to have an N-terminal signal peptide that targets the protein to the endomembrane system. The four other BGAL proteins possibly locate in the cytoplasm or nucleus. The GH35 domain contains two active site glutamate residues. The active site consensus sequence G-G-P-[LIVM](2)-x(2)-Q-x-E-N-**E**-[FY] is common to all GH35 BGALs, and contains the Glu residue (bold) that acts as a proton donor during hydrolysis. The motif P-N-K-x-x-K-P-KM-W-T-**E**-x-W is present in all BGALs except BGAL17, and carries the Glu residue (bold) that acts as a nucleophile (Ahn et al.,

2007). Apart from the GH35 domain, ten BGALs also carry an additional gal_lectin domain in the C-terminus (Figure 1.2C). BGAL14 has an additional PRP1 domain C-terminal to the gal_lectin domain. BGAL11 and BGAL16 carry an additional BetaGal4.5 domain between GH35 and gal_lectin domain whereas BGAL13 carries a GH2N domain between GH35 and gal_lectin domain. The functional significance of these extra domains is yet unclear. It has been suggested that the gal_lectin domain might contribute to substrate specificity of BGAL (Ahn et al., 2007; Gantulga et al., 2009).

Eight Arabidopsis BGALs have been biochemically characterized for their beta-galactosidase activities (Figure 1.2C). Six of these belong to the subfamily a1 (*BGAL1-5*, *BGAL12*) and the other two belong to subfamilies a5 (*BGAL10*) and c2 (*BGAL6*). Subfamily a1 enzymes can hydrolyze artificial substrates with galactose or fucose as glycone moiety (Gantulga et al., 2009). Specificity for aglycone moieties has not been observed for these enzymes. Enzyme assays have also been performed with more natural substrates such as galactose-based oligosaccharides and cell wall fractions of different plants. These experiments revealed that subfamily a1 enzymes generally prefer galacto-oligosaccharides with β(1-3) or β(1-4) linkage (Gantulga et al., 2009). The exception is BGAL12, which can hydrolyze galacto-oligosaccharides having all three linkages: β(1-3), β(1-4) and β(1-6) (Gantulga et al., 2009). Galactosidic activities of BGAL6 and BGAL10 has been verified using PNP-β-D-galactopyranoside and XLLG, a xyloglucan oligosaccharide, respectively (Dean et al., 2007a; Sampedro et al., 2012a). These studies show that the subfamily a1 BGALs are genuine beta galactosidases with slightly different substrate specificities.

Immunogold labelling followed by Transmission Electron Microscopy (TEM) of root sections has revealed that BGAL1 and BGAL12 reside in the thickened cell walls of xylem cells (Gantulga et al., 2009). Cell wall localization of BGAL6 has been observed using a fusion with Green Fluorescent Protein (GFP), transiently expressed in *Nicotiana tabacum* leaves (Dean et al., 2007a). BGAL2 and BGAL5 have been detected in cell wall fractions of Arabidopsis leaves by dotblotting (Gantulga et al., 2008), whilst and BGAL8 has been detected in the cell walls of Arabidopsis stems by proteomics (Wei et al., 2015). In conclusion, all six characterized BGALs in Arabidopsis to date are localized in the cell wall, implicating their role in cell wall remodelling and expansion (Figure 1.2D).

Gene expression analysis using eFP browser (Winter et al., 2007) indicates that *BGAL* genes have distinct organ-specific expression patterns (Figure 1.2E). *BGAL7, -11, and -13* are expressed mostly in flowers whereas *BGAL17* is mostly expressed in the stem. Other BGALs are expressed in multiple organs, but still follow different expression patterns. *BGAL12, -14 and -16* are poorly expressed in the selected tissues, consistent with RT-PCR analysis of these genes (Ahn et al., 2007).

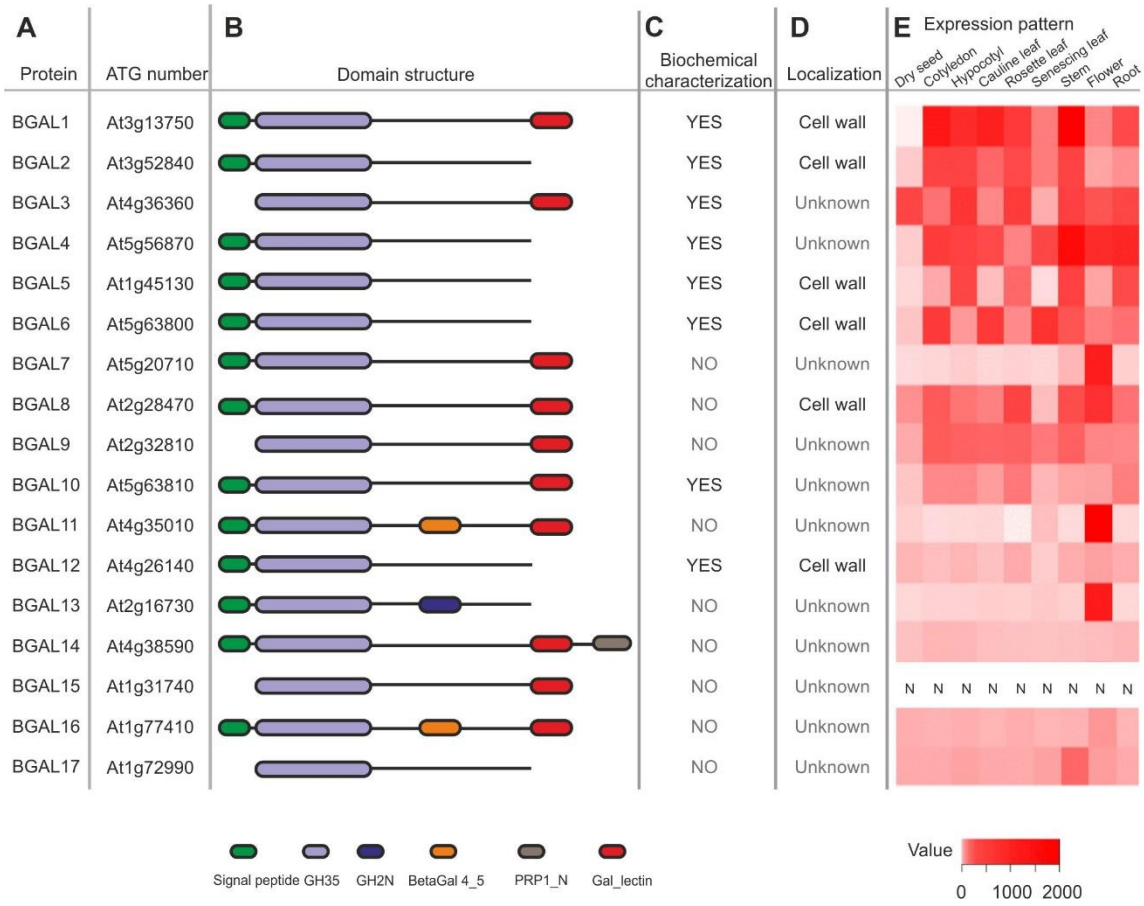

Figure 1.2 BGALs of *Arabidopsis thaliana*

(A) Protein name and accession numbers. (B) Domains in BGAL proteins. Represented domains are not on scale. (C) Biochemically characterized BGALs. (D) Experimentally validated subcellular protein localization. (E) Expression pattern of BGALs in various tissues of Arabidopsis. The expression data of Arabidopsis BGALs for these tissues were extracted using the eFP browser (Winter et al., 2007). Expression data were converted into heat maps using R. Expression data for *BGAL15* were not available (N).

The physiological roles of only two Arabidopsis BGALs have been characterized. Mucilage mutant-2 (*mum2*) fails to extrude mucilage from the apoplast upon hydration and is caused by the *bgal6* mutant allele (Figure 1.3A), indicating that BGAL6 alters the hydration properties of mucilage by modifying carbohydrate structures (Dean et al., 2007a). By contrast, BGAL10 seems to be the only or main beta galactosidase acting on xyloglucan cell wall substrates because unusual xyloglucan residues were observed in cell walls of *bgal10* mutant flowers (Sampedro et al., 2012a). This unusual xyloglucan accumulation correlates with a reduced silique and sepal length of *bgal10* mutant plants (Figure 1.3B). Characterization of the physiological functions of the remaining Arabidopsis BGALs is an unexplored area in plant biology.

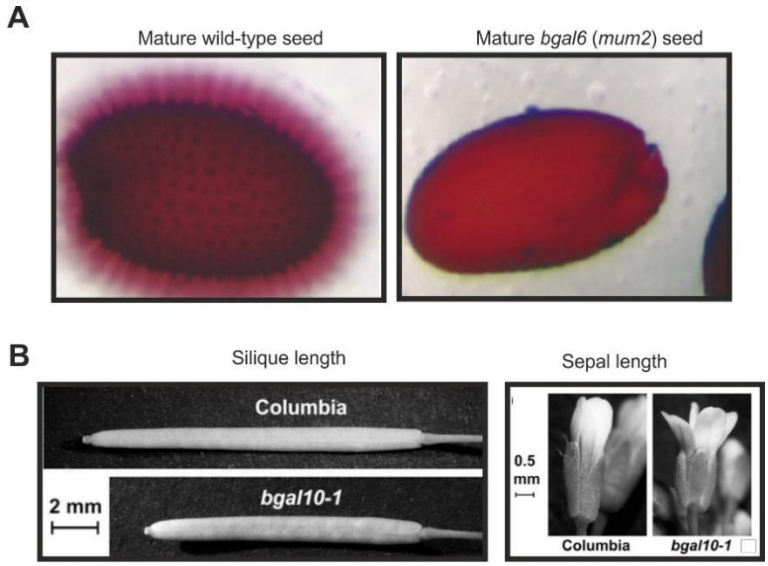

Figure 1.3 Phenotypes of *bgal* mutants of *Arabidopsis thaliana*

(A) Failure to extrude the mucilage in *bgal6 (mum2)* mutant seeds. The wild type and T-DNA insertion mutant seeds of *bgal6* were stained with Ruthenium Red to visualize the mucilage layer in the seeds. These pictures were reprinted from Dean et al., 2007 (Dean et al., 2007a) with permission. (B) *bgal10* T-DNA mutants have a reduced silique and sepal length. The pictures are reprinted from Sampedro et al., 2012 (Sampedro et al., 2012a) with permission.

1.4 Tomato BGALs

The tomato genome contains 17 genes encoding putative BGALs. All these proteins contain the GH35 domain with typical consensus sequences and both active site residues. Two additional proteins (Solyc07g038120 and Solyc07g038130), share some similarity with the GH35 domain but lack the active site consensus sequences. Seven genes are expressed during various stages of tomato fruit development (Smith and Gross, 2000)(Smith and Gross, 2000). These seven genes have been named *TBG1-7* (Tomato Beta Galactosidase). We named the remaining 10 tomato *BGAL* genes as *TBG8-17*, in chronological order of their accession number (Figure 1.4).

Phylogenetic analysis using protein sequences of both Arabidopsis and tomato revealed that tomato BGALs fall into the same seven groups as Arabidopsis BGALs (Figure 1.5). This indicates that BGAL diversification occurred early in plant evolution and that orthologs in Arabidopsis and tomato may have similar, distinct functions. To extend the evolutionary analysis of the BGAL family, we have included the 15 BGALs of the monocot *Oryza sativa* (Rice) (Tanthanuch et al., 2008) and six BGALs of the moss *Physcomitrella patens* (Goodstein et al., 2012) in our phylogenetic analysis (Figure 4). The grouping of the BGALs in the phylogenetic tree indicates that BGALs of groups I and VI existed since the evolution of land plants since they are also present in moss. By contrast,

BGALs of groups II, III, IV and VII may have evolved later, but probably before the angiosperms evolved because they are present in both eudicot and monocot plant species. This includes groups III, IV and VII, of which individual BGALs were shown to act in fruit development (see below) and flower development (Sampedro et al., 2012b) and seed mucilage release (Dean et al., 2007b), consistent with the absence of these genes in moss. BGALs in groups II and III contain more than one ortholog, suggesting their distinct functions, whereas BGALS in group VI tend to have duplicated and diversified within each of the four plant species. The presence of additional domains seems less conserved within plants. The C-terminal lectin domain is absent in group I and present in group II, IV, V and VI, but irregularly present in groups III and VII. The GH2N domain is occasionally found in group I, III, IV, VI and VIIs and the remaining additional domains are only found in groups VI and VII. Thus, these data indicate that plant BGALs have ancient origins in the plant kingdom, though the additional domains are not consistently present.

Biochemical characterization has been performed for three tomato BGALs. All these characterized TBGs are expressed during tomato fruit development. TBG4 is the first enzyme to be biochemically characterized. Earlier in 1980's this enzyme (β-galactosidase II) was found to be abundant in ripe tomato fruits and was purified from the tomato fruit extracts and shown to hydrolyze galactose residues from cell wall polysaccharides and artificial substrates (Carey et al., 1995; Pressey, 1983). In another study, the gene encoding TBG4 was cloned and the enzyme was expressed in yeast and purified. The purified TBG4 had β(1-4) galactosidase/exogalactanase activity, meaning it can hydrolyze galactose from galactan, lactose and other synthetic substrates (Smith et al., 2002). A similar strategy has been used to characterize TBG1 and TBG5, which both have β(1-4) galactosidase and β(1-4) exogalactanase activity (Carey et al., 2001; Moctezuma et al., 2003a). The other 14 TBGs remain to be biochemically characterized.

The role of beta galactosidases in tomato fruit ripening has been well studied. Fruit ripening is a complicated physiological process involving alterations in fruit texture and cell wall degradation. A key biochemical event during ripening is the loss of galactosyl residues from the cell wall fractions (mainly pectins) and the accumulation of soluble free galactose residues (Gross, 1983, 1984; Gross and Wallner, 1979; Wallner and Bloom, 1977). Galactose, when injected into tomato fruits, causes enhanced ethylene production and promotes early ripening (Gross, 1985). Hence, galactose released from the cell walls during ripening might have the same effect as enhancing ethylene production.

Down regulation of *TBG4* transcript levels by antisense *TBG4* resulted in transgenic tomato lines with reduced exogalactanase activity and low levels of galactose (Smith et al., 2002). These *TBG4*-silenced plants also produced fruits with a 40% increased fruit firmness

compared to the controls (Smith et al., 2002). By contrast, downregulating 90% of *TBG1* transcript levels had no effect on exogalactanase activity or galactose levels and did not affect the firmness of the fruit (Carey et al., 2001).

Notably, antisense suppression of the *TBG6* gene resulted in a tomato fruit with high beta-galactosidase activity at day 20 after pollination (Moctezuma et al., 2003b). An interesting, unexpected observation is that although the mRNA levels of *TBG6* were significantly downregulated, the anti-sense lines had higher total beta galactosidase activity than the wild type plants. However, at 30 days after pollination or three days after the breaker stage, the total beta galactosidase activity was comparable to the wild type. Unexpectedly, fruits from *TBG6*-silenced plants had reduced galactosyl residues in cell walls and enhanced fruit softening. In addition, *TBG6* gene suppression also had some notable external and internal fruit morphological phenotypes. The fruits from these transgenic lines were elongated and had vertical ‘zipper like scars’ along their epidermis (Figure 1.6). Furthermore, the internal locular space was decreased or absent in these fruits.

Though the anti-sense approach had helped in these studies to understand the involvement of TBG’s in tomato fruit development process, possible effects due to off-target effects cannot be neglected. Hence independent genetic knock-outs by genome editing or complementation of the transgenic line with a synthetic *TBG* gene that is insensitive for silencing, may be needed to confirm the role of *TBGs* during fruit development. To our knowledge, the exact functions of other *TBGs* which are expressed during fruit development and elsewhere during development still remains to be elucidated.

Protein	Accession number	A Structural domains of TBG proteins	B Biochemical characterization	C Phenotype after silencing
TBG1	Solyc12g044880		YES	No phenotype on fruit [41]
TBG2	Solyc09g092160		NO	Unknown
TBG3	Solyc03g121540		NO	Unknown
TBG4	Solyc12g008840		YES	Enchanged fruit firmness [40]
TBG5	Solyc11g069270		YES	Unknown
TBG6	Solyc02g084720		NO	Fruit Scars, locular space, fruit softening [48]
TBG7	Solyc03g019890		NO	Unknown
TBG8	Solyc01g110000		NO	Unknown
TBG9	Solyc01g111540		NO	Unknown
TBG10	Solyc02g078950		NO	Unknown
TBG11	Solyc04g080840		NO	Unknown
TBG12	Solyc06g062580		NO	Unknown
TBG13	Solyc06g062660		NO	Unknown
TBG14	Solyc07g042220		NO	Unknown
TBG15	Solyc10g055470		NO	Unknown
TBG16	Solyc11g018490		NO	Unknown
TBG17	Solyc11g018500		NO	Unknown

Figure 1.4 BGALs of tomato

(A) Domains in BGAL proteins. Represented domains are not on scale. (B) Biochemically characterized BGALs. (C) Phenotypes of tomato fruit upon silencing tomato BGAL.

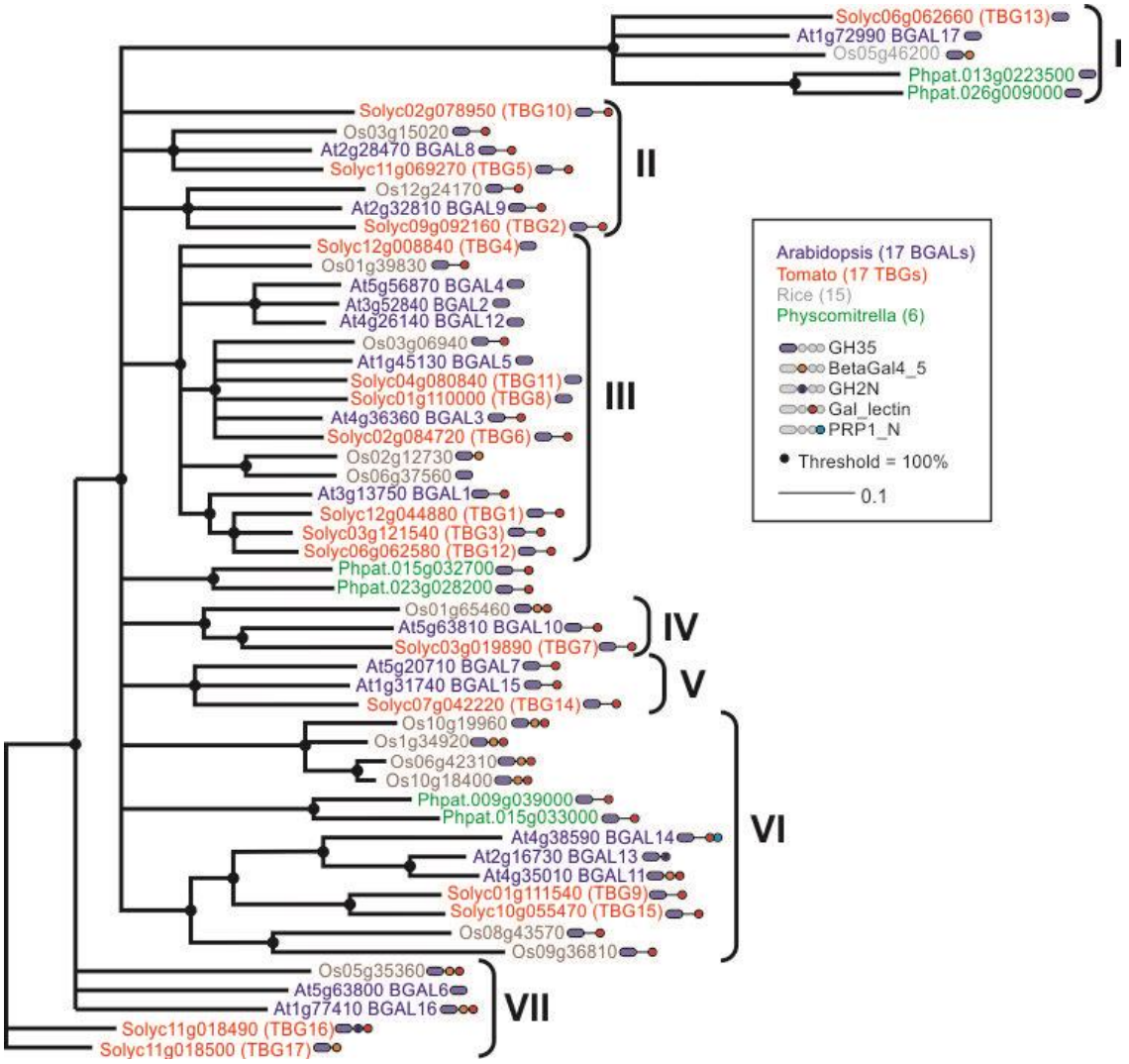

Figure 1.5 Phylogenetic analysis of Arabidopsis, tomato, rice and moss BGALs

An unrooted phylogenetic tree was built with the amino acid sequences of 17 BGALs of Arabidopsis, 17 TBGs of tomato, 15 BGALs of rice and 5 BGALS of *Physcomitrella patens*. The 54 sequences were aligned using Clustal Omega and an unrooted tree was built using Geneious Tree Builder with the Neighbour Joining Method and the Jukes-Cantour genetic distances. Threshold percentage values are indicated at the nodes (1000 replication used for analysis) and genetic distance scale is indicated on the right. The presence of additional domains are indicated.

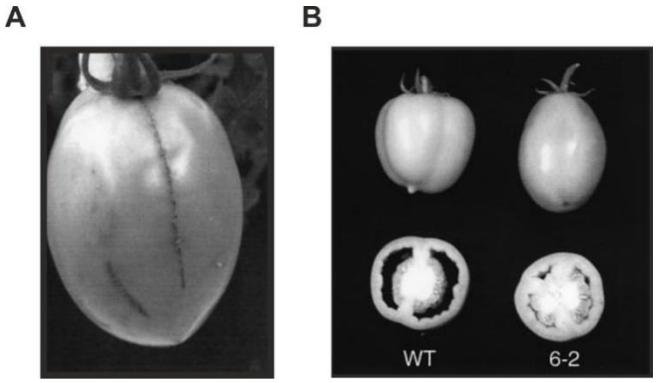

Figure 1.6 Morphological phenotypes of tomato fruits from transgenic line 6-2 carrying antisense *TBG6*

(A) Transgenic line 6-2 has elongated tomato fruits with 'zipper like scars' on epidermis. (B) The transgenic line 6-2 lacks internal locular space in their fruits. These pictures are reprinted from Moctezuma et al., 2003 (Moctezuma et al., 2003a) with permission.

1.5 Roles of BGALs in other plant species

The physiological roles of BGALs have also been studied in other plant species. BGAL activities are important during ripening of fruits like apple, mango, strawberry, banana and bell pepper (Ali et al., 1995; Ogasawara et al., 2007; Ross et al., 1994; Trainotti et al., 2001). BGALs acting on galactans are also involved in formation of secondary cell walls in flax fibres (Gorshkova et al., 1997). By contrast, a BGAL from radish seeds acts on β(1-3) and β(1-6) linked galactose residues on arabinogalactan proteins (AGPs) (Kotake et al., 2005; Sekimata et al., 1989).The functional significance of BGALs in degrading this natural substrate is still unknown. In another study, upregulation of a BGAL has been observed during abscission of mature orange fruits (Wu and Burns, 2004), suggesting that BGAL activity might play an important role during this abscission process. Hence it is evident from these studies that, similar to Arabidopsis and tomato, the majority of BGALs from other plant species also find their significance in cell wall associated biological processes.

1.6 Activity-based protein profiling of BGAL and other glycosidases

Despite the importance of GH enzymes, physiological and biochemical functions are assigned to only a few glycosidases (Minic, 2008). A bottleneck for studying glycosidases are their substrates, which are challenging to identify and difficult to synthesize. Also the majority of the glycosidases are regulated by post-translational modification and are inactive under *in vitro* conditions. Activity-based protein profiling (ABPP) is a powerful tool to monitor enzyme activities without knowing their natural substrates (Cravatt et al., 2008; Kołodziejek and van der Hoorn, 2010). ABPP involves the use of chemical probes, which reacts with active site residues in an activity-dependent manner (Figure 1.7). Thus ABPP displays the availability

and reactivity of active site residues in proteins, which are hallmarks for enzyme activity (Kobe and Kemp, 1999). ABPP is particularly attractive because the profiling can be done without purifying the enzymes and can be performed in cell extracts or in the living cells. Another key advantage of ABPP is that the activities of large mulltigene enzyme families can be monitored using broad range probes. ABPP has made a significant impact into plant science. After the introduction of probes for papain-like cysteine proteases (van der Hoorn et al., 2004; Richau et al., 2012) these probes revealed increased protease activities in the tomato and maize apoplast during immune responses (van der Linde et al., 2012; Shabab et al., 2008) and that these immune proteases are targeted by unrelated inhibitors secreted by fungi, oomycetes and nematodes (Dong et al., 2014; Hörger et al., 2012; Kaschani et al., 2010; Lozano-Torres et al., 2012; Mueller et al., 2013; Rooney et al., 2005; Song et al., 2009; Tian et al., 2007). Likewise, probes for the proteasome displayed unexpected increased proteasome activities during immune responses (Gu et al., 2010) and that the bacterial effector molecule Syringolin A targets the nuclear proteasome (Kolodziejek et al., 2011). We anticipate that more will be discovered using probes introduced for serine hydrolases, metalloproteases, vacuolar processing enzymes, ATP binding proteins and glutathione transferases (Gu et al., 2013; Kaschani et al., 2009; Lenger et al., 2012; Misas-Villamil et al., 2013; Nickel et al., 2012; Villamor et al., 2013).

Figure 1.7 Activity-based protein profiling

Activity-based protein profiling involves usage of chemical probes which labels proteins in an activity-dependent manner.

1.7 Aim and outline of the thesis

Cyclophellitol aziridine-based probes were previously used in animal proteomes to target retaining glucosidases (Kallemeijn et al., 2012). The cyclophellitol-aziridine based probes displayed specificity for only retaining beta-glucosidases like GBA1, GBA2, GBA3 and LPH present in the mammalian and non-mammalian proteomes. Furthermore, these probes targeted retaining beta-glucosidases belonging to diverse GH families such as GH1, GH3, GH30 and GH11. These probes were synthesized in the laboratory of Prof. Dr. Hermen

Overkleeft (Leiden Institute of Chemistry, the Netherlands) and were made available prior to my PhD studies. The important aims of my PhD thesis are:

1. Establishing glycosidase activity profiling in plants using the cyclophellitol aziridine activity-based probes;

2. Applying the validated probes to investigate the active status of apoplastic glycosidases in leaves of *Nicotiana benthamiana* during *Pseudomonas syringae* infection;

3. Elucidate the mechanism and biological relevance of glycosidases having differential activity upon *P. syringae* infection.

The research outline of various chapters of this thesis are summarized below:

Chapter 1

This chapter introduces glycosidases and their mechanisms of glycosidic bond cleavage. Retaining glycosidases are abundant in plants and play major role during various biological processes. The various functional roles of several characterized plants glycosidases are discussed. Furthermore, the physiological roles of beta-galactosidases in *Arabidopsis thaliana* and tomato are reviewed in detail.

Chapter 2

In this chapter, we apply activity-based glycosidase profiling using cell permeable small molecular probes that react covalently with the active site nucleophile of retaining glycosidases in an activity-dependent manner. Using mass spectrometry we detect the active state of dozens of myrosinases, glucosidases, xylosidases, and galactosidases representing seven different retaining glycosidase families. The method is simple and applicable on different organs, different plant species, in living cells and in subproteomes.

Chapter 3

In this chapter, ABPP has been used to investigate the activities of apoplastic glycosidases during bacterial infections. When glycosidase activity profiling was applied to *Nicotiana benthamiana* plants infected with the bacterial pathogen *Pto*DC3000, we discovered that the activity of an extracellular beta-galactosidase (BGAL) is suppressed during infection. Convolution ABPP, an inhibitor discovery approach, revealed that the suppression of BGAL is caused by a small, heat-stable inhibitor that is produced by the pathogen.

Chapter 4

In this chapter, a novel reporter-based functional assay has been developed to detect the BGAL inhibitor produced by *Pto*DC3000 *in vivo*. This assay was used for random mutagenesis using *mini-tn5* transposons. The established functional screening assay proved to be a viable

approach tool to isolate *Pto*DC3000 mutants lacking the BGAL inhibitor. Finally, TAIL-PCR combined with genome sequencing has revealed novel genes encoding biosynthesis enzymes and regulators involved in BGAL inhibitor production in *Pto*DC3000.

Chapter 5

In this chapter, biochemical methods have been employed to enrich for the BGAL inhibitor produced by *Pto*DC3000 in the minimal medium. These enrichment procedures have been instrumental to identify the crystal structure of the BGAL inhibitor through crystal soaking. Next, the candidate BGAL inhibitor was chemically synthesized and used as a reference. We next detect this BGAL inhibitor in the samples of infected plants and bacterial culture medium using analytical techniques like GC-MS and HRMS.

Chapter 6

In this chapter, the significance of BGAL inhibition at the plant-pathogen interface is investigated. Reverse genetics combined with pathogen assays have been employed to understand the importance of the candidate BGAL present in the apoplast of *N. benthamiana* leaves. Furthermore, the *Δbim4* and *Δbim5* mutants and other BGAL inhibitor mutants (*Δbim*) have been used for pathogen assays to investigate the biological significance of BGAL inhibitor production by *Pto*DC3000.

Chapter 7

In this chapter, processing of BGAL is investigated. The full length *BGAL* gene was transiently expressed in *N. benthamiana* plants to monitor the cleavage from the full-length protein. Extracellular active PLCPs were identified from agroinfiltrated plants and plants silenced for some these PLCPs display altered BGAL processing.

Chapter 8:

In this chapter, the concept of annotation of glycosidases using inhibition by monosaccharide products of glycosides labeling is investigated.

Chapter 9:

This chapter describes about the two additional discoveries or observations made during my PhD research. First, I discovered an increased glycosidase activities in the growth medium of *Pto*DC3000 mutants lacking an ABC transporter. Second, I discovered an unexpected inhibitory activity of commonly used antibiotics on various plant beta-glycosidases.

Chapter 10:

In this chapter, I summarize the most important future prospects on various research projects which I have been involved during my PhD studies are summarized.

1.8 References

Ahn, Y.O., Zheng, M., Bevan, D.R., Esen, A., Shiu, S.-H., Benson, J., Peng, H.-P., Miller, J.T., Cheng, C.-L., Poulton, J.E., et al. (2007). Functional genomic analysis of *Arabidopsis thaliana* glycoside hydrolase family 35. Phytochemistry *68*, 1510–1520.

Ali, Z.M., Armugam, S., and Lazan, H. (1995). β-galactosidase and its significance in ripening mango fruit. Phytochemistry *38*, 1109–1114.

Bansal, S., Oberoi, H.S., Dhillon, G.S., and Patil, R.T. (2008). Production of β-galactosidase by *Kluyveromyces marxianus* MTCC 1388 using whey and effect of four different methods of enzyme extraction on β-galactosidase activity. Indian J. Microbiol. *48*, 337–341.

Carey, A.T., Holt, K., Picard, S., Wilde, R., Tucker, G.A., Bird, C.R., Schuch, W., and Seymour, G.B. (1995). Tomato exo-(1-4)-[beta]-D-galactanase (Isolation, changes during ripening in normal and mutant tomato fruit and characterization of a related cDNA Clone). Plant Physiol. *108*, 1099–1107.

Carey, A.T., Smith, D.L., Harrison, E., Bird, C.R., Gross, K.C., Seymour, G.B., and Tucker, G.A. (2001). Down-regulation of a ripening-related β-galactosidase gene (*TBG1*) in transgenic tomato fruits. J. Exp. Bot. *52*, 663–668.

Cheeke, P.R. (2001). Glycosides: naturally occurring. In Encyclopedia of Life Sciences, John Wiley & Sons, Ltd, ed. (Chichester: John Wiley & Sons, Ltd),.

Chen, W., Chen, H., Xia, Y., Zhao, J., Tian, F., and Zhang, H. (2008). Production, purification, and characterization of a potential thermostable galactosidase for milk lactose hydrolysis from *Bacillus stearothermophilus*. J. Dairy Sci. *91*, 1751–1758.

Coutinho, P.M., Stam, M., Blanc, E., and Henrissat, B. (2003). Why are there so many carbohydrate-active enzyme-related genes in plants? Trends Plant Sci. *8*, 563–565.

Cravatt, B.F., Wright, A.T., and Kozarich, J.W. (2008). Activity-based protein profiling: from enzyme chemistry to proteomic chemistry. Annu. Rev. Biochem. *77*, 383–414.

Davies, G., and Henrissat, B. (1995). Structures and mechanisms of glycosyl hydrolases. Structure *3*, 853–859.

Dean, G.H., Zheng, H., Tewari, J., Huang, J., Young, D.S., Hwang, Y.T., Western, T.L., Carpita, N.C., McCann, M.C., Mansfield, S.D., et al. (2007). The Arabidopsis *MUM2* gene encodes a beta-galactosidase required for the production of seed coat mucilage with correct hydration properties. Plant Cell *19*, 4007–4021.

Deane, J.E., Graham, S.C., Kim, N.N., Stein, P.E., McNair, R., Cachón-González, M.B., Cox, T.M., and Read, R.J. (2011). Insights into krabbe disease from structures of galactocerebrosidase. Proc. Natl. Acad. Sci. *108*, 15169–15173.

Dong, S., Stam, R., Cano, L.M., Song, J., Sklenar, J., Yoshida, K., Bozkurt, T.O., Oliva, R., Liu, Z., Tian, M., et al. (2014). Effector specialization in a lineage of the Irish potato famine pathogen. Science *343*, 552–555.

Dörmann, P. (2001). Galactolipids in plant membranes. In eLS, (John Wiley & Sons, Ltd),.

Gantulga, D., Turan, Y., Bevan, D.R., and Esen, A. (2008). The Arabidopsis *At1g45130* and *At3g52840* genes encode β-galactosidases with activity toward cell wall polysaccharides. Phytochemistry *69*, 1661–1670.

Gantulga, D., Ahn, Y.O., Zhou, C., Battogtokh, D., Bevan, D.R., Winkel, B.S.J., and Esen, A. (2009). Comparative characterization of the Arabidopsis subfamily a1 β-galactosidases. Phytochemistry *70*, 1999–2009.

Goodstein, D.M., Shu, S., Howson, R., Neupane, R., Hayes, R.D., Fazo, J., Mitros, T., Dirks, W., Hellsten, U., Putnam, N., et al. (2012). Phytozome: a comparative platform for green plant genomics. Nucleic Acids Res. *40*, D1178–D1186.

Gorshkova, T.A., Chemikosova, S.B., Lozovaya, V.V., and Carpita, N.C. (1997). Turnover of galactans and other cell wall polysaccharides during development of flax plants. Plant Physiol. *114*, 723–729.

Gross, K.C. (1983). Changes in free galactose, myo-inositol and other monosaccharides in normal and non-ripening mutant tomatoes. Phytochemistry *22*, 1137–1139.

Gross, K.C. (1984). Fractionation and partial characterization of cell walls from normal and non-ripening mutant tomato fruit. Physiol. Plant. *62*, 25–32.

Gross, K.C. (1985). Promotion of ethylene evolution and ripening of tomato fruit by galactose. Plant Physiol. *79*, 306–307.

Gross, K.C., and Wallner, S.J. (1979). Degradation of cell wall polysaccharides during tomato fruit ripening 1. Plant Physiol. *63*, 117–120.

Gu, C., Kolodziejek, I., Misas-Villamil, J., Shindo, T., Colby, T., Verdoes, M., Richau, K.H., Schmidt, J., Overkleeft, H.S., and van der Hoorn, R.A.L. (2010). Proteasome activity profiling: a simple, robust and versatile method revealing subunit-selective inhibitors and cytoplasmic, defense-induced proteasome activities. Plant J. Cell Mol. Biol. *62*, 160–170.

Gu, C., Shannon, D.A., Colby, T., Wang, Z., Shabab, M., Kumari, S., Villamor, J.G., McLaughlin, C.J., Weerapana, E., Kaiser, M., et al. (2013). Chemical proteomics with sulfonyl fluoride probes reveals selective labeling of functional tyrosines in glutathione transferases. Chem. Biol. *20*, 541–548.

Henrissat, B. (1991). A classification of glycosyl hydrolases based on amino acid sequence similarities. Biochem. J. *280 (Pt 2)*, 309–316.

Hirata, H., Negoro, S., and Okada, H. (1985). High production of thermostable β-galactosidase of *Bacillus stearothermophilus* in *Bacillus subtilis*. Appl. Environ. Microbiol. *49*, 1547–1549.

Van der Hoorn, R.A.L., Leeuwenburgh, M.A., Bogyo, M., Joosten, M.H.A.J., and Peck, S.C. (2004). Activity profiling of papain-like cysteine proteases in plants. Plant Physiol. *135*, 1170–1178.

Hörger, A.C., Ilyas, M., Stephan, W., Tellier, A., Hoorn, R.A.L. van der, and Rose, L.E. (2012). Balancing selection at the tomato RCR3 guardee gene family maintains variation in strength of pathogen defense. PLOS Genet. *8*, e1002813.

Hoyoux, A., Jennes, I., Dubois, P., Genicot, S., Dubail, F., François, J.M., Baise, E., Feller, G., and Gerday, C. (2001). Cold-adapted β-galactosidase from the antarctic psychrophile *Pseudoalteromonas haloplanktis*. Appl. Environ. Microbiol. *67*, 1529–1535.

Hsu, C.A., Lee, S.L., and Chou, C.C. (2007). Enzymatic Production of galactooligosaccharides by β-galactosidase from *Bifidobacterium longum* BCRC 15708. J. Agric. Food Chem. *55*, 2225–2230.

Jacob, F., and Monod, J. (1961). Genetic regulatory mechanisms in the synthesis of proteins. J. Mol. Biol. *3*, 318–356.

Juers, D.H., Matthews, B.W., and Huber, R.E. (2012). LacZ β-galactosidase: Structure and function of an enzyme of historical and molecular biological importance. Protein Sci. Publ. Protein Soc. *21*, 1792–1807.

Kaschani, F., Gu, C., Niessen, S., Hoover, H., Cravatt, B.F., and van der Hoorn, R.A.L. (2009). Diversity of serine hydrolase activities of unchallenged and botrytis-infected *Arabidopsis thaliana*. Mol. Cell. Proteomics MCP *8*, 1082–1093.

Kaschani, F., Shabab, M., Bozkurt, T., Shindo, T., Schornack, S., Gu, C., Ilyas, M., Win, J., Kamoun, S., and van der Hoorn, R.A.L. (2010). An effector-targeted protease contributes to defense against *Phytophthora infestans* and is under diversifying selection in natural hosts. Plant Physiol. *154*, 1794–1804.

Kobe, B., and Kemp, B.E. (1999). Active site-directed protein regulation. Nature *402*, 373–376.

Kołodziejek, I., and van der Hoorn, R.A. (2010). Mining the active proteome in plant science and biotechnology. Curr. Opin. Biotechnol. *21*, 225–233.

Kolodziejek, I., Misas-Villamil, J.C., Kaschani, F., Clerc, J., Gu, C., Krahn, D., Niessen, S., Verdoes, M., Willems, L.I., Overkleeft, H.S., et al. (2011). Proteasome activity imaging and profiling characterizes bacterial effector Syringolin A. Plant Physiol. *155*, 477–489.

Kotake, T., Dina, S., Konishi, T., Kaneko, S., Igarashi, K., Samejima, M., Watanabe, Y., Kimura, K., and Tsumuraya, Y. (2005). Molecular cloning of a β-galactosidase from radish that specifically hydrolyzes β-(1-3) and β-(1-6)-galactosyl residues of arabinogalactan Protein. Plant Physiol. *138*, 1563–1576.

Kötzler, M.P., Hancock, S.M., and Withers, S.G. (2001). Glycosidases: functions, families and folds. In eLS, (John Wiley & Sons, Ltd),.

Lenger, J., Kaschani, F., Lenz, T., Dalhoff, C., Villamor, J.G., Köster, H., Sewald, N., and van der Hoorn, R.A.L. (2012). Labeling and enrichment of *Arabidopsis thaliana* matrix metalloproteases using an active-site directed, marimastat-based photoreactive probe. Bioorg. Med. Chem. *20*, 592–596.

van der Linde, K., Mueller, A.N., Hemetsberger, C., Kashani, F., van der Hoorn, R.A.L., and Doehlemann, G. (2012). The maize cystatin CC9 interacts with apoplastic cysteine proteases. Plant Signal. Behav. *7*, 1397–1401.

Liu, G.X., Kong, J., Lu, W.W., Kong, W.T., Tian, H., Tian, X.Y., and Huo, G.C. (2011). β-galactosidase with transgalactosylation activity from *Lactobacillus fermentum* K4. J. Dairy Sci. *94*, 5811–5820.

Lombard, V., Ramulu, H.G., Drula, E., Coutinho, P.M., and Henrissat, B. (2014). The carbohydrate-active enzymes database (CAZy) in 2013. Nucleic Acids Res. *42*, D490–D495.

Lozano-Torres, J.L., Wilbers, R.H.P., Gawronski, P., Boshoven, J.C., Finkers-Tomczak, A., Cordewener, J.H.G., America, A.H.P., Overmars, H.A., Van 't Klooster, J.W., Baranowski, L., et al. (2012). Dual disease resistance mediated by the immune receptor Cf-2 in tomato requires a common virulence target of a fungus and a nematode. Proc. Natl. Acad. Sci. U. S. A. *109*, 10119–10124.

McCarter, J.D., and Stephen Withers, G. (1994). Mechanisms of enzymatic glycoside hydrolysis. Curr. Opin. Struct. Biol. *4*, 885–892.

Minic, Z. (2008). Physiological roles of plant glycoside hydrolases. Planta *227*, 723–740.

Misas-Villamil, J.C., Toenges, G., Kolodziejek, I., Sadaghiani, A.M., Kaschani, F., Colby, T., Bogyo, M., and van der Hoorn, R.A.L. (2013). Activity profiling of vacuolar processing enzymes reveals a role for VPE during oomycete infection. Plant J. Cell Mol. Biol. *73*, 689–700.

Moctezuma, E., Smith, D.L., and Gross, K.C. (2003a). Effect of ethylene on mRNA abundance of three β-galactosidase genes in wild type and mutant tomato fruit. Postharvest Biol. Technol. *28*, 207–217.

Moctezuma, E., Smith, D.L., and Gross, K.C. (2003b). Antisense suppression of a β-galactosidase gene (*TBG6*) in tomato increases fruit cracking. J. Exp. Bot. *54*, 2025–2033.

Mueller, A.N., Ziemann, S., Treitschke, S., Aßmann, D., and Doehlemann, G. (2013). Compatibility in the Ustilago maydis-maize interaction requires inhibition of host cysteine proteases by the fungal effector Pit2. PLOS Pathog. *9*, e1003177.

Nakagawa, T., Ikehata, R., Uchino, M., Miyaji, T., Takano, K., and Tomizuka, N. (2006). Cold-active acid β-galactosidase activity of isolated psychrophilic-basidiomycetous yeast *Guehomyces pullulans*. Microbiol. Res. *161*, 75–79.

Nakagawa, T., Ikehata, R., Myoda, T., Miyaji, T., and Tomizuka, N. (2007). Overexpression and functional analysis of cold-active β-galactosidase from *Arthrobacter psychrolactophilus* strain F2. Protein Expr. Purif. *54*, 295–299.

Nickel, S., Kaschani, F., Colby, T., van der Hoorn, R.A.L., and Kaiser, M. (2012). A para-nitrophenol phosphonate probe labels distinct serine hydrolases of Arabidopsis. Bioorg. Med. Chem. *20*, 601–606.

OGASAWARA, S., ABE, K., and NAKAJIMA, T. (2007). Pepper β-Galactosidase 1 (PBG1) plays a significant role in fruit ripening in bell Pepper (*Capsicum annuum*). Biosci. Biotechnol. Biochem. *71*, 309–322.

Ohto, U., Usui, K., Ochi, T., Yuki, K., Satow, Y., and Shimizu, T. (2012). Crystal Structure of human β-galactosidase. Structural basis of GM1 gangliosidosis and morquio B diseases. J. Biol. Chem. *287*, 1801–1812.

Panesar, P.S., Kumari, S., Panesar, R., Panesar, P.S., Kumari, S., and Panesar, R. (2010). Potential applications of immobilized β-galactosidase in food processing industries, potential applications of immobilized β-galactosidase in food processing industries. Enzyme Res. Enzyme Res. *2010, 2010*, e473137.

Perez Almeida, I.B. (2004). Arabidopsis cell wall beta-galactosidase gene family: Expression, catalytic activities and biological function in galactose dynamics. Ph.D. thesis. Purdue University.

Pressey, R. (1983). β-galactosidases in ripening tomatoes. Plant Physiol. *71*, 132–135.

Redgwell, R.J., Fischer, M., Kendal, E., and MacRae, E.A. (1997). Galactose loss and fruit ripening: high-molecular-weight arabinogalactans in the pectic polysaccharides of fruit cell walls. Planta *203*, 174–181.

Regenhardt, S.A., Mammarella, E.J., and Rubiolo, A.C. (2013). Hydrolysis of lactose from cheese whey using a reactor with β-galactosidase enzyme immobilised on a commercial UF membrane. Chem. Process Eng. *34*, 375–385.

Richau, K.H., Kaschani, F., Verdoes, M., Pansuriya, T.C., Niessen, S., Stüber, K., Colby, T., Overkleeft, H.S., Bogyo, M., and Van der Hoorn, R.A.L. (2012). Subclassification and biochemical analysis of plant papain-like cysteine proteases displays subfamily-specific characteristics. Plant Physiol. *158*, 1583–1599.

Rojas, A.L., Nagem, R.A.P., Neustroev, K.N., Arand, M., Adamska, M., Eneyskaya, E.V., Kulminskaya, A.A., Garratt, R.C., Golubev, A.M., and Polikarpov, I. (2004). Crystal structures of β-galactosidase from *Penicillium sp.* and its complex with galactose. J. Mol. Biol. *343*, 1281–1292.

Rooney, H.C.E., Van't Klooster, J.W., van der Hoorn, R.A.L., Joosten, M.H.A.J., Jones, J.D.G., and de Wit, P.J.G.M. (2005). Cladosporium Avr2 inhibits tomato Rcr3 protease required for Cf-2-dependent disease resistance. Science *308*, 1783–1786.

Ross, G.S., Wegrzyn, T., MacRae, E.A., and Redgwell, R.J. (1994). Apple beta-galactosidase. activity against cell wall polysaccharides and characterization of a related cDNA clone. Plant Physiol. *106*, 521–528.

Sampedro, J., Gianzo, C., Iglesias, N., Guitián, E., Revilla, G., and Zarra, I. (2012). *AtBGAL10* is the main xyloglucan β-galactosidase in Arabidopsis, and its absence results in unusual xyloglucan subunits and growth defects. Plant Physiol. *158*, 1146–1157.

Sekimata, M., Ogura, K., Tsumuraya, Y., Hashimoto, Y., and Yamamoto, S. (1989). A β-galactosidase from radish (*Raphanus sativus* L.) seeds. Plant Physiol. *90*, 567–574.

Shabab, M., Shindo, T., Gu, C., Kaschani, F., Pansuriya, T., Chintha, R., Harzen, A., Colby, T., Kamoun, S., and Hoorn, R.A.L. van der (2008). Fungal effector protein AVR2 targets diversifying defense-related cys proteases of tomato. Plant Cell *20*, 1169–1183.

Showalter, A.M. (2001). Arabinogalactan-proteins: structure, expression and function. Cell. Mol. Life Sci. CMLS *58*, 1399–1417.

Smith, D.L., and Gross, K.C. (2000). A family of at least seven β-galactosidase genes is expressed during tomato fruit development. Plant Physiol. *123*, 1173–1184.

Smith, D.L., Abbott, J.A., and Gross, K.C. (2002). Down-regulation of tomato β-galactosidase 4 results in decreased fruit softening. Plant Physiol. *129*, 1755–1762.

Song, J., Win, J., Tian, M., Schornack, S., Kaschani, F., Ilyas, M., Hoorn, V.D., A.l, R., and Kamoun, S. (2009). Apoplastic effectors secreted by two unrelated eukaryotic plant pathogens target the tomato defense protease RCR3. Proc. Natl. Acad. Sci. U. S. A.

Sturgeon, R.J. (2001). Carbohydrates. In eLS, (John Wiley & Sons, Ltd).

Szczodrak, J. (2000). Hydrolysis of lactose in whey permeate by immobilized β-galactosidase from *Kluyveromyces fragilis*. J. Mol. Catal. B Enzym. *10*, 631–637.

Tanthanuch, W., Chantarangsee, M., Maneesan, J., and Ketudat-Cairns, J. (2008). Genomic and expression analysis of glycosyl hydrolase family 35 genes from rice (*Oryza sativa* L.). BMC Plant Biol. *8*, 84.

Tian, M., Win, J., Song, J., Hoorn, R. van der, Knaap, E. van der, and Kamoun, S. (2007). A *Phytophthora infestans* cystatin-like protein targets a novel tomato papain-like apoplastic protease. Plant Physiol. *143*, 364–377.

Torres, D.P.M., Gonçalves, M. do P.F., Teixeira, J.A., and Rodrigues, L.R. (2010). Galacto-oligosaccharides: production, properties, applications, and significance as prebiotics. Compr. Rev. Food Sci. Food Saf. *9*, 438–454.

Trainotti, L., Spinello, R., Piovan, A., Spolaore, S., and Casadoro, G. (2001). β-galactosidases with a lectin-like domain are expressed in strawberry. J. Exp. Bot. *52*, 1635–1645.

Villamor, J.G., Kaschani, F., Colby, T., Oeljeklaus, J., Zhao, D., Kaiser, M., Patricelli, M.P., and van der Hoorn, R.A.L. (2013). Profiling protein kinases and other ATP binding proteins in Arabidopsis using Acyl-ATP probes. Mol. Cell. Proteomics MCP *12*, 2481–2496.

Vuong, T.V., and Wilson, D.B. (2010). Glycoside hydrolases: catalytic base/nucleophile diversity. Biotechnol. Bioeng. *107*, 195–205.

Wallner, S.J., and Bloom, H.L. (1977). Characteristics of tomato cell wall degradation *in vitro*. Plant Physiol. *60*, 207–210.

Wei, H., Brunecky, R., Donohoe, B.S., Ding, S.-Y., Ciesielski, P.N., Yang, S., Tucker, M.P., and Himmel, M.E. (2015). Identifying the ionically bound cell wall and intracellular glycoside hydrolases in late growth stage Arabidopsis stems: implications for the genetic engineering of bioenergy crops. Front. Plant Sci. *6*.

Wierzbicka-Woś, A., Cieśliński, H., Wanarska, M., Kozłowska-Tylingo, K., Hildebrandt, P., and Kur, J. (2011). A novel cold-active β-D-galactosidase from the *Paracoccus sp.* 32d - gene cloning, purification and characterization. Microb. Cell Factories *10*, 108.

Winter, D., Vinegar, B., Nahal, H., Ammar, R., Wilson, G.V., and Provart, N.J. (2007). An “electronic fluorescent pictograph” browser for exploring and analysing large-scale biological data sets. PLoS ONE *2*.

Wu, Z., and Burns, J.K. (2004). A β-galactosidase gene is expressed during mature fruit abscission of “Valencia” orange (*Citrus sinensis*). J. Exp. Bot. *55*, 1483–1490.

Yapo, B.M. (2011). Rhamnogalacturonan-I: a structurally puzzling and functionally versatile polysaccharide from plant cell walls and mucilages. Polym. Rev. *51*, 391–413.

Zhang, S., McCarter, J.D., Okamura-Oho, Y., Yaghi, F., Hinek, A., Withers, S.G., and Callahan, J.W. (1994). Kinetic mechanism and characterization of human β-galactosidase precursor secreted by permanently transfected Chinese hamster ovary cells. Biochem. J. *304*, 281–288.

Chapter 2: Broad range glycosidase activity profiling

This chapter has been published as: Chandrasekar, B., Colby, T., Emon, A.E.K., Jiang, J., Hong, T.N., Villamor, J.G., Harzen, A., Overkleeft, H.S., and Van der Hoorn, R.A.L. (2014). Broad-range glycosidase activity profiling. *Mol. Cell. Proteomics 13*, 2787–2800. **(*Highlighted in Oxford Biochemical society Journal, Phenotype, 24th issue, Trinity term, 2016*)**

2.1 Introduction

Plants produce hundreds of glycosidases. Despite their importance in cell wall (re)-modelling, protein and lipid modification and metabolite conversion, very little is known of this large class of glycolytic enzymes, partly because of their post-translational regulation and their elusive substrates. Consequently, glycosidases are poorly defined in plants and other organisms. Here, we apply activity-based glycosidase profiling using cell permeable small molecular probes that react covalently with the active site nucleophile of retaining glycosidases in an activity-dependent manner. Using mass spectrometry we detect the active state of dozens of myrosinases, glucosidases, xylosidases, and galactosidases representing seven different retaining glycosidase families. The method is simple and applicable on different organs, different plant species, in living cells and in subproteomes. We displayed the active state of previously uncharacterized glycosidases, one of which encoded by a previously declared pseudogene. Interestingly, glycosidase activity profiling also revealed the active state of a diverse range of putative xylosidases, galactosidases, glucanases and heparanase in the cell wall of *Nicotiana benthamiana*. Our data illustrate that this powerful approach displays a new and important layer of functional proteomic information on the active state of glycosidases.

2.2 Results

2.2.1 Labeling of leaf proteomes with cyclophellitol aziridine activity-based probes

JJB70, JJB111 and KY371 are the three activity-based probes that carry an aziridine analog of cyclophellitol as their warhead. JJB70 carries a bodipy as its reporter tag and is slightly different from the previously described ABP3 (Kallemeijn et al., 2012) by having the triazole linker in reverse orientation (Figure 2.1A). JJB111 (previously called ABP4) and KY371 carry biotin and alkyne minitags, respectively (Figure 2.1A). The electrophilic acyl-aziridine group in the probes react with the nucleophilic active site glutamate/aspartate residue of retaining glycosidases, resulting in a reversible covalent ester bond (Figure 2.1B)**.**

To test plant extracts for labeling, Arabidopsis leaf extracts were incubated with and without 2 µM JJB70 or JJB111. After 1 h labeling, proteins were separated on protein gels and labeled proteins were detected by fluorescent scanning (JJB70) or protein blot analysis using

streptavidin-linked horseradish peroxidase (strep-HRP) (for JJB111). Two major signals were detected at 68 (grey circle) and 75 kDa (black circle) (Figure 2.1C)**.** These signals were not detected in the no-probe-control and suppressed in the samples preincubated with KY371 (Figure 2.1C). These data indicate that JJB70 and JJB111 target similar proteins in Arabidopsis leaf extracts and that labeling with these probes is specific. Further characterization of labeling parameters revealed that one hour labeling time is sufficient to reach maximum labeling; that labeling is saturated at 1 µM JJB70; and that labeling is optimal at slightly acidic pH (Figure 2.2A). These experiments show that labeling strongly depends on labeling conditions.

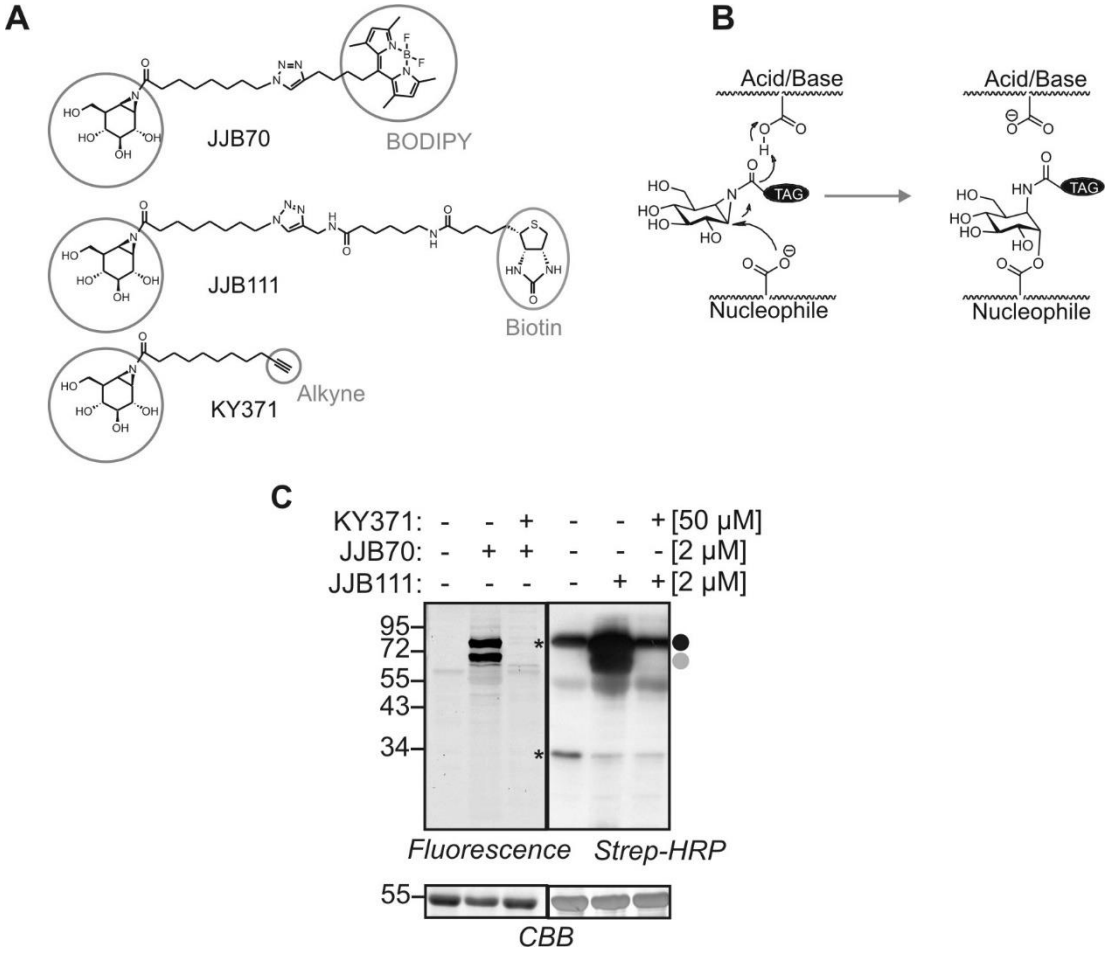

Figure 2.1 Glycosidase profiling with cyclophellitol aziridine activity-based probes

(A) Structures of cyclophellitol aziridine activity-based probes. All the three probes have an aziridine analog of cyclophellitol as warhead followed by a linker. JJB70 has a BODIPY fluorescent reporter tag. JJB111 has an extended linker and a biotin reporter tag. KY371 carries an alkyne minitag. (B) Mechanism of labeling retaining glycosidases (Kallemeijn et al., 2012). The nucleophilic oxygen of one of the two catalytic glutamic acids attacks the electrophilic carbon next to nitrogen in the aziridine ring to form a covalent, reversible ester bond. (C) Labeling profiles of JJB70 and JJB111 on Arabidopsis leaf extracts. *Arabidopsis thaliana* leaf exacts containing ~1.5 mg/ml total soluble proteins were pre-incubated with and without 50 µM KY371 for 30 min and labeled with 2 µM JJB70

or JJB111 for 1 h at pH 7.5. The labeled proteins were either analyzed by in-gel fluorescent scanning (left) or detection on protein blot using streptavidin conjugated to horseradish peroxidase (strep-HRP) (right). The two major signals are indicated by grey and black circles; *, endogenously biotinylated proteins; CBB, Coomassie-Brilliant Blue.

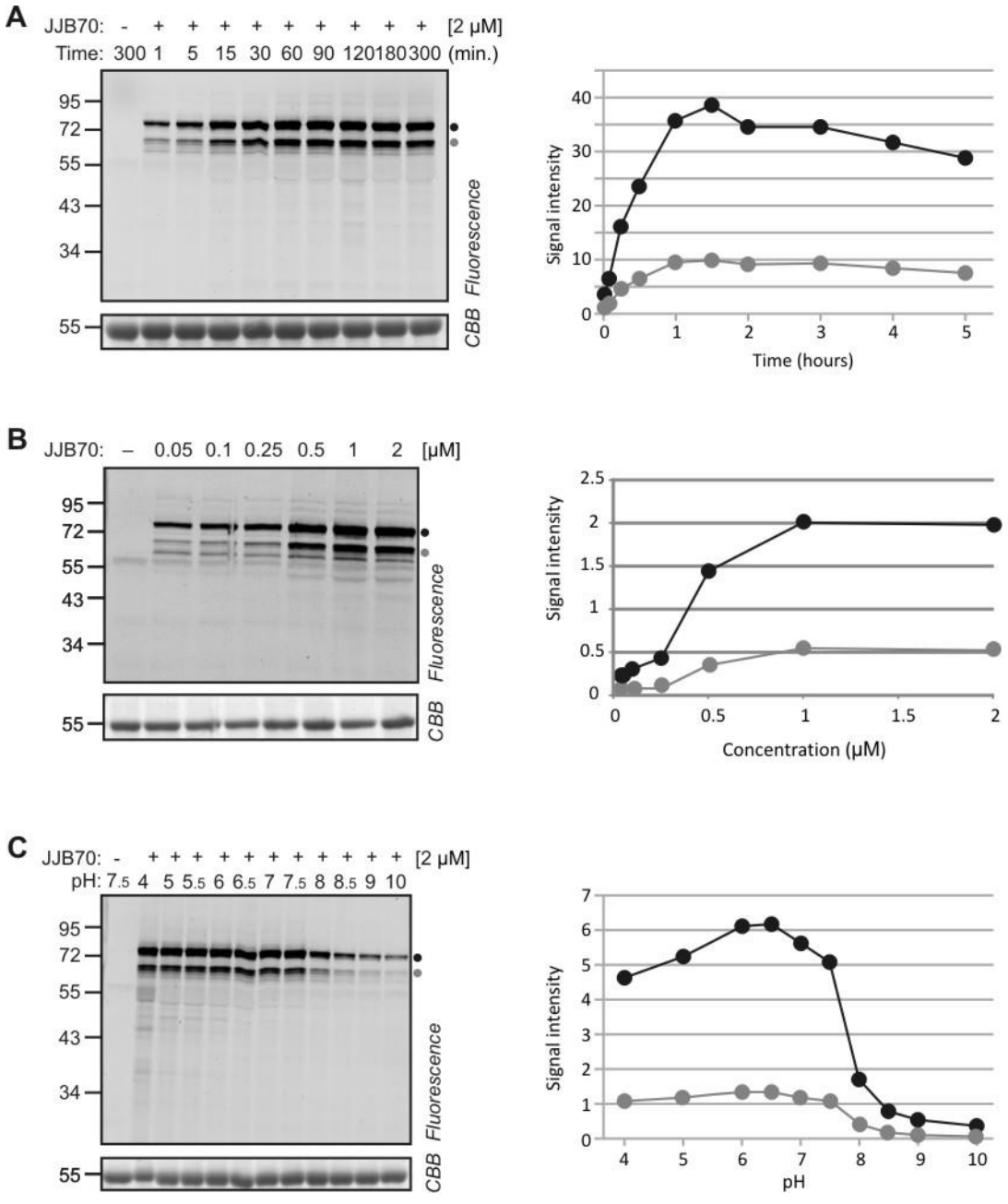

Figure 2.2 Conditions affecting myrosinase labeling with JJB70

(A) Labeling occurs within one hour. Leaf extracts containinig ~1.5 mg/ml total soluble proteins were incubated at pH 7.5 with 2 µM JJB70 and protein samples were collected at various time points. (B) Labeling reaches saturation at 1 µM JJB70. Leaf extracts were incubated at pH 7.5 with 0.05-2 µM of JJB70. (C) Labeling is optimal at slightly acidic pH. Leaf extracts were incubated with 2 µM JJB70 at pH 4-10 for 1 h. *(*A-C) Labeled proteins were detected by in-gel fluorescent scanning. The fluorescence was quantified and plotted against labeling time, probe

concentration and pH. The gel was stained with coomassie to show the equal loading. Two major signals are indicated by grey and black circles.

2.2.2 Active site labeling of myrosinases TGG1 and TGG2

To identify the labeled proteins, large scale labeling was performed from JJB111-labeled leaf extracts. The labeled proteins were enriched on streptavidin beads, separated on a protein gel, stained with SYPRO Ruby and detected by fluorescent scanning. The detected protein bands were excised, treated with trypsin, and the peptides were identified by ion-trap mass spectrometry. Similar to small scale labeling, two strong signals at 68 and 75 kDa were enriched and these signals were absent in the no-probe-control (Figure 2.3A). MS analysis showed that the majority of the peptide spectra from the 68 kDa signal originated from β-thioglucoside glucohydrolase TGG2, whereas the 75 kDa signal contained peptides mostly from TGG1 (Figure 2.3B)**.** TGG1 and TGG2 are myrosinases mediating the conversion of glucosinolates during herbivore attack (Barth and Jander, 2006). Myrosinases have one catalytic glutamate residue whereas the second catalytic residue has been replaced by glutamine residue (Burmeister et al., 1997).

To identify the labeling site, the expected modification by JJB111 (735.386 Da) on potentially reactive residues (E and D) was included in the searches. One labeled peptide of TGG1 was identified (black in Figure 3B). Further analysis of the MS2 fragmentation spectrum revealed that b-ions up to T419 and y-ions down to E420 of this peptide are unmodified. In contrast, b-ions beyond E420 or y-ions starting at T419 or before carry the modification (Figure 2.3C). These data demonstrate that the modification is either at E420 or T419. This is consistent with the fact that E420 has been annotated as the nucleophilic active site residue (Zhou et al., 2012). Notably, in addition to the labeled active site peptide, also the spectra of the unmodified active site peptide were found amongst the peptide spectra. This can be explained by the fact that the ester bond between the probe and the active site (Figure 2.1B) can hydrolyze in water. This is the first time that a modification of the active site with cyclophellitol-aziridine is identified by MS.

2.2.3 TGG1 and TGG2 cause the major signals in Arabidopsis leaf extracts

The TGG1 and TGG2 signals migrate at a higher apparent molecular weight (MW) than calculated from the plain amino acid sequence of the mature enzyme (59 and 60.4 kDa, respectively). The increased apparent MW could be due to *N*-glycosylation since TGG1 and TGG2 carry nine and four putative *N*-glycosylation sites, respectively (Figure 2.3E). To examine if TGG1 and TGG2 are *N*-glycosylated, the labeled leaf proteins were incubated with and without deglycosylation enzyme PNGaseF. After PNGaseF treatment, labeled TGG1 and

TGG2 migrated in their expected MW (Figure 2.3E) demonstrating that TGG1 and TGG2 are *N*-glycosylated. The presence of *N*-glycosylation is also consistent with the absence of tryptic peptides carrying putative glycosylation sites from the MS data (Figure 2.3B)**.**

To confirm that the major signals are caused by myrosinases TGG1 and TGG2, leaf extracts of wild-type (WT*)* and *tgg1-3*, *tgg2-1* and *tgg1-3/tgg2-1* knockout plants (Barth and Jander, 2006) were incubated with and without JJB70. Surprisingly, both the major signals were absent in the *tgg1-3* and *tgg1-3/tgg2-1* mutants and only the 68 kDa signal was absent in the *tgg2-1* mutant (Figure 2.3F). It has previously been noted that solubility of TGG2 depends on the presence of TGG1, unless the proteins are extracted in the presence of 500 mM NaCl (Zhou et al., 2012). Indeed, the 68 kDa signal was recovered by extraction in 500 mM NaCl only in the *tgg1-3* mutant but remained absent in *tgg2-1* and *tgg1-3/tgg2-1* mutants. A third signal at 60 kDa was detected in all plants upon extraction in 500 mM NaCl. Taken together, these data demonstrate that the TGG1 and TGG2 cause the two major signals in Arabidopsis leaf extracts labeled with JJB70 and JJB111.

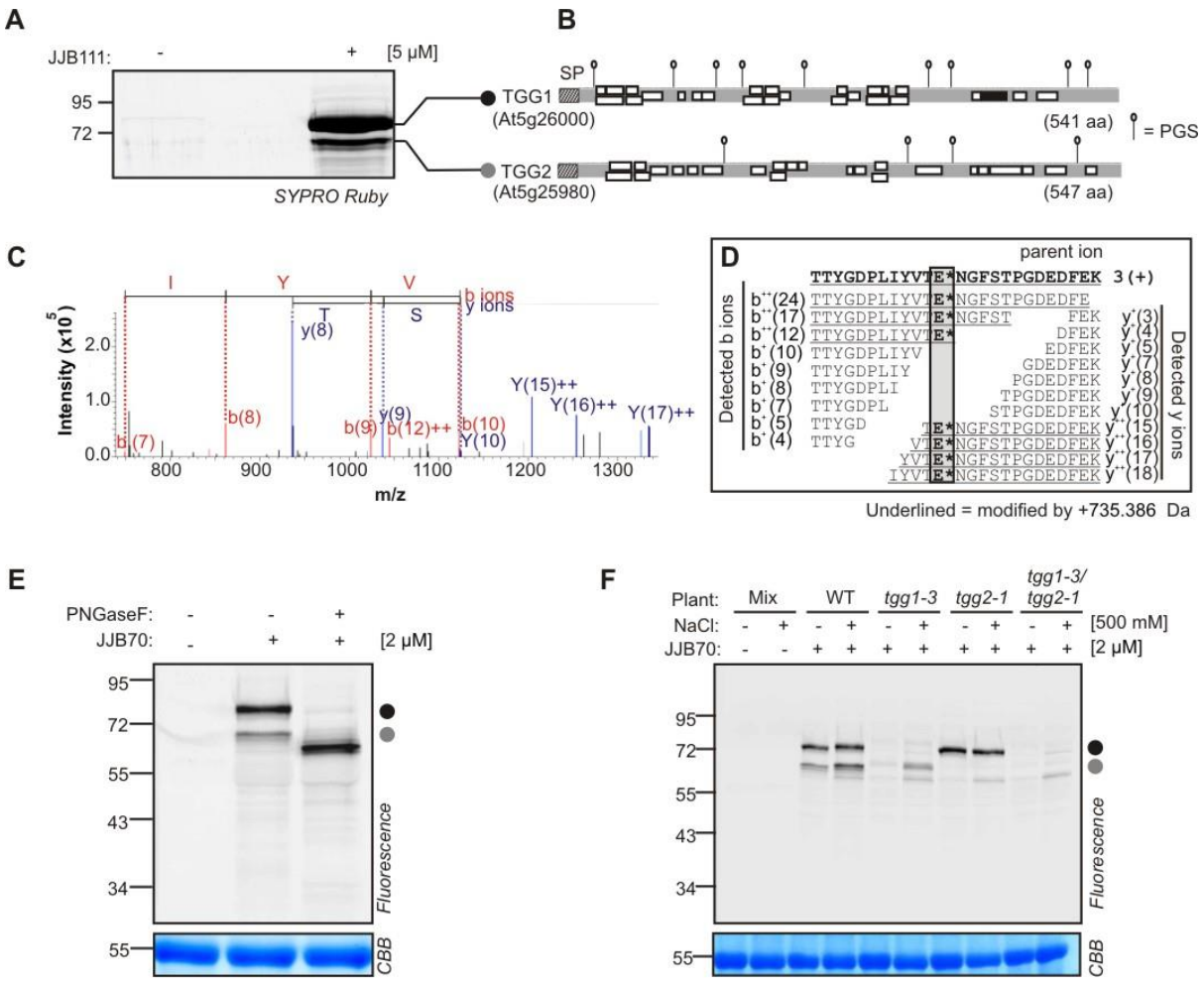

Figure 2.3 Myrosinase activity profiling in Arabidopsis leaf extracts

(A) Identification of proteins labeled by JJB111. Large scale labeling was performed by incubating Arabidopsis leaf extracts with and without 5 µM JJB111. Biotinylated proteins were purified with streptavidin beads and separated on protein gels. The proteins were visualized by SYPRO Ruby staining and fluorescent scanning. Bands were excised, treated with trypsin and the peptides were identified by ion trap mass spectrometry. (B) Peptide coverage of myrosinases TGG1 and TGG2. The identified peptides of TGG1 and TGG2 are indicated by white boxes. The black box represents the labeled active site peptide of TGG1. The signal peptide (SP) and putative *N*-glycosylation sites (PGS) are indicated. (C) Fragmentation of modified active site peptide of TGG1. Region of MS2 fragmentation spectrum showing ions that indicate the labeling site. Peaks from the annotated b- and y-ions are indicated. (D) Summary of all detected ions of modified peptide in the MS2 fragmentation spectrum. (E) the active site residue. All underlined ions carry an extra modification by the probe (735.386 Da). *E,* TGG1 and TGG2 migrate at their predicted molecular weight upon deglycosylation. Leaf extracts of wild type (*WT*) plants were incubated at pH 6.0 with and without 2 µM JJB70. The labeled proteomes were denatured, treated with and without PNGaseF, separated on protein gel and detected by in-gel fluorescence scanning. (F) Labeling of mutant Arabidopsis lines confirms that signals are caused by TGG1 and TGG2. Leaf proteins of wild type (*WT*) and *tgg1-3*, *tgg2-1* and *tgg1-3/tgg2-1* mutant plants were extracted with and without 500 mM NaCl and labeled with 2 µM JJB70. Mixtures of these extracts (mix) were used as no-probe-control.

2.2.4 JJB probes label a second layer of glycosidases representing new GH families

Further examination of the labeling profiles of the *tgg1-3/tgg2-1* double mutant revealed another 13 weak signals at longer exposure times (Figure 2.4A). These signals are also present in *WT* plants but covered by the strong TGG1 and TGG2 signals (Figure 2.4A). Importantly, pre-incubation with KY371 blocked the labeling of all these proteins in both WT and *tgg1-3/tgg2-1* plants (Figure 2.4B). These data demonstrate that JJB70 labels proteins in addition to myrosinases TGG1 and TGG2.

To identify these additional labeled proteins we extended the MS analyses of JJB111 labeled proteins by analyzing the weaker signals. This analysis revealed an additional 18 proteins that were annotated as glycosidases in the CAZY database (Figure 2.4C). This includes myrosinase TGG3 with two unique peptides (Figure 2.4C). TGG3 was previously classified as pseudogene with no ascribed functions (Zhang et al., 2002). Detection of TGG3 upon JJB111-labeling demonstrates that this enzyme is in an active state in Arabidopsis leaves. Nine additional proteins include the endogenously biotinylated proteins BCCP2 and MCCA and abundant proteins such as ribulose-1,5-bisphosphate carboxylase/oxygenase (RuBisCO). These non-glycosidases are usually also detected in no-probe-controls and were not included in further analysis.

The genome of *Arabidopsis thaliana* encodes for 260 retaining glycosidases subdivided into 24 glycosyl hydrolase (GH) families. Mapping the identified glycosidases onto a genome-wide phylogenetic tree of Arabidopsis retaining glycosidases shows that the detected glycosidases are not clustered in the tree but represent members from families GH1, GH3, GH35 and GH79 (Figure 2.5A). This broad range of GH families extends the target list

of these probes beyond the previously described GH1, GH3, and GH30 families (Kallemeijn et al., 2012). Of the twenty identified glycosidases only eight enzymes have been previously characterized for their biochemical and molecular functions. This includes three enzymes from the GH1 family (TGG1, TGG2 and BGLU44), three enzymes from the GH3 family (BXL1, BXL4 and BXL6), one enzyme from the GH35 family (BGAL6) and one enzyme from the GH79 family (GUS2) (Arsovski et al., 2009; Dean et al., 2007; Eudes et al., 2008; Hrubá et al., 2005; Minic et al., 2004; Xu et al., 2004; Zhou et al., 2012). These data show that the probes also display activities of a broad range of glycosidases.

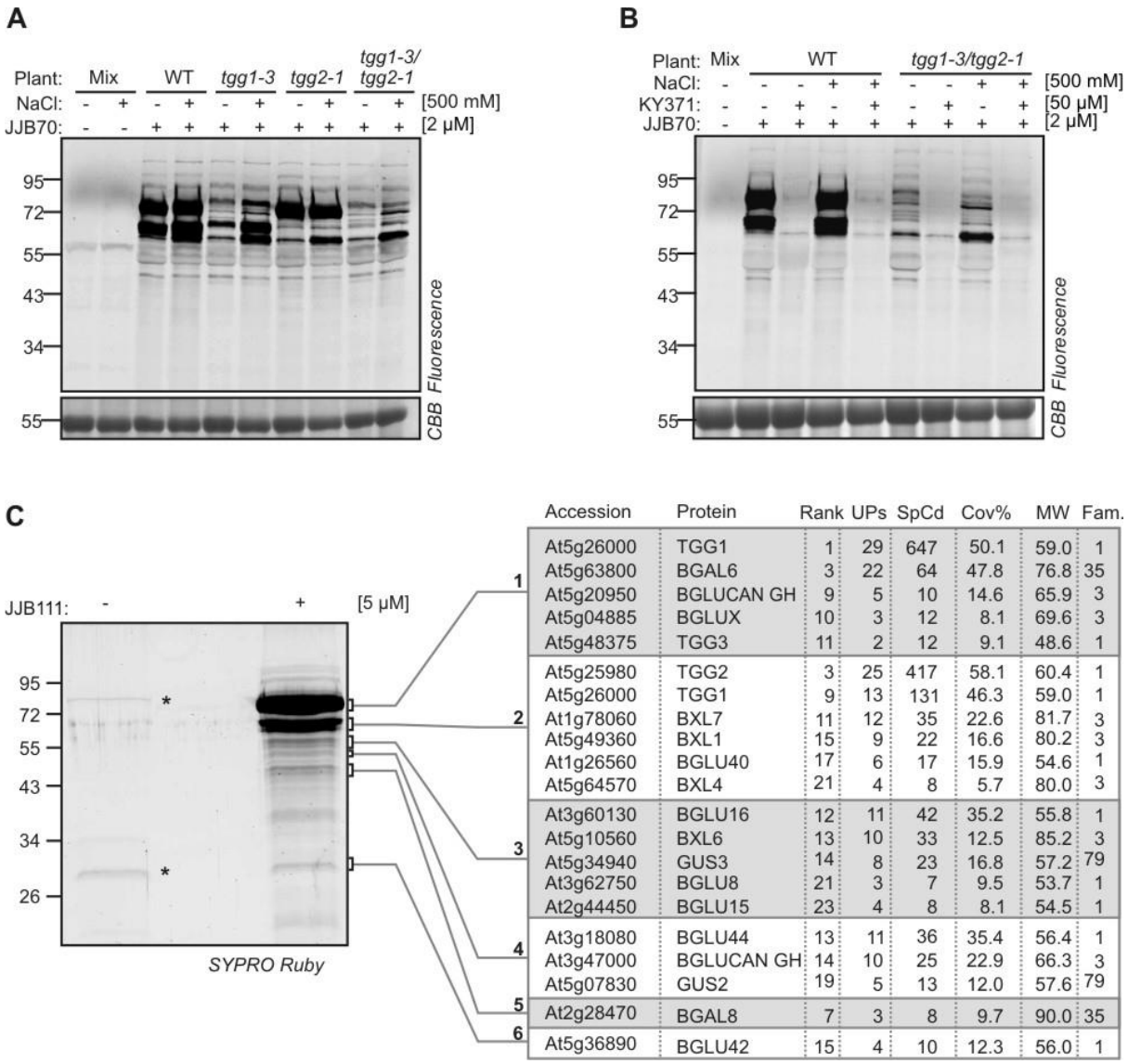

	Accession	Protein	Rank	UPs	SpCd	Cov%	MW	Fam.
1	At5g26000	TGG1	1	29	647	50.1	59.0	1
	At5g63800	BGAL6	3	22	64	47.8	76.8	35
	At5g20950	BGLUCAN GH	9	5	10	14.6	65.9	3
	At5g04885	BGLUX	10	3	12	8.1	69.6	3
	At5g48375	TGG3	11	2	12	9.1	48.6	1
2	At5g25980	TGG2	3	25	417	58.1	60.4	1
	At5g26000	TGG1	9	13	131	46.3	59.0	1
	At1g78060	BXL7	11	12	35	22.6	81.7	3
	At5g49360	BXL1	15	9	22	16.6	80.2	3
	At1g26560	BGLU40	17	6	17	15.9	54.6	1
	At5g64570	BXL4	21	4	8	5.7	80.0	3
3	At3g60130	BGLU16	12	11	42	35.2	55.8	1
	At5g10560	BXL6	13	10	33	12.5	85.2	3
	At5g34940	GUS3	14	8	23	16.8	57.2	79
	At3g62750	BGLU8	21	3	7	9.5	53.7	1
	At2g44450	BGLU15	23	4	8	8.1	54.5	1
4	At3g18080	BGLU44	13	11	36	35.4	56.4	1
	At3g47000	BGLUCAN GH	14	10	25	22.9	66.3	3
	At5g07830	GUS2	19	5	13	12.0	57.6	79
5	At2g28470	BGAL8	7	3	8	9.7	90.0	35
6	At5g36890	BGLU42	15	4	10	12.3	56.0	1

Figure 2.4 JJB probes label a second layer of glycosidases

(A) Prolonged exposure of protein gels revealed additional proteins labeled by JJB70. The labeled proteins in Figure 2E were detected by prolonged exposure. (B) Competition assay confirms specific labeling of additional proteins. Leaf proteins of *WT* and *tgg1-3/tgg2-1* plants were extracted with and without 500 mM NaCl, pre-incubated with and without KY371 for 30 min and labeled with JJB70 at pH 6.0. Mixtures of these proteins were used as no-probe-control (mix). (C) The additional labeled proteins are glycosidases. Purified JJB111-labeled proteins (Figure 2A) were detected by prolonged exposure of the SYPRO Ruby-stained protein gel. Six bands were excised, treated with trypsin and analyzed by MS. Summarized are: rank of protein in the list of identified proteins; number of unique peptides (Ups); spectral counts of all peptides (SpCd); sequence coverage (Cov%); expected molecular weight (MW) and GH family (Fam).

2.2.5 Selectivity of glycosidase labeling

To investigate possible preferential labeling of certain glycosidases (e.g. TGG1 and TGG2) in Arabidopsis leaves, we compared our data with the abundance of transcript and peptide spectra present in the AtGenExpress database and the Arabidopsis proteome database,

respectively. We retrieved the transcript levels of the vegetative rosette from the Botany Array Resource (Toufighi et al., 2005) and raw spectral details of juvenile leaves from the pep2pro database (Hirsch-Hoffmann et al., 2012) for all 260 retaining glycosidases. The majority of the glycosidases are detected at various transcript levels (Figure 2.5B). Peptides of 90 retaining glycosidases were detected in the juvenile leaves of Arabidopsis with different frequencies (Figure 2.5B). Next, we compared transcript levels and the spectral counts with the spectra of our MS data (Figure 2.5B). We are aware that such a comparison is not fully meaningful because the used materials and methods are not identical. Nevertheless, this comparative analysis indicates that major signals caused by TGG1 and TGG2 in leaf extracts are not caused by a greater affinity of the probe for TGGs but by the high abundance of these enzymes when compared to other glycosidases. Additional glycosidases that we detected occur in relatively low abundance in leaf extracts. However, we did not detect all retaining glycosidases present in leaf proteomes, despite the fact that some occur at reasonable abundance. This may be caused by a different affinity for the probe, or because these proteins are not active under the chosen extraction and labeling conditions.

To analyze the diversity of the 20 identified glycosidases, we annotated substrates for these enzymes based on the names in the UniprotKB and NCBI databases. In these databases, protein names are assigned either based on the experimental evidence or homology with characterized enzymes. All the nine identified enzymes from the GH1 family are classified as β-D-glucosidases. Three GH3 family members are assigned as β-D-glucan exohydrolase-like proteins (At3g47000 & At5g20950) or β-glucosidase related protein (At5g04885). We consider these enzymes as being β-D-glucosidases because the β-D-glucan exohydrolases show β-D-glucosidase activity (Hrmova et al., 1996). The other four enzymes from the GH3 family were classified as β-D-xylosidases. Both enzymes from the GH35 family are assigned as β-galactosidases and both enzymes from the GH79 family are assigned as β-glucuronidases. The structural differences in the glycoside substrates of these enzymes deviate only slightly from the reactive group of the JJB probes (Figure 2.5C), explaining why these proteins are labeled despite having different substrates.

To confirm that glycosidases other than glucosidases can be labeled, we tested if commercially available xylosidase from PROZOMIX (http://www.prozomix.com/home) can also be labeled with JJB70. This well-characterized xylosidase is from the soil bacterium *Opitutus terrae* PB90-1 (ACB77584) and belongs to the GH52 family. This experiment revealed that also this classical xylosidase can be labeled with JJB70 and that labeling is competed with KY371 and pH dependent (Figure 2.6). These experiments demonstrate that JJB probes have a much broader range of target retaining glycosidases than originally thought.

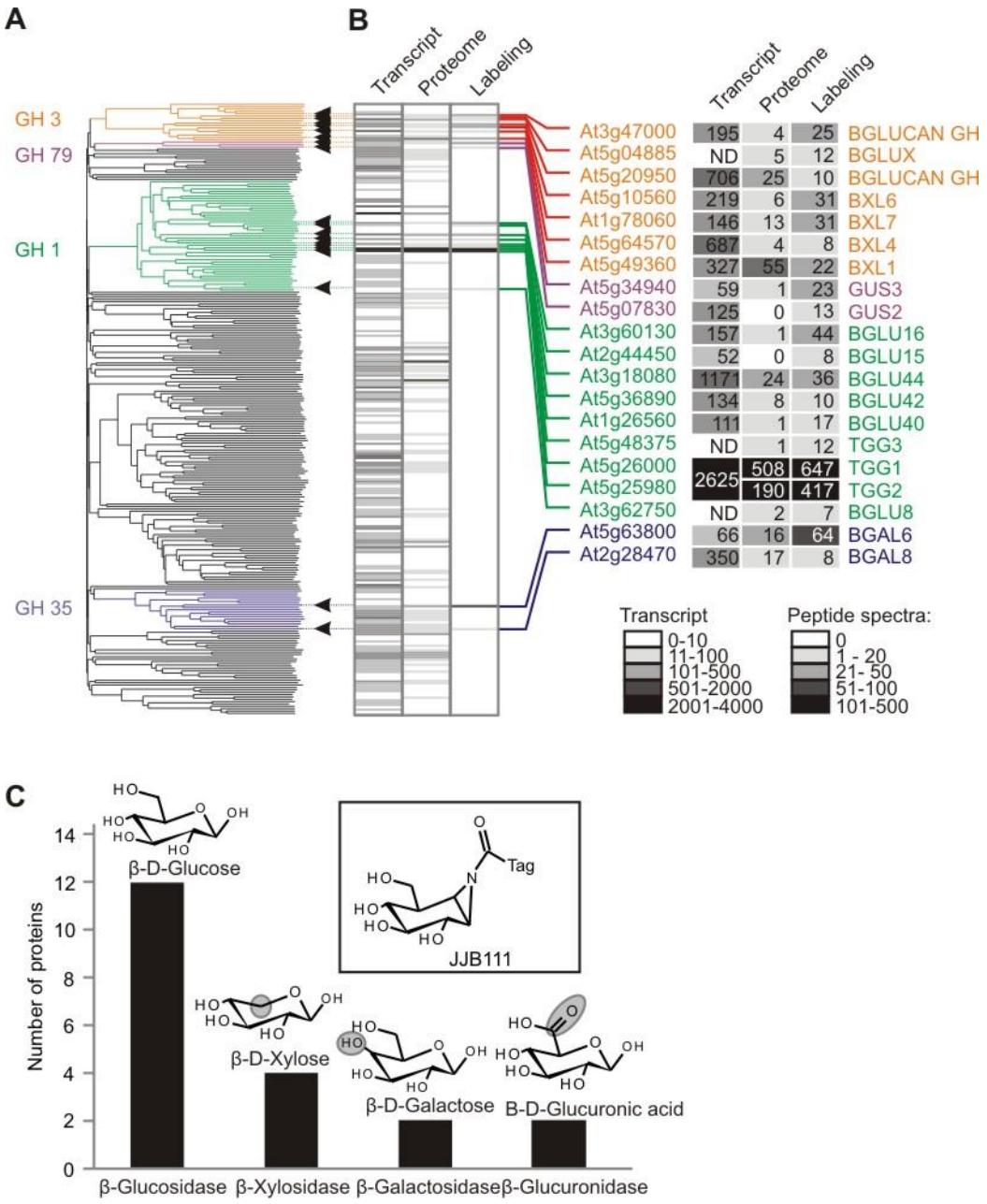

Figure 2.5 Identified glycosidases are diverse in phylogeny and have related putative substrates

(A) Identified glycosidases represent four major families. The unrooted phylogenetic tree of Arabidopsis retaining glycosidases was constructed with protein sequences of 260 retaining glycosidases annotated in the CAZY database. The extended lines on the right indicate the proteins identified in this study. (B) Comparison of transcript and protein abundance with activity of retaining glycosidases in leaf proteomes. The transcript levels (transcript: retrieved from the AtGenExpress database) and the protein levels (proteome: spectral counts retrieved from the pep2pro database) of each retaining glycosidases detected in leaves is compared with the spectral count of JJB111 labeled proteins (labeling). ND, not determined. (C) Identified glycosidases have related but distinct putative substrates. The putative substrate for the glycosidases was identified based on UniProtKB and NCBI databases. The key differences with the probe (inset) are indicated with circles.

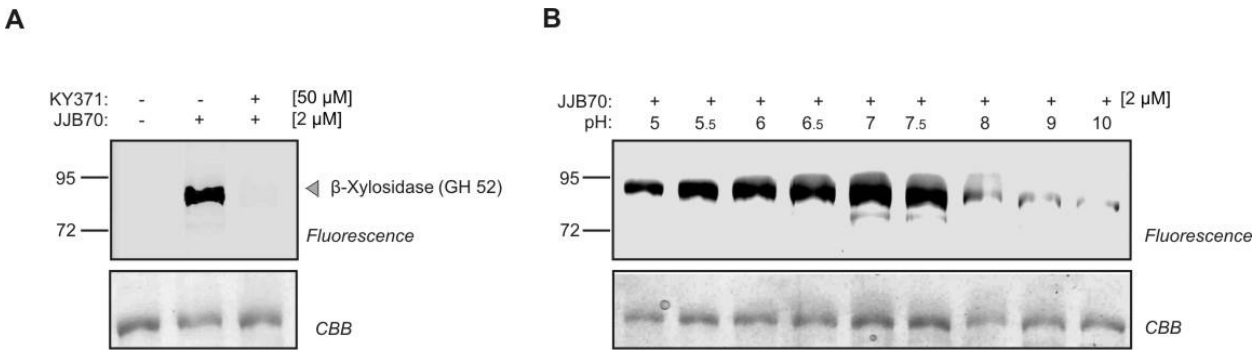

Figure 2.6 JJB70 labels a characterized GH52 β-D-xylosidase

(A) Labeling of a commercially available β-D-xylosidase from the soil bacterium *Opitutus terrae*. 3 µg of purified β-D Xylosidase was pre-incubated with and without 50 µM KY371 for 30 min and labeled with 2 µM JJB70 for 1 h at pH 6.5. (B) Labeling is optimal at neutral pH. 3 µg of β-D-xylosidase was incubated with 2 µM JJB70 at pH 5-10 for 1 h. The labeled protein was detected by in-gel fluorescent scanning. CBB, Coomassie-Brilliant Blue.

2.2.6 Glycosidase profiling is widely applicable

To investigate if glycosidases profiling could be extended to different organs of Arabidopsis, we labeled extracts from seeds, seedlings, leaves, senescing leaves and flowers with JJB70. Profiles are very different between organs (Figure 2.7A). Notably, many signals were detected in flower extracts. Labeling of these proteins is blocked upon pre-incubation with KY371 and most signals remain in the *tgg1-3/tgg2-1* double mutant extracted with and without NaCl (Figure 2.7B).

To extend glycosidase profiling to different plant species, leaf extracts of other dicot and monocot plants were incubated with and without JJB70. Labeling was observed in all tested plant extracts with different profiles and different intensities (Figure 2.7C). Labeling of these proteins was suppressed by pre-incubation with KY371. Taken together, these data demonstrate that glycosidase activity profiling is broadly applicable in plant science.

To test if JJB70 can label proteins in living cells, Arabidopsis cell cultures were pre-incubated with and without KY371 and labeled with JJB70 in duplicate. Proteins were extracted by grinding the cell cultures with SDS-containing gel loading buffer (GLB) to stop the labeling reaction. JJB70 labeling caused two major signals at 56 and 72 kDa and these signals were suppressed by KY371 pre-incubation (Figure 1.7D). Protein extraction in the presence of JJB70 also causes labeling (Ctr1) but this *ex-vivo* labeling is completely abolished if the extraction is performed in SDS-containing GLB (Ctr2; Figure 2.7D). This shows that JJB70 does not label proteins under denaturing conditions and demonstrates that the probe can label proteins in living cells. Interestingly, the labeling profile of the cell culture medium is distinct from that of the cells as it displays two faint signals at 55 kDa that are suppressed

upon pre-incubation with KY371, indicating that the probe also displays activities of secreted glycosidases.

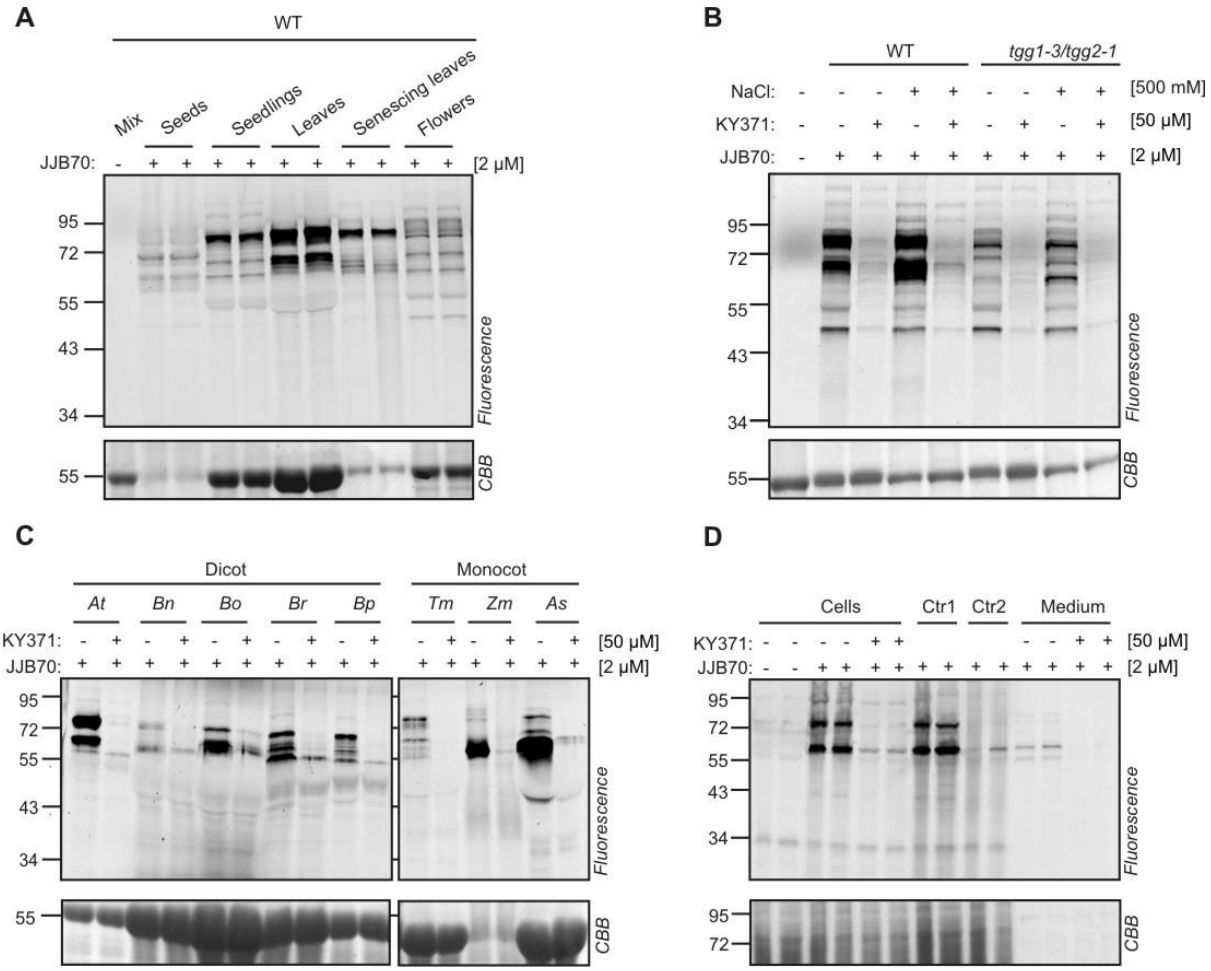

Figure 2.7 Glycosidase profiling is broadly applicable

(A) Glycosidase activity profiles differ in different organs of wild-type *Arabidopsis thaliana*. Organ extracts containing ~1.0-1.5 mg/ml soluble proteins were labeled with and without 2 µM JJB70 for 1 h. The different organ proteomes were mixed and used as a no-probe-control (mix). (B) Flowers contain a diversity of active glycosidase in addition to TGG1 and TGG2. Flower proteins of *WT* and *tgg1-3/tgg2-1* plants were extracted with and without 500 mM NaCl, pre-incubated with and without KY371 for 30 min and labeled with JJB70 at pH 6.0. (C) Glycosidase profiling in different plant species. Leaf extracts of various dicot and monocot plants were pre-incubated with and without 50 µM KY371 for 30 minutes and incubated with 2 µM JJB70 for 1 h. The labeled proteins were detected by in-gel fluorescent scanning. *At*, *Arabidopsis thaliana; Bn, Brassica napus; Bo, Brassica oleracea; Br, Brassica rapa; Bp, Brassica pekinensis; Tm,Triticum monococcum; Zm, Zea mays; As, Avena sativa*. (D) JJB70 labels glycosidases in living cells. Arabidopsis cell cultures were pre-incubated with and without 50 µM KY371 for 30 minutes and incubated with 2 µM JJB70 for 1h. The cell cultures were ground with SDS-containing gel-loading buffer (GLB) to stop the labeling reaction. For control-1 (Ctr1), untreated cell cultures were ground with JJB70 for 30s, followed by adding GLB. For control-2 (Ctr2), untreated cell cultures were ground in GLB containing 2 µM

JJB70. Liquid medium of cell cultures incubated with the probes was separated and concentrated using acetone precipitation.

2.2.7 Glycosidase Profiling of Secreted Proteomes

To investigate the secreted glycosidases further, we identified active glycosidases in the extracellular space (apoplast) of *Nicotiana benthamiana*, an important model plant having large leaves that are ideal for apoplast extraction. The apoplast of plants contains many glycosidases involved in cell wall remodeling and defense (Günl et al., 2011; Minic and Jouanin, 2006). To monitor the active state of apoplastic glycosidases, apoplastic proteomes were isolated from *N. benthamiana* leaves and incubated with and without 2 µM JJB70 for 1h. The labeled proteins were separated on protein gel and detected by fluorescent scanning. Three major signals at 45, 55 and 72 kDa, a weak signal at 43 kDa and a series of weaker signals below 40 kDa were detected in the probe-labeled sample (Figure 2.8A). Similar, but much weaker signals were detected in the total extracts (Figure 2.8A). These signals were absent in the no-probe-control and suppressed in the samples preincubated with KY371. Furthermore, labeling is optimal at acidic pH (Figure 2.8B), consistent with the pH of the apoplast.

To identify the labeled proteins, JJB111-labeled proteins were purified, separated on protein gels and detected by SYPRO Ruby staining. Labeled proteins were enriched in the JJB111-labeled sample and these signals were not detected in the no-probe-control (Figure 2.8C). Seven protein bands from the JJB111-labeled sample and the corresponding regions from no-probe-control were excised and treated with trypsin. MS anaysis of peptides identified 19 different glycosidases from six different GH families: GH1, GH3, GH5, GH35, GH51 and GH79. Members of GH5 and GH51 families were not detected before in labeling experiments, which signifies the potential of JJB probes to label retaining glycosidases from additional GH families. Of the 19 identified glycosidases, β-D-galactosidase (BGAL) (NbS00024332g0007) and α-L-arabinofuranosidase/β-D-xylosidase (AFU/BXLU) (NbS00011746g0004.1) migrated at an apparent MW (45 and 56 kDa, respectively), which is much lower than their theoretical MW (89.7 and 83.9, respectively; Figure 2.8C). The MS analysis identified 12 unique peptides from BGAL and four unique peptides of AFU/BXLU. All the identified peptides of BGAL originate from the GH35 catalytic domain and not from the C-terminal half of this protein (Figure 2.8D). This indicates that the active state of BGAL is a 45 kDa truncated protein consisting of only the catalytic domain.

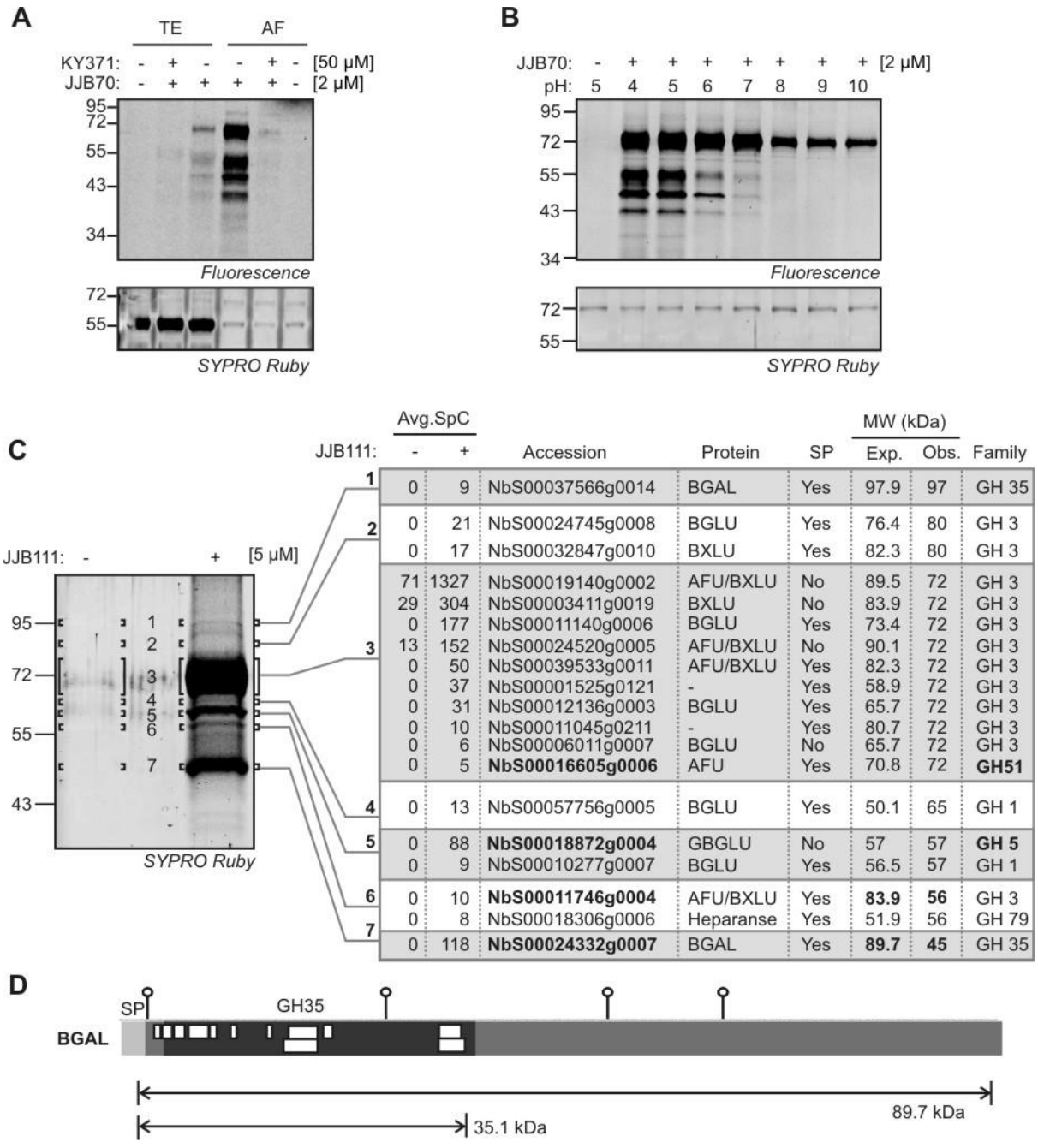

	JJB111:	Avg.SpC -	Avg.SpC +	Accession	Protein	SP	MW (kDa) Exp.	MW (kDa) Obs.	Family
1		0	9	NbS00037566g0014	BGAL	Yes	97.9	97	GH 35
2		0	21	NbS00024745g0008	BGLU	Yes	76.4	80	GH 3
		0	17	NbS00032847g0010	BXLU	Yes	82.3	80	GH 3
3		71	1327	NbS00019140g0002	AFU/BXLU	No	89.5	72	GH 3
		29	304	NbS00003411g0019	BXLU	No	83.9	72	GH 3
		0	177	NbS00011140g0006	BGLU	Yes	73.4	72	GH 3
		13	152	NbS00024520g0005	AFU/BXLU	No	90.1	72	GH 3
		0	50	NbS00039533g0011	AFU/BXLU	Yes	82.3	72	GH 3
		0	37	NbS00001525g0121	-	Yes	58.9	72	GH 3
		0	31	NbS00012136g0003	BGLU	Yes	65.7	72	GH 3
		0	10	NbS00011045g0211	-	Yes	80.7	72	GH 3
		0	6	NbS00006011g0007	BGLU	No	65.7	72	GH 3
		0	5	**NbS00016605g0006**	AFU	Yes	70.8	72	**GH51**
4		0	13	NbS00057756g0005	BGLU	Yes	50.1	65	GH 1
5		0	88	**NbS00018872g0004**	GBGLU	No	57	57	**GH 5**
		0	9	NbS00010277g0007	BGLU	Yes	56.5	57	GH 1
6		0	10	**NbS00011746g0004**	AFU/BXLU	Yes	**83.9**	**56**	GH 3
7		0	8	NbS00018306g0006	Heparanse	Yes	51.9	56	GH 79
		0	118	**NbS00024332g0007**	BGAL	Yes	**89.7**	**45**	GH 35

Figure 2.8 The plant apoplast contains a diversity of active glycosidases

(A) Labeling of total extracts (TE) and apoplastic fluids (AF) isolated from *N. benthamiana* leaves. TE and AF were isolated from leaves of *N. benthamiana*, pre-incubated with and without 50 µM KY371 for 30 min and labeled with 2 µM JJB70 at pH 5. (B) Labeling is optimal at acidic (apoplastic) pH. Apoplastic fluids were incubated with 2 µM JJB70 at pH 4-10 for 1 h. *A-B* Labeled proteins were detected by in-gel fluorescent scanning. The gel was stained with coomassie to show the equal loading. (C) Identification of the JJB111-labeled glycosidases. Large scale labeling was performed by incubating 10 ml of apoplastic fluids from *N. benthamiana* leaves with and without 5 µM JJB111. Biotinylated proteins were purified, separated on protein gels and visualized by fluorescent scanning of SYPRO Ruby-stained protein gels. Bands were excised, treated with trypsin and the peptides were identified by ion trap mass spectrometry by performing two independent MS runs. Proteins identified in both runs were selected

and the average spectral counts are summarized. Band 3 was sub-sliced into 3a, 3b, and 3c and the peptides were identified from each sub-slice. Avg.SpC, average spectral counts; SP, predicted signal peptide; MW, molecular weight; Exp., expected MW; Obs, observed MW. *D,* Peptide coverage of a truncated beta-galactosidase (BGAL). The identified peptides of BGAL are represented by white boxes. Putative *N*-glycosylation sites (PGS) and the theoretical molecular weight of GH35 domain in BGAL and mature protein without signal peptide (SP) are indicated.

2.3 Discussion

We introduced broad-range activity profiling of glycosidases and demonstrated its potential to uncover unexpected post-translational regulation of these enzymes. Using cyclophellitol-aziridine probes, we have detected the active state of nearly 40 different retaining glycosidases of Arabidopsis and *N. benthamiana*. These identified glycosidases belong to seven different GH families and are likely to have different substrate specificities. The majority of the detected glycosidases are uncharacterized enzymes. Glycosidase activity profiling revealed the active state of apoplastic glycosidases in *N. benthamiana*.

2.3.1 Activity-based glycosidase profiling

Several experiments demonstrate that glycosidase labeling is activity dependent. First, glycosidase labeling depends on pH. For example, myrosinases TGG1 and TGG2 and apoplastic glycosidases were labeled intensively at slightly acidic or acidic pH, consistent with *in vitro* studies of these enzymes (Rather and Mishra, 2013; Zhou et al., 2012) and the location of these enzymes in the acidic apoplast, lysosome or vacuole (Grignon and Sentenac, 1991). In general, bio-molecules have evolved to perform their functions at conditions of the compartments where they are located (Talley and Alexov, 2010). Second, the identified glycosidases are all retaining enzymes. This selectivity is in agreement with the proposed mechanism of these probes to label the active site of retaining glycosidases with a covalent glycosyl-enzyme intermediate. Third, spectral analysis of the JJB111-labeled peptide of TGG1 indicated that the nucleophilic glutamate active site residue was indeed labeled by the probe. This confirms that the warhead of the probe enters the substrate-binding pocket of glycosidases to label the active site. Identification of both labeled and unlabeled versions of active site peptides from TGG1 is explained by the reversible nature of the ester bond formed between the probe and the enzymes, sensitive for hydrolysis during the chemical proteomics workflow. This also explains why we did not identify labeled peptides from the other detected glycosidases. Fourth, labeling of proteins in cell cultures was abolished under denaturing conditions, implying that a native protein structure is essential for labeling. Fifth, competition assays by pre-incubation with glycosidase inhibitor KY371 blocked labeling. Taken together,

these experiments show that the probes label glycosidases based on their active state rather than their abundance.

2.3.2 Broad range glycosidase profiling

We discovered the potential of JJB probes to label a larger number of glycosidases than originally thought. Cyclophellitol-aziridine based probes were initially designed to label retaining glucosidases (Kallemeijn et al., 2012). In addition to glucosidases, we have detected glycosidases with additional specificities including xylosidases, galactosidases, glucuronidase and glucanases. Interestingly, we also identified an α-L-arabinofuranosidase and heparanase whose substrates are α-L-arabinofuranoside and heparan sulphate, respectively. Furthermore, labeling of a well-characterized xylosidase confirms that the JJB probes do not target only glucosidases. Detection of a large number of different glycosidases in plant proteomes is consistent with the fact plant genomes have more glycosidase-related genes when compared to animals (Coutinho et al., 2003). We have detected the active state of 39 different glycosidases representing six different retaining GH families of Arabidopsis and *N. benthamiana*. The labeled purified xylosidase is a representative of the seventh GH family. In addition to labeling members of GH1, GH3, and GH30 (Kallemeijn et al., 2012), we have now detected labeling of members of GH5, GH35, GH79, GH51, GH52 families, which comprise 100 genes in Arabidopsis. Hence JJB probes offer a great potential to study the active state of a large number of glycosidases in plants.

2.3.3 Opportunities offered by glycosidase profiling

Being a large super family, glycosidases are challenging to characterize. Glycosidase profiling can be used to study which and when these enzymes are in their active state. Some glycosidases do not show activities when heterologously expressed and purified. For example, recombinant TGG2 did not have myrosinase activity upon heterologous expression and *in vitro* enzyme assays (Andersson et al., 2009). This highlights the importance of profiling activities of enzymes under native conditions. To our knowledge, activities contributed by TGG1 or TGG2 have not been studied in wild-type Arabidopsis plants before. To study myrosinase activities contributed by TGG2, a tedious extraction and purification procedure had to be followed using *tgg1* mutant plants (Zhou et al., 2012). We displayed the active state of TGG1 and TGG2 in wild-type plants without using knockout lines and without complex extraction procedures. Hence glycosidase activity profiling significantly simplifies future studies on myrosinases and other glycosidases.

The synthesis of putative substrates by organic chemistry to characterize the glycoside specificities is a bottle-neck in glycobiology (Minic and Jouanin, 2006). Furthermore, some

glycosidases, like plant α-D-xylosidases, hydrolyze only their natural substrates but not commercially available synthetic substrates (Fanutti et al., 1991; Minic and Jouanin, 2006). Glycosidase activity profiling bypasses these bottle-necks by displaying active site availability and reactivity, which are hallmarks for enzyme activity (Kobe and Kemp, 1999). Hence active glycosidases can be monitored with ABPP without knowing the natural substrates. We also detected active glycosidases that were assumed to be inactive. Detection of TGG3 for example, shows that this enzyme is active even though it was originally classified as a pseudogene (Zhang et al., 2002). Glycosidase profiling is not restricted to the proteomes from which we have identified labeled proteins. We also profiled for active glycosidases in extracts of different organs and leaves of different dicot and monocot plant species. Hence glycosidase profiling can be used to unravel roles of glycosidases in other plant species. We have also demonstrated that both fluorescent probe JJB70 and inhibitor KY371 enter living cells and label glycosidases *in vivo*. These experiments demonstrate that KY371 is an excellent broad range glycosidase inhibitor in living cells. Hence KY371 can now be used in chemical knock out studies to display phenotypes associated with loss of broad range glycosidase functions at a time point and dosis of choice.

2.3.4 Active glycosidases in the apoplast

The extracellular space and the cell wall jointly constitute an important part of a plant called the apoplast. In this study, we chose *Nicotiana benthamiana* as a model system to study the active glycosidases in the leaf apoplast. Apoplastic glycosidases can selectively alter cell wall polysaccharides to remodel the cell wall architecture during plant growth and development. By labeling apoplastic proteomes, we have detected the active state of four putative bi-functional α-L-arabinofuranosidase/β-D-xylosidases (AFU/BXLU); two putative β-D-xylosidases; five putative β-D-glucosidases; two putative β-D-galactosidases; one putative heparanase; one putative β-D-glucanase and one putative α-L-arabinofuranosidase. Glycosidases with these substrate hydrolyzing activities process the major cell wall polysaccharides including glucan, xylan, arabinoxylan, galactan and arabinan during cell wall assembly and re-organization (Minic, 2008). Hence glycosidase profiling reveal the active state of glycosidases that likely play a role in cell wall remodeling. Furthermore, we have also detected two GH3 family enzymes with unknown glycosidic activities. Hence glycosidase profiling allows for the detection of the active state of these enzymes without knowing their substrates.

The activity of glycosidases is tightly regulated at post-translational level. For example, cell wall proteome analysis suggested that glycosidases can be regulated by proteases (Minic et al., 2007). Consistent with this, we found that the labeled BGAL (NbS00024332g0007) is a

truncated protein, which consists of only the GH35 catalytic domain. Such truncation has also been observed in an animal lysosomal β-galactosidase where the C-terminal half is removed to release a mature enzyme in an acidic environment (van der Spoel et al., 2000). Interestingly, a C-terminal truncation of a bacterial β-galactosidase resulted in an efficient transgalactosylase (Jørgensen et al., 2001). Likewise the truncated BGAL in the plant apoplast might have acquired transglycosylase activity and may catalyze the transfer of galactose to acceptor molecules. In addition, the loss of the C-terminal half of the protein may also have altered the location of this enzyme in the apoplast. The role of proteolytic regulation of BGAL is therefore an interesting topic for further studies.

2.4 References

Andersson, D., Chakrabarty, R., Bejai, S., Zhang, J., Rask, L., and Meijer, J. (2009). Myrosinases from root and leaves of *Arabidopsis thaliana* have different catalytic properties. Phytochemistry *70*, 1345–1354.

Arsovski, A.A., Popma, T.M., Haughn, G.W., Carpita, N.C., McCann, M.C., and Western, T.L. (2009). *AtBXL1* encodes a bifunctional beta-D-xylosidase/alpha-L-arabinofuranosidase required for pectic arabinan modification in Arabidopsis mucilage secretory cells. Plant Physiol. *150*, 1219–1234.

Barth, C., and Jander, G. (2006). Arabidopsis myrosinases TGG1 and TGG2 have redundant function in glucosinolate breakdown and insect defense. Plant J. Cell Mol. Biol. *46*, 549–562.

Burmeister, W.P., Cottaz, S., Driguez, H., Iori, R., Palmieri, S., and Henrissat, B. (1997). The crystal structures of *Sinapis alba* myrosinase and a covalent glycosyl-enzyme intermediate provide insights into the substrate recognition and active-site machinery of an S-glycosidase. Struct. Lond. Engl. 1993 *5*, 663–675.

Coutinho, P.M., Stam, M., Blanc, E., and Henrissat, B. (2003). Why are there so many carbohydrate-active enzyme-related genes in plants? Trends Plant Sci. *8*, 563–565.

Dean, G.H., Zheng, H., Tewari, J., Huang, J., Young, D.S., Hwang, Y.T., Western, T.L., Carpita, N.C., McCann, M.C., Mansfield, S.D., et al. (2007). The Arabidopsis *MUM2* gene encodes a beta-galactosidase required for the production of seed coat mucilage with correct hydration properties. Plant Cell *19*, 4007–4021.

Eudes, A., Mouille, G., Thévenin, J., Goyallon, A., Minic, Z., and Jouanin, L. (2008). Purification, cloning and functional characterization of an endogenous beta-glucuronidase in *Arabidopsis thaliana*. Plant Cell Physiol. *49*, 1331–1341.

Fanutti, C., Gidley, M.J., and Reid, J.S.G. (1991). A xyloglucan-oligosaccharide-specific α-d-xylosidase or exo-oligoxyloglucan-α-xylohydrolase from germinated nasturtium (*Tropaeolum majus* L.) seeds. Planta *184*, 137–147.

Grignon, C. (Ecole N.S.A., and Sentenac, H. (1991). pH and ionic conditions in the apoplast. Annu. Rev. Plant Physiol. Plant Mol. Biol. USA.

Günl, M., Neumetzler, L., Kraemer, F., de Souza, A., Schultink, A., Pena, M., York, W.S., and Pauly, M. (2011). *AXY8* encodes an α-fucosidase, underscoring the importance of apoplastic metabolism on the fine structure of Arabidopsis cell wall polysaccharides. Plant Cell *23*, 4025–4040.

Hirsch-Hoffmann, M., Gruissem, W., and Baerenfaller, K. (2012). pep2pro: the high-throughput proteomics data processing, analysis, and visualization tool. Front. Plant Sci. *3*, 123.

Hrmova, M., Harvey, A.J., Wang, J., Shirley, N.J., Jones, G.P., Stone, B.A., Høj, P.B., and Fincher, G.B. (1996). Barley beta-D-glucan exohydrolases with beta-D-glucosidase activity. Purification, characterization, and determination of primary structure from a cDNA clone. J. Biol. Chem. *271*, 5277–5286.

Hrubá, P., Honys, D., Twell, D., Capková, V., and Tupý, J. (2005). Expression of beta-galactosidase and beta-xylosidase genes during microspore and pollen development. Planta *220*, 931–940.

Jørgensen, F., Hansen, O.C., and Stougaard, P. (2001). High-efficiency synthesis of oligosaccharides with a truncated beta-galactosidase from *Bifidobacterium bifidum*. Appl. Microbiol. Biotechnol. *57*, 647–652.

Kallemeijn, W.W., Li, K.-Y., Witte, M.D., Marques, A.R.A., Aten, J., Scheij, S., Jiang, J., Willems, L.I., Voorn-Brouwer, T.M., van Roomen, C.P.A.A., et al. (2012). Novel activity-based probes for broad-spectrum profiling of retaining β-exoglucosidases *In Situ* and *In Vivo*. Angew. Chem. Int. Ed. *51*, 12529–12533.

Kobe, B., and Kemp, B.E. (1999). Active site-directed protein regulation. Nature *402*, 373–376.

Minic, Z. (2008). Physiological roles of plant glycoside hydrolases. Planta *227*, 723–740.

Minic, Z., and Jouanin, L. (2006). Plant glycoside hydrolases involved in cell wall polysaccharide degradation. Plant Physiol. Biochem. PPB *44*, 435–449.

Minic, Z., Rihouey, C., Do, C.T., Lerouge, P., and Jouanin, L. (2004). Purification and characterization of enzymes exhibiting β-d-xylosidase activities in stem tissues of Arabidopsis. Plant Physiol. *135*, 867–878.

Minic, Z., Jamet, E., Négroni, L., Arsene der Garabedian, P., Zivy, M., and Jouanin, L. (2007). A sub-proteome of *Arabidopsis thaliana* mature stems trapped on Concanavalin A is enriched in cell wall glycoside hydrolases. J. Exp. Bot. *58*, 2503–2512.

Rather, M.Y., and Mishra, S. (2013). β-glycosidases: An alternative enzyme based method for synthesis of alkyl-glycosides. Sustain. Chem. Process. *1*, 7.

van der Spoel, A., Bonten, E., and d'Azzo, A. (2000). Processing of lysosomal beta-galactosidase. The C-terminal precursor fragment is an essential domain of the mature enzyme. J. Biol. Chem. *275*, 10035–10040.

Talley, K., and Alexov, E. (2010). On the pH-optimum of activity and stability of proteins. Proteins *78*, 2699–2706.

Toufighi, K., Brady, S.M., Austin, R., Ly, E., and Provart, N.J. (2005). The Botany array resource: e-Northerns, expression angling, and promoter analyses. Plant J. Cell Mol. Biol. *43*, 153–163.

Xu, Z., Escamilla-Treviño, L., Zeng, L., Lalgondar, M., Bevan, D., Winkel, B., Mohamed, A., Cheng, C.-L., Shih, M.-C., Poulton, J., et al. (2004). Functional genomic analysis of *Arabidopsis thaliana* glycoside hydrolase family 1. Plant Mol. Biol. *55*, 343–367.

Zhang, J., Pontoppidan, B., Xue, J., Rask, L., and Meijer, J. (2002). The third myrosinase gene TGG3 in *Arabidopsis thaliana* is a pseudogene specifically expressed in stamen and petal. Physiol. Plant. *115*, 25–34.

Zhou, C., Tokuhisa, J.G., Bevan, D.R., and Esen, A. (2012). Properties of β-thioglucoside hydrolases (TGG1 and TGG2) from leaves of *Arabidopsis thaliana*. Plant Sci. Int. J. Exp. Plant Biol. *191-192*, 82–92.

Chapter 3: Glycosidase activity profiling of secreted proteome during *Pseudomonas syringae* infections

Part of this chapter has been published as: (Chandrasekar, B., Hong, T.N., and van der Hoorn, R.A.L. (2017). Inhibitor Discovery by Convolution ABPP. Methods Mol. Biol. Clifton NJ *1491*, 47–56).

3.1 Introduction

In plants, the majority of glycosidases are secreted into the apoplast and play an important role in cell wall associated biological processes. For example, retaining glycosidases like BGAL10, a beta-galactosidase from family GH35, and XYL1, a xylosidase from family GH3 (Pauly and Keegstra, 2016; Sampedro et al., 2012), act on cell wall polysaccharides like xyloglucans to modulate the primary growth of plants during cell elongation. Seed apoplastic glycosidases like BGAL6 act on polysaccharides like mucilage to alter its hydration properties (Dean et al., 2007). Some apoplastic glycosidases in seeds also act on storage polysaccharides to generate monosaccharide sugars like glucose which serves as an energy source for growing seedlings (Pauly and Keegstra, 2016). Apoplastic glycosidases in plants also play a major role during plant-pathogen interactions. For example, a well characterized pathogenesis-related protein like β-1,3-glucanase (PR-2) and chitinases (PR-3) accumulate in high amounts in the apoplast during plant defence. Although overexpression of these enzymes in crop plants has resulted in enhanced disease resistance, the actual roles of these enzymes are still unclear.

In this chapter, ABPP has been used to investigate the activities of apoplastic glycosidases during bacterial infections. *Nicotiana benthamiana* and *Pseudomonas syringae* pv. *tomato* (*Pto*) DC3000 has been chosen as a model organism in my study. *Nicotiana benthamiana* serves as a good model plant system for leaf apoplastic proteome studies. This is because large volumes of apoplastic proteomes can be isolated from its leaves with relatively low cytoplasmic protein contaminations. Furthermore, *Nicotiana benthamiana* is also a host for variety of plant pathogens infecting solanaceae species and hence the obtained research information's could be applied to related solanaceae crop plants like tomato, pepper and potato (Goodin et al., 2008). *Pseudomonas syringae* pv. *tomato* (*Pto*) DC3000 is a good model pathogen to study bacterial pathogenesis inside the plant apoplast. *Pto*DC3000 is a weak epiphytic bacteria but becomes an aggressive pathogen once inside the plant apoplast (Xin and He, 2013). Furthermore, the genome sequence of *Pto*DC3000 are well annotated and hence the bacterial genetic experiments like random mutagenesis or targeted gene knock-out are possible in this bacterium.

To study apoplastic glycosidase activities in *N. benthamiana* leaves during bacterial infections, we used two different strains of *Pseudomonas syringae* pv. *tomato* (*Pto*) DC3000. *Pto*DC3000(*WT)* causes disease on tomato and Arabidopsis. In *N. benthamiana*, however, *Pto*DC3000(*WT)* triggers a Type-II non-host response causing HR-like cell death triggered by the recognition of the Type-III effector HopQ1-1. Consequently, the mutant of *Pto*DC3000 lacking effector protein HopQ1-1, the *Pto*DC3000(Δ*HQ*) causes bacterial speck disease when inoculated on *N. benthamiana* leaves (Wei et al., 2007).

3.2 Results

3.2.1 Profiling of active apoplastic glycosidases during *Pseudomonas syringae* infections

To study apoplastic glycosidase activities during bacterial infection, *N. benthamiana* leaves were infiltrated with *Pto*DC3000(*WT)* or *Pto*DC3000(Δ*HQ*) at 10^6 bacteria/ml concentrations using a needleless syringe. At 2 dpi, the leaves inoculated with *Pto*DC3000(*WT)* are at an early stage of cell death whereas the leaves infected with *Pto*DC3000(Δ*HQ*) show no symptoms. Importantly, the glycosidase labeling profile of apoplastic fluids isolated from infected plants were remarkably different compared to the untreated or mock infiltrated samples (Figure 3.1A). An extra signal appeared at 36 kDa only in the apoplastic fluids of *Pto*DC3000(*WT)* infiltrated sample. A similar signal appeared on the SYPRO Ruby-stained gel. MS analysis of this protein revealed that this protein is β-1-3-glucanase (NbS00010129g0001), the tobacco ortholog of PR2, a GH17 retaining glycosidase (Figure 3.1A). This indicates that the fluorescent signal at 36 kDa in the apoplast of *Pto*DC3000(*WT)* infected plants is caused by this glucanase. Interestingly, labeling of many enzymes was reduced in apoplastic fluids of infected samples compared to the noninfected samples. We decided to focus our attention on a 45 kDa signal whose labeling intensity was dramatically reduced in the apoplastic fluids of both *Pto*DC3000(*WT)* and *Pto*DC3000(Δ*HQ*) infected samples (Figure 3.1B). The MS analysis indicated that the 45 kDa signal corresponded to a truncated protein β-D-galactosidase (NbS00024332g0007) which belongs to GH35 family (Figure 1.8D).

To determine if the reduced labeling of BGAL is caused due to its reduced protein levels, we performed shotgun proteomics to determine the BGAL abundance. The apoplastic proteomes were isolated from the infected and the noninfected samples at 2 dpi, digested with trypsin/lysC mixture and label free quantification was performed using LC/MS. In our MS analysis, five different BGALs belonging to GH35 family were detected in the apoplastic proteomes of the infected and the noninfected samples. Interestingly, the candidate BGAL (NbS00024332g0007) was abundant among diiferent BGALs and their protein levels

remained unchanged during infection with the *Pto*DC3000(*WT)* and *Pto*DC3000(Δ*HQ*) compared to the control samples (Figure 3.1C). Taken together, these data demonstrate that the suppression of BGAL labeling in the apoplastic fluids during infection is due to decrease in active site availability and not due to decreased in BGAL protein levels.

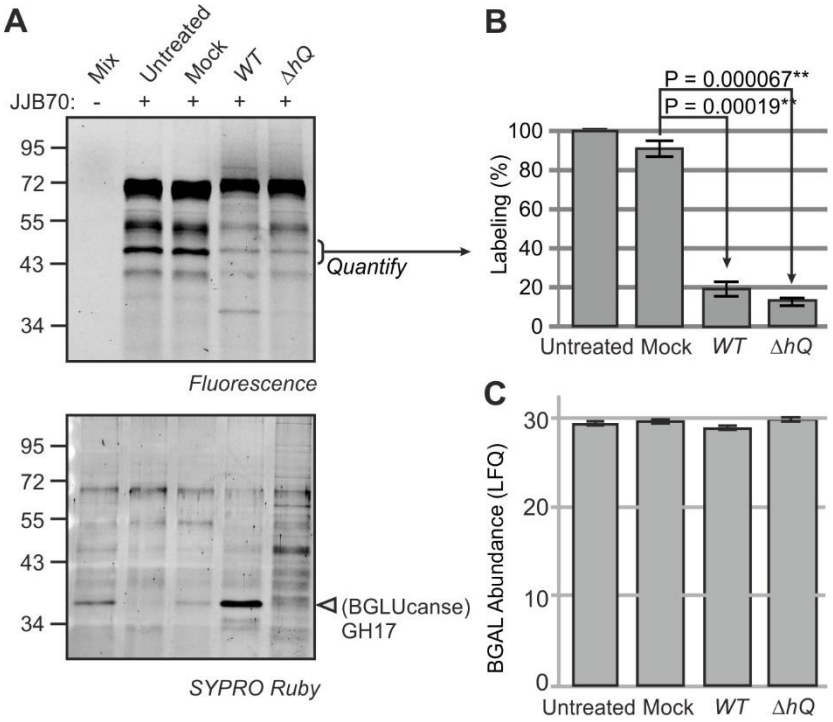

Figure 3.1 Glycosidase profiling reveals suppression of a beta-galactosidase (BGAL) labeling during bacterial infection

(A) Infection and labeling of apoplastic fluids. *N. benthamiana* leaves were infiltrated with *Pto*DC3000(*WT)* or *Pto*DC3000(Δ*HQ*) at 10^6 bacteria/ml. For mock inoculations, the leaves were infiltrated with water. Apoplastic fluids were isolated after 2 dpi and labeled with and without 2 µM JJB70 for 1 h at pH 5.0. Labeled proteins were detected using in-gel fluorescent scanning. Proteins were detected by SYPRO Ruby staining. The 38 kDa signal appearing in *Pto*DC3000(*WT)* infected plants was excised and identified by MS as a beta-glucanase of the GH17 (white arrow at bottom panel). (B) Quantification of BGAL signals detected in (A). Signals were quantified using ImageQuant and the labeling percentages were calculated with respect to labeling intensity of the untreated sample. Error bars represent SEM of three independent experiments. Student's *t*-test was used to calculate the indicated P-values. (C) Estimation of BGAL protein levels by shotgun proteomics combined with label free quantification. The apoplastic proteomes of untreated, mock, *WT* and Δ*HQ* were digested with trypsin/lysC mixture and the tryptic peptides were identified and quantified using LC/MS. The BGAL abundance in the interested samples are represented as log2 scale of label free quantification values (MS^1 intensity of detected peptides).

3.2.2 Convolution ABPP – a simple approach to detect inhibitors in biological samples

To test if the reduced labeling of BGAL is caused by an excess inhibitor present in the infected samples, we established a simple method called convolution ABPP (Chandrasekar et al., 2017). Traditionally, ABPP is classified as either comparative or competitive ABPP.

Comparative ABPP involves the comparison of the active status of proteins in two or more biological samples (e.g different treatments). In competitive ABPP, a proteome is preincubated with putative inhibitors and subsequently with the activity-based probes to label the non-inhibited proteins. Both of these approaches have emerged as powerful tools to study active proteins in crude proteomes. Convolution ABPP takes benefit from both the competitive and comparative ABPP. This method indicates if a reduced signal observed by comparative ABPP is due to the presence of inhibitors.

To illustrate the principle of convolution ABPP, two proteomes (A and B) are shown as example (Figure 3.2A). Labeling of proteomes A and B displays a signal that is reduced in sample B when compared to sample A. Convolution ABPP can be applied in this situation to determine if an excess of inhibitors in proteome B has caused the reduced labeling. Convolution ABPP is a simple, two-step protocol. The first step involves preparation of proteome D, which is a mix of one volume of proteome A with one volume of proteome B. In the second step, proteomes A, B, and D are labeled with an activity-based probe. As a control to display the average signals of samples A and B, one volume of labeled sample A and one volume of labeled sample B are mixed together, resulting in sample C (label-and-mix). In short, the proteomes are mix-and-label (sample D) or label-and-mix (sample C). The fluorescent intensities of labeled proteins in sample C should be the mean of the labeling intensities in samples A and B. Reduced labeling of any protein in sample D when compared to sample C indicates the presence of an inhibitor excess in proteome B (Figure 3.2A).

To present the proof-of-concept of convolution ABPP, we performed an experiment with a known, specific inhibitor of beta-galactosidase called galactostatin bisulphite. Galactostatin bisulphite inhibits the labeling of beta-galactosidase in the apoplastic fluids with JJB70 probe at 10 µm concentration (Proteome B, Figure 3.2C). When convolution ABPP was performed with the excess inhibitor treated sample (proteome B) against the untreated apoplastic fluids (Proteome A), reduced labeling of the 45 kDa BGAL protein was observed in the sample D compared to sample C (Figure 3.2D). Hence this experiment indicates that convolution ABPP with JJB70 probe can be used as a tool to detect excess inhibitors in biological samples.

To test if excess inhibitors cause the suppression of BGAL labeling during infections, we applied convolution ABPP with *Pto*DC3000(Δ*HQ*) treated apoplastic fluids (Proteome B) against the mock treated apoplastic fluids (Proteome A). Remarkably, the labeling intensity of BGAL protein was suppressed in the sample D (mix and label) compared to sample C (label and mix) (Figure 3.3). These results demonstrate the presence of an excess inhibitor in the *Pto*DC3000(Δ*HQ*) treated apoplastic fluids.

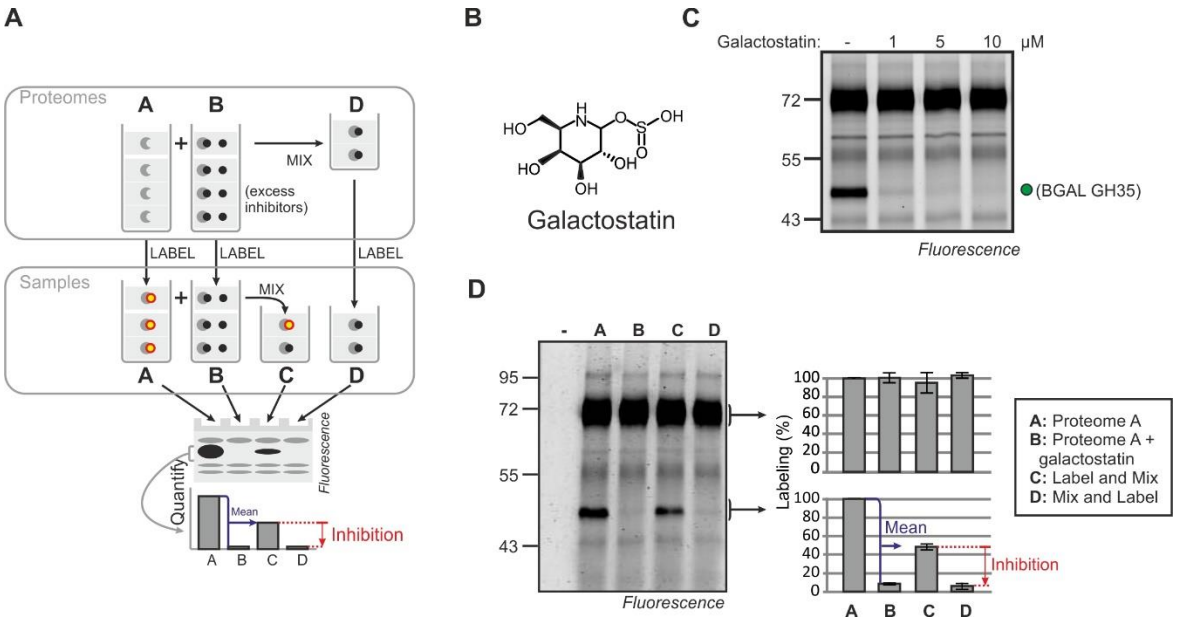

Figure 3.2 Procedure of convolution ABPP

(A) This approach can be used if a reduced labeling of a protein is observed in a sample (e.g. any biological treatment, Proteome B) compared to its control (Proteome A). To test if there is an inhibitor excess (black dots) in proteome B, one volume of proteome A and B are mixed together and the mixed proteome (Proteome D) is then labelled (mix-and-label Sample D). As a control for sample D, one volume of labeled samples A and B are mixed together (label-and-mix Sample C). Signals in Sample C should be the average of the signals in Samples A and B. If there is an excess inhibitor in Proteome B then the signal intensity in Sample D will be lower than in Sample C. (B) Structure of galactostatin bisulphite, a beta-galactosidase inhibitor. (C) Competitive ABPP with increasing galactostatin bisulphite concentrations and apoplastic fluids isolated from untreated *N. benthamiana* leaves. (D) Convolution ABPP with a proteome containing an excess of a known inhibitor. Proteome A is an apoplastic fluid from untreated *N. benthamiana* leaves and proteome B is the same proteome containing 10 µM galactostatin bisulphite. Equal volumes of proteome A and proteome B were mixed together, resulting in proteome D. Proteomes A, B and D were labeled with 2 µM JJB70 for one hour. After labeling, one volume of labeled samples A and B were mixed together (label-and-mix Sample C). The labeled samples A, B, C, D were separated on a protein gel, detected by in-gel fluorescent scanning and the labeling intensity was quantified. Error bars indicate the standard error of means from three independent experiments. Black dots, inhibitors; yellow/red dots; activity-based probes; grey moons, enzyme.

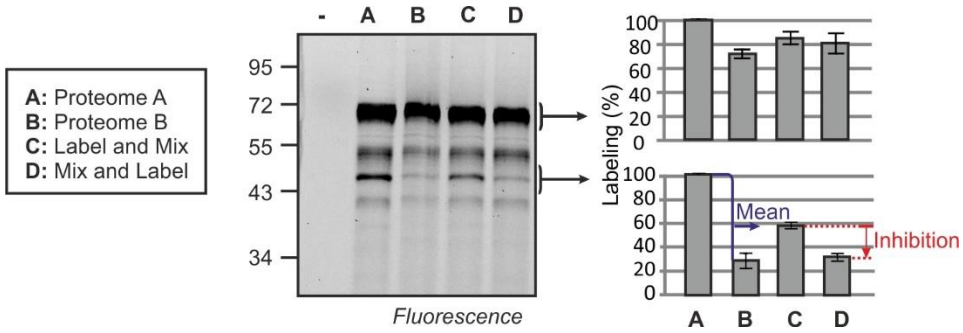

Figure 3.3 Convolution ABPP with *Pto*DC3000(Δ*HQ*) treated apoplastic fluids

Convolution ABPP indicates the presence of excess BGAL inhibitor in *P. syringae*-infected *N. benthamiana* leaves. Proteome A represents apoplastic fluids from the mock-infiltrated *N. benthamiana* leaves and Proteome B represents apoplastic fluids from *P. syringae*-infiltrated *N. benthamiana* leaves.

3.2.3 Characterization of the BGAL inhibitor produced during infection

3.2.3.1 Characterization of molecular size of the BGAL inhibitor produced during infections

To characterize the inhibitor further apoplastic fluids of *Pto*DC3000(Δ*HQ*)-treated leaves were separated into <3 kDa (F1) and >3 kDa fractions (F2). These fractions were normalized to equal volumes and convolution ABPP was performed against the apoplastic fluids of mock-treated leaves. Interestingly, the < 3kDa (F1) caused suppressed labeling of BGAL compared to sample C and no significant suppression was detected with the >3 kDa fraction (F2) (Figure 3.4A & B). To investigate the thermal stability of the inhibitor, the <3 kDa (F1) fraction was heated at 95°C for 5 minutes and convolution ABPP was performed against the apoplastic fluids of mock-treated leaves. Significant suppression in BGAL labeling was detected with the heated F1 (Figure 3.4A & B). These data demonstrate that a heat stable, small molecule inhibitor is produced during infection with *Pto*DC3000(Δ*HQ*) and is responsible for the suppressed BGAL labeling in infected plants.

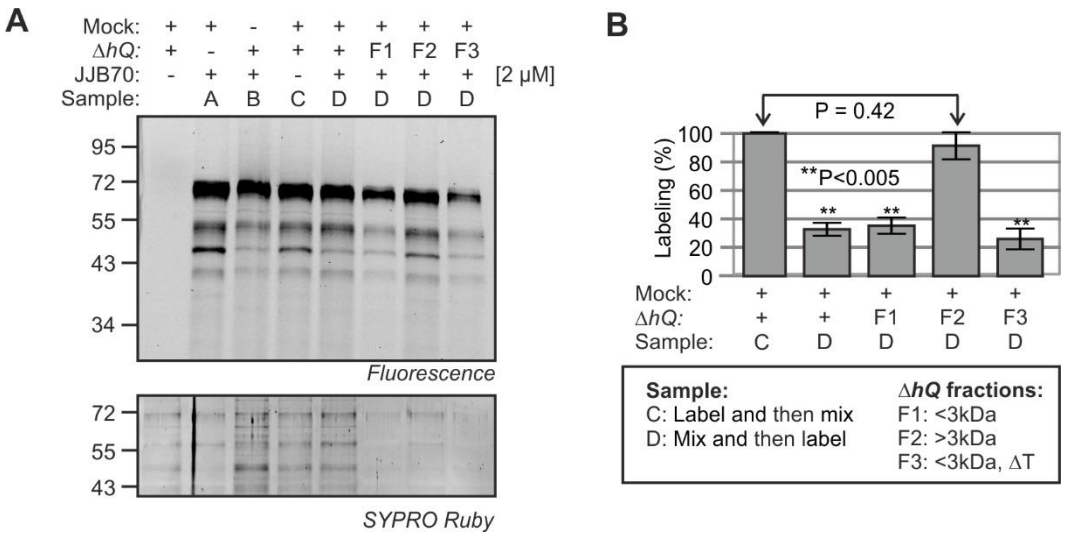

Figure 3.4 Suppressed labeling of BGAL is due to a heat-stable small molecule inhibitor

(A) Mixing and labeling of apoplastic fluids. *N. benthamiana* leaves were infiltrated with Δ*HQ* at 10^6 bacteria/ml. For mock inoculations, the leaves were infiltrated with sterilized water. Apoplastic fluids were isolated from the leaves at 2 dpi. An aliquot of apoplastic fluids from Δ*HQ* treated leaves was concentrated using ultrafiltration spin colums to remove the <3 kDa low molecular weight compounds. The filtrate (<3 kDa) and the concentrate (>3 kDa) were normalized to equal starting volumes and these fractions were marked as F1 and F2, respectively. Fraction F3 was obtained by heating the filtrate (<3 kDa) at 95 ºC for 5 min. For mixing procedure D (mix and then label), apoplastic fluids from mock and the Δ*HQ* treated samples were first mixed in a 1:1 ratio and then labeled with JJB70 at pH 5.0. The labeling reaction was stopped by adding gel loading buffer and heating at 95 ºC. Mixing procedure D was also followed with the fractions F1 , F2 and F3. For mixing procedure C (label and then mix), the apoplastic fluids of mock and Δ*HQ* treated samples were separately labeled with JJB70 at pH 5.0 for 1 h. After stopping the labeling reaction, the labeled proteomes of both were mixed in 1:1 ratio. The proteomes were separated on protein gels, detected by in-gel fluorescent scanning and subsequently stained with SYPRO Ruby. (B) Quantification of suppressed of BGAL labeling. Fluorescence of labeled BGAL was quantified using ImageQuant from three independent experiments. Labeling intensity was normalized to mixing procedure C and expressed as a percentage. Error bars represent SEM of three independent experiments. Student's *t*-test was used to calculate P-values.

3.2.3.2 Identification of source of BGAL inhibitor

To determine if *Pseudomonas syringae* is the source of BGAL inhibitor, *Pto*DC3000(*WT)* or *Pto*DC3000(Δ*HQ*) strains were grown overnight in nitrogen limiting mannitol-glutamate minimal medium in the presence or absence of iron. Convolution ABPP was performed with these bacteria grown medium against the untreated apoplastic fluids of *N. benthamiana* leaves. Remarkably, BGAL inhibitor could be detected in both minimal mediums (+/- iron) inoculated with *Pto*DC3000(*WT)* or *Pto*DC3000(Δ*HQ*) but not in the nutrient rich LB medium (Figure 3.5A). These results strongly suggest that *Pto*DC3000 produces the BGAL inhibitor produced during infection. Furthermore, the BGAL inhibitor production in the bacteria is not strictly dependent on bioavailability of the iron.

To gain more insights in the genetic regulation of BGAL inhibitor production, the *Pto*DC3000 knock out strains like *Pto*DC3000(Δ*hrcC*), *Pto*DC3000(Δ*gacA*) and *Pto*DC3000(Δ*gacS*) were grown overnight in mannitol-glutamate minimal and convolution ABPP was applied. Interestingly, BGAL inhibitor could be detected in the minimal medium inoculated with all these strains (Figure 3.5A & 3.5B). This data indicates that the secretion of the BGAL inhibitor into the plant apoplast is independent of Type-III secretion system and two component system GacS/GacA are not involved in regulating the BGAL inhibitor production in *Pseudomonas syringae*.

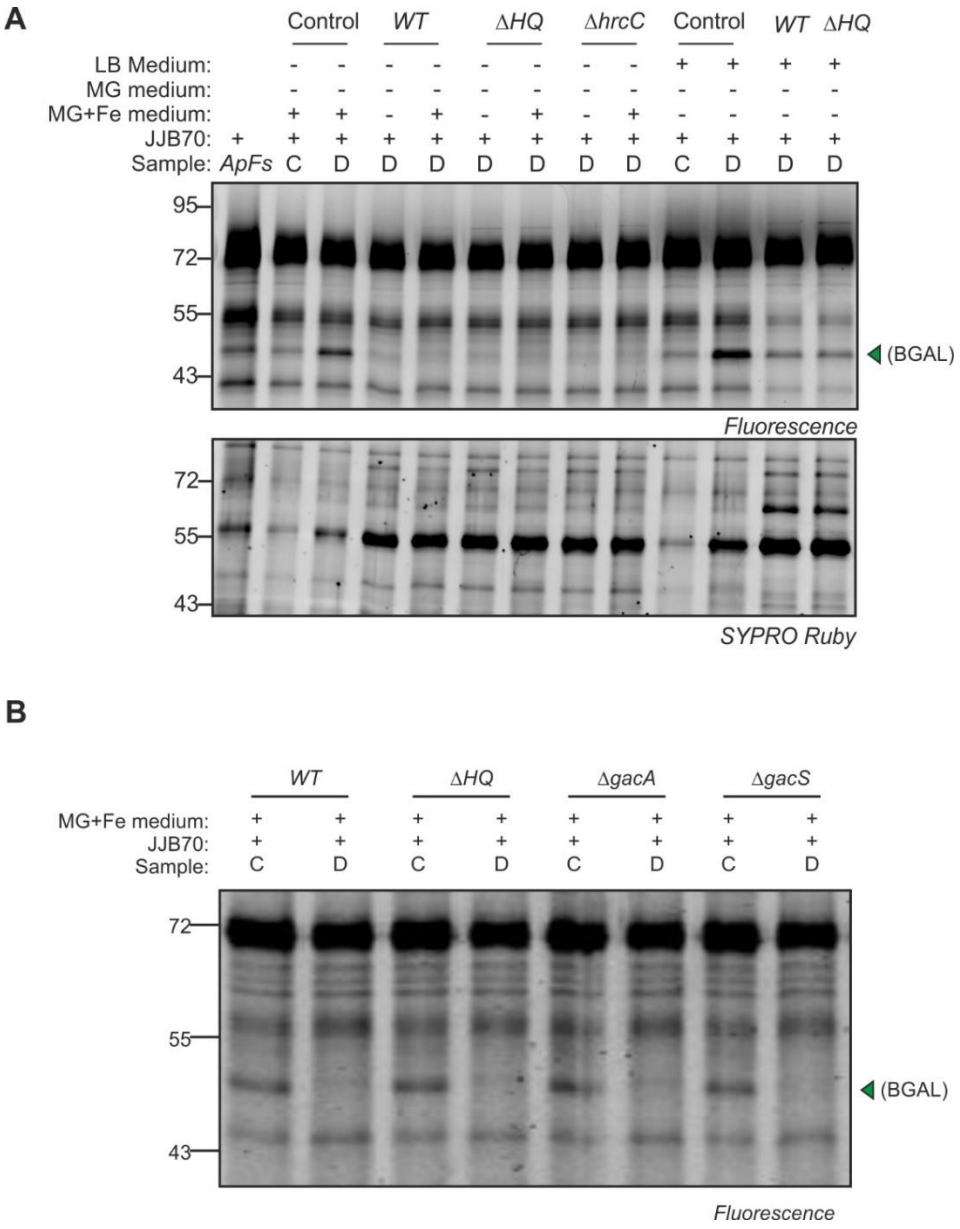

Figure 3.5. Convolution ABPP with minimal medium reveals the source of BGAL inhibitor

A. and B. Convolution ABPP with bacterial minimal medium against the apoplastic fluids isolated from *N. benthamiana* leaves. The *P. syringae* strains *Pto*DC3000(*WT)*, *Pto*DC3000(Δ*HQ*), *Pto*DC3000(Δ*hrcC*), *Pto*DC3000(Δ*gacA*) and *Pto*DC3000(Δ*gacS*) were inoculated at O.D=0.5 and grown in the mannitol-glutamate medium (minimal) or LB medium (nutrient rich). The overnight (16h) grown bacterial cultures were centrifuged, the mediums were collected and convolution ABPP was performed with the apoplastic fluids isolated of *N. benthamiana* leaves.

3.2.3.3 Minimal medium assay with different strains of Pseudomonas

To investigate if BGAL inhibitor production is common to other Pseudomonas strains, we applied convolution ABPP with the bacteria grown in minimal medium from different strains of Pseudomonas. Remarkably, BGAL inhibitor could be detected in the minimal medium inoculated with NCPPB1106, an ancestor strain of *Pto*DC3000 but not in the minimal medium of other isolates of tomato pathovars (Figure 3.6A). Furthermore, BGAL inhibitor could be also detected in the minimal medium inoculated with *Pseudomonas syrinagae* pathovars like *P.s.* pv *maculicola* KN91, *P.s.* pv. *glycinea* race4 and *P.s.* pv. *pisi* race6 but not in other tested Pseudomonas pathovars (Figure 3.6B). Hence these data indicate that only certain *Pseudomonas syrinagae* pathovars produce the BGAL inhibitor.

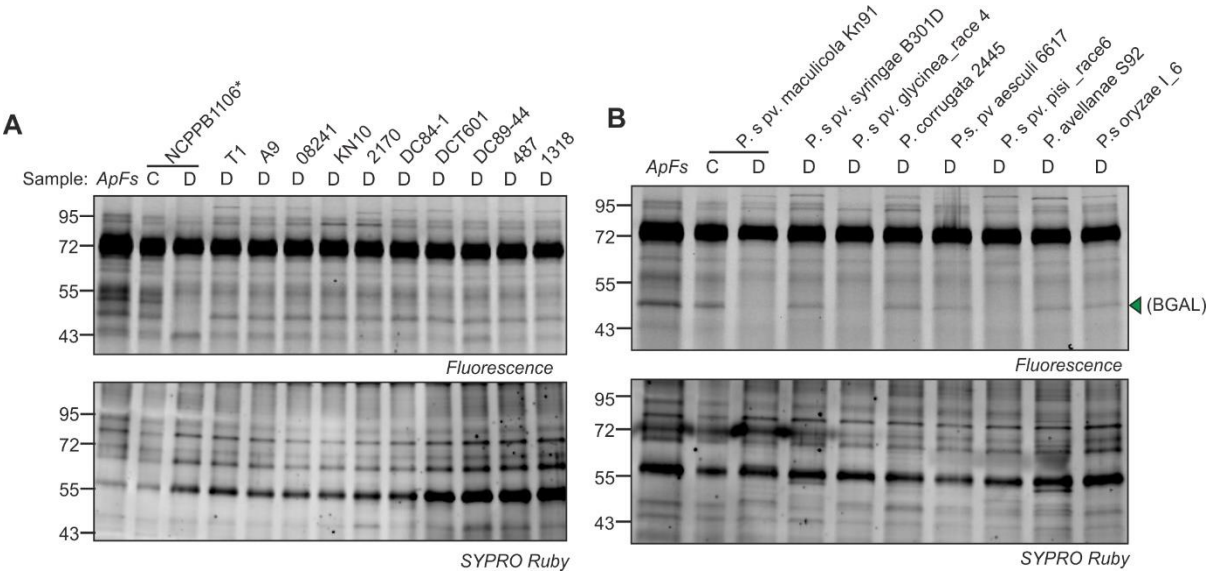

Figure 3.6 BGAL inhibitor production by other Pseudomonas strains

(A) PtoDC3000 is unique in producing BGAL inhibitor compared to other tomato field isolates of *Pseudomonas syringae*. (B) *Pseudomonas syringae* strains belonging to different pathovars produce the BGAL inhibitor. The different Pseudomonas strains were inoculated at O.D=0.5 and grown in the mannitol-glutamate medium (minimal). The overnight (16h) grown bacterial cultures were centrifuged, the mediums were collected and convolution ABPP was performed medium against the apoplastic fluids isolated of *N. benthamiana* leaves.

3.3 Discussion

In apoplastic fluids of *Pto*DC3000(*WT)* or *Pto*DC3000(Δ*HQ*) infiltrated *Nicotiana benthamiana* leaves, the labeling of a beta galactosidase (BGAL, NbS00024332g0007) with JJB70 was significantly reduced. Labeling with JJB70 reflects the active site avalability of the protein or enzymes. Hence the reduced labeling of BGAL signifies that the activity of this enzyme is reduced during *Pto*DC3000 infection. Reduced labeling of BGAL might be due to: (i) reduced BGAL secretion, (ii) increased BGAL protein degradation, or (iii) BGAL inhibition. Label-free quantification of apoplastic proteomes has revealed that the abundance of BGAL enzyme remains unchanged during infection with *Pto*DC3000. Hence the reduced labeling of BGAL is not due to its decreased secretion or degradation.

Convolution ABPP is a simple tool to detect inhibitors in extracts of interest against any proteome whose labeling profile is well-characterized. Applying convolution ABPP with apoplastic fluids has revealed the presence of excess BGAL inhibitor in infected samples. Hence the presence of BGAL inhibitor must have caused the suppression of BGAL enzyme during infections. Furthermore, reduced BGAL labeling was also observed with heated < 3 kDa fraction derived from apoplastic fluids of infected plants. These experiments revealed that a heat stable, small molecule inhibitor(s) in apoplastic fluids of infected plants is responsible for the suppression of BGAL labeling. Hence by profiling glycosidases with JJB70, we have discovered that the BGAL activities are suppressed due to a small molecule inhibitor during infections.

Performing convolution ABPP with the *Pto*DC3000(*WT)* or *Pto*DC3000(Δ*HQ*) grown minimal mediums has reaveled that the *Pto*DC3000 produces a BGAL inhibitor. Interestingly, these strains produce the BGAL inhibitor only under nitrogen limiting conditions but not under nutrient rich conditions. Nitrogen limiting conditions are prevalent in the plant apoplast during infection and it has been shown that such conditions induce the production of bacterial and fungal virulence factors (Ackerveken et al., 1994). Hence the nitrogen limiting conditions might be a trigger in the plant apoplast to induce the BGAL inhibitor production in *Pto*DC3000.

Pseudomonas syringae deploys Type-III secretory system to inject multitude of effector proteins into the host cytoplasm (Xin and He, 2013). *Pto*DC3000(Δ*hrcC*) lacks HrcC, an important outer membrane protein thereby defective in Type-III secretion (Yuan and He, 1996). Interestingly, *Pto*DC3000(Δ*hrcC*) still produced the BGAL inhibitor when grown in minimal medium. This implies that *Pto*DC3000 must employ other secretion systems to inject the inhibitor into the host apoplast.

In *Pseudomonas syring*ae, large number of secreted virulence factors are controlled by important micro nutrients or regulatory proteins. For example, bioavailabilty of iron in the

plant apoplast is an important regulator for production of the secondary metabolities and virulence factors in *P.syring*ae (Bronstein et al., 2008). However, both *Pto*DC3000(*WT)* and *Pto*DC3000(Δ*HQ*) produced BGAL inhibitor in the minimal medium even in the absence of iron. Hence BGAL inhibitor production in *Pto*DC3000 is not strictly dependent on iron bioavailablity. *gacS/gacA* are yet another important master regulators involved in controlling expression of virulence genes and secondary metabolities in *Pto*DC3000 (Heeb and Haas, 2001). Interestingly, knockout mutants *Pto*DC3000(Δ*gacS*) and *Pto*DC3000(Δ*gacA*) still produced the BGAL inhibitor in the minimal medium. Hence *gacS/gacA* are not involved in BGAL inhibitor production and BGAL inhibitor production must be controlled by other regulators.

Among the different tomato pathovars of *Pseudomonas syringae, Pto*DC3000 and NCPPB1106, an acestror strain of *Pto*DC3000 are unique in producing the BGAL inhibitor (Xin and He, 2013). Other tested tomato pathovars did not produce the BGAL inhibitor under the minimal medium conditions. Comparison of genomes of *Pto*DC3000 and *Pseudomonas syringae* pv. tomato strain A1 has revealed a unique repertoires of Type-III effectors (Almeida et al., 2008). Hence, in the evolutionary context, *Pto*DC3000 might have acquired a distinct repertoire of genes involved in BGAL inhibitor production. Furthermore, BGAL inhibitor production is not restricted to *Pto*DC3000. *P.s.* pv *maculicola* KN91, *P.s.* pv*. glycinea* race4 and *P.s.* pv. *pisi* race6 can also produced the BGAL inhibitor. Other tested *Pseudomonas syringae* pathovars like *P.s.* pv. syringae B301D, *P.s.* pv. aesculi 6617, *P.s.* pv. oryzae I_6 and *P. avellanae* S92 and *P.corrugata* 2445 did not produce the BGAL inhibitor. Hence, comparative genomics with *P. syringae* strains which can produce the BGAL inhibitor versus *P. syringae* strains which do not produce the inhibitor might provide insights about the genes which are involved in BGAL inhibitor production.

3.4 References

Ackerveken, G.F.J.M.V. den, Dunn, R.M., Cozijnsen, A.J., Vossen, J.P.M.J., Broek, H.W.J.V. den, and Wit, P.J.G.M.D. (1994). Nitrogen limitation induces expression of the avirulence gene avr9 in the tomato pathogen *Cladosporium fulvum*. Mol. Gen. Genet. MGG *243*, 277–285.

Almeida, N.F., Yan, S., Lindeberg, M., Studholme, D.J., Schneider, D.J., Condon, B., Liu, H., Viana, C.J., Warren, A., Evans, C., et al. (2008). A draft genome sequence of *Pseudomonas syringae* pv. tomato T1 reveals a Type-III effector repertoire significantly divergent from that of *Pseudomonas syringae* pv. tomato DC3000. Mol. Plant. Microbe Interact. *22*, 52–62.

Bronstein, P.A., Filiatrault, M.J., Myers, C.R., Rutzke, M., Schneider, D.J., and Cartinhour, S.W. (2008). Global transcriptional responses of *Pseudomonas syringae* DC3000 to changes in iron bioavailability in vitro. BMC Microbiol.

Chandrasekar, B., Hong, T.N., and van der Hoorn, R.A.L. (2017). Inhibitor discovery by convolution ABPP. Methods Mol. Biol. Clifton NJ *1491*, 47–56.

Dean, G.H., Zheng, H., Tewari, J., Huang, J., Young, D.S., Hwang, Y.T., Western, T.L., Carpita, N.C., McCann, M.C., Mansfield, S.D., et al. (2007). The Arabidopsis MUM2 gene encodes a β-galactosidase required for the production of seed coat mucilage with correct hydration properties. Plant Cell *19*, 4007–4021.

Goodin, M.M., Zaitlin, D., Naidu, R.A., and Lommel, S.A. (2008). *Nicotiana benthamiana*: its history and future as a model for plant-pathogen interactions. Mol. Plant-Microbe Interact. MPMI *21*, 1015–1026.

Heeb, S., and Haas, D. (2001). Regulatory roles of the GacS/GacA two-component system in plant-associated and other Gram-negative bacteria. Mol. Plant-Microbe Interact. MPMI *14*, 1351–1363.

Pauly, M., and Keegstra, K. (2016). Biosynthesis of the plant cell wall matrix polysaccharide xyloglucan. Annu. Rev. Plant Biol. *67*, 235–259.

Sampedro, J., Gianzo, C., Iglesias, N., Guitián, E., Revilla, G., and Zarra, I. (2012). AtBGAL10 is the main xyloglucan β-galactosidase in Arabidopsis, and its absence results in unusual xyloglucan subunits and growth defects. Plant Physiol. *158*, 1146–1157.

Wei, C.-F., Kvitko, B.H., Shimizu, R., Crabill, E., Alfano, J.R., Lin, N.-C., Martin, G.B., Huang, H.-C., and Collmer, A. (2007). A *Pseudomonas syringae* pv. tomato DC3000 mutant lacking the Type-III effector HopQ1-1 is able to cause disease in the model plant *Nicotiana benthamiana*. Plant J. Cell Mol. Biol. *51*, 32–46.

Xin, X.-F., and He, S.Y. (2013). *Pseudomonas syringae* pv. tomato DC3000: a model pathogen for probing disease susceptibility and hormone signaling in plants. Annu. Rev. Phytopathol. *51*, 473–498.

Yuan, J., and He, S.Y. (1996). The *Pseudomonas syringae* Hrp regulation and secretion system controls the production and secretion of multiple extracellular proteins. J. Bacteriol. *178*, 6399–6402.

Chapter 4: Generation of BGAL inhibitor mutants (*Δbim*)

4.1 Introduction

The BGAL inhibitor produced by *Pto*DC3000 during infections in *Nicotiana benthamiana* is a heat stable, small molecular compound. I hypothesized that the BGAL inhibitor might be a secondary metabolite produced by *Pto*DC3000. Many of the secondary metabolites are controlled by GacS/GacA, an important two-component signalling system in *Pseudomonas syringae* strains. However, independent knock out mutants of *gacS/gacA* genes still produced the BGAL inhibitor under minimal medium conditions (Figure 3.5B). Hence it is necessary to identify other genes encoding biosynthesis enzymes or regulators which are involved in BGAL inhibitor production. The identification of these genes would be of threefold advantage: First, identified genes might provide information about the nature of BGAL inhibitor produced by Pseudomonas. Second, the mutants would be a valuable source for pathogen assays to understand the biological significance of BGAL inhibitor production. Third, the mutants should also be helpful during comparative metabolomics when performed with the wild-type bacteria to identify the BGAL inhibitor molecule. Hence this necessitated to identify of mutants of *Pto*DC3000 that do not produce the BGAL inhibitor.

In this chapter, a novel reporter-based functional assay has been developed to detect the BGAL inhibitor produced by *Pto*DC3000 *in vivo*. Next, random mutagenesis was performed in the genome of *Pto*DC3000 using *mini-tn5* transposons. The established functional screening assay proved to be a powerful tool to isolate *Pto*DC3000 mutants lacking the BGAL inhibitor. Finally, TAIL-PCR combined with genome sequencing has revealed novel genes encoding BGAL inhibitor biosynthesis enzymes and regulators in *Pto*DC3000.

4.2 Results

4.2.1 *In vivo* reporter-based functional assay to detect BGAL inhibitor

To detect the BGAL inhibitor produced by *Pto*DC3000 *in vivo*, a functional screening assay has been established using LacZ, a well-characterized beta galactosidase enzyme. pHRP308, a plasmid which carries the *lacZ* reporter gene was transformed into both *Pto*DC3000(*WT*) and *Pto*DC3000(*ΔHQ*) bacteria (Figure 4.1A). The resulting *Pto*DC3000(*WT_lacZ*) or *Pto*DC3000(*ΔHQ_lacZ*) strains were plated onto X-gal containing, nutrient-rich LB medium or mannitol-glutamate minimal medium. As expected, *Pto*DC3000(*WT_lacZ*) and *Pto*DC3000(*ΔHQ_lacZ*) appeared blue on the X-gal containing LB agar medium (Figure 4.1B). However, both these strains appeared white on the X-gal containing mannitol-glutamate minimal medium (Figure 4.1B). These data indicate that LacZ could be used as reporter

enzyme to detect the produced BGAL inhibitor in *Pto*DC3000 under minimal medium conditions, despite being an *E. coli* enzyme of the GH2 family.

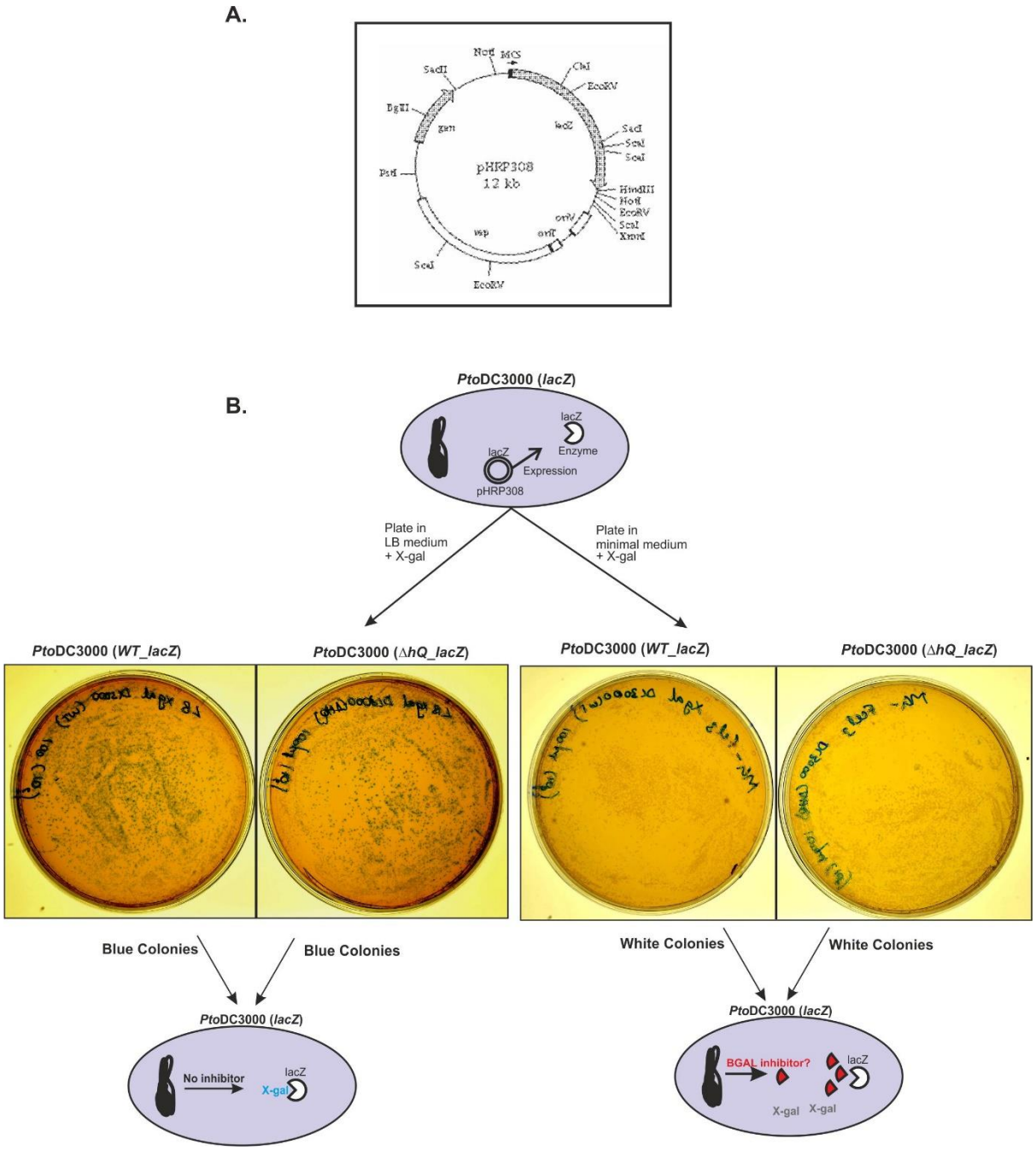

Figure 4.1 *In vivo* reporter-based functional screening assay to detect the BGAL inhibitor produced by *Pto*DC3000

(A) pHRP308, a broad range cloning vector used functional screening assay. pHRP308 is a RSF1010-based plasmid belonging to incompatibility group IncQ. This plasmid carries the full-length *lacZ* gene from *E.coli*. In this plasmid, the *lacZ* gene does not contain its own promoter, instead the *lacZ* gene is expressed along with the gentamycin resistance gene by read-through transcription. (B) LacZ serves as a reporter enzyme to detect BGAL inhibitor production *in vivo* in *Pto*DC3000. The pHRP308 plasmid containing the *lacZ* reporter gene was transformed into *Pto*DC3000(*WT*) or *Pto*DC3000(*ΔHQ*). The transformed bacterial strains *Pto*DC3000(*WT_lacZ*)

and *Pto*DC3000(*ΔHQ_lacZ*) were grown overnight in LB liquid medium, diluted to 10^6 bacteria/ml and 100 µl was plated either onto X-gal containing LB medium or X-gal containing mannitol-glutamate minimal medium and incubated at 28^0C for 36 hours.

4.2.2 Random mutagenesis of *Pto*DC3000(*ΔHQ_lacZ*) to generate BGAL inhibitor mutants (*Δbim*)

To generate mutants of *Pto*DC3000 which do not produce the BGAL inhibitor, random mutagenesis was performed on *Pto*DC3000(*ΔHQ_lacZ*) strain using *mini-tn5* transposons (de Lorenzo et al., 1990). *Mini-tn5* transposons are engineered *Tn5* transposons which creates random and stable knockouts in the genome of gram-negative bacteria. The mutagenized bacteria were plated onto X-gal containing mannitol-glutamate agar minimal medium and screened for blue colonies on this medium. In total, 130,000 colonies were screened and 40 putative blue colonies were selected the functional screening assay (Figure 4.2A).

To check if the selected blue colonies do not produce the BGAL inhibitor, two confirmation experiments were performed. First, all the obtained blue mutants were grown in mannitol-glutamate liquid minimal medium and convolution ABPP was performed with their <3kDa medium fraction against the apoplastic fluids of *Nicotiana benthamiana* leaves. Second, all the blue mutants were re-plated onto the X-gal containing mannitol-glutamate medium and the blue appearance was compared with the parental *Pto*DC3000(*ΔHQ_lacZ*) strain within a single plate. Of the 40 putative blue mutants, 29 did not produce the BGAL inhibitor in convolution ABPP and also appeared blue in the single plate assay. These mutants were called BGAL inhibitor mutants (*Δbim*).

The remaining mutants were white in the single plate assay and produced the BGAL inhibitor in the convolution ABPP assay. Hence these were mutants were considered false positives and were not included in further studies. A typical validation screen with nine different putative blue mutants is presented (Figure 4.2B). Among the nine tested mutants, five mutants did not produce the BGAL inhibitor in the convolution ABPP assay with the <3kDa medium and also appeared blue on the single plate assay (Figure 4.2B).

To validate if the obtained *Δbim* mutants do not produce the BGAL inhibitor during infection, the 28 *Δbim* mutants were infiltrated into the leaves of *Nicotiana benthamiana* at 10^6 bacteria/ml concentrations using a needleless syringe. The BGAL inhibitor mutant *Δbim8* grew very slowing in the LB medium and hence was not used for the analysis. At 2 dpi, the apoplastic fluids were isolated and labelled with JJB70 probe. Of the 28 tested mutants, 18 mutants did not inhibit the BGAL in the apoplastic fluids of *Nicotiana benthamiana* (Figure 4.2C, Table 4.1). Hence these 18 *Δbim* mutants are the true BGAL inhibitor mutants. The remaining 10 *Δbim* mutants are the false positives since they produce the BGAL inhibitor during infection.

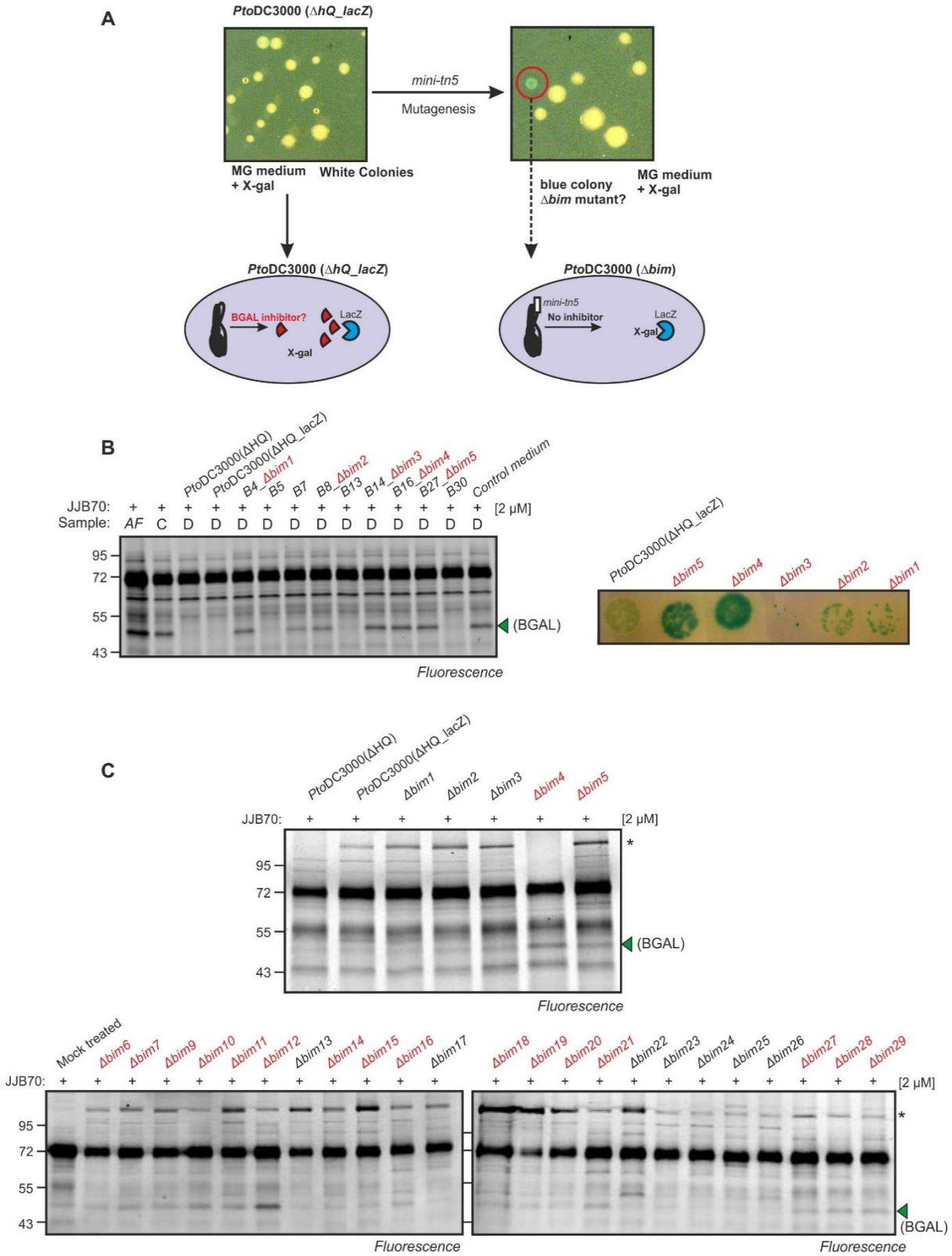

Figure 4.2 Generation and validation of BGAL inhibitor mutants (*Δbim*)

(A) Random mutagenesis to obtain blue mutants in mannitol-glutamate minimal medium. Tri-parental mating was performed by mixing recipient strain: *Pto*DC3000(*ΔHQ _lacZ*), donor strain: *E.coli* (*mini-tn5*-km2) and helper strain:

E.coli (pRK2013). After 6 hours, the conjugation mix was suspended in 1ml of mannitol-glutamate minimal medium and 100 µl aliquots of the suspension were plated onto X-gal mannitol-glutamate minimal medium. (B) Validation of obtained blue mutants by convolution ABPP with <3kDa medium. The candidate blue mutants obtained after the *mini-tn5* mutagenesis were inoculated at O.D=0.5 and grown in the mannitol-glutamate medium. The overnight (16h) grown bacterial cultures were centrifuged, the mediums were fractionated using 3kDa cut off filters and convolution ABPP was performed with <3kDa medium fractions against the apoplastic fluids of *N. benthamiana* leaves. In parallel, the bacterial cultures re-plated on X-gal containing mannitol-glutamate agar minimal medium. (C) Validation of BGAL inhibitor mutants (*Δbim*) by infection assays. The *Δbim* mutants obtained from the previous validation experiments, were infiltrated into *N. benthamiana* leaves at 10^6 bacteria/ml. After 2dpi, apoplastic fluids were isolated and labeled with JJB70 for one hour at room temperature. Labeled proteins were detected using in-gel fluorescent scanning.*, Signal specific to *Pto*DC3000(*ΔHQ _lacZ*) and *Δbim* mutants. This band is absent in the infection assay with the *Δbim4* mutant because this mutant is drastically reduced in virulence and does not grow well in plants.

Table 4.1 Overview of the 29 BGAL inhibitor mutants (*Δbim*)

Mutant	Putative Insertion site[1]	Complementation[2]	Inhibitor in MM[3]	Inhibitor in AF[4]
ΔHQ _lacZ	Parental strain (G)	Parental strain	+	+
Δbim1	NS (T)	ND	-	+
Δbim2	PSPTO_1977 (T + G)	ND	-	+
Δbim3	PSPTO_1978 (T + G)	ND	-	+
Δbim4	PSPTO_1379 (T + G)	S	-	-
Δbim5	PSPTO_0259 (T + G)	NS	-	-
Δbim6	PSPTO_3724 (T)	ND	-	-
Δbim7	NS (T)	ND	-	-
Δbim8	NS (T)	ND	-	-
Δbim9	NS (T)	ND	-	-
Δbim10	PSPTO_0341 (T)	ND	-	-
Δbim11	NS (T)	ND	-	-
Δbim12	NS (T)	ND	-	-

Δbim13	PSPTO_1778 (T)	ND	-	+
Δbim14	PSPTO_4225 (T)	ND	-	-
Δbim15	PSPTO_1075 (T)	ND	-	-
Δbim16	PSPTO_2863 (T)	ND	-	-
Δbim17	NS (T)	ND	-	+
Δbim18	PSPTO_3959 (T)	ND	-	-
Δbim19	PSPTO_4705 (T)	ND	-	-
Δbim20	NS (T)	ND	-	-
Δbim20	NS (T)	ND	-	-
Δbim21	NS (T)	ND	-	-
Δbim22	NS (T)	ND	-	+
Δbim23	PSPTO_1778 (T)	ND	-	+
Δbim24	PSPTO_1778 (T)	ND	-	+
Δbim25	PSPTO_4353 (T)	ND	-	+
Δbim26	PSPTO_0219 (T)	ND	-	+
Δbim27	PSPTO_2222 (T)	ND	-	-
Δbim28	NS (T)	ND	-	-
Δbim29	PSPTO_2222 (T)	ND	-	-

1. The insertion site of the *mini-tn5* transposons was identified using TAIL-PCR (T) and genome sequencing (G) of the bacterial strains. 2. Complementation experiments were performed by using the candidate genes into the pME based vectors. 3. Detected by convolution ABPP with the >3kDa fraction of bacteria grown minimal medium (MM) against the apoplastic fluids of *N. benthamiana* leaves. 4. Detected by ABPP of the apoplastic fluids (AF) collected from the *N. benthamiana* leaves infiltrated with *Δbim* mutants using JJB70. ND, Not determined. NS, Not successful. S, successful. T, Tail-PCR. G, genome sequencing. +, BGAL suppression detected. -, BGAL suppression not detected.

4.2.3 Identification of insertion site of *mini-tn5* transposons in *Δbim4* and *Δbim5*

An overview of the 29 *Δbim* mutants and the details about the insertion of *mini-tn5* transposons in these mutants, the status of complementation experiments performed with these mutants and their BGAL inhibitor production phenotype detected by convolution ABPP in the minimal medium and apoplastic fluids are represented (Table 4.1). In this chapter, *Δbim4* and *Δbim5* were chosen for further characterization. To identify the genes which are responsible for the BGAL inhibitor production, the insertion sites of *mini-tn5* transposons in *Δbim4* and *Δbim5* were identified using TAIL-PCR (Liu and Whittier, 1995). Sequencing the TAIL-PCR products revealed that the *mini-tn5* transposon was inserted in *hrpR* (PSPTO_1379) in *Δbim4* and *gabt-1* (PSPTO_0259) in *Δbim5* (Figure 4.3A). PCR performed with gene- and transposon-specific primer confirmed the insertion of *mini-tn5* transposon at the respective gene loci in these mutants (Figure 4.3B). Furthermore, a single copy *mini-tn5* transposon insertion in these genes has been confirmed in the genomes of *Δbim4* and *Δbim5* by genome sequencing of these strains. These data indicate that the *hrpR* and *gabT-1* genes are required for BGAL inhibitor production.

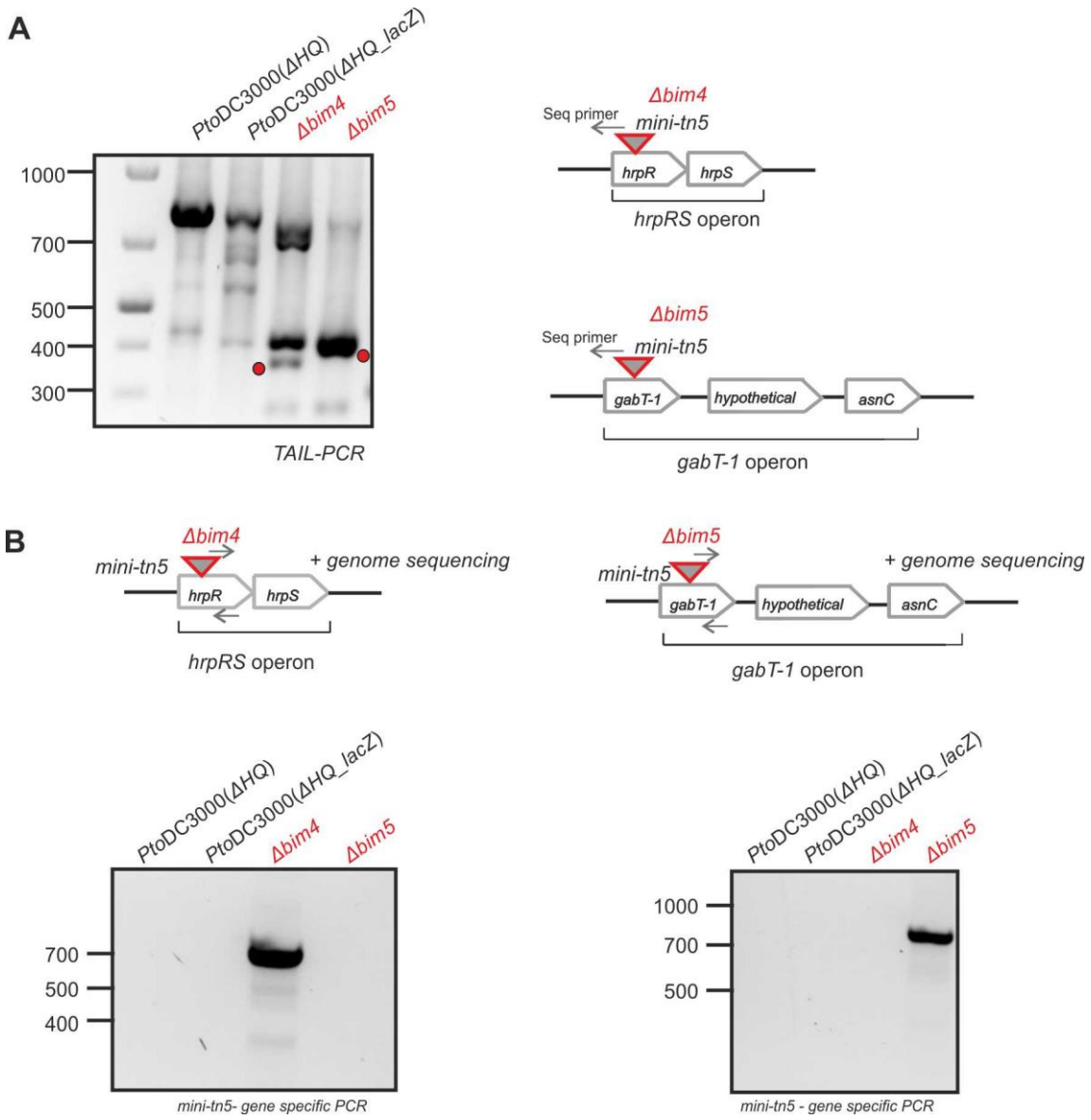

Figure 4.3. Identification of insertion site of *mini-tn5* transposons

(A) Insertion site of *mini-tn5* transposons in *Δbim4* and *Δbim5*. Thermal asymmetric interlaced polymerase chain reaction (TAIL PCR) was performed with the genomic DNA of *Δbim4*, *Δbim5*, *ΔHQ_lacZ* and *ΔHQ* strains using arbitrary primers and transposon-specific primer pairs. The TAIL PCR products were sequenced using transposon-specific primers. The PCR product at 400bp which had the information about the insertion site is indicated with a red dot. The other bands above 400bp were also sequenced and were found to be unspecific PCR products with no insertion site information. (B) Confirmation of insertion site of *mini-tn5* transposons. Colony PCR was performed with *Δbim4*, *Δbim5*, *ΔHQ_lacZ* and *ΔHQ* strains using gene- and transposon-specific primers. Genome sequencing of *Δbim4*, *Δbim5* and *ΔHQ_lacZ* strains were performed by hi-seq illumina sequencing technology offered by microbesNG facility at University of Birmingham, UK.

4.2.4 *hrpRS*-mediated production of BGAL inhibitor in *Pto*DC3000

To confirm if the *hrpRS* operon is required for BGAL inhibitor production in *Pto*DC3000, two different complementation constructs carrying the *hrpRS* operon were created using pME-

based vectors (Heeb et al., 2000). In the first construct (pBK17), the *hrpRS* operon was cloned into the pME6010 expression vector behind a kanamycin promoter with an added ribosome binding site (RBS) (Figure 4.4A). In the second construct (pBK18), the *hrpRS* operon was cloned with its native promoter into the pME6031 cloning vector (Figure 4.4A). The plasmids were transformed into *Δbim4*. These transformed strains were inoculated in mannitol-glutamate minimal liquid medium and convolution ABPP was performed with the overnight grown bacterial medium against the apoplastic fluids of *Nicotiana benthamiana* leaves. In parallel, these strains were also plated onto X-gal containing mannitol-glutamate minimal medium. Importantly, the *Δbim4* mutant transformed with pBK18 construct produced the BGAL inhibitor in mannitol-glutamate liquid medium whereas the *Δbim4* mutant transformed with empty vector pME6031 failed to produce the BGAL inhibitor (Figure 4.4B). In addition, the *Δbim4* mutant transformed with pBK18 appeared white on the X-gal containing mannitol-glutamate medium whereas *Δbim4* transformed with empty vector pME6031 appeared blue (Figure 4.4B). Unfortunately, the *Δbim4* transformed with pBK17 was not complementing for the BGAL inhibitor production phenotypes. This might be because the *hrpRS* operon may not be properly expressed from the pME6010 expression vector.

To further validate the involvement of *hrpR* and *hrpS* genes in BGAL inhibitor production, convolution ABPP was performed with the bacteria grown minimal mediums isolated from the independent knock out strains of *Pto*DC3000 for *hrpR* gene *Pto*DC3000 (*ΔhrpR*) and *hrpS* gene *Pto*DC3000 (*ΔhrpS*) against the apoplastic fluids of *Nicotiana benthamiana* leaves. These mutants were obtained from Prof. Dr. Jorg Schumacher, Imperial College, London (unpublished data). Notably, both *ΔhrpR* and *Δhrps* mutants of *Pto*DC3000 failed to produce the BGAL inhibitor (Figure 4.4C). Taken together, these results demonstrate that the *hrpRS* operon is required for BGAL inhibitor production in *Pto*DC3000 and the absence of either *hrpR* or *hrpS* is not sufficient to abolish BGAL inhibitor production.

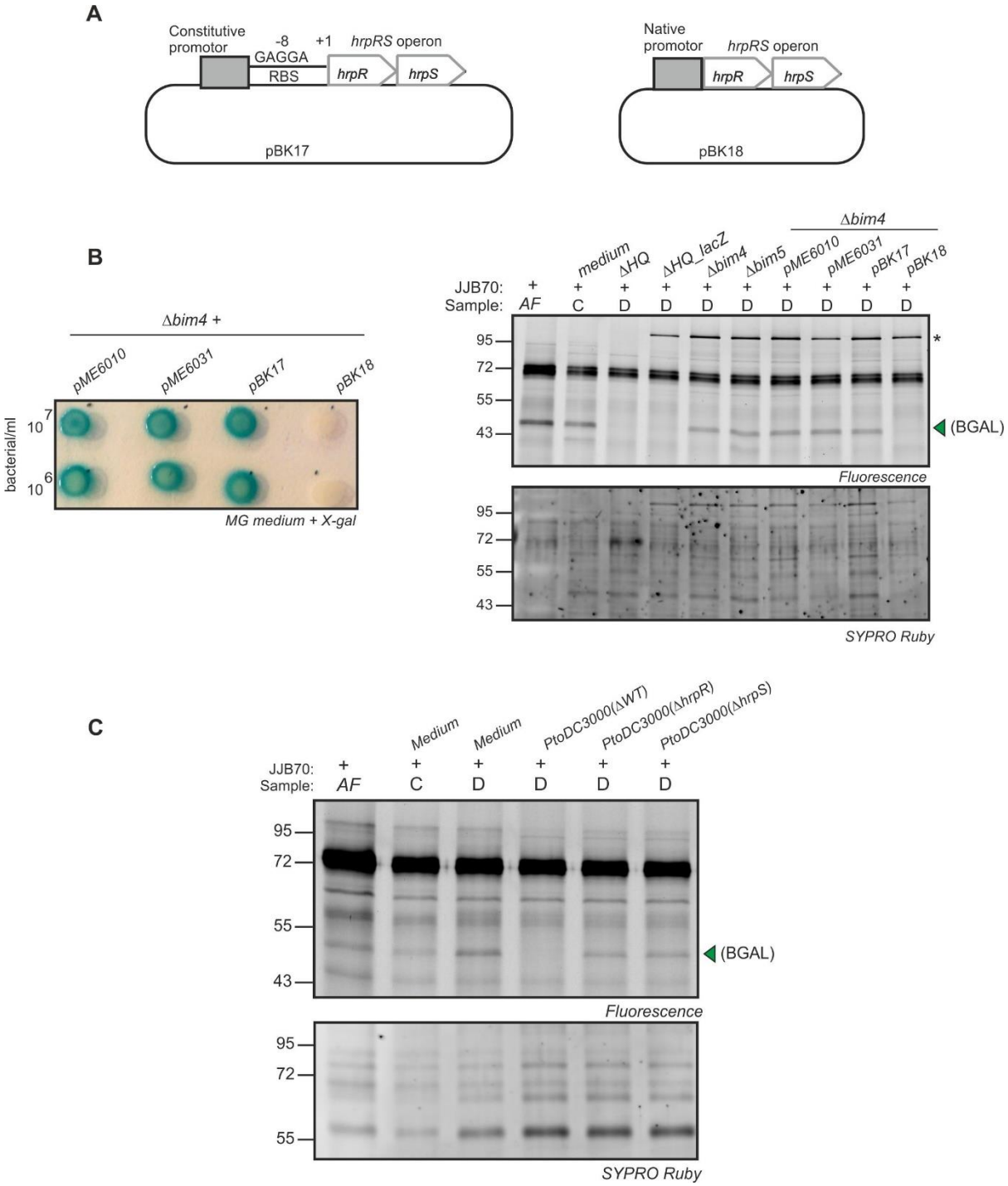

Figure 4.4 *hrpR* and *hrpS* are required for the production of BGAL inhibitor in *Pto*DC3000

(A) Constructs for complementation studies with *Δbim4*. pBK17 carries the *hrpRS* operon cloned with a ribosome binding site (RBS) into the pME6010 expression vector driven by kanamycin promoter. pBK18 carries the *hrpRS* operon cloned with its native promoter the pME6031 cloning vector. (B) *hrpRS* operon is involved in BGAL inhibitor production. The constructs pBK17, pBK18 and the empty vectors pME6031 and pME6010 were transformed into *Δbim4* by electroporation. The transformed constructs were inoculated at O.D=0.5 and grown in the mannitol-glutamate minimal medium. The overnight (16h) grown bacterial cultures were centrifuged and convolution ABPP was performed with the isolated medium against the apoplastic fluids (AF) of *N. benthamiana* leaves. In parallel,

the bacterial cultures were plated onto the X-gal containing mannitol-glutamate minimal medium and incubated at 28^0C for 36 hours. *, Signal specific to *Pto*DC3000(*ΔHQ _lacZ*) and *Δbim* mutants. Signal is absent when convolution ABPP is performed with the <3kDa fraction(see also, Figure 4.2B). (C) Both *hrpR* and *hrpS* genes are required to regulate the BGAL inhibitor production. The independent knock out strains of *Pto*DC3000 for *hrpR* and *hrpS* were inoculated at O.D=0.5 and grown in the mannitol-glutamate minimal medium. The overnight (16h) grown bacterial cultures were centrifuged and convolution ABPP was performed with the isolated medium against the apoplastic fluids of *N. benthamiana* leaves.

4.2.4 *Δbim5* mutant is affected in asparagine biosynthetic pathway for BGAL inhibitor production

In the *Pto*DC3000 genome, *gabT-1* (PSPTO_0259) is clustered together with a hypothetical gene (PSPTO_0260) and a gene which encodes AsnC-family transcriptional regulator (PSPTO_0261). In the Pseudomonas genome database, these three genes have been computationally predicted to function together as an operon (*gabT-1* operon). To understand if the annotated *gabT-1* operon is involved in BGAL inhibitor production in *Pto*DC3000, two different plasmid constructs carrying the *gabT-1* operon were created using pME-based vectors similar to *hrpRS* complementation (Figure 4.5A). In pBK15, the *gabT-1* operon was cloned with added ribosome binding site (RBS) into pME6010. In pBK16, the *gabT-1* operon was cloned with its native promoter into pME6031. The plasmids were transformed into *Δbim5*. These transformed strains were inoculated in mannitol-glutamate minimal medium and convolution ABPP was performed with the overnight grown bacterial medium against the apoplastic fluids of *Nicotiana benthamiana* leaves. In parallel, these strains were plated onto X-gal containing mannitol-glutamate minimal medium. Unfortunately, the *Δbim5* mutant transformed with constructs pBK15 or pBK16 was not complemented for BGAL inhibitor production (Figure 4.5B). The transformants failed to produce the BGAL inhibitor both in liquid and X-gal containing mannitol glutamate minimal medium (Figure 4.5B). The reason for *Δbim5* transformed with pBK15 for not complementing BGAL inhibitor production might because the *gabT-1* operon may not be properly expressed from the pME6010 expression vector.

Despite several attempts, the *Δbim5* mutant was not complemented for BGAL inhibitor production when transformed with the construct pBK16. We speculated that the *mini-tn5* transposon in the *Δbim5* mutant might have caused secondary effects such as polar or non-polar mutations. Due to such secondary effects the pBK16 transformed *Δbim5* mutant might have lost their ability to sense the apoplast mimicking conditions in the minimal medium to activate regulatory networks or pathways for the proper expression of *gabT-1 operon* or functioning of the GabT-1 enzyme. We hypothesized that by supplementing 4-aminobutyrate (GABA), an important plant specific signalling molecule in the minimal medium might mimic plant-like environment and thereby activate networks or pathways needed for the proper functioning of pBK16 in *Δbim5* mutant. Furthermore, GabT-1, as an aminotransferase

encoded by the *gabT-1* operon has been proposed to be involved in GABA metabolism (Park et al., 2010). Hence we also speculated that GABA as substrate might help proper expression of *gabT-1* operon or functioning of the GabT-1 enzyme in the pBK16 transformed ***Δbim5*** mutant. To investigate this hypothesis, ***Δbim5*** mutants transformed with pBK16 or the empty vector (pME6031) were inoculated in mannitol-glutamate medium supplemented with 50 mM GABA. Unfortunately, both the strains failed to produce the BGAL inhibitor under this condition (Second panel, Figure 4.C). Hence the presence of GABA in the minimal medium is not essential for complementation experiment.

In this line of thinking, when I looked carefully on the annotated *gabT-1* operon, there existed a gene encoding AsnC-family transcriptional regulator. AsnC family of transcriptional factors has been shown to regulate biosynthesis of leucine as leucine responsive protein (Lrp) or biosynthesis of asparagine as AsnC protein (Deng et al., 2011). I hypothesized that in the ***Δbim5*** mutant biosynthesis of leucine or asparagine or related amino acid like glutamate for the BGAL inhibitor production might have been affected due to the insertion of *mini-tn5* transposon in the *gabT-1* gene. Hence I speculated that amino acids such as leucine or asparagine or glutamate might be required for the proper functioning of pBK16 in ***Δbim5*** mutant. To investigate this hypothesis, the ***Δbim5*** mutants transformed with pBK16 or the empty vector (pME6031) were inoculated in mannitol-glutamate minimal medium supplemented with 50 mM amino acids like leucine or asparagine or glutamate. Surprisingly, both these strains produced the BGAL inhibitor in the mannitol-glutamate minimal medium supplemented with 50 mM asparagine but not with the other tested amino acids (First, third and fourth panel, Figure 4.C). Hence this result suggests that in the ***Δbim5*** mutant, an asparagine biosynthesis pathway for the BGAL inhibitor production might have been affected due to the insertion of a *mini-tn5* transposon at the *gabT-1* operon.

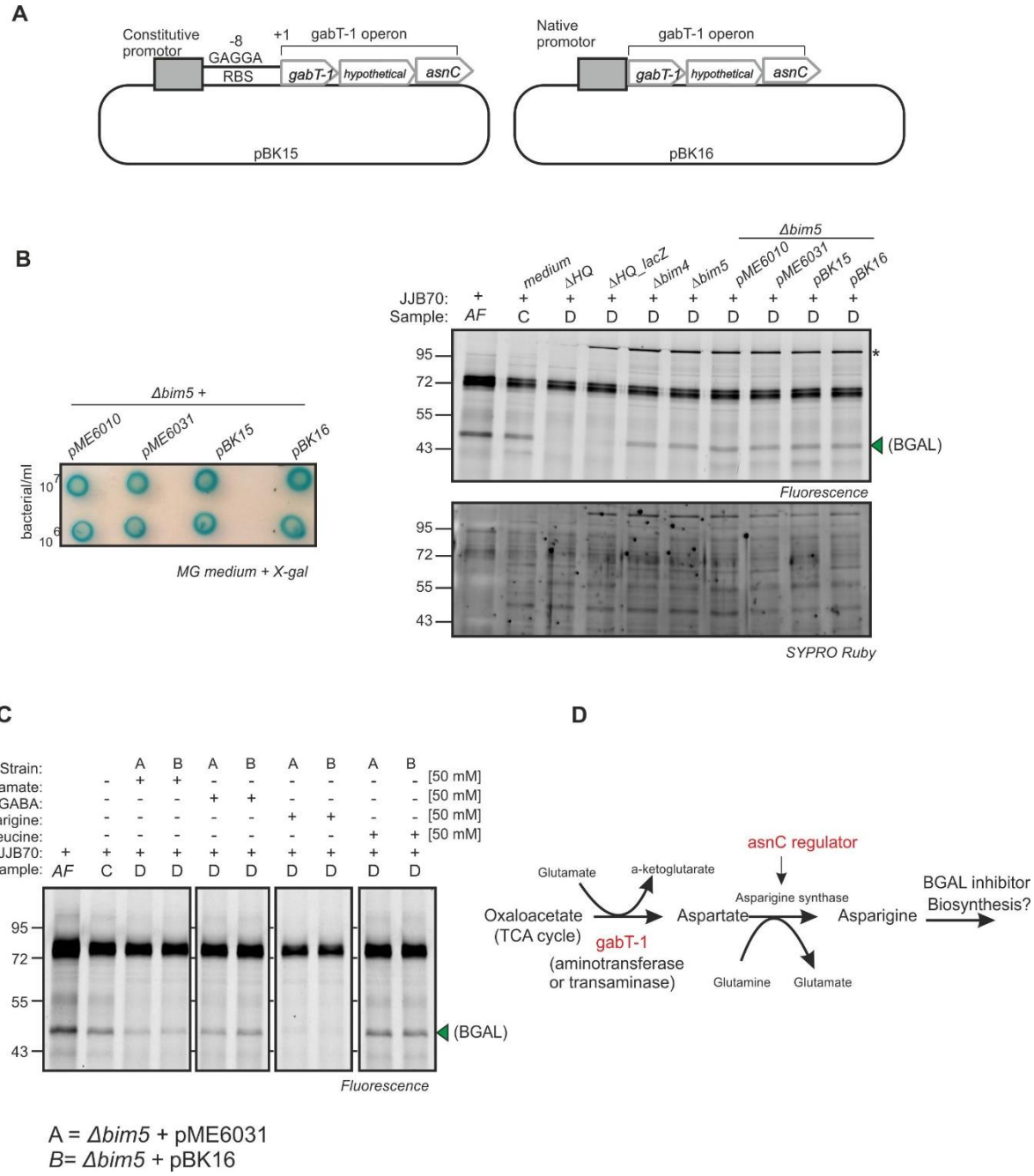

Figure 4.5 *Δbim5* mutant is affected in asparagine biosynthetic pathway

(A) Constructs for complementation studies with *Δbim5*. pBK15: *gabT-1* operon was cloned with a ribosome binding site (RBS) into the pME6010 expression vector behind a constitutive kanamycin promoter. pBK16: the *gabT-1* operon was cloned with the native promoter into the pME6031 cloning vector. (B) *Δbim5* mutant transformed with pBK15 and pBK16 did not complement for the BGAL inhibitor phenotype. The pBK15, pBK16 and the empty vectors pME6031 and pME6010 were transformed into *Δbim5* by electroporation. The transformants constructs were inoculated at O.D=0.5 and grown in the mannitol-glutamate minimal medium. The overnight (16h) grown bacterial cultures were centrifuged and convolution ABPP was performed with the isolated medium against the apoplastic fluids (AF) of *N. benthamiana* leaves. In parallel, the bacterial cultures were plated onto X-gal containing mannitol-glutamate minimal medium and incubated at 28^{0}C for 36 hours. (C) *Δbim5* grown in mannitol-glutamate minimal

medium supplemented with asparagine produces the BGAL inhibitor. The *Δbim5* mutant transformed with pBK16 and the empty vector pME6031 were inoculated in mannitol glutamate minimal medium supplemented with 50 mM amino acids like glutamate, GABA, asparagine and leucine. The overnight (16h) grown bacterial cultures were centrifuged and convolution ABPP was performed with the isolated <3kDa medium fraction against the apoplastic fluids of *N. benthamiana* leaves. (D) Proposed pathwy for the production of the BGAL inhibitor. *gabT-1* and *asnC* genes present at the gabT-1 operon might be involved in asparagine biosynthesis pathway. GabT-1 enzyme might acts as transaminase by transferring the amine group from glutamate to the oxaloacetate thereby producing aspartate. AsnC protein might regulate an unidentified asparagine synthase which converts aspartate to asparagine. *, This signal is specific to *Pto*DC3000(*ΔHQ _lacZ*) and *Δbim* mutants. Signal is absent when convolution ABPP is performed with the <3kDa fraction isolated from the *ΔHQ _lacZ* or *Δbim* grown in minimal medium (Figure 4.2B).

4.3 Discussion

LacZ, a beta-galactosidase from *E.coli,* has been successfully used as a reporter enzyme to detect the BGAL inhibitor produced by *Pto*DC3000 *in vivo*. Although the LacZ enzyme belongs to the GH2 family, it follows a retaining mechanism of hydrolysis like GH35 BGALs. In this study, pHRP308, a RSF1010-based plasmid carrying the *lacZ* gene, was used for the *in vivo* functional screening assay to detect the BGAL inhibitor. pHRP308 is a stable, medium copy number plasmid and belongs to incompatibility group incQ (Parales and Harwood, 1993). The distinct feature of this plasmid is that the *lacZ* gene is expressed together with the gentamycin resistance gene (gm^R) by read-through transcription, mediated by the gentamycin promoter located upstream of gm^R gene. Hence the uncertainty about the *lacZ* gene expression can be avoided using the gentamycin in the screening assay. The established LacZ-based functional screening assay combined with random mutagenesis using *mini-tn5* transposons has been a powerful tool to identify mutants of *Pto*DC3000 which do not produce the BGAL inhibitor. Identification of the insertion sites of *mini-tn5* transposon in the *Δbim* mutants has revealed important genes required for BGAL inhibitor production. In this chapter, two BGAL inhibitor mutants (*Δbim4 and Δbim5*) have been characterized in detail.

In the *Δbim4* mutant, a *mini-tn5* transposon was inserted into a gene called *hrpR* (PSPTO_1380). HrpR is an enhancer binding protein which acts in co-operation with HrpS to regulate the σ^{54}-dependent transcription of the *hrpL* gene (PSPTO_1404). In the *Pto*DC3000 genome, *hrpR* and *hrpS* genes are clustered as an operon whose expression is driven by the *hrpR* promoter, $hrpR_p$. In this study, pME-based plasmid vectors pME6010 and pME6031 were chosen for gene complementation experiments. This is due to the fact that, pME vectors belongs has a pVS1 origin-of-replication and is compatible with different of incompatibility group plasmids (Heeb et al., 2000). Hence during the gene complementation experiments, these plasmid would be stably maintained and inherited together with pHRP308 plasmid which has the incQ origin-of-replication. The pBK18, which carries the *hrpRS* operon with its native

promoter has successfully complemented the BGAL inhibitor phenotype when transformed into the *Δbim4* mutant. This confirms the requirement of *hrpRS* genes in BGAL inhibitor production. In addition, the independent knock strains for *hrpR* and *hrpS* genes has also failed to produce the BGAL inhibitor. Δ*hrpR*) and Δ*hrpS* were created by gene replacements and the effect of mutation is non-polar (Prof. Dr. Jorg Schumacher, personal communication). Consequently, the expression of *hrpS* gene is not affected in the Δ*hrpR* strain and *vice* versa. Hence in *Pto*DC3000, both the proteins HrpR and HrpS are required to regulate the BGAL inhibitor production. This is in agreement with the strict co-dependent functions of HrpR and HrpS proteins which have been observed in earlier studies. In *Pto*DC3000, the HrpR and HrpS proteins interact with each other and their interactions are strictly essential in *Pto*DC3000 to regulate the expression HrpL, an alternative sigma factor associated with Type-III secretion system (Hutcheson et al., 2001;Jovanovic et al., 2011). In the previous chapter, we have confirmed that the BGAL inhibitor secretion is independent of the Type-III secretion system. Hence, this chapter indicates that the *hrpRS* operon might also regulate biosynthesis of the BGAL inhibitor which is secreted independent of the Type-III secretion system.

In the *Δbim5* mutant, *mini-tn5* transposon was inserted into a gene called *gabT-1*. GabT-1 in the *Pto*DC3000 genome is annotated as 4-aminobutyrate (GABA) aminotransferase. GABA-aminotransferases are important enzymes in GABA metabolism, where the GABA molecules are converted into succinic semialdehyde (Park et al., 2010). In the *Pto*DC3000 genome, *gabT-1* (PSPTO_0259) is clustered together with a hypothetical gene (PSPTO_0260) and a gene encoding AsnC-family of transcriptional regulator (PSPTO_0261). These three genes has been computationally annotated to function together as an operon. Unfortunately, the pBK16 construct, which carries the *gabT-1* operon with its own promoter did not complement the BGAL inhibitor phenotype when transformed into the *Δbim5* mutant. Although pBK16 was constructed similar to pBK18, which carries the *hrpRS* operon, the reason for not complementing the BGAL inhibitor phenotype is not known. Expression profiling should be carried out on the *Δbim5* mutant transformed with pBK16 construct to ensure that all the three genes in the operon are properly expressed in this mutant.

Initially, we hypothesized that supplementing the mannitol-glutamate minimal medium with additional amino acids might be helpful for the *Δbim5* mutant transformed with pBK16 to produce the BGAL inhibitor. Surprisingly, the *Δbim5* mutant produced the BGAL inhibitor when the mannitol-glutamate minimal medium was supplemented with asparagine, indicating that asparagine might be an important amino acid needed for BGAL inhibitor production in *Pto*DC3000. Sequential enzymatic activity of a transaminase and an asparagine synthase are important in asparagine biosynthesis pathway of Gram negative bacteria like *E.coli* (Meta Cyc database (Caspi et al., 2016)). I propose that the *gabT-1* and the gene encoding AsnC-family

transcriptional regulator in the *gabT-1* operon might be involved in asparagine biosynthesis pathway specifically for the BGAL inhibitor production (Figure 4.5D). The GabT-1 enzyme might acts as a transaminase by transferring amine group from glutamate to oxaloacetate thereby producing aspartate. The AsnC protein might regulate an unknown asparagine synthase which converts aspartate to asparagine as studied in *E.coli* (Kölling and Lother, 1985) (Figure 4.5D) and that asparagine might serve as a nitrogen source for BGAL inhibitor production. Asparagine has been shown to be an important amino acid source for many nitrogen containing compounds like alkaloids in plants (Chatterjee, 1944) (Olea et al., 2004) and microorganisms (Rehácek et al., 1977). This suggests that the BGAL inhibitor produced by *Pto*DC3000 might be a nitrogen containing compound.

4.4 References

Caspi, R., Billington, R., Ferrer, L., Foerster, H., Fulcher, C.A., Keseler, I.M., Kothari, A., Krummenacker, M., Latendresse, M., Mueller, L.A., et al. (2016). The MetaCyc database of metabolic pathways and enzymes and the BioCyc collection of pathway/genome databases. Nucleic Acids Res. *44*, D471–D480.

Chatterjee, R. (1944). The Origin and function of the alkaloids in *Mahonia Nepalensis* DC. (Berberis Nepalensis Spreng.)**From St. Joseph's College, Darjeeling, India. J. Am. Pharm. Assoc. Sci. Ed *33*, 205–210.

Deng, W., Wang, H., and Xie, J. (2011). Regulatory and pathogenesis roles of Mycobacterium Lrp/AsnC family transcriptional factors. J. Cell. Biochem. *112*, 2655–2662.

Heeb, S., Itoh, Y., Nishijyo, T., Schnider, U., Keel, C., Wade, J., Walsh, U., O'Gara, F., and Haas, D. (2000). Small, stable shuttle vectors based on the minimal pVS1 replicon for use in Gram negative, plant-associated bacteria. Mol. Plant. Microbe Interact. *13*, 232–237.

Hutcheson, S.W., Bretz, J., Sussan, T., Jin, S., and Pak, K. (2001). Enhancer-binding proteins HrpR and HrpS interact to regulate hrp-encoded Type-III protein secretion in *Pseudomonas syringae* Strains. J. Bacteriol. *183*, 5589–5598.

Jovanovic, M., James, E.H., Burrows, P.C., Rego, F.G.M., Buck, M., and Schumacher, J. (2011). Regulation of the co-evolved HrpR and HrpS AAA+ proteins required for *Pseudomonas syringae* pathogenicity. Nat. Commun. *2*, 177.

Kölling, R., and Lother, H. (1985). AsnC: an autogenously regulated activator of asparagine synthetase A transcription in *Escherichia coli.* J. Bacteriol. *164*, 310–315.

Liu, Y.-G., and Whittier, R.F. (1995). Thermal asymmetric interlaced PCR: automatable amplification and sequencing of insert end fragments from P1 and YAC clones for chromosome walking. Genomics *25*, 674–681.

de Lorenzo, V., Herrero, M., Jakubzik, U., and Timmis, K.N. (1990). *Mini-Tn5* transposon derivatives for insertion mutagenesis, promoter probing, and chromosomal insertion of cloned DNA in Gram-negative eubacteria. J. Bacteriol. *172*, 6568–6572.

Olea, F., Pérez-García, A., Cantón, F.R., Rivera, M.E., Cañas, R., Ávila, C., Cazorla, F.M., Cánovas, F.M., and Vicente, A. de (2004). Up-regulation and localization of asparagine synthetase in tomato leaves infected by the bacterial pathogen *Pseudomonas syringae*. Plant Cell Physiol. *45*, 770–780.

Park, D.H., Mirabella, R., Bronstein, P.A., Preston, G.M., Haring, M.A., Lim, C.K., Collmer, A., and Schuurink, R.C. (2010). Mutations in γ-aminobutyric acid (GABA) transaminase genes in plants or *Pseudomonas syringae* reduce bacterial virulence. Plant J. *64*, 318–330.

Rehácek, Z., Desai, J.D., Sajdl, P., and Pazoutová, S. (1977). The cellular role of nitrogen in the biosynthesis of alkaloids by submerged culture of *Claviceps purpurea* (Fr.) Tul. Can. J. Microbiol. *23*, 596–600.

Chapter 5: Identification and detection of the BGAL inhibitor produced by *Pto*DC3000

5.1 Introduction

This chapter describes the identification and detection of the BGAL inhibitor produced by *Pto*DC3000 using various biochemical approaches. Two major clues from the previous chapters paved the way for designing experiments to enrich for the BGAL inhibitor produced by *Pto*DC3000 in minimal medium and apoplastic fluids. First, the amino acid feeding experiment in the last chapter hinted on the nature of the BGAL inhibitor produced by *Pto*DC3000. The *Δbim5* mutant supplemented with asparagine in the minimal medium produced the BGAL inhibitor. Asparagine is an important amino acid source for nitrogen containing compounds and hence I speculate that the BGAL inhibitor might be an alkaloid. Second, GabT-1, a transaminase from *Bacillus subtilis* MOR1 is an important enzyme involved in the production of 1-Deoxynojirimycin (DNJ), an imino sugar (Kang et al., 2011). Imino sugars such as DNJ are analogues of natural sugars, in which the oxygen is replaced by a nitrogen in the ring structure (Nash et al., 2011). Imino sugars are well known to inhibit various glycosidases and have been used for the treatment of human diseases (Asano, 2003). In the *Δbim5* mutant, the *mini-tn5* transposon was inserted in the *gabT-1* gene. Based on these clues, I suspected that the BGAL inhibitor produced by *Pto*DC3000 should be an imino sugar i.e. a polyhydroxy alkaloid.

In this chapter, biochemical methods have been employed to enrich for the BGAL inhibitor produced by *Pto*DC3000 in the minimal medium. These enrichment procedures have been instrumental to identify the crystal structure of the BGAL inhibitor through crystal soaking approach. Next, the candidate BGAL inhibitor was chemically synthesized and used as a reference to detect the BGAL inhibitor in the samples using analytical techniques like GC-MS and HRMS.

5.2 Results

5.2.1 Activity-guided enrichment of BGAL inhibitor produced by *Pto*DC3000*(ΔHQ)* in the minimal medium

The fractionation experiments with apoplastic fluids isolated from the infected leaves of *Nicotiana benthamiana* indicated that the BGAL inhibitor produced by *Pto*DC3000*(ΔHQ)* is a heat stable and <3 kDa small molecule inhibitor (Figure 3.4). The BGAL inhibitor production can be induced in the *Pto*DC3000*(ΔHQ)* by growing them in the apoplast mimicking mannitol-glutamate minimal medium (Figure 3.5). To reduce the complexity and ease the process of identifying the BGAL inhibitor, we used *Pto*DC3000*(ΔHQ)* grown in minimal medium.

Biochemical approaches were followed to enrich for the BGAL inhibitor produced by *Pto*DC3000(*ΔHQ*). First, the *Pto*DC3000*(ΔHQ)* grown minimal medium was subjected to chloroform-methanol precipitation. As a result of adding the chloroform-methanol mixture, the minimal medium was separated into three different phases: the upper hydrophilic (methanol/water) phase, the lower hydrophobic (chloroform) phase, and the protein phase in between (Figure 5.1A). Since the BGAL inhibitor is speculated to be a heat stable small molecular weight compound, the hydrophilic and hydrophobic phases were tested for the presence of the BGAL inhibitor. Both these phases were freeze-dried separately, dissolved in water and fractionated with 3 kDa cut-off filters. The filtrate (<3 kDa) fraction was heated at 95 ^{0}C for 5 minutes and competitive ABPP was performed with the apoplastic fluids isolated from *Nicotiana benthamiana* leaves. Interestingly, the BGAL inhibitor could be detected only in the hydrophilic (methanol/water) phase but not in the hydrophobic (chloroform) phase of *Pto*DC3000*(ΔHQ)* minimal medium sample (Figure 5.1B). In addition, the BGAL inhibitor could not be detected in the both phases of the control samples (Figure 5.1B). This result indicates that the BGAL inhibitor produced by *Pto*DC3000*(ΔHQ)* in the minimal medium can be enriched using chloroform-methanol precipitation and the BGAL inhibitor is a hydrophilic small molecular compound.

Next the BGAL inhibitor-enriched hydrophilic (methanol/water) phase was subjected to cation exchange chromatography using Dowex resins (Figure 5.2A). The freeze dried hydrophilic (methanol/water) fraction from the *Pto*DC3000*(ΔHQ)* minimal medium sample was dissolved with water, acidified to pH 3.5 and passed through the cation-exchange column, The flow-through was collected (A), the column was washed (B) and eluted with the ammonium hydroxide (NH_4OH) (C). The ammonium hydroxide was used for elution because I hypothesized that the BGAL inhibitor might be a nitrogen-containing compound and the excess NH_4OH can compete with the compound bound to the resin. All the three fractions (A, B and C) were freeze-dried using lyophilizer. The freeze-dried fractions had different colours: Fractions A and B were white, and the fraction C was yellowish brown (Figure 5.2B). To detect the presence of the BGAL inhibitor, these fractions were dissolved in water and competitive ABPP was performed with apoplastic fluids isolated from the leaves of *Nicotiana benthamiana*. Interestingly, the BGAL inhibitor could be enriched only in the NH_4OH eluate fraction C but not in the water-wash fraction B (Figure 5.2C). The BGAL inhibitor could also be detected in the flow through fraction A. Probably because not all BGAL inhibitor was absorbed by the column. This might be the unbound BGAL inhibitor which has passed through the column because the BGAL inhibitor was enriched more in the fraction C compared to fraction A (Figure 5.2C). The BGAL inhibitor could not be detected in the NH_4OH eluate fraction C from the *Δbim4* and *Δbim5* mutants grown minimal mediums or the control medium (Figure 5.2C and 5.2D). These

results demonstrate that the BGAL inhibitor can be enriched using the cation exchange chromatography and suggest that the BGAL inhibitor produced by *Pto*DC3000*(ΔHQ)* is most likely containing nitrogen.

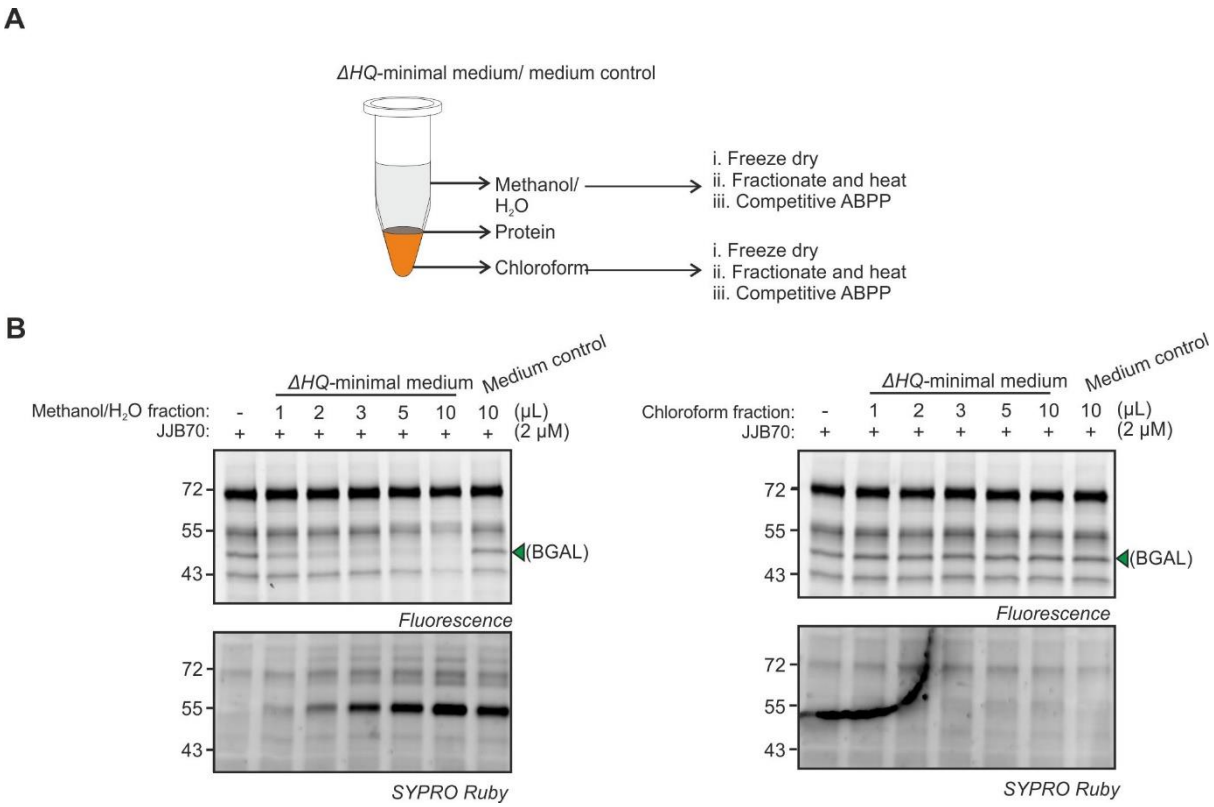

Figure 5.1 The BGAL inhibitor produced by *Pto*DC3000 in minimal medium is a hydrophilic small molecule

(A) Chloroform-methanol precipitation method to isolate the BGAL inhibitor produced by *Pto*DC3000 in mannitol-glutamate minimal medium. The *Pto*DC3000(Δ*HQ*) strain was inoculated at OD=0.5 and grown in mannitol-glutamate medium (minimal). The overnight (16h) grown bacterial cultures were centrifuged and the supernatant of bacteria grown in minimal medium was collected. Chloroform-methanol precipitation was performed by adding equal volume of metabolite isolation buffer containing chloroform-methanol-water in the ratio 1: 2.5:1 to 4 ml of bacterial grown minimal medium or only minimal medium as control. (B) The BGAL inhibitor produced by *Pto*DC3000 in the minimal medium is a methanol/water soluble small molecule. The upper hydrophilic phase (methanol/ water) and the lower hydrophobic phase (chloroform) were collected and freeze-dried separately. The freeze dried fractions were dissolved in water and concentrated using ultrafiltration spin colums to remove the <3 kDa low molecular weight compounds. The <3 kDa (filtrate) fractions were collected, heated at 95ºC for 5 min and competitive ABPP was performed with the apoplastic fluids isolated of *N. benthamiana* leaves using JJB70.

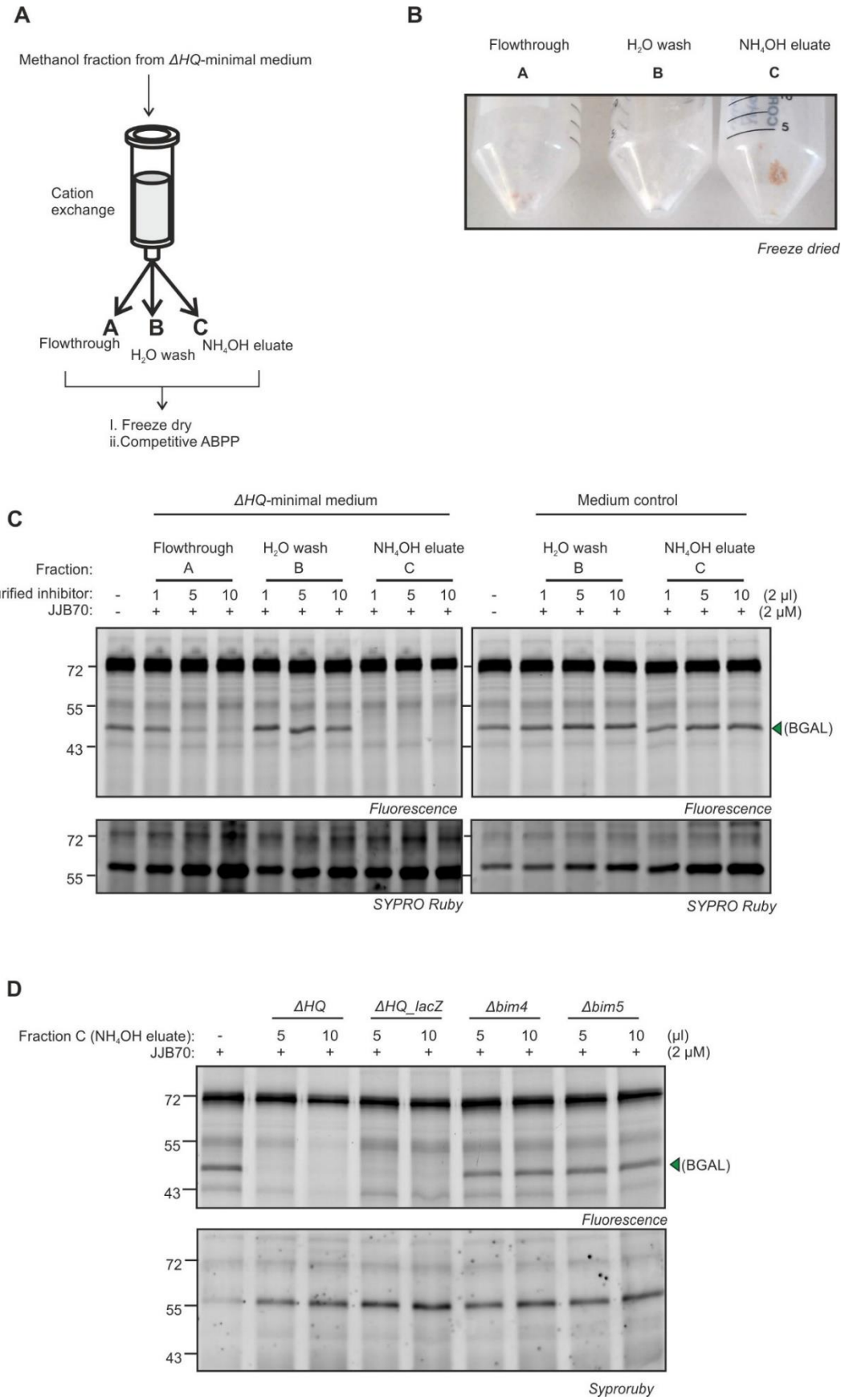

Figure 5.2 The BGAL inhibitor produced by *Pto*DC3000 is a nitrogen-containing small molecule.

(A) Cation exchange chromatography to enrich the BGAL inhibitor. Large scale chloroform-methanol precipitation was performed with 40 ml supernatant of *Pto*DC3000(Δ*HQ*) culture grown in mannitol-glutamate medium or only minimal medium as control. The freeze dried hydrophilic phase (methanol/water) was dissolved in 50 ml of water, adjusted to pH 3.5 and added to the prepared cation-exchange dowex50 resin column. The flow-through was collected and labelled as Fraction A. The column was washed with water and the water-wash fraction was labelled as Fraction B. The cation-exchange column were eluted using 2.5 M ammonium hydroxide (NH_4OH) and the eluate was labelled as Fraction C. (B) Colour of the fractions after cation exchange chromatography and freeze drying. (C) The BGAL inhibitor produced by *Pto*DC3000 in the minimal medium is enriched in the ammonium hydroxide (NH_4OH) eluate fraction C. The freeze dried fractions A, B and C from the ***ΔHQ***-minimal medium sample and freeze dried fractions B and C from the medium control samples were dissolved in water and competitive ABPP was performed with the apoplastic fluids isolated of *N. benthamiana* leaves using JJB70. (D) The BGAL inhibitor is not detected in the enriched NH_4OH eluate fraction C of ***Δbim4*** and ***Δbim5*** minimal medium samples. Large scale chloroform-methanol precipitation and cation exchange chromatography were performed with the ***Δbim4*** and ***Δbim5*** grown in minimal mediums. The freeze-dried fraction C i.e the NH_4OH eluate was dissolved in water and competitive ABPP was performed with the apoplastic fluids isolated of *N. benthamiana* leaves using JJB70.

5.2.2 Identification of the BGAL inhibitor by crystal soaking and X-ray crystallography

*Cj*BglGH35A is a GH35 family BGAL from *Cellvibrio japonicus* for which the crystals were available in the laboratory of Prof. Gideon Davis, University of York, UK (Larsbrink et al., 2014). To investigate if the BGAL inhibitor produced by *Pto*DC3000***(ΔHQ)***can also inhibit *Cj*BglGH35A competitive ABPP was performed with the NH_4OH eluate fraction from *Pto*DC3000***(ΔHQ)*** minimal medium sample and the purified *Cj*BglGH35A enzyme. Interestingly, the labelling of *Cj*BglGH35A was inhibited upon increasing the amount of the NH_4OH eluate fraction from the *Pto*DC3000***(ΔHQ)*** sample (Figure 5.3A). This data indicate the BGAL inhibitor produced by *Pto*DC3000 can also inhibit *Cj*BglGH35A

To identify the BGAL inhibitor, the NH_4OH eluate fraction from *Pto*DC3000***(ΔHQ)*** minimal medium sample was soaked together with the protein crystals of *Cj*BglGH35A enzyme and the soaked crystals were imaged using X-ray crystallography (Figure 5.3B). The crystal soaking experiment and analysis was performed by Dr. Wendy Offen in the laboratory of Prof. Gideon Davis, University of York, UK. A strong electron density of a small molecule was observed near the active site of the *Cj*BglGH35A enzyme at resolution of 1.5 Å. The detected electron density was fitted to various candidate inhibitors using the *Crystallographic Object-Oriented Toolkit* (COOT) program (Emsley et al., 2010). Surprisingly, the electron density in the active site perfectly matched a meso stereoisomer of 3,4,5 trihydroxy piperidine (THP-MESO) (Figure 5.3C). The annotation of this electron density to THP is as follows: The electron indicated 1.) A six membered ring with a boat conformation suggesting saturation; 2.) Three adjacent hydroxyl groups probably making hydrogen bonds with five nearby asparagine amino acid residues of *Cj*BglGH35A: N383, N57, N134, N135 and N204; 3.) Possibly a nitrogen in the ring opposite to the trihydroxy groups; This nitrogen would interact directly with

the active site E349. Having nitrogen fits with the basic property of the BGAL inhibitor and with the involvement of GabT-1 for its biosynthesis.

The meso stereoisomer of trihydroxy piperidine (THP-MESO) was chemically synthesized by Richard van den Berg in the laboratory of Prof. Dr. Hermen Overkleeft, the Leiden Institute of Chemistry, The Netherlands. To investigate if the synthetic THP-MESO can also inhibit BGAL from *Nicotiana bentha*miana, competitive ABPP was performed with the synthetic THP-MESO on apoplastic fluids isolated from the leaves of *Nicotiana benthamiana*. Importantly, the labelling of BGAL in apoplastic fluids completely inhibited with 4 mM concentration of synthetic THP-MESO and partially inhibited with 200 µM (Figure 5.3D). These results indicate that the meso stereoisomer of 3,4,5 trihydroxy piperidine (THP-MESO) is most likely the BGAL inhibitor produced by *Pto*DC3000*(ΔHQ)* in minimal medium. However, relatively high concentrations of THP-MESO are required to inhibit BGAL present in the apoplastic fluids of *Nicotiana benthamiana* leaves.

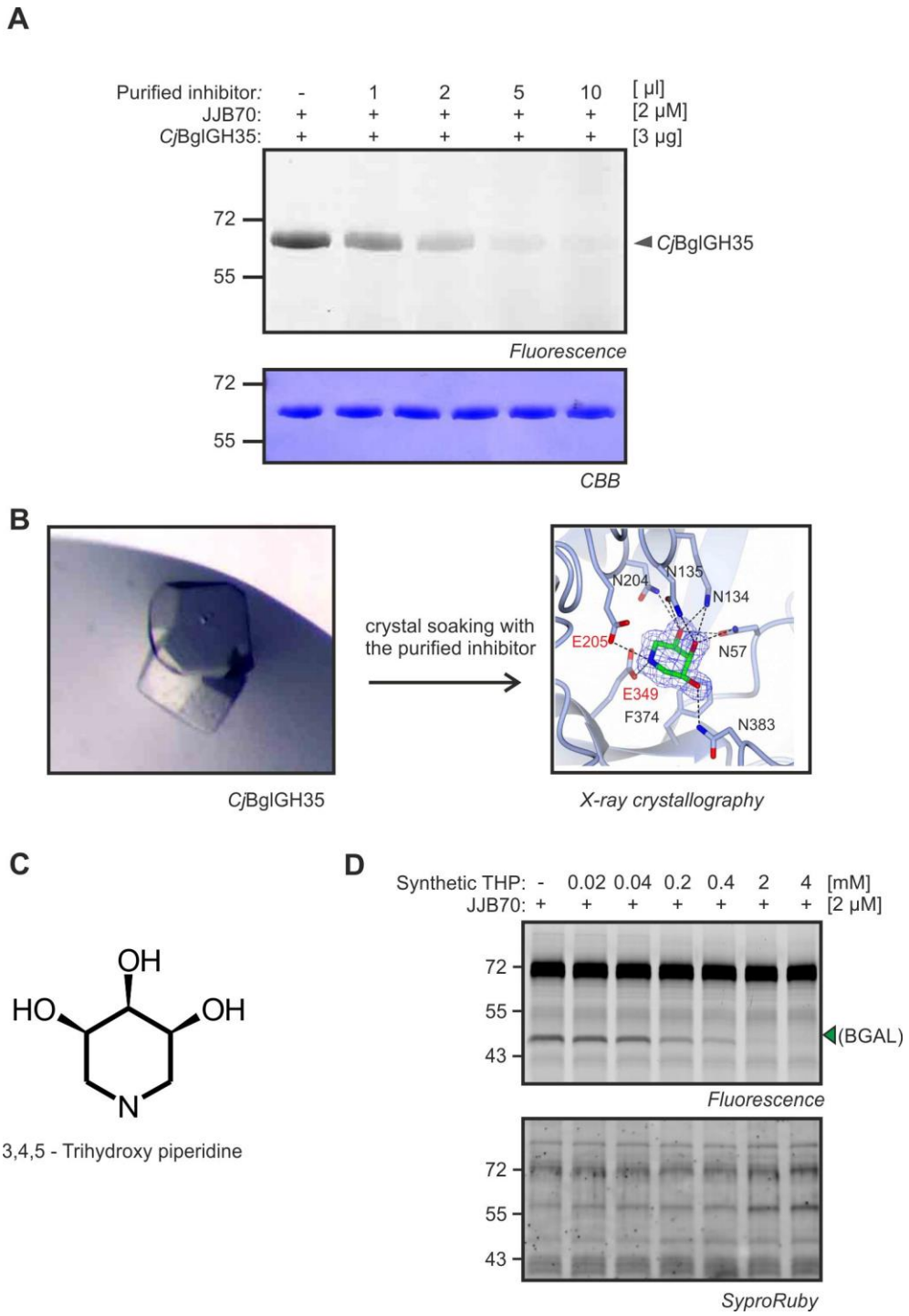

Figure 5.3 3,4,5 trihydroxy piperidine (THP-MESO) is the candidate BGAL inhibitor produced by *Pto*DC3000 in the minimal medium

(A) The BGAL inhibitor enriched in the NH_4OH eluate fraction from the *Pto*DC3000*(ΔHQ)* minimal medium sample also inhibits a microbial BGAL from GH35 family. The NH_4OH eluate fraction from the *Pto*DC3000*(ΔHQ)* minimal medium sample was dissolved in water and 3 µg of purified *Cj*BglGH35 enzyme was pre-incubated the NH_4OH eluate fraction at different volumes for 30 minutes. The pre-incubated protein was labelled with JJB70 for one hour at pH 5.0. The labeling reaction was stopped by adding gel loading buffer and heating at 95ºC. The proteomes were separated on protein gels, detected by in-gel fluorescent scanning and subsequently stained with coomassie brilliant blue (CBB). (B) Soaking crystal approach to identify the BGAL inhibitor. *Cj*BglGH35A crystal was soaked

into the NH_4OH eluate fraction solution from the *Pto*DC3000*(ΔHQ)* sample. This was performed by Dr. Wendy Offen and Prof. Dr. Gideon Davis at the University of York, UK. The soaked crystals were analysed by X-ray crystallography at the Diamond Light Source Synchrotron Science Facility, located near Oxford, UK. The detected electron density near the active site glutamate residues E205 and E349 was modelled using Crystallographic Object-Oriented Toolkit (COOT). The possible hydrogen bonding interactions of the functional groups present in the molecule with the active site amino acid residues in the *CjBgl*GH35A enzyme is depicted. (C) Identified structure from the electron density. (D)The synthetic trihydroxy piperidine (THP-MESO) inhibits the BGAL from *Nicotiana benthamiana*. THP-MESO was chemically synthesized at the University of Leiden, the Netherlands. Apoplastic fluids from *Nicotiana benthamiana* leaves were pre-incubated with the synthetic THP-MESO at different concentrations for 30 minutes. The pre-incubated proteome was labelled with JJB70 for one hour at pH 5.0. The labeling reaction was stopped by adding gel loading buffer and heating at 95 ºC. The proteomes were separated on protein gels, detected by in-gel fluorescent scanning and subsequently stained with SYPRO Ruby.

5.2.3 Detection of trihydroxy piperidine (THP) in the *Pto*DC3000*(ΔHQ)* minimal medium using gas chromatography mass spectrometry (GC-MS)

To investigate if the trihydroxy piperidine (THP) is produced by *Pto*DC3000*(ΔHQ)* in the minimal medium, the NH_4OH eluate fraction was analysed using gas chromatography mass spectrometry (GC-MS). Firstly the synthetic trihydroxy piperidine (THP-MESO) was analysed using GC-MS to make sure that the compound can be detected by GC-MS. When the compound was injected into GC-MS machine without any modifications, the THP-MESO could not be detected (data not shown). Hence, THP-MESO has to be modified to detect it using GC-MS. The synthetic THP-MESO compound was silylated using N-methyl-N-trimethylsilyl-trifluoroacetamide (MSTFA*)* and the derivatized compound was analysed using GC-MS (Lisec et al., 2006). An abundant peak at the retention time (RT) of 27.2 minutes was observed in the GC-MS chromatogram with a mass/charge (m/z) molecular ion at 421.1 Da. THP-MESO molecule has four potential sites for silylated reaction sites (3xOH + N) and the fully derivitized compound is therefore expected to have a molecular mass of 421.1 Da (Figure 5.4A). Hence the peak at the retention time (RT) of 27.2 minutes corresponds to the fully silylated THP (Figure 5.4A). We were able to annotate eight other possible structures to m/z ions derived from the silylated THP (Figure 5.4B). The m/z fragment ion at 215.1 Da with high intensity is the base peak of the silylated-THP compound and the m/z fragment ion at 73 Da is the trimethylsilane (TMS). The minor peaks detected over various retention times in the total ion chromatogram of GC-MS might be the partially derivitized THP-MESO. These results demonstrate that the synthetic THP-MESO can be detected using GC-MS after silylation using MSTFA.

Having a protocol standardized to detect THP-MESO using GC-MS, we aimed to detect THP-MESO in the minimal medium of *Pto*DC3000(*ΔHQ*) cultures. Therefore, NH_4OH eluate fractions from the minimal medium samples of *Pto*DC3000(*ΔHQ*), *Δbim4, Δbim5* and the medium control were silylated using MSTFA and analysed using GC-MS. To detect the

candidate silylated-THP molecule in these samples, the GC-MS chromatograms were analysed using the GC-MS analysis program, AMDIS (Automated Mass Spectral Deconvolution and Identification System) (Du and Zeisel, 2013). First, a target spectral library was built based on the m/z fragment ions of fully silylated synthetic THP-MESO using the AMDIS program (Figure 5.5A). The extracted ion chromatograms (EIC) contain representative m/z fragments at: 200, 215, 331 and 421 Da (Figure 5.5B) and all the m/z fragment ions of fully derivitized THP-MESO used for building the target library are represented (Figure 5.5C).

Next, the GC-MS chromatograms from the minimal medium samples of *Pto*DC3000(*ΔHQ*), *Δbim4, Δbim5* and the medium control were analysed using the AMDIS program. This program performs automated deconvolution of the entire total ion chromatogram (TIC) and searches for the target THP compound in these samples. Importantly, the target silylated THP molecule was detected in the peak at a retention times of 26.5 minutes from *Pto*DC3000*(ΔHQ)* minimal medium sample (Figure 5.6A). The retention time of the detected silylated THP in the *Pto*DC3000*(ΔHQ)* samples are slightly different between experiments. This is due to the fact that the overall chromatogram profile is slightly shifted because of the exchange of new GC-MS columns over the years.

The extracted ion chromatograms (EIC) of selected m/z fragments (200, 215, 331 and 421 Da) show the silylated THP in the peak from the *Pto*DC3000*(ΔHQ)* sample (Figure 5.6B). The peak at this retention time (26.5 minutes) also contained the co-eluting silylated glutamate which has the base m/z fragment ion at 246.1 Da (Figure 5.6C). The extracted spectrum at 26.5 minutes, contains the m/z fragment ions of silylated THP from the *Pto*DC3000*(ΔHQ)* sample are represented (Figure 5.6D). Importantly, this silylated THP molecule could not be detected in *Δbim4, Δbim5* and the medium control samples, when the deconvolution analysis were performed using the AMDIS program (Figure 5.7A, 5.8A, 5.9A). The peak at 26.5 minutes retention time in the *Δbim4 and Δbim5* minimal medium samples, contained only glutamate as a major component (Figure 5.7B&C, 5.8B&C). The medium control sample contained a major peak at 25.3 minutes retention time, which corresponds to partially silylated glutamate (Figure 5.9A). In a second independent experiment (data not shown), the silylated THP molecule could be detected in the *Pto*DC3000*(ΔHQ)* minimal medium sample but not in the *Δbim4* sample. In this experiment, traces of silylated THP could be detected in the *Δbim5* sample but less abundant than *Pto*DC3000*(ΔHQ)* sample. Taken together, these results demonstrate that a trihydroxy piperidine (THP) is produced by *Pto*DC3000*(ΔHQ)* but not by the BGAL inhibitor mutant *Δbim4* and reduced or absent *Δbim5* mutant.

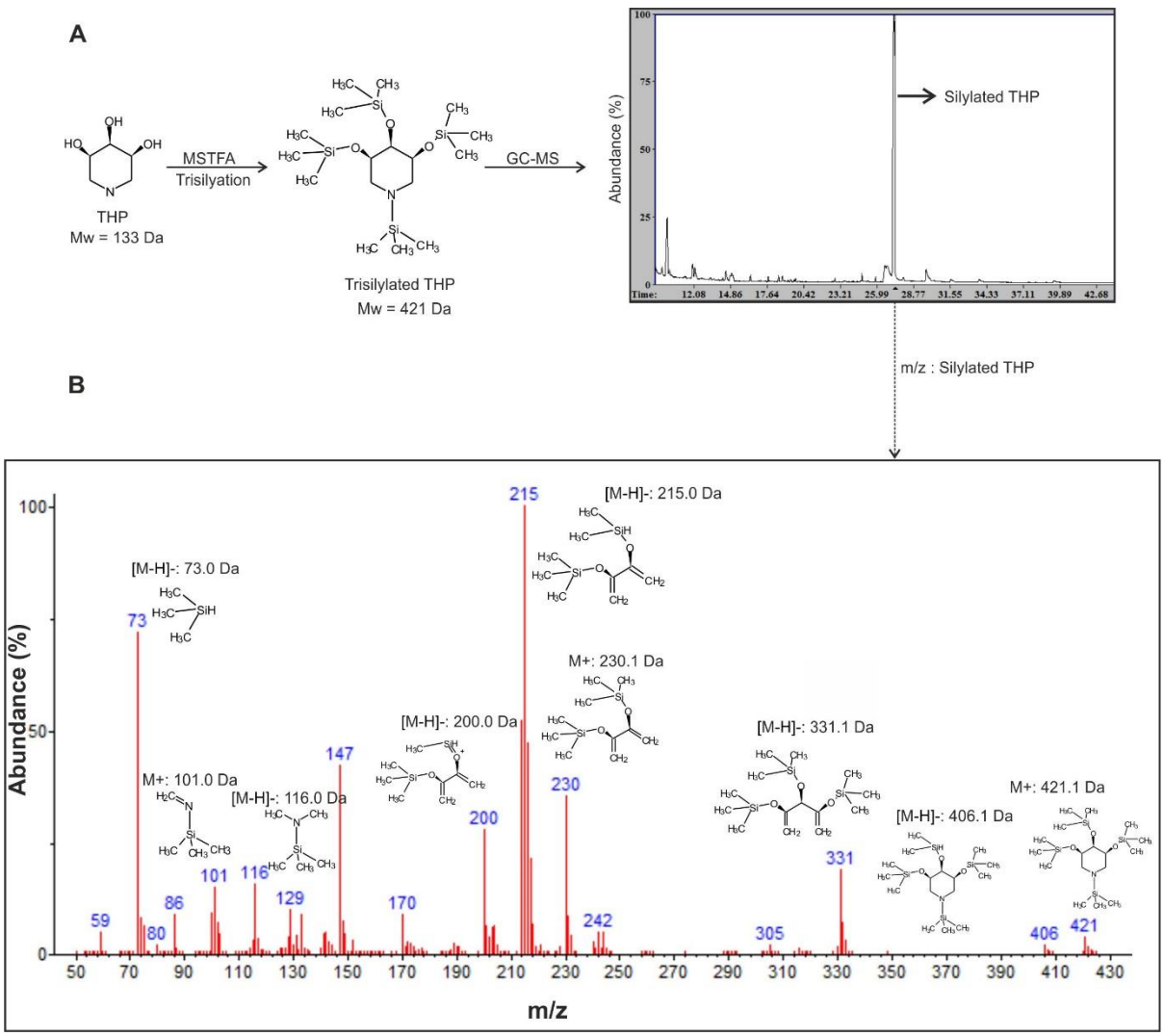

Figure 5.4 Analysis of the synthetic silylated trihydroxy piperidine (THP-MESO) using GC-MS

(A) Derivatization and GC-MS analysis of synthetic trihydroxy piperidine (THP-MESO). Synthetic THP-MESO was silylated using *N*-Trimethylsilyl-*N*-methyl trifluoroacetamide (MSTFA) at 60^{0}C for 90 minutes. The derivitized molecule was injected into GC-MS for further analysis. (B) Fragmentation pattern of silylated THP-MESO molecule. The mass/charge (m/z) fragment ions of silylated THP-MESO molecule at retention time 27.2 are shown. The predicted or proposed structures of the m/z fragment ions generated from fully silylated THP-MESO are shown. The m/z fragment ion at 421 Da is the molecular ion peak and m/z fragment at 215 Da is the base peak of silylated THP-MESO.

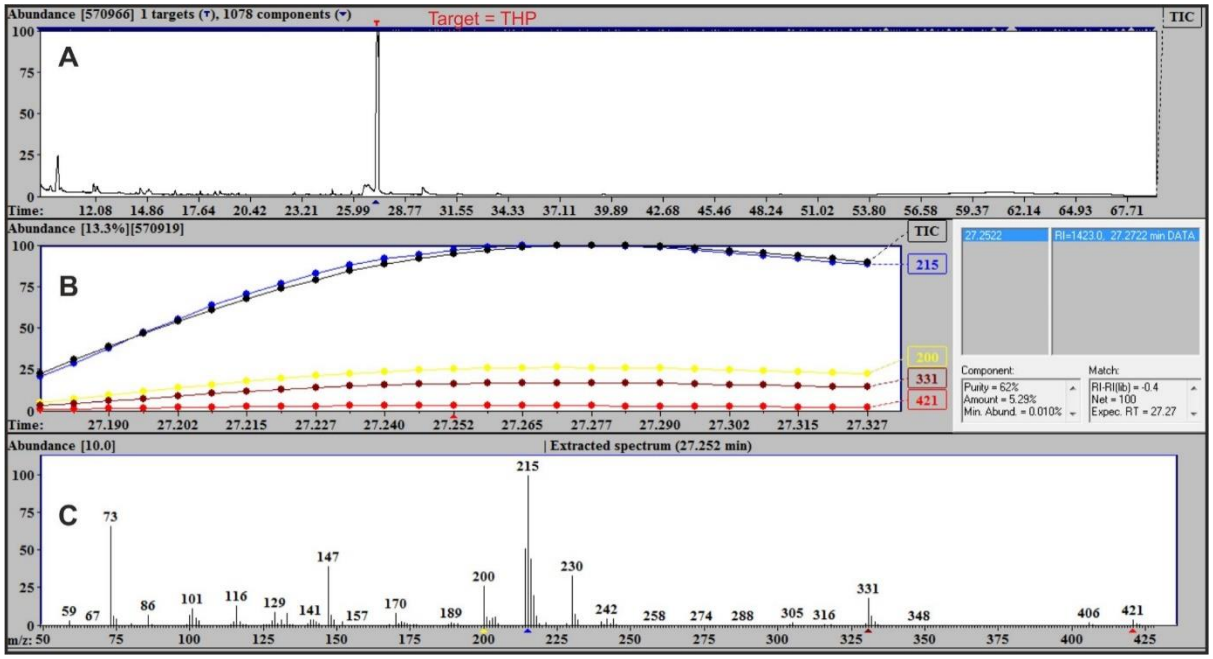

Figure 5.5 Spectral library construction for synthetic silylated THP-MESO

(A) The total ion chromatogram (TIC) of silylated synthetic THP-MESO. (B) The extracted ion chromatogram (EIC) of selected m/z fragment ions: 200, 215, 331 and 421 Da which signifies the silylated THP-MESO compound. The (C) The mass/charge (m/z) fragment ions of silylated THP-MESO at 27.2 minutes retention time.

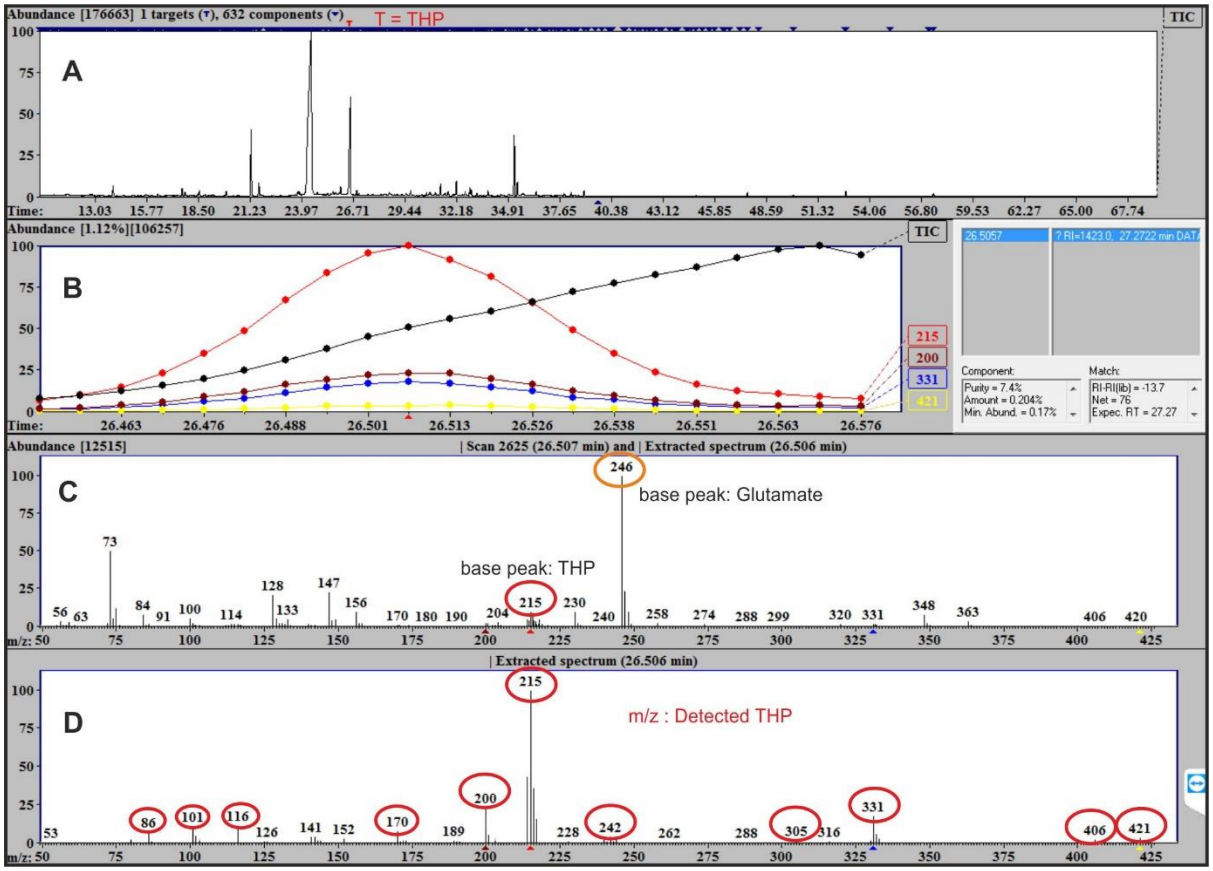

Figure 5.6 THP is detected in the metabolome of *Pto*DC3000*(ΔHQ)* cultures

(A) The total ion chromatogram (TIC) of silylated NH_4OH eluate from the *Pto*DC3000*(ΔHQ)* minimal medium culture sample. The analysed peak in the TIC at 26.5 minutes retention time is indicated as T (red). (B) The extracted ion chromatogram (EIC) of selected m/z fragments: 200, 215, 331 and 421 Da signify the detected silylated THP. (C) The mass/charge (m/z) fragment ions detected at 26.5 minutes retention time. The m/z fragment ion at 215 Da is the base peak of silylated THP and m/z fragment ion at 246 Da is the base peak of silylated glutamic acid. (D) The extracted spectrum which contains majority of m/z fragment ions of the detected silylated THP present in the *Pto*DC3000*(ΔHQ)* minimal medium sample. The m/z fragment ions representing the silylated THP molecule is indicated with red circles.

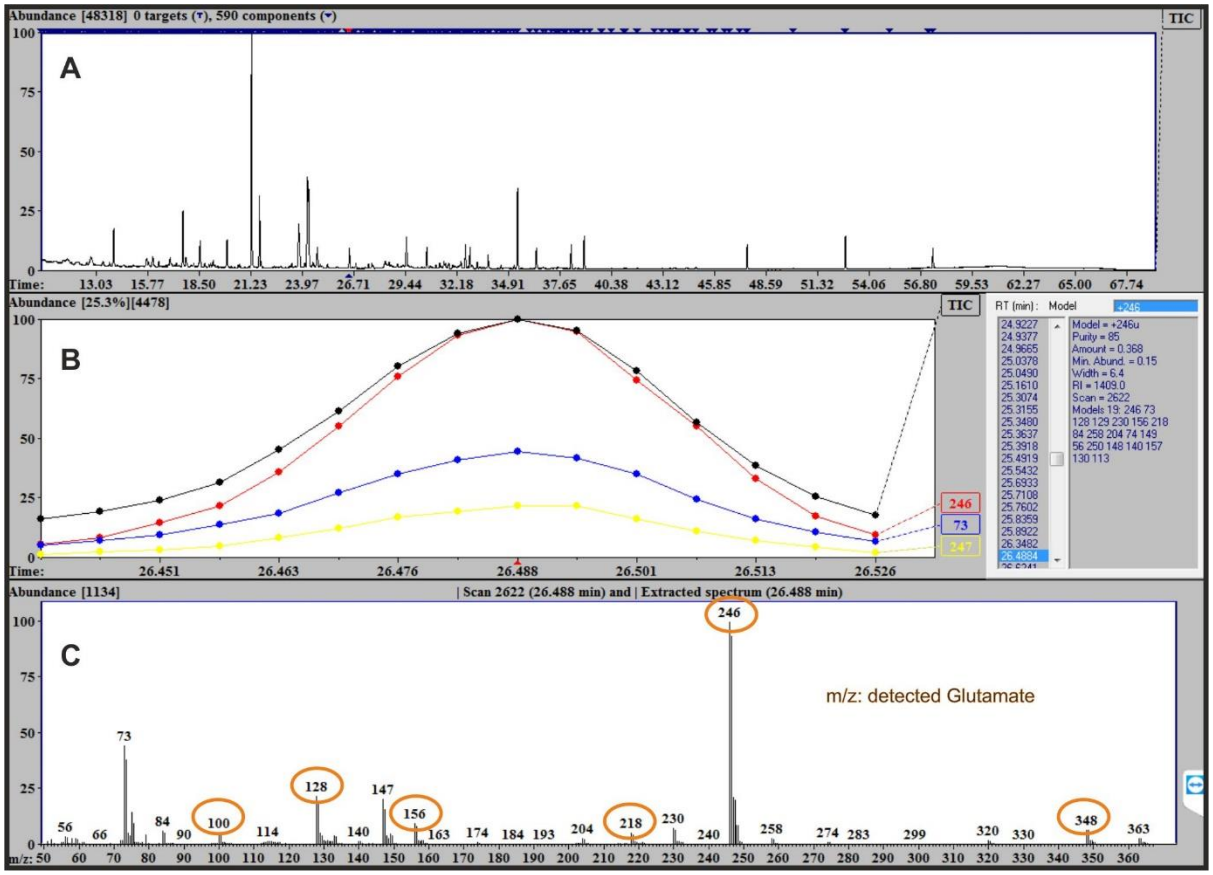

Figure 5.7 THP is not detected in the metabolome of *Δbim4* cultures

(A) The total ion chromatogram (TIC) of silylated NH_4OH eluate from the *Δbim4* minimal medium sample. (B) The extracted ion chromatogram (EIC) of selected m/z fragments: 246, 73 and 247 signifying the detected silylated glutamic acid. (C) The mass/charge (m/z) fragment ions detected at 26.5 minutes retention time. The m/z fragment ion: 246 Da is the base peak of silylated glutamic acid. The m/z fragment ions representing the silylated glutamic acid is indicated as orange circles.

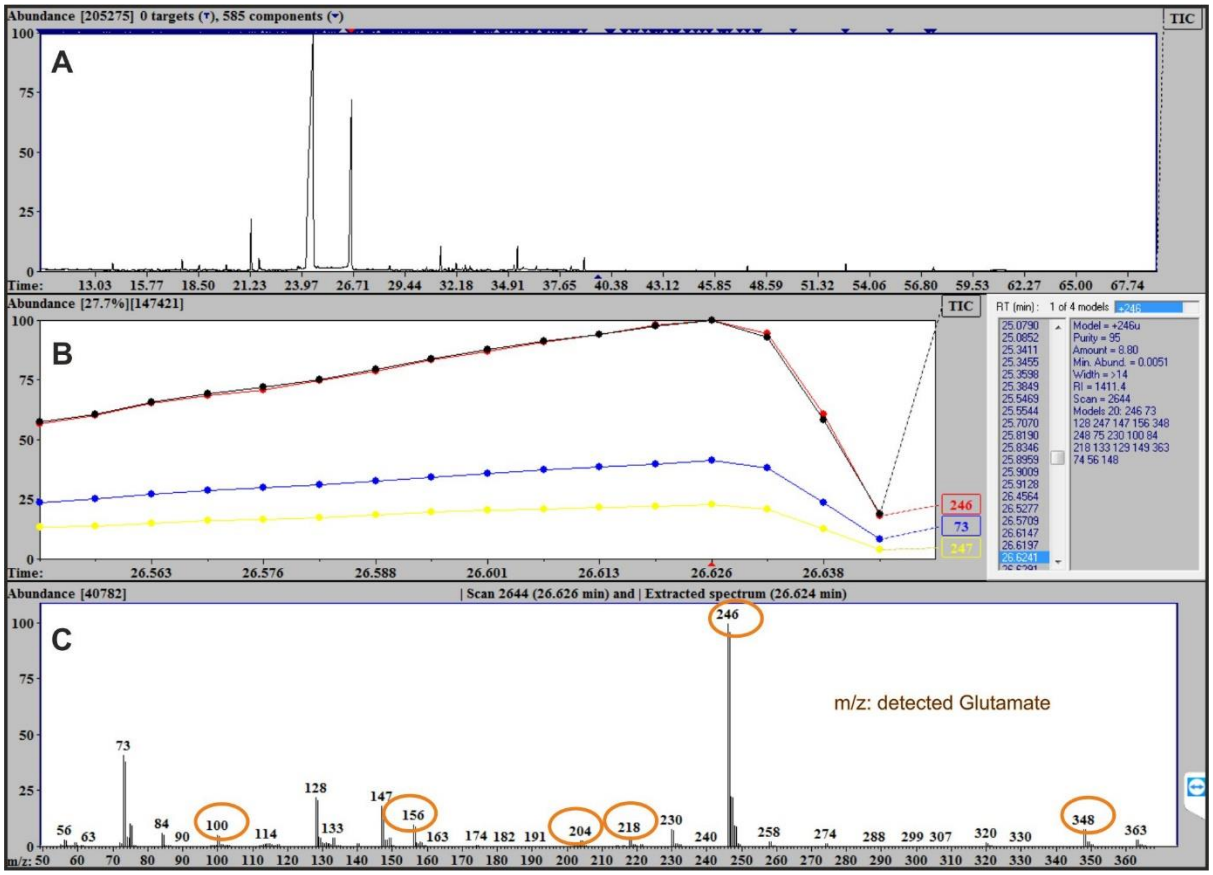

Figure 5.8 THP is not detected in the metabolome of *Δbim5* cultures

(A) The total ion chromatogram (TIC) of silylated NH_4OH eluate from the *Δbim5* minimal medium sample. (B) The extracted ion chromatogram (EIC) of selected m/z fragments 246, 73 and 247 signify the detected silylated glutamic acid. (C) The mass/charge (m/z) fragment ions detected at 26.5 minutes retention time. The m/z fragment ion at 246 Da is the base peak of silylated glutamic acid. The m/z fragment ions representing the silylated glutamic acid is indicated as orange circles.

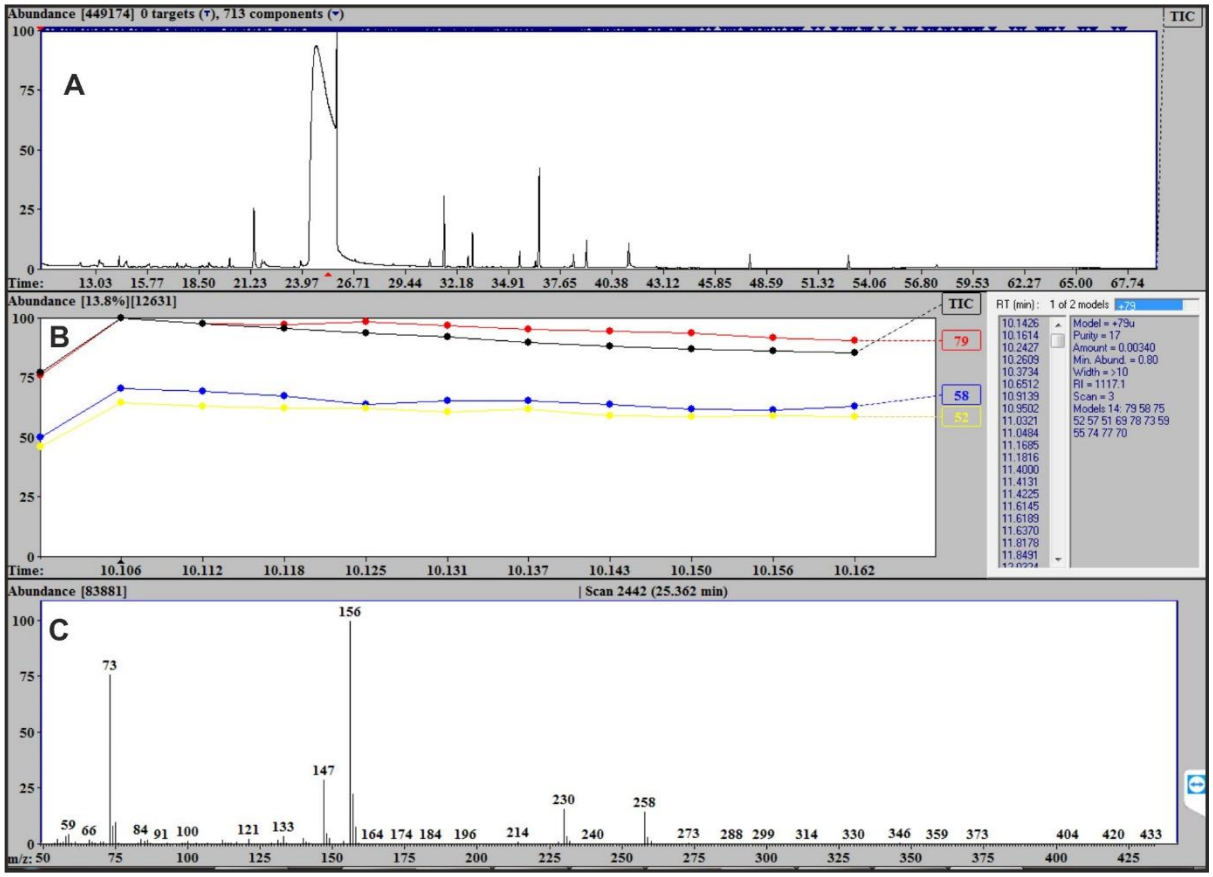

Figure 5.9 THP is not detected in the minimal medium control sample.

(A) The total ion chromatogram (TIC) of silylated NH_4OH eluate from the minimal medium control sample. (B) The extracted ion chromatogram (EIC) of selected m/z fragments: 79, 58 and 52 Da signify the detected partially silylated glutamic acid. (C) The mass/charge (m/z) fragment ions detected at 26.5 minutes retention time. The m/z fragment ion: 156 Da is the base peak of partially silylated glutamic acid.

5.2.4 Purification of the BGAL inhibitor produced by *Pto*DC3000*(ΔHQ)* in minimal medium using gel-filtration chromatography

To purify the BGAL inhibitor for downstream analysis like Nuclear Magnetic Resonance spectroscopy (NMR) and high resolution mass spectrometry (HRMS), the NH_4OH eluate fraction from the *Pto*DC3000*(ΔHQ)* minimal medium sample was subjected to gel-filtration chromatography. In this method, the compounds present in the sample are separated based on their molecular size. Fourteen different fractions were collected after gel-filtration chromatography and these fractions were freeze dried (Figure 5.10A). The freeze-dried fractions were dissolved in water and competitive ABPP was performed with the apoplastic fluids isolated from *N. benthamiana* leaves. The BGAL inhibitor was detected in fractions 2 and 3 but not in other fractions (Figure 5.10B).

To test the purity of the samples, fractions 2 and 3 were subjected to GC-MS analysis. The samples were silylated using MSTFA and the GC-MS chromatograms were analysed

using AMDIS. The candidate silylated THP molecule was detected in the peak at 27.4 minutes retention time from fractions 2 and 3 (Figure 5.11A & 5.12A). The absolute abundance of this peak was higher in the fraction 2 (38213 counts) compared to fraction 3 (931 counts) which suggests that the THP molecule is more abundant in fraction 2. In both samples, at 27.4 minutes retention time, the peak also contained the co-eluting silylated glutamate which has the base m/z fragment ion at 246.1 Da (Figure 5.11C & 5.12C). The spectrum at 27.4 minutes retention time which contains the m/z fragment ions of silylated THP molecule in the fractions 2 and 3 was extracted using AMDIS program (Figure 5.11D & 5.12D). Unfortunately both fractions 2 and 3 were not pure since many other compounds could be detected in these sample over different retention times (Figure 5.11A & 5.12A).

To have a further assurance about the detection of trihydroxy piperidine (THP) in the *Pto*DC3000*(ΔHQ)* minimal medium, the BGAL inhibitor enriched samples: fractions 2 and 3 were subjected to High Resolution Mass Spectrometry (HRMS) analysis. The HRMS and the elemental composition analysis were performed by Prof. Dr. Dmitri Filippov at the Leiden Institute of Chemistry, the Netherlands. The advantage of using HRMS is that the mass and elemental composition of various compounds present in the sample can be obtained. First, the synthetic THP-MESO was analysed to make sure that the compound can be detected using HRMS. In this analysis, the protonated form of synthetic THP-MESO was detected as the major component at 0.09-0.3 minutes retention time with molecular mass of 134.08119 Da predicting its elemental composition as $C_5H_{12}N_1O_3$ (Figure 5.13A&B). Having the chromatogram profile of synthetic THP-MESO as reference, the HRMS chromatograms from fractions 2 and 3 were analysed. Importantly, a compound with molecular mass of 134.08117 Da with predicted elemental composition of $C_5H_{12}N_1O_3$ could be detected in fraction 2 at 0.08-0.3 minutes retention time (Figure 5.14A&B). Unfortunately, the compound was not detected in the fraction 3 sample using HRMS (Figure 5.15A&B). This results confirm that THP is indeed present in the BGAL inhibitor enriched fraction 2 obtained from *Pto*DC3000*(ΔHQ)* minimal medium. The most likely reason for not detecting THP in fraction 3 is that it may not be abundant enough.

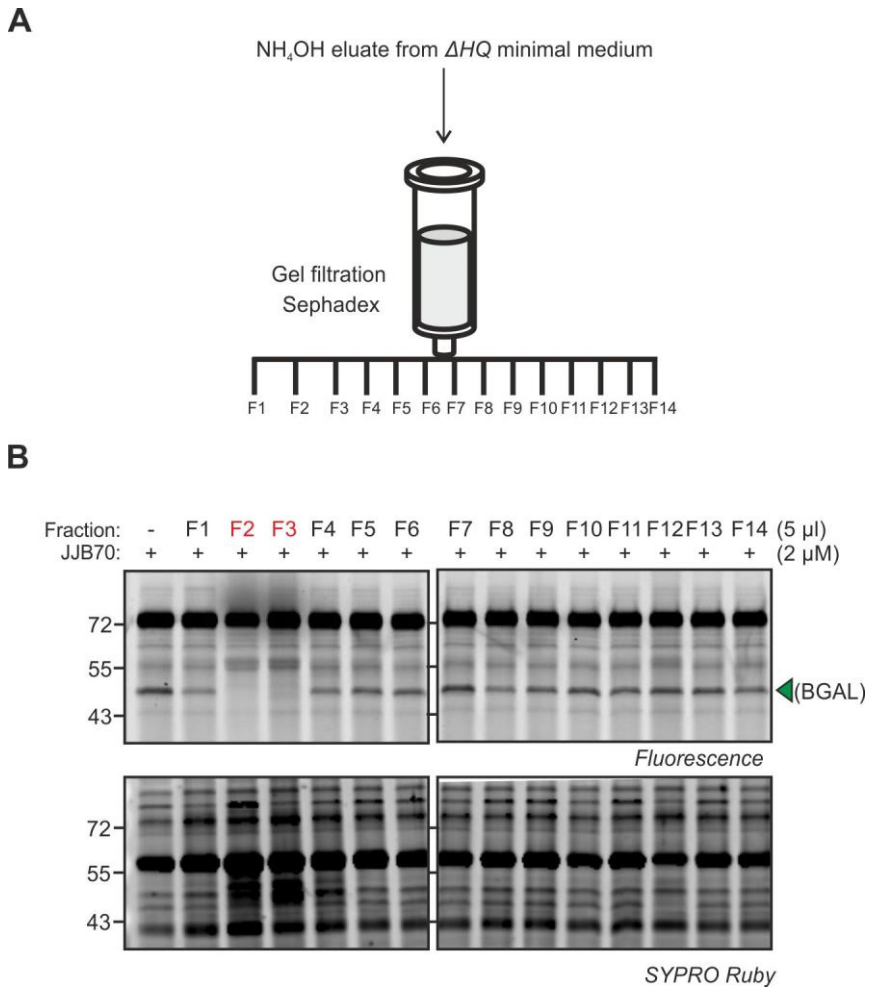

Figure 5.10 Fractionation of NH_4OH eluate using gel-filtration chromatography

(A) Fractionation using gel-filtration chromatography. The NH_4OH eluate fraction was obtained from the two litres of *Pto*DC3000*(ΔHQ)*inoculated minimal medium. The NH_4OH was dissolved in methanol: water (9:1) and loaded to the prepared sephax gel filtration column. The fraction were collected and freeze dried separately. (B) Fraction 2 and 3 are enriched with the BGAL inhibitor. The freeze-dried fractions from (A) were dissolved in water and competitive ABPP was performed with apoplastic fluids isolated from the leaves of *N. benthamiana* using JJB70.

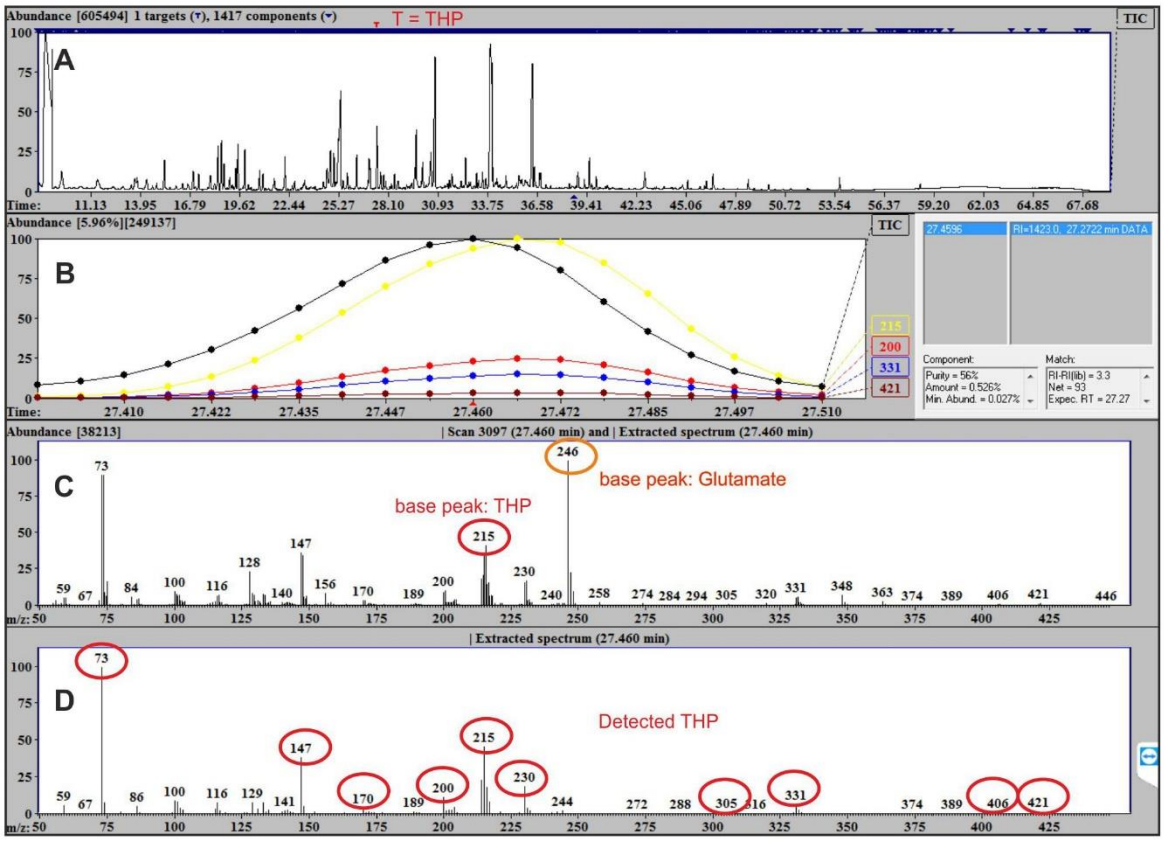

Figure 5.11 Trihydroxy piperidine (THP) is detected in the fraction 2 after gel-filtration chromatography using HRMS

(A) The total ion chromatogram (TIC) of silylated fraction 2 from the *Pto*DC3000*(ΔHQ)* inoculated minimal medium sample. The analysed peak in the TIC at 27.4 minutes retention time is indicated as T (red). (B) The extracted ion chromatogram (EIC) of selected m/z fragments: 200, 215, 331 and 421 Da signify the detected silylated THP (Figure 5.10). (C) The mass/charge (m/z) fragment ions detected at 27.4 minutes retention time. The m/z fragment ion: 215 Da is the base peak of silylated THP and m/z fragment ion: 246 Da is the base peak of silylated glutamic acid. (D) The spectrum at 27.4 minutes retention time which contains the m/z fragment ions of silylated THP molecule in the fractions 2 was extracted using AMDIS program. The m/z fragment ions representing the silylated THP molecule is indicated with red circles.

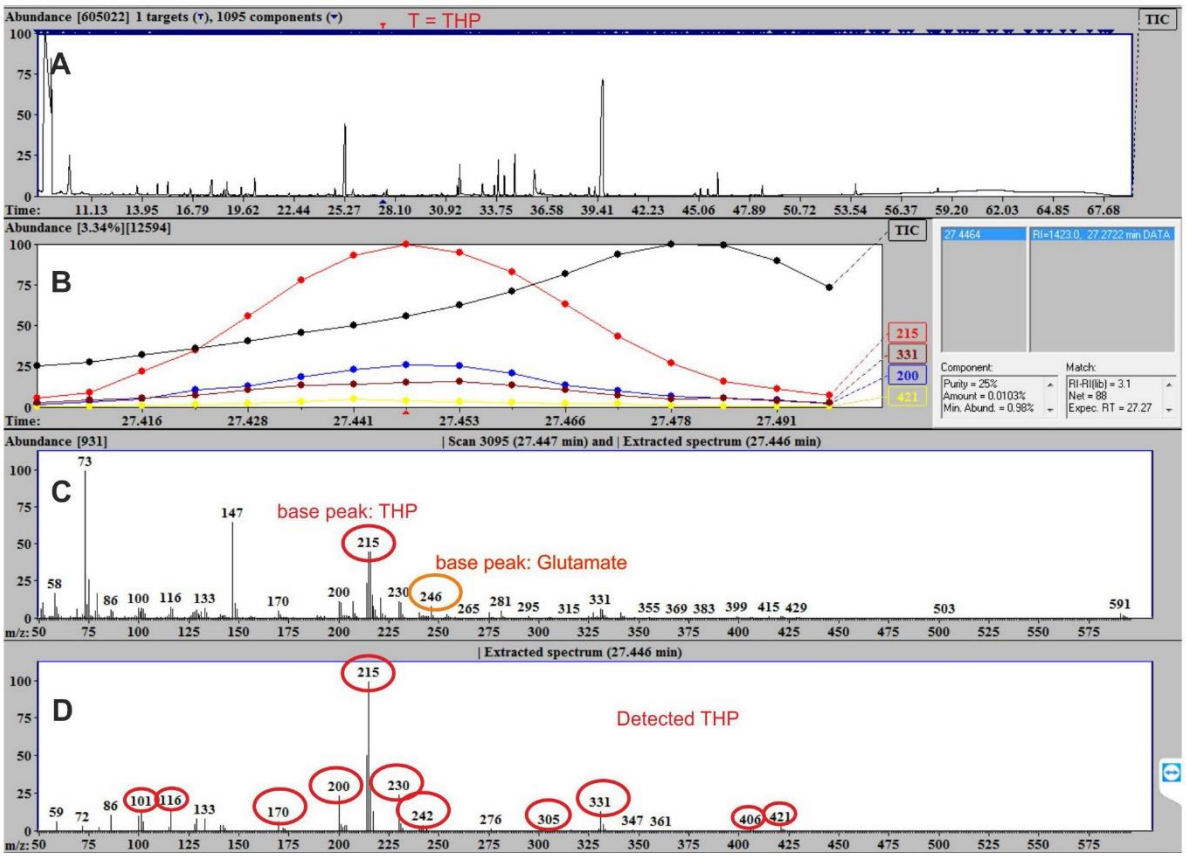

Figure 5.12 Trihydroxy piperidine (THP) is detected in the fraction 3 after gel-filtration chromatography using HRMS

(A) The total ion chromatogram (TIC) of silylated fraction 3 from the *Pto*DC3000*(ΔHQ)* inoculated minimal medium sample (Figure 5.10). The analysed peak in the TIC at 27.4 minutes retention time is indicated as T (red). (B) The extracted ion chromatogram (EIC) of selected m/z fragments: 200, 215, 331 and 421 Da signify the detected silylated THP. (C) The mass/charge (m/z) fragment ions detected at 27.4 minutes retention time. The m/z fragment ion: 215 Da is the base peak of silylated THP and m/z fragment ion: 246 Da is the base peak of silylated glutamic acid. (D) The spectrum at 27.4 minutes retention time which contains the m/z fragment ions of silylated THP molecule in the fractions 3 was extracted using AMDIS program. The m/z fragment ions representing the silylated THP molecule is indicated with red circles.

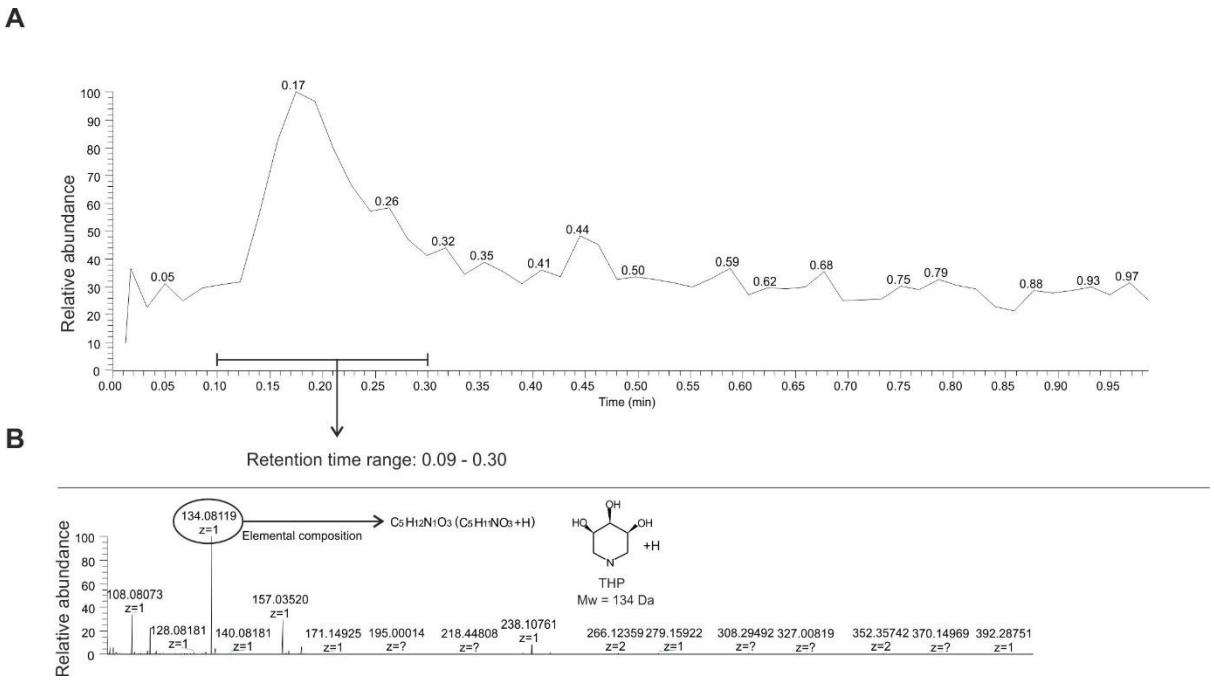

Figure 5.13 Analysis of synthetic THP-MESO using HRMS

(A&B) The chemically synthesized THP-MESO was dissolved in water containing 2% of acetonitrile and 0.05% of formic acid and analysed by HRMS. The mass and elemental composition of the detected THP-MESO at 0.09-0.3 minutes retention time. This analysis was performed by Prof. Dmitri Filippov, Leiden institute of chemistry.

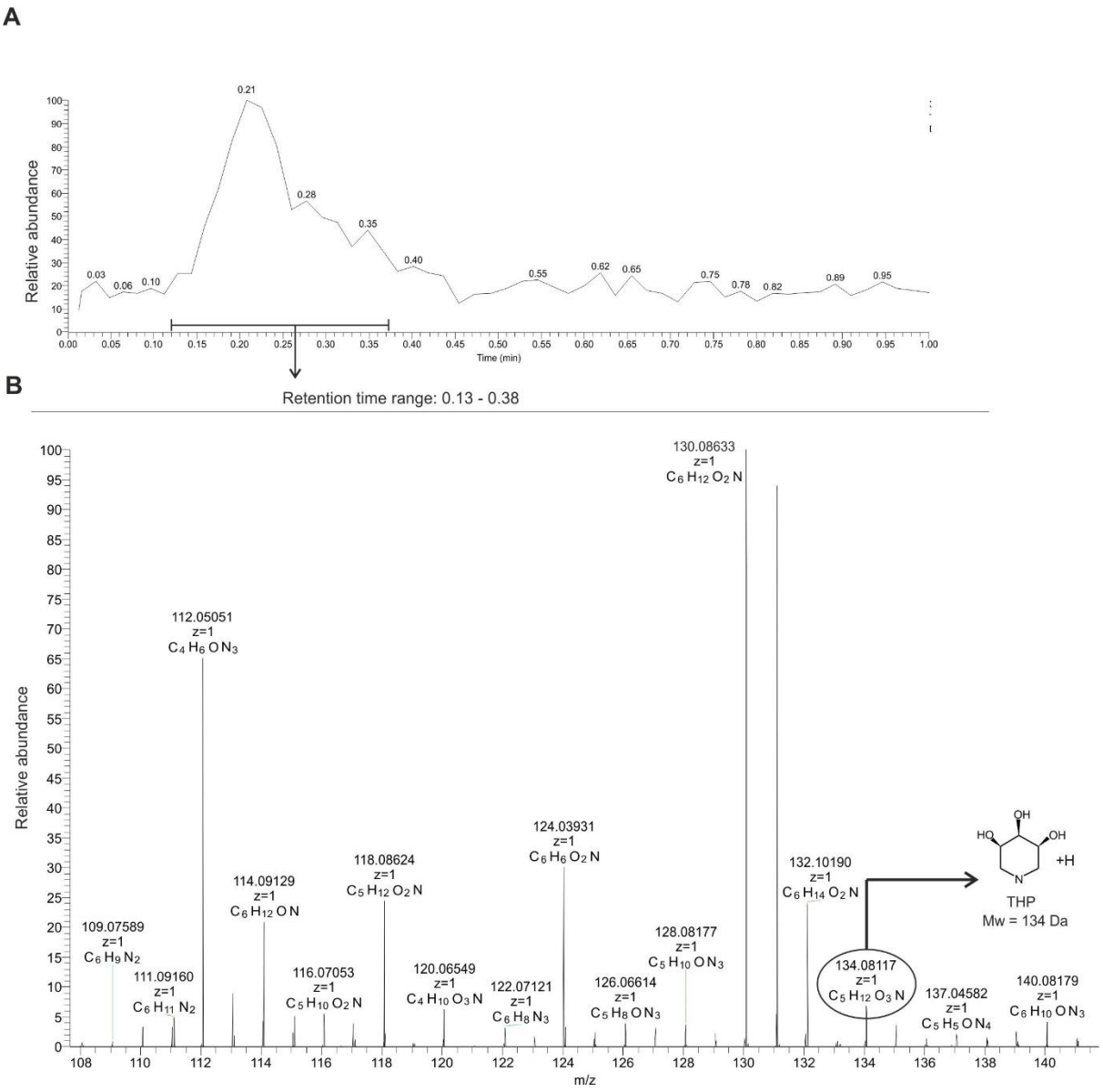

Figure 5.14 Trihydroxy piperidine (THP) is detected in fraction 2 after gel-filtration chromatography using HRMS

(A&B) The BGAL inhibitor enriched fraction 2 after gel-filtration were dissolved in water containing 2% of acetonitrile and 0.05% of formic acid and analysed by HRMS. The mass and elemental composition various compounds detected at 0.13-0.30 minutes retention time. This analysis was performed by Prof. Dmitri Filippov, Leiden Institute of Chemistry.

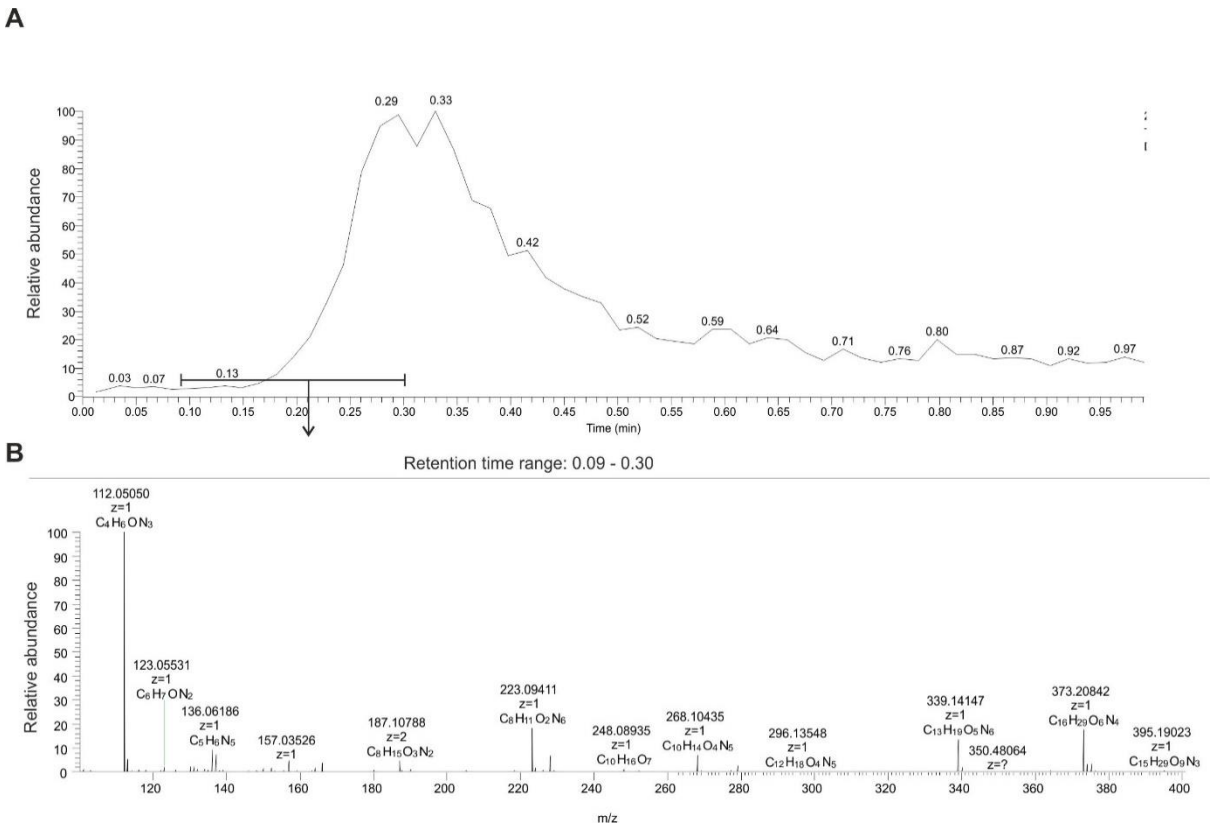

Figure 5.15 Trihydroxy piperidine (THP) is not detected in fraction 3 after gel-filtration chromatography using HRMS

(A&B) The BGAL inhibitor enriched fraction 2 after gel-filtration were dissolved in water containing 2% of acetonitrile and 0.05% of formic acid and analysed by HRMS. The mass and elemental composition various compounds detected at 0.13-0.30 minutes retention time. This analysis was performed by Prof. Dmitri Filippov, Leiden Institute of Chemistry.

5.2.5 Detection of candidate trihydroxy piperidine (THP) molecule from the *Pto*DC3000*(ΔHQ)* minimal medium sample using an improved protocol

In the GC-MS analysis of the NH_4OH eluate fraction from the *Pto*DC3000*(ΔHQ)* culture in minimal medium, glutamate co-eluted with the candidate THP (Figure 5.6B). The glutamate should have come from the medium which is not used by the bacteria. Hence, the protocol was adjusted to reduce glutamate as much as possible to improve the detection of candidate THP in the *Pto*DC3000*(ΔHQ)* inoculated minimal medium. Two major changes were made. First, the bacteria were grown in minimal medium as 2 ml aliquots in slanting position for 38 hours. The assumption is that growing bacteria in reduced volume and with longer incubation could complete the metabolization of glutamate present in the medium. Second, the methanol fraction was acidified to pH=3.75 instead of pH=3.5 before adding into the cation exchange to improve the binding of THP to the cation exchange column. Having these changes included in the protocol, a new NH_4OH eluate obtained from the *Pto*DC3000*(ΔHQ)* culture grown in minimal medium was analysed using GC-MS. The sample was silylated using MSTFA and the chromatograms were analysed using AMDIS. Interestingly, the candidate silylated-THP was detected in the peak at 27.2 minutes retention time from the *Pto*DC3000*(ΔHQ)* minimal medium sample (Figure 5.16A). The extracted ion chromatograms (EIC) of selected m/z fragments: 200, 215, 331 and 421 signify the presence the silylated THP molecule in the peak (Figure 5.16B). The peak contained almost all the m/z fragment of ions of silylated THP with traces of silylated glutamate having a base m/z fragment ion at 246 Da (Figure 5.16C). The extracted spectrum at 27.2 minutes retention time contained almost all the m/z fragment ions of the silylated THP (Figure 5.16D). This result indicates that the new developed protocol improved the detection of silylated THP in the *Pto*DC3000*(ΔHQ)* minimal medium sample.

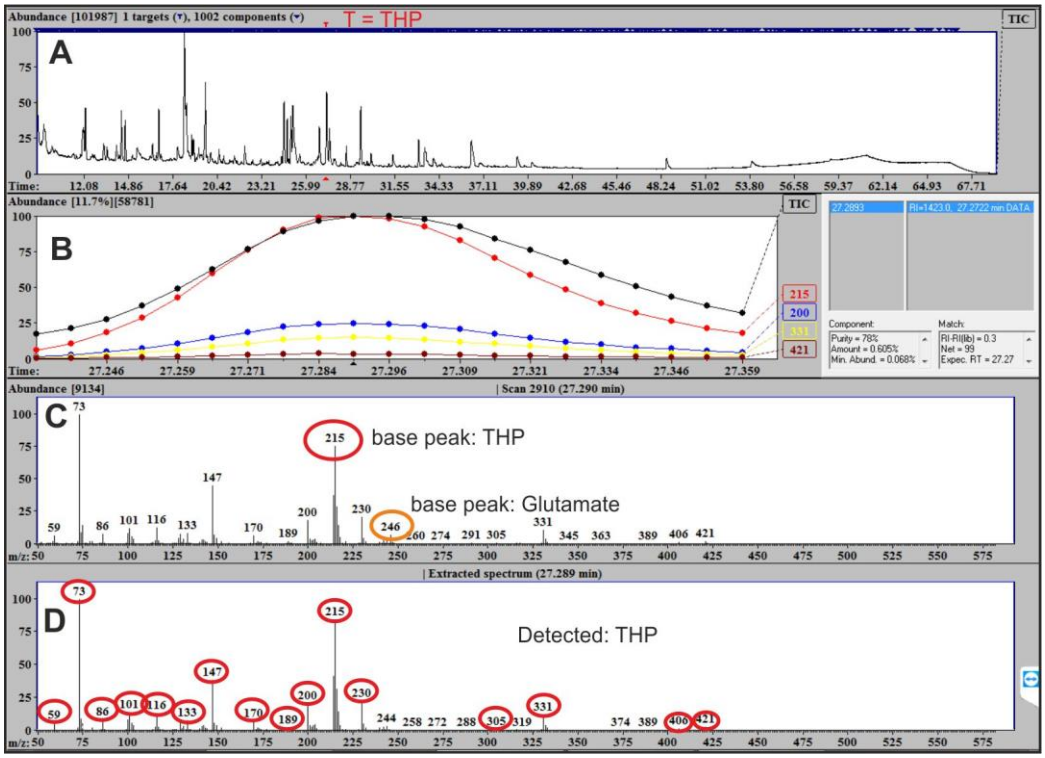

Figure 5.16 Detection of THP using an improved protocol

THP is detected in the *Pto*DC3000*(ΔHQ)* minimal medium sample. *Pto*DC3000*(ΔHQ)* was inoculated at O.D=0.5 in 500 ml mannitol glutamate minimal medium. This was further aliquoted into 2ml in the bacteria culture tubes and incubated at 23^{0}C. After for 38 hours of incubation, the medium was isolated and subjected to chloroform-methanol precipitation. The hydrophilic phase was freeze dried, dissolved in 50 ml water, acidified to pH=3.75 and loaded to the cation exchange dowex50 column. The NH_4OH eluate fraction was silylated using MSTFA at 60^{0}C for 90 minutes. The derivitized molecule was injected into the GC-MS and the chromatogram was analysed using AMDIS. The target silylated THP compound was searched in the total ion chromatogram (TIC) by deconvolution analysis. (A) The total ion chromatogram (TIC) of silylated NH_4OH eluate. The detected silylated THP in the TIC at 27.2 minutes retention time is indicated as T (Red). (B) The extracted ion chromatogram (EIC) of selected m/z fragments: 200, 215, 331 and 421 Da signify the detected silylated THP. (C) The mass/charge (m/z) fragment ions detected at 26.5 minutes retention time. The m/z fragment ion: 215 Da is the base peak of silylated THP (red) and m/z fragment ion: 246 Da is the base peak of silylated glutamic acid (orange). (D) The extracted spectrum contains the majority of m/z fragment ions of the detected silylated THP. The m/z fragment ions derived from silylated-THP molecule are indicated with red circles.

5.2.6 THP is detected in apoplastic fluids of *Nicotiana benthamiana* leaves upon *Pto*DC3000(*ΔHQ*) infection

To investigate if THP is produced during *Pto*DC3000 infection, *Pto*DC3000*(ΔHQ)* was infiltrated into leaves of *Nicotiana benthamiana*. At 2 dpi, the apoplastic fluids were isolated from *Pto*DC3000*(ΔHQ)* and mock infiltrated leaves. These apoplastic fluids were subjected to chloroform-methanol precipitation and the hydrophilic (methanol/water) and hydrophobic (chloroform) phases were separated and freeze dried. The freeze dried fractions were dissolved in water, passed through 3 kDa cut-off filters and the filtrate fractions (<3 kDa) were heated at 95 ^{0}C for 5 minutes (Figure 5.17A). Competitive ABPP was performed with the heated the filtrate fractions (<3 kDa) and apoplastic fluids isolated from the unchallenged leaves of *Nicotiana benthamiana* using JJB70. Importantly, in the *Pto*DC3000*(ΔHQ)* infiltrated sample, the BGAL inhibitor could be detected only in the hydrophilic (methanol/water) phase but not in the hydrophobic (chloroform) phase (Figure 5.17B). The BGAL inhibitor could not be detected in both hydrophilic phase (methanol/water) and hydrophobic phase (chloroform) of mock treated sample (Figure 5.17B). This result indicates that the BGAL inhibitor produced during infection with *Pto*DC3000*(ΔHQ)* is enriched in the hydrophilic (methanol/water) phase.

To detect the trihydroxy piperidine (THP), the freeze-dried methanol fraction obtained from apoplastic fluids of *Pto*DC3000*(ΔHQ)* and mock infiltrated leaves were dissolved in water, acidified to pH=3.75 and subjected to the cation exchange chromatography. The NH_4OH eluate fraction from these samples were subjected to GC-MS analysis. The samples were silylated using MSTFA and the GC-MS chromatograms were analysed using AMDIS. Importantly, the candidate silylated THP molecule was detected in the peak at 27.2 minutes retention time from the *Pto*DC3000*(ΔHQ)* sample but not the mock infiltrated treated sample (Figure 5.18A & 5.19A). The extracted ion chromatograms (EIC) of selected m/z fragments: 200, 215, 331 and 421 Da signify the presence the silylated THP molecule in the peak from *Pto*DC3000*(ΔHQ)* infiltrated leaves (Figure 5.18B). In both *Pto*DC3000*(ΔHQ)* and mock infiltrated samples, this fraction also contained the co-eluting silylated glutamate which has the base m/z fragment ion at 246.1 Da (Figure 5.18C & 5.19C). The extracted spectrum at retention time of 27.2 minutes contains the m/z fragment ions of the detected silylated-THP molecule from the *Pto*DC3000*(ΔHQ)* infiltrated sample (Figure 5.18D & 5.19C). In addition, the extracted spectrum at 27.2 minute retention time contains the m/z fragment ions of silylated glutamate from the mock infiltrated leaves (Figure 5.19C). These results demonstrate that THP is produced in the leaves of *Nicotiana benthamiana* during infection with *Pto*DC3000 (*ΔHQ*).

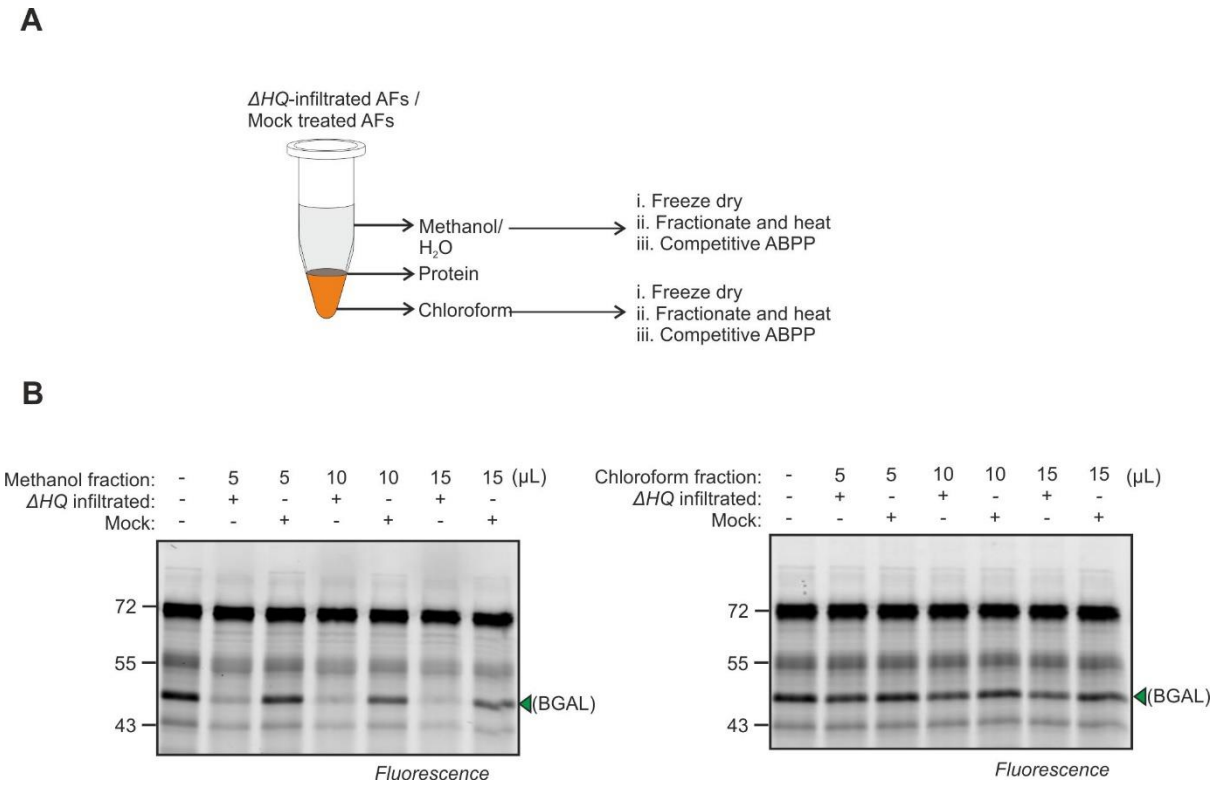

Figure 5.17 The BGAL inhibitor produced during *Pto*DC3000 infection is also a hydrophilic small molecule

(A) *N. benthamiana* leaves were infiltrated with *Pto*DC3000(Δ*HQ*) at 10^6 bacteria/ml or with water as control. Apoplastic fluids were isolated after 2 dpi from these samples and chloroform-methanol precipitation was performed by adding equal volumes of metabolite isolation buffer to 50 ml apoplastic fluids. (B) The BGAL inhibitor produced during *Pto*DC3000 infections is a methanol/water-soluble small molecule. The upper hydrophilic phase (methanol/ water) and the lower hydrophobic phase (chloroform) were collected and freeze-dried separately. The freeze-dried fractions were dissolved in water and concentrated using ultrafiltration spin colums to collect the <3 kDa low molecular weight compounds. The <3 kDa fractions were collected, heated at 95 ºC for 5 min and competitive ABPP was performed with the apoplastic fluids isolated from *N. benthamiana* leaves using JJB70.

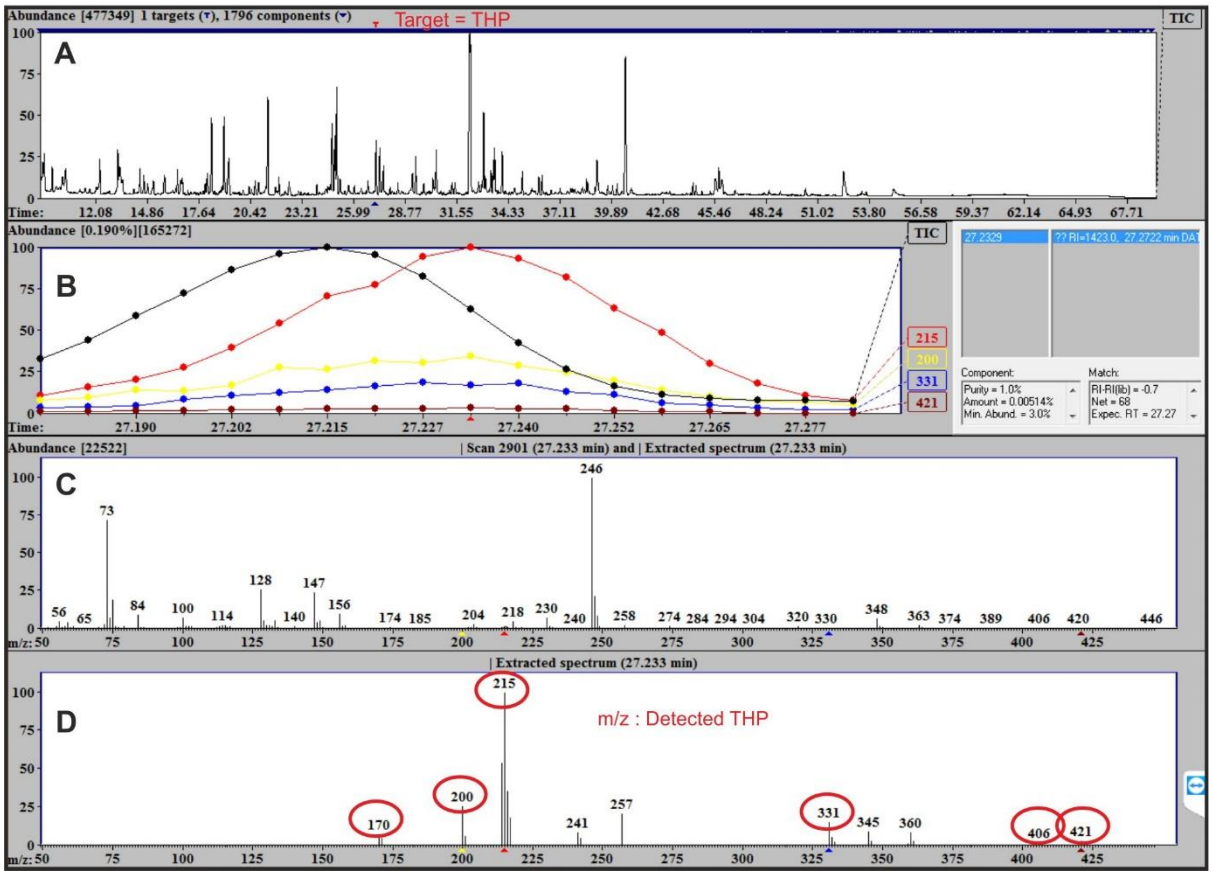

Figure 5.18 Trihydroxy piperidine (THP) is produced during infections with *Pto*DC3000

Large scale chloroform-methanol precipitation was performed with the 50 ml of apoplastic fluids isolated from *N. benthamiana* leaves infiltrated with *Pto*DC3000(*ΔHQ*). The freeze-dried hydrophilic phase (methanol/ water) was dissolved in 50 ml of water, adjusted to pH 3.75 and added to the prepared cation-exchange dowex50 column. The bound molecules to the cation-exchange column were eluted using 2.5 N ammonium hydroxide (NH_4OH) and the NH_4OH eluate was silylated using MSTFA reagent at 60 ºC for 90 minutes. The derivitized molecule was injected into GC-MS and the chromatogram was analysed using AMDIS. The target silylated THP compound was searched in the total ion chromatogram (TIC) by deconvolution analysis. (A) The total ion chromatogram (TIC) of silylated NH_4OH eluate from the *Pto*DC3000*(ΔHQ)*infiltrated sample. The analysed peak in the TIC at 27.2 minutes retention time is indicated as T (red). (B) The extracted ion chromatogram (EIC) of selected m/z fragments: 200, 215, 331 and 421 Da signify the detected silylated THP. (C) The mass/charge (m/z) fragment ions detected at 27.2 minutes retention time. The m/z fragment ion: 215 Da is the base peak of silylated THP and m/z fragment ion: 246 Da is the base peak of silylated glutamic acid. (D) The extracted spectrum which contains majority of m/z fragment ions of the detected silylated THP present in the *Pto*DC3000*(ΔHQ)* infiltrated sample. The m/z fragment ions representing the silylated THP molecule is indicated with red circles.

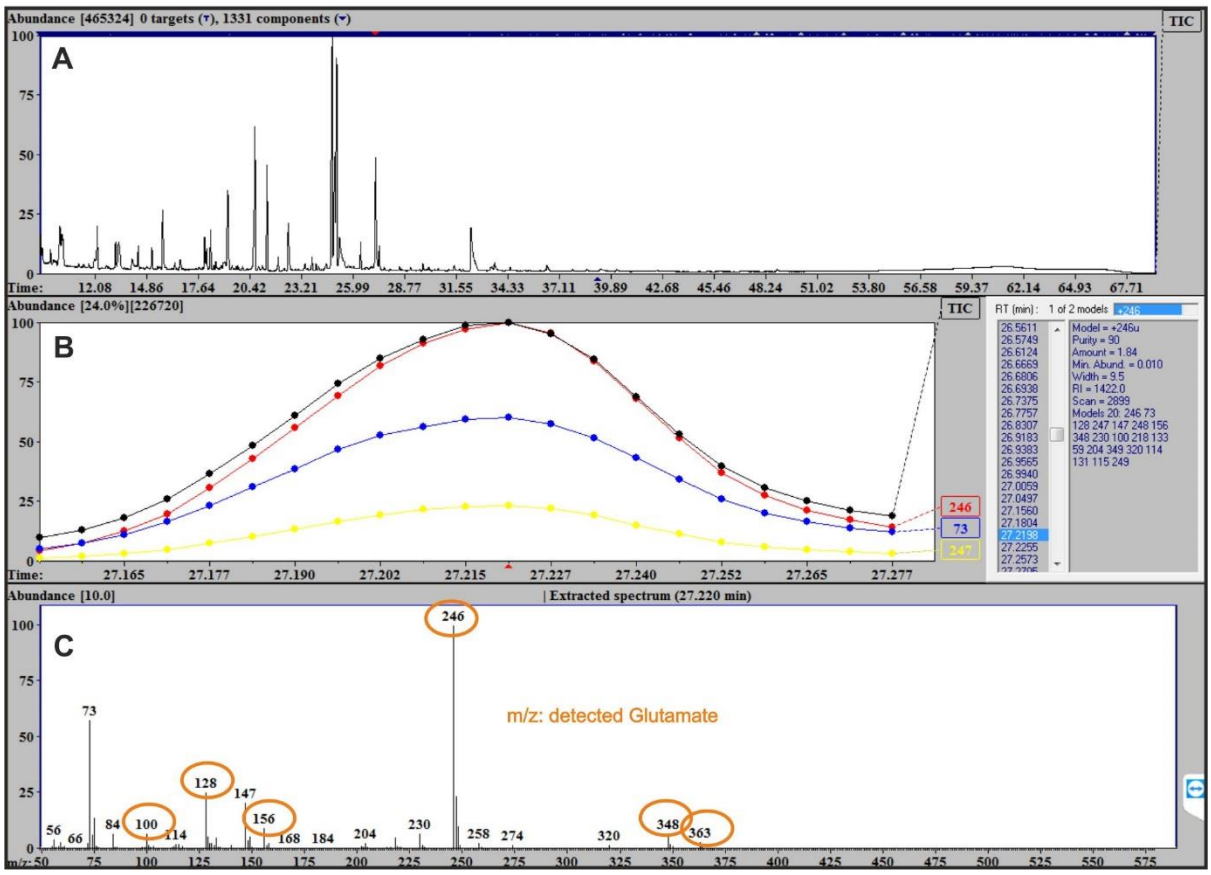

Figure 5.19 Trihydroxy piperidine (THP) is not detected in mock infiltrated leaves

(A) The total ion chromatogram (TIC) of silylated NH_4OH eluate from the mock infiltrated leaves sample. (B) The extracted ion chromatogram (EIC) of selected m/z fragments: 246, 73 and 247 signifying the detected silylated glutamic acid. (C) The mass/charge (m/z) fragment ions detected at 27.2 minutes retention time. The m/z fragment ion: 246 Da is the base peak of silylated glutamic acid. The m/z fragment ions representing the silylated glutamic acid is indicated as orange circles.

5.3 Discussion

5.3.1. 3,4,5 trihydroxy piperidine (THP) is the BGAL inhibitor produced by *Pto*DC3000

Several lines of evidence indicate that the 3,4,5-trihydroxy piperidine (THP) is the BGAL inhibitor produced by *Pto*DC3000*(ΔHQ)* during infection. First, the crystal soaking experiment using the microbial beta-galactosidase *Cj*BglGH35A and the BGAL enriched fraction from the *Pto*DC3000*(ΔHQ)* minimal medium has revealed the presence of the meso stereo isoform of THP near the active site of the enzyme (Figure 5.3B). Second, the chemically synthesized THP can inhibit the candidate apoplastic BGAL from *Nicotiana benthamiana* leaves (Figure 5.3B). Third, using GC-MS the presence of THP could be detected in the minimal medium sample from *Pto*DC3000*(ΔHQ)* but not two BGAL inhibitor mutant samples, *Δbim4* and *Δbim5*

(Figure 5.6A). Fourth, HRMS analysis on the BGAL inhibitor enriched fraction from the *Pto*DC3000*(ΔHQ)* minimal medium has the right mass and elemental composition of THP (Figure 5.14B). Fifth, using GC-MS, THP was detected only in apoplastic fluids of *Nicotiana benthamiana* leaves infiltrated with *Pto*DC3000*(ΔHQ)* but not in the mock controls (Figure 5.18A). In addition, the activity-guided enrichment assay revealed properties that perfectly correlate with the chemical property of THP. (Figures 5.1A, 5.1C and 5.17B). Taken together, the imino sugar THP is the putative BGAL inhibitor produced by *Pto*DC3000(*ΔHQ*).

5.3.2. Trihydroxy piperidine (THP-MESO-I) is the candidate stereoisomer produced by *Pto*DC3000*(ΔHQ)* to inhibit the BGAL from *N. benthamiana*

THP can exist in four different stereoisomeric forms (Figure 5.20). The stereoisomers I and II are meso compounds, due to the super-imposability of their mirror images. Different stereoisomers of trihydroxy piperidine (THP) has been shown to have moderate beta-galactosidase and other glycosidase inhibitory activities with tested enzymes. The stereoisomers II and IV has been shown to be potent beta-glucosidase and alpha-mannosidase inhibitors respectively (Bernotas et al., 1990); Genjiro-kusano et al., 1990). The stereoisomers I and III has been shown to have only moderate beta-galactosidase inhibitory activities with tested enzymes (Bernotas et al., 1990); Genjiro-kusano et al., 1990; (Front et al., 2016).

Due to the moderate inhibitory activity of stereoisomer I, additional groups like alkyl group have been added to this compound to increase the inhibitory activity towards beta-galactosidases in a recent study (Front et al., 2016). Hence there is a reasonable chance that the BGAL inhibitor, THP detected in apoplastic fluids of *Nicotiana benthamiana* might be stereoisomer I or III.

In this study, the electron density detected in the co-crystal demonstrated that the three hydroxyl groups are oriented in same direction, hence the stereoisomer I (THP-MESO-I) is at least one of the stereoisomer produced by *Pto*DC3000(*ΔHQ*). Moderate beta-galactosidase inhibitory activity of THP-MESO-I is in agreement with the fact that high concentration 4 mM of THP-MESO-I was required to inhibit the labelling of BGAL from *Nicotiana benthamiana* completely (Figure 5.3B). Convolution ABPP (Figure 3.5) and activity-guided enrichment experiments performed with *Pto*DC3000*(ΔHQ)* minimal medium sample (Figure 5.2) completely inhibited the labelling of BGAL present in apoplastic fluids of *Nicotiana benthamiana*. Hence under the minimal medium conditions, *Pto*DC3000 might produce large amounts of THP-MESO-I. To add further strength to the claim for THP-MESO-I to be the actual BGAL inhibitor, the THP produced in the apoplastic fluids during *Pto*DC3000 infection could be isolated to perform 1D and 2D-NMR. Also to determine the specificity, enzymatic assays with the purified BGAL enzyme the four stereoisomer of THP and could be performed to

determine the inhibition constants (Ki). Furthermore, chemical complementation experiments by supplementing trihydroxy piperidine (THP) to the BGAL inhibitor mutants (*Δbim*) should be also performed.

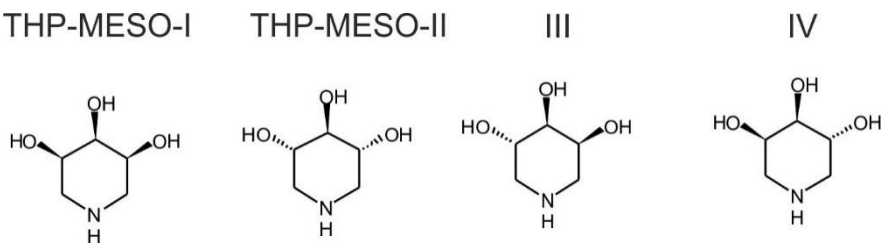

Figure 5.20 The four different stereoisomers of Trihydroxy piperidine (THP)

References

Asano, N. (2003). Glycosidase inhibitors: update and perspectives on practical use. Glycobiology *13*, 93R – 104R.

Bernotas, R.C., Papandreou, G., Urbach, J., and Ganem, B. (1990). A new family of five-carbon iminoalditols which are potent glycosidase inhibitors. Tetrahedron Lett. *31*, 3393–3396.

Du, X., and Zeisel, S.H. (2013). Spectral deconvolution for gas chromatography mass spectrometry-based metabolomics: current status and future perspectives. Comput. Struct. Biotechnol. J. *4*.

Emsley, P., Lohkamp, B., Scott, W.G., and Cowtan, K. (2010). Features and development of Coot. Acta Crystallogr. D Biol. Crystallogr. *66*, 486–501.

Front, S., Gallienne, E., Charollais-Thoenig, J., Demotz, S., and Martin, O.R. (2016). N-Alkyl, 1-C-Alkyl-, and 5-C-Alkyl-1,5-dideoxy-1,5-imino-(l)-ribitols as galactosidase inhibitors. ChemMedChem *11*, 133–141.

Kang, K.-D., Cho, Y.S., Song, J.H., Park, Y.S., Lee, J.Y., Hwang, K.Y., Rhee, S.K., Chung, J.H., Kwon, O., and Seong, S.-I. (2011). Identification of the genes involved in 1-deoxynojirimycin synthesis in *Bacillus subtilis* MORI 3K-85. J. Microbiol. Seoul Korea *49*, 431–440.

Larsbrink, J., Thompson, A.J., Lundqvist, M., Gardner, J.G., Davies, G.J., and Brumer, H. (2014). A complex gene locus enables xyloglucan utilization in the model saprophyte *Cellvibrio japonicus*. Mol. Microbiol. *94*, 418–433.

Lisec, J., Schauer, N., Kopka, J., Willmitzer, L., and Fernie, A.R. (2006). Gas chromatography mass spectrometry–based metabolite profiling in plants. Nat. Protoc. *1*, 387–396.

Nash, R.J., Kato, A., Yu, C.-Y., and Fleet, G.W. (2011). Iminosugars as therapeutic agents: recent advances and promising trends. Future Med. Chem. *3*, 1513–1521.

Toshiaki, S., Makio, S and Genjiro, K (1995). Three trihydroxy piperidines, glycosidase inhibitors, from *Eupatorium fortune* TURZ. Nature medicines 49, 332-335

Chapter 6: Biological significance of BGAL inhibition during *Pto*DC3000 infection

6.1 Introduction

In the previous chapter it was found that *Pto*DC3000 produces a trihydroxy piperidine (THP) to inhibit an apoplastic beta-galactosidase (BGAL) from *Nicotiana benthamiana*. Two important questions can be raised based on this observation. First, what is the biological significance of BGAL inhibitor production by *Pto*DC3000 during infection? Second, does BGAL from *N. benthamiana* play a role during infections with *Pto*DC3000? The BGAL inhibitor mutants (*Δbim*) will be helpful to address biological significance of BGAL inhibitor production by *Pto*DC3000. The virulence of *Pto*DC3000 as a result of loss of inhibitor production can be studied through pathogen assays with wild-type *N. benthamiana*. In Chapter 4, it was found that the *hrpRS* operon is responsible for regulating the BGAL inhibitor production in *Pto*DC3000. *hrpR/S* together with *hrpL* are important in regulating the Type-III secretion system in *Pto*DC3000 (Hutcheson et al., 2001). *hrpS* and *hrpL* genes also regulate the expression of all known Type-III effectors genes associated with virulence (Zwiesler-Vollick et al., 2002). Hence the BGAL inhibitor produced in the apoplast might also be an important and unexplored virulence-associated compound produced by *Pto*DC3000.

In this chapter, the significance of BGAL inhibition at the plant-pathogen interface is investigated. Reverse genetics combined with pathogen assays will be employed to understand the importance of the candidate BGAL present in the apoplast of *N. benthamiana* leaves. Furthermore, the well-characterized *Δbim4 (hrpRS*) and *Δbim5 (gabT-1*) mutants and other BGAL inhibitor mutants will be used for pathogen assays to unravel the biological significance of BGAL inhibitor production by *Pto*DC3000.

6.2 Results

6.2.1 Depletion of BGAL levels in *Nicotiana benthamiana* favours the growth of *Pto*DC3000(*ΔHQ*)

To investigate the importance of BGAL during infections, transcript levels of the *BGAL* gene were suppressed using virus-induced gene silencing (VIGS) (Lu et al., 2003). Two different constructs, *TRV::BGALa* and *TRV::BGALb* were created to silence the *BGAL* gene (Figure 6.1A). *TRV::BGALa* carried a 300 bp fragment of the *BGAL* gene (NbS00024332g0007) cloned into the pTRV2 vector (Senthil-Kumar and Mysore, 2014). *TRV::BGALb* carried a different 500 bp fragment from the same *BGAL* gene cloned into the pTRV2 vector. The fragments for the *BGAL* silencing were selected using the VIGS tool available in the

solgenomics website (Fernandez-Pozo et al., 2015). VIGS was initiated in *N. benthamiana* plants upon infiltration of pTRV1 with *TRV::BGALa* or *TRV::BGALb*. In this experiment, an Agrobacterium strain carrying TRV with a fragment from Green Fluorescent Protein (*GFP*) (*TRV::GFP*) gene was used as a negative control.

To investigate the effect of *BGAL* silencing, the apoplastic fluids were isolated from *TRV::BGAL* and *TRV::GFP* plants and labelled with JJB70. Interestingly, the active BGAL enzyme could not be detected in the apoplastic fluids of *TRV::BGALa* plants generated and BGAL labelling was not affected in the *TRV::GFP* control plants (Figure 6.1A). Furthermore, the *TRV::BGALa* plants appeared consistently shorter in height compared to the *TRV::GFP* control plants (Figure 6.1B). In *TRV::BGALb* plants, the active BGAL enzyme could still be detected in apoplastic fluids but the intensity of labelling was reduced compared to the *TRV::GFP* control plants (Figure 6.1A). This result indicates that the VIGS using *TRV::BGALa* is more efficient to deplete BGAL from *Nicotiana benthamiana*.

To investigate the effect of *BGAL* gene silencing on pathogen growth, *Pto*DC3000(*ΔHQ*) bacteria were infiltrated into the leaves of the VIGS plants generated using *TRV::BGALa* and *TRV::BGALb*. The growth of *Pto*DC3000(*ΔHQ*) inside the plant was quantified using the standard colony counting assays (Katagiri et al., 2002). Interestingly, *Pto*DC3000(*ΔHQ*) grows significantly more in the *TRV::BGALa* plants compared to the *TRV::GFP* control plants (Figure 6.1C). The growth of *Pto*DC3000(*ΔHQ*) in the *TRV::BGALb* compared to the TRV:: GFP control plants was not significantly different (Figure 6.1C). This experiment was repeated twice with four biological replicates and similar results were observed. In the third repetition time no significant growth difference of the *Pto*DC3000(*ΔHQ*) bacteria was observed between *TRV::BGALa* plants and the *TRV::GFP* control plants. However, in this third assay when apoplastic fluids were isolated from the wild-type *N. benthamiana* plants and labelled with JJB70, active BGAL could not detected in these plants. The reason for not detecting active BGAL in the wild-type plants is not known. Taken together, this result indicates that the depletion of BGAL levels using *TRV::BGALa* favours growth of *Pto*DC3000(*ΔHQ*) in leaves of *N. benthamiana*.

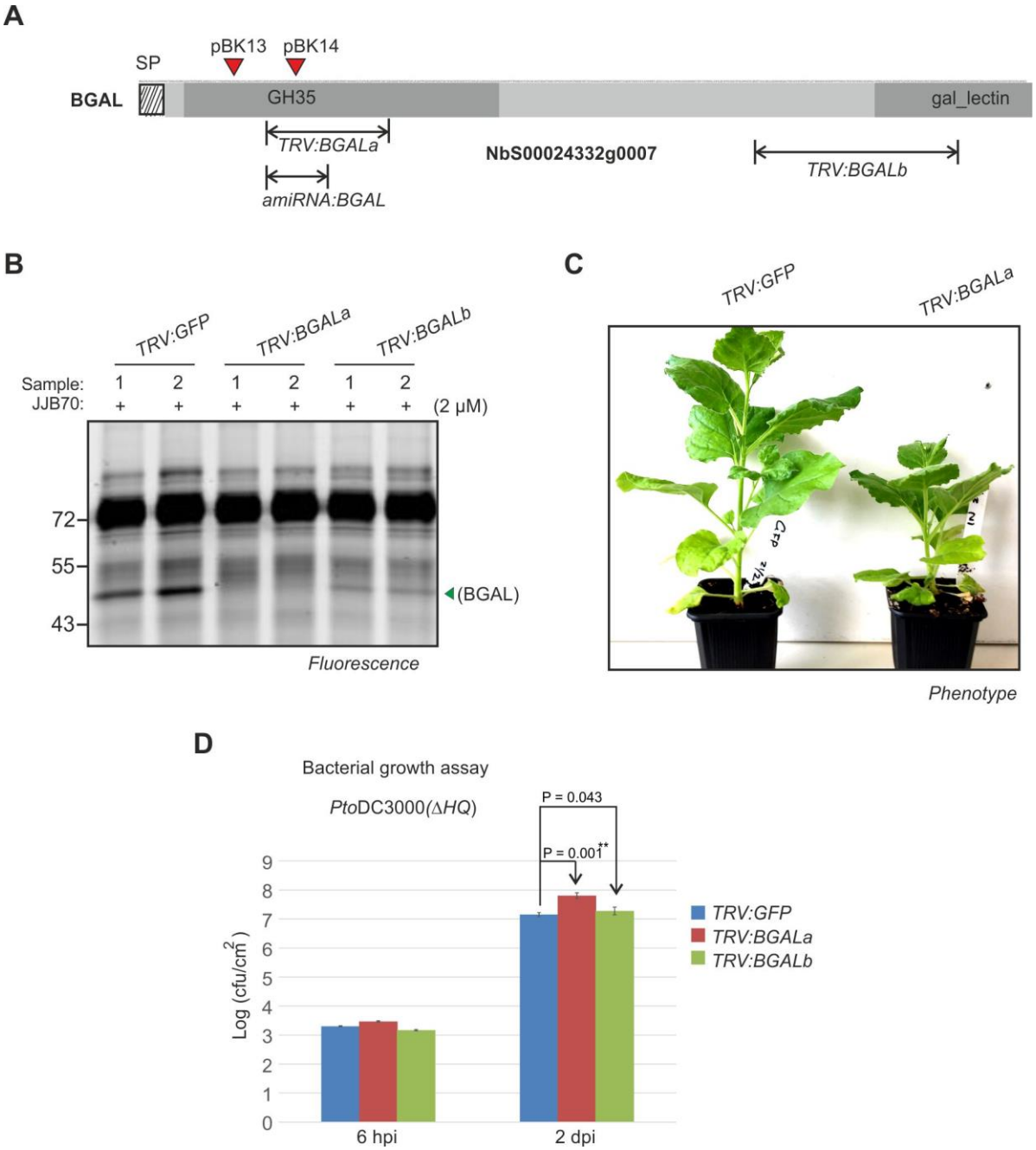

Figure 6.1 BGAL depleted plants are more susceptible to *Pto*DC3000(*ΔHQ*)

(A) Fragments to silence *BGAL* gene expression. *TRV::BGALa* carried a 300 bp fragment of the *BGAL* gene (NbS00024332g0007) cloned into the pTRV2 vector. *TRV::BGALb* carried a different 500 bp fragment from the same *BGAL* gene cloned into the pTRV2 vector. *amiRNA:BGAL* construct carried a 75 bp fragment from the *BGAL* gene. pBK13 and pBK14 carried a 20 bp guide RNA which were designed to target two different locations: at 106 bp and 147 bp respectively, on the *BGAL* gene. (B) Knock-down of *BGAL* gene expression using virus-induced gene silencing (VIGS). Three different Agrobacterium strains carrying the *TRV::BGALa*, *TRV::BGALb* or *TRV::GFP* were mixed individually with the Agrobacterium strain carrying pTRV1 vector in 1:1 ratio. The mixed cultures having OD = 0.5 were infiltrated into leaves of 10 day old *N. benthamiana* plants and incubated at 23^0C degrees in the growth chamber. After 3 weeks, apoplastic fluids were isolated from the infiltrated plants and labelled with 2 µM JJB70 for 1 h at pH 5.0. Labeled proteins were detected by in-gel fluorescent scanning. Proteins were detected by

SYPRO Ruby staining. (C) *TRV::BGALa* plants appeared shorter in height compared to the *TRV::GFP* control plants. A representative from the *TRV::GFP* and *TRV::BGALa* infiltrated *N. benthamiana* plants were photographed at 5 weeks after infiltration. The phenotype was observed consistently in all experiments. (D) The *BGAL* silenced plants are more susceptible to *Pto*DC3000(*ΔHQ*). *N. benthamiana* leaves were infiltrated with *Pto*DC3000(Δ*HQ*) at $2X10^5$ bacteria/ml. The leaf discs were isolated from the *N. benthamiana* plants at 4 hours post infiltration (hpi) and 2 days post infiltration, surface sterilized with 15% hydrogen peroxide and ground in 1ml water. The samples were then serially diluted with water, plated onto LB medium and incubated at 28^0C. After 36 hours, the colony forming units (CFU) were counted. Error bars represent SEM of four independent biological replicates. Student's *t*-test was used to calculate P-values. The experiment was repeated twice with similar results.

6.2.3 The BGAL inhibitor contributes to virulence of *Pto*DC3000

To understand the biological significance of the BGAL inhibitor production, the BGAL inhibitor mutants, *Δbim4* (*hrpR/S*) and *Δbim5* (*gabT-1*) were used for growth assays (Chapter 4). The bacterial strains were infiltrated into leaves of *N. benthamina* and the growth of bacteria was quantified using standard colony counting assays (Katagiri et al., 2002). Notably, the growths of *Δbim4* and *Δbim5* were significantly reduced compared to the parent *Pto*DC3000(*ΔHQ_lacZ*) strain. Furthermore, the growth of *Δbim4* was drastically reduced compared to the *Δbim5* and the bacterial growth population declined even at 1 and 2 dpi compared to 2 hpi (Figure 6.2A).

To investigate if the *Δbim4* and *Δbim5* are also compromised in their growth *in vitro*, these bacteria strains were grown under the apoplast mimicking minimal medium conditions and the growth of these bacteria was monitored using a plate reader. Importantly, the *Δbim5* and *Pto*DC3000(*ΔHQ_lacZ*) had similar growth rate and whereas the growth rate of *Δbim4* was slightly higher than *Δbim5* and *Pto*DC3000(*ΔHQ_lacZ*) (Figure 6.2B). Taken together, these results indicate that the BGAL inhibitor mutants *Δbim4* and *Δbim5* are reduced in virulence only inside the *N. benthamina* leaf tissues, implicating that the BGAL inhibitor might contribute to virulence of *Pto*DC3000.

To investigate, if other the BGAL inhibitor mutants are also reduced in their virulence, the bacterial strains *Pto*DC3000(Δ*HQ_lacZ*), Δ*bim7*, Δ*bim9,* Δ*bim12* and Δ*bim21* were infiltrated into the leaves of *N. benthamina* and growth of bacteria was quantified using standard colony counting assays. Growth of these selected BGAL inhibitor mutants were significantly reduced when compared to the parent *Pto*DC3000(*ΔHQ_lacZ*) (Figure 6.3B). Furthermore, the growth of *Δbim12* was drastically reduced compared to the other tested BGAL inhibitor mutants (Figure 6.3B). Hence the *Δbim12* mutant might have been disrupted for a major transcriptional regulator similar to *Δbim4* lacking *hrpRS*. The other BGAL inhibitor mutants, (Δ*bim7*, Δ*bim9* and Δ*bim21*) display slightly reduced virulence similar to *Δbim5* (*gabT-1*) and therefore might been disrupted for a biosynthesis gene for BGAL inhibitor

production. Hence it will be interesting to identify the disrupted genes in these mutants due to the insertion of *mini-tn5* transposons.

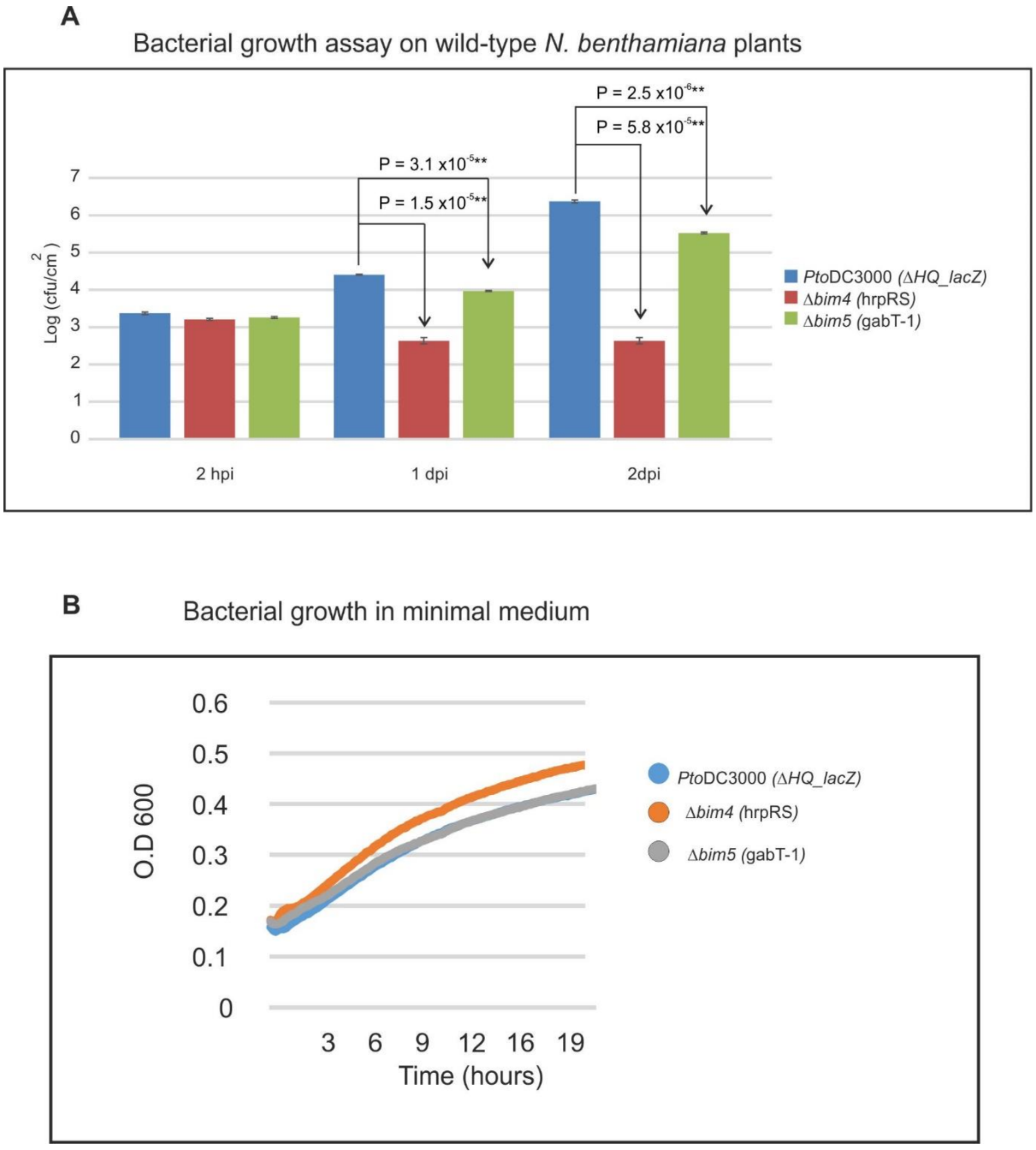

Figure 6.2 *Δbim4* and *Δbim5* mutants display reduced virulence upon infection

(A) Bacterial growth assay on wild-type *N. benthamiana* plants using the BGAL inhibitor mutants (*Δbim*). *N. benthamiana* leaves were infiltrated with *Pto*DC3000(Δ*HQ_lacZ*), Δ*bim4* and Δ*bim5* strains at 2X10^5 bacteria/ml. Leaf discs were isolated from the *N. benthamiana* plants at 2 hours post infiltration (hpi), 1 dpi, and 2 dpi, surface sterilized with 15% hydrogen peroxide and ground in 1ml water. The samples were then serially diluted with water, plated on LB medium and incubated at 28^{0}C. After 36 hours, the colony forming units (CFU) were counted. Error

bars represent SEM of three independent biological replicates. Student's *t*-test was used to calculate P-values. The experiment was repeated the second time with four biological relicates with similar results. (B) Bacterial growth assay on mannitol-glutamate minimal medium using the BGAL inhibitor mutants (*Δbim*). The bacterial strains *Pto*DC3000(Δ*HQ_lacZ*), Δ*bim4* and Δ*bim5* strains were grown in LB medium. The overnight cultures were re-inoculated in the mannitol-glutamate medium at O.D=0.1 and growth of the bacteria was monitored using a plate reader. The experiment was repeated three time with similar results.

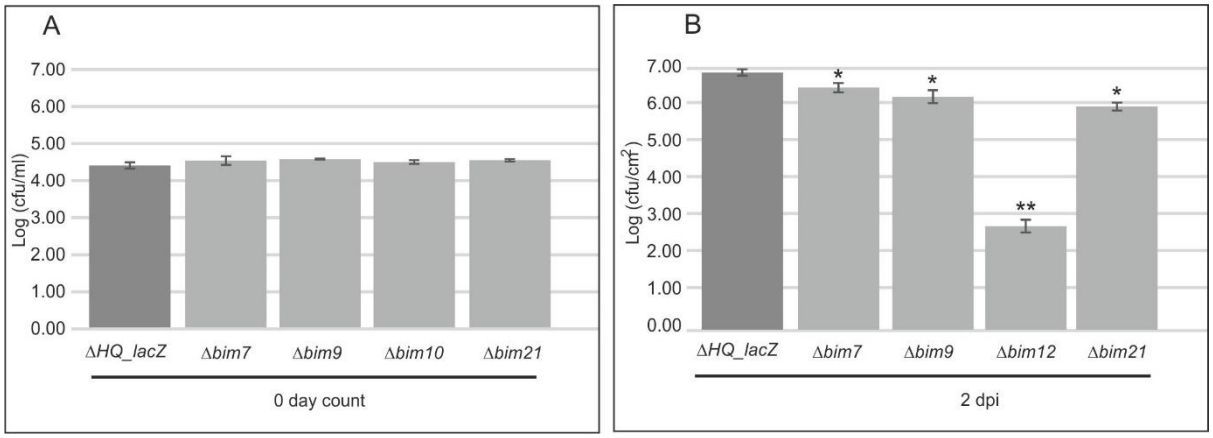

Figure 6.3 Other BGAL inhibitor mutants also display reduced virulence upon infection

(A) Bacterial growth assay on wild-type *N. benthamiana* plants using the BGAL inhibitor mutants (*Δbim*). The bacterial strains *Pto*DC3000(Δ*HQ_lacZ*), Δ*bim7*, Δ*bim9,* Δ*bim12* and Δ*bim21* used for the growth assay were diluted $2X10^5$ bacteria/ml. The diluted bacterial solutions were serially diluted with water, plated on LB medium and incubated at 28^0C. After 36 hours, the colony forming units (CFU) were counted. Error bars represent SEM of three independent biological replicates. (B) *N. benthamiana* leaves were infiltrated with the diluted bacterial strains at $2X10^5$ bacteria/ml. The leaf discs were excised from *N. benthamiana* plants at 2 dpi, surface sterilized with 15% hydrogen peroxide and ground in 1ml water. The samples were then serially diluted with water, plated on LB medium and incubated at 28^0C. After 36 hours, the colony forming units (CFU) were counted. Error bars represent SEM of four independent biological replicates. Student's *t*-test was used to calculate P-values.The experiment was done once with four biological replicates except for Δ*bim21*. The Δ*bim21* pathogen assay was performed by David Miron the second time with four biological replicates with similar results.

6.2.4 Silencing of *BGAL* gene expression using amiRNA technology

To generate stable transgenic plants which are silenced of *BGAL* gene expression, the transcript levels of the *BGAL* gene were suppressed using artificial microRNA (amiRNA) technology (Carbonell et al., 2014). The *amiRNA:BGAL* construct carried a 75 bp fragment from the *BGAL* gene cloned into the *pMDC123SB-AtMIR390a-B/c* vector (highlighted in Figure 6.1A). The construct was transformed into *N. benthamiana* plants using Agrobacterium medium transformation. To investigate the effect of *BGAL* silencing, apoplastic fluids were isolated from the primary transformants (T_0) of *T_0-amiRNA:BGAL* plants and labelled with JJB70. Interestingly, the active BGAL enzyme could not be detected in the *T_0-amiRNA:BGAL*

plant 2 and labeling of BGAL was not affected in the other *T_0-amiRNA:BGAL* plants or the wild-type *N. benthamiana* plant (Figure 6.4A). The seeds were collected from *the T_0-amiRNA:BGAL* plant 2 and its T_1 progeny was screened for *BGAL* silencing using RT-PCR. Importantly, the transcript levels of the *BGAL* gene were suppressed in the *T_1-amiRNA:BGAL* plant 9 (ami9) compared to other *T_1-amiRNA:BGAL* plants and the wild type *N. benthamiana* plant (Figure 6.4B). The seeds of *T_1-amiRNA:BGAL* plant 9 (ami9) were collected and their T_2 progenies were screened for *BGAL* silencing using RT-PCR. This analysis showed that the tested T_2 plants were not silenced for the *BGAL* gene expression and hence stable transgenic *amiRNA:BGAL* lines which are silenced for *BGAL* gene expression could not be obtained in the T_2 generation (data not shown).

In addition, two different constructs for knocking out the *BGAL* gene in *Nicotiana benthamiana* plants were created using the CRISPR/Cas9 technology (Bortesi and Fischer, 2015). The pBK13 and pBK14 carried a 20 bp guide RNA which were designed to target two different locations: at 106 bp and 147 bp respectively, on the *BGAL* gene (highlighted in Figure 6.1A). These constructs were transformed into *N. benthamiana* plants using Agrobacterium medium transformation techniques. The primary transformants (T_0), are being screened for the *BGAL* gene knock out.

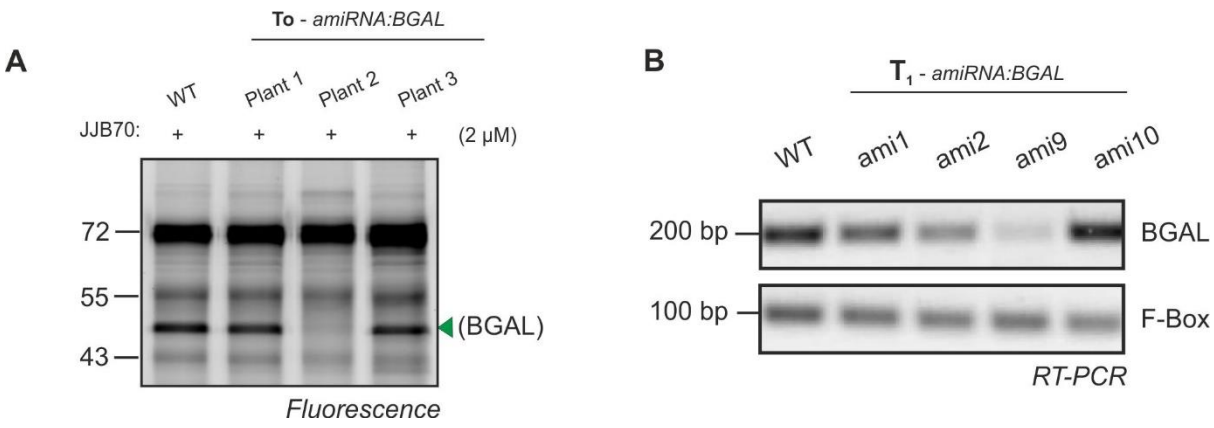

Figure 6.4 Silencing of *BGAL* gene expression using amiRNA technology

(A) Knock-down of *BGAL* gene expression using artificial microRNA (amiRNA) technology. The *amiRNA:BGAL* construct was transformed into *N. benthamiana* plants using Agrobacterium-mediated transformation techniques. Apoplastic fluids were isolated from three primary transformants (T_0) of *T_0-amiRNA:BGAL* plants and labelled with 2 µM JJB70 for 1 h at pH 5.0. Labeled proteins were detected by in-gel fluorescent scanning. (B) RT-PCR analysis of *T_1-amiRNA:BGAL* plants. RNA were isolated from the leaf tissues and converted into cDNA. The obtained cDNA was used as template for RT-PCR using gene-specific primers for *BGAL*. The RT-PCR was also performed with these samples using gene-specific primers for *F-Box* to show the equal the amount of RNA used for the analysis.

6.3 Discussion

6.3.1 Efficient silencing of *BGAL* gene expression using *TRV::BGALa*

Of the two constructs designed for virus-induced gene silencing (VIGS), *TRV::BGALa* was more efficient in silencing the *BGAL* gene expression. Robust depletion of active BGAL levels could be detected in the apoplastic fluids of VIGS plants generated using *TRV::BGALa* compared to *TRV::BGALb*. This is in agreement with the fact that gene fragments larger than 300 bp in VIGS are less efficient in gene silencing (Senthil-Kumar and Mysore, 2014). Hence the *TRV::BGALa*, which carries the 300bp fragment of the *BGAL* gene is the best construct to silence the *BGAL* gene expression in *N. benthamiana* using VIGS.

6.3.2 Active BGAL might have a functional role during plant-pathogen interactions

Increased growth of *Pto*DC3000(*ΔHQ*) was detected in *TRV::BGALa* plants in which the active BGAL levels were depleted. This increased growth of *Pto*DC3000(*ΔHQ*) was not observed on *TRV::BGALb* plants in which the active BGAL could be still detected. The increased bacterial growth in *TRV::BGALa* plants was also not observed when no active BGAL was detected in control plants. Hence, BGAL in *N. benthamiana* plants suppresses *Pto*DC3000 growth.

6.3.3 Loss of inhibitor production reduces the virulence of *Pto*DC3000

In the pathogen growth assay, BGAL inhibitor mutants *Δbim4* and *Δbim5* displayed reduced growth on wild-type *N. benthamiana* leaves when compared to *Pto*DC3000(*ΔHQ_lacZ*). By contrast, these strains had similar growth rate under *in vitro* conditions. Hence the reduced growth of *Δbim4* and *Δbim5* on wild-type *N. benthamiana* plants reflects their reduced virulence during infections. Of the two mutants, the growth of *Δbim4* was drastically reduced and declined from their inoculation levels compared to *Δbim5* on the wild-type plants. This was expected because the *hrpR* gene is disrupted in the *Δbim4* mutant (Figure 4.3B). The *hrpR/S* operon is a major regulator of the Type-III secretion system and Type-III effectors. The *Δbim4* bacteria are therefore severely reduced in their virulence (Xin and He, 2013). The loss of BGAL inhibitor production in *Δbim4* might not be the major reason their reduced virulence. In contrast, in the *Δbim5* mutant, the loss of BGAL inhibitor production might be the major reason for its reduced virulence, because it carries a disrupted *gabT-1* gene or *gabT-1* operon which might be required for BGAL inhibitor biosynthesis. Furthermore, the other tested BGAL inhibitor mutants also displayed reduced virulence in pathogen assays. These data indicate that the BGAL inhibitor is a novel virulence factor produced by *Pto*DC3000. Nevertheless, to add further strength to the claim to THP being this virulence factor, chemical complementation experiments by supplementing THP to the BGAL inhibitor mutants should be performed. In

addition, pathogen assay with the *Δbim* mutants on the BGAL depleted plants would be helpful to show that BGAL is the main target of THP.

6.4 References

Bortesi, L., and Fischer, R. (2015). The CRISPR/Cas9 system for plant genome editing and beyond. Biotechnol. Adv. *33*, 41–52.

Carbonell, A., Takeda, A., Fahlgren, N., Johnson, S.C., Cuperus, J.T., and Carrington, J.C. (2014). New generation of artificial MicroRNA and synthetic trans-acting small interfering RNA vectors for efficient gene silencing in Arabidopsis. Plant Physiol. pp.113.234989.

Fernandez-Pozo, N., Menda, N., Edwards, J.D., Saha, S., Tecle, I.Y., Strickler, S.R., Bombarely, A., Fisher-York, T., Pujar, A., Foerster, H., et al. (2015). The Sol Genomics Network (SGN)--from genotype to phenotype to breeding. Nucleic Acids Res. *43*, D1036–D1041.

Hutcheson, S.W., Bretz, J., Sussan, T., Jin, S., and Pak, K. (2001). Enhancer binding proteins HrpR and HrpS interact to regulate hrp-Encoded Type-III protein secretion in *Pseudomonas syringae* Strains. J. Bacteriol. *183*, 5589–5598.

Katagiri, F., Thilmony, R., and He, S.Y. (2002). The *Arabidopsis thaliana-Pseudomonas Syringae* Interaction. Arab. Book Am. Soc. Plant Biol. *1*.

Lu, R., Martin-Hernandez, A.M., Peart, J.R., Malcuit, I., and Baulcombe, D.C. (2003). Virus-induced gene silencing in plants. Methods *30*, 296–303.

Senthil-Kumar, M., and Mysore, K.S. (2014). Tobacco rattle virus–based virus-induced gene silencing in *Nicotiana benthamiana*. Nat. Protoc. *9*, 1549–1562.

Xin, X.-F., and He, S.Y. (2013). *Pseudomonas syringae* pv. tomato DC3000: a model pathogen for probing disease susceptibility and hormone signaling in plants. Annu. Rev. Phytopathol. *51*, 473–498.

Zwiesler-Vollick, J., Plovanich-Jones, A.E., Nomura, K., Bandyopadhyay, S., Joardar, V., Kunkel, B.N., and He, S.Y. (2002). Identification of novel hrp-regulated genes through functional genomic analysis of the *Pseudomonas syringae* pv. tomato DC3000 genome. Mol. Microbiol. *45*, 1207–1218.

Chapter 7: Involvement of Papain-like cys proteases to mature the BGAL enzyme

7.1 Introduction

During my PhD studies, I was involved in a project to identify the active Papain-like Cysteine Proteases (PLCPs) present in the apoplastic fluids of *Nicotiana benthamiana*. The project aims to deplete PLCPs that degrades pharmaceutically important antibodies during the transient expression of proteins using Agroinfiltration technique (Kapila et al., 1997). During this study, the observation was made that the presence of full length BGAL protein was detected in *N. benthamiana* plants which were silenced for *PLCPs*. Hence the activity of BGAL protein could be regulated by PLCPs present in the apoplast of *Nicotiana benthamiana* plants.

In this chapter, the involvement of apoplastic PLCPs to mature BGAL is investigated. The full length *BGAL* gene was cloned with a Strep-II epitope tag into a binary plasmid vector and transiently expressed in the plants silenced for *PLCPs*. The BGAL was detected by western blotting and immuno-detection using anti-Strep-II antibodies.

7.2 Results

7.2.1 The active BGAL at 45 kDa is a truncated protein

In the chapter 2, we found that the identified peptides of BGAL originate from the GH35 catalytic domain and not from the C-terminal half of this protein (Figure 2.8D). This indicates that BGAL accumulates as a 45 kDa truncated protein consisting of only the catalytic domain, consistent with the 45 kDa signal detected upon JJB70 labeling.

7.2.2 Profiling active PLCPs in the apoplast using DCG-04

To investigate extracellular proteases, we identified active PLCPs in the apoplast of *Nicotiana benthamiana*, an important model plant for expressing pharmaceutical important antibodies. The apoplast contains many PLCPs involved in plant defense (Jashni et al., 2015; Misas-Villamil et al., 2016; Shabab et al., 2008) and these PLCPs might degrade the expressed pharmaceutical important antibodies.

To monitor the apoplastic PLCPs which are active during Agroinfiltration, *N. benthamiana* leaves were infiltrated with Agrobacterium strain GV3101:pMP90 carrying the silencing inhibitor p19 expression plasmid at OD=0.5 or the infiltration buffer. At 4 dpi, the apoplastic proteomes were isolated from these *N. benthamiana* leaves and pre-incubated with or without cysteine protease inhibitor E-64 (Matsumoto et al., 1999) for 30 minutes. The pre-incubated proteomes were then labelled with 10 µM DCG-04 probe for 4 hours. The DCG-04 probe consists of a electrophilic E-64 as warhead and biotin reporter tag (Greenbaum et al.,

2000). The DCG-04 probe has been applied in plants to display the activities of several PLCPs (van der Hoorn et al., 2004).

To identify the labeled proteins, biotinylated proteins were purified, separated on protein gels and detected by SYPRO Ruby staining. Three protein bands could be detected in the 43-36 kDa region from the DCG-04-labelled samples and these signals were absent in the samples pre-incubated with E-64 (Figure. 7.1A). The three protein bands and the corresponding regions from the mock treated apoplastic fluid sample were excised and treated with trypsin. MS analysis of the peptides identified 11 different proteases from six different PLCP sub families: RD21, CTB, XBCP, XCP, RD19 & ALP (Figure. 7.1A). Importantly, seven active PLCPs were detected only in the agroinfiltrated sample compared to the mock control. Six active PLCPs were detected in both agroinfiltrated and mock control samples. Of these six active PLCPs, two from the sub families RD21 (RD50) and CTB (CTB48) were detected in high abundance in the agroinfiltrated compared to the mock control sample. The four active PLCPs had their abundance level nearly same in the agroinfiltrated and mock control samples. These results indicate that the activities of two PLCPs increased and seven additional PLCPs are appear upon Agroinfiltration.

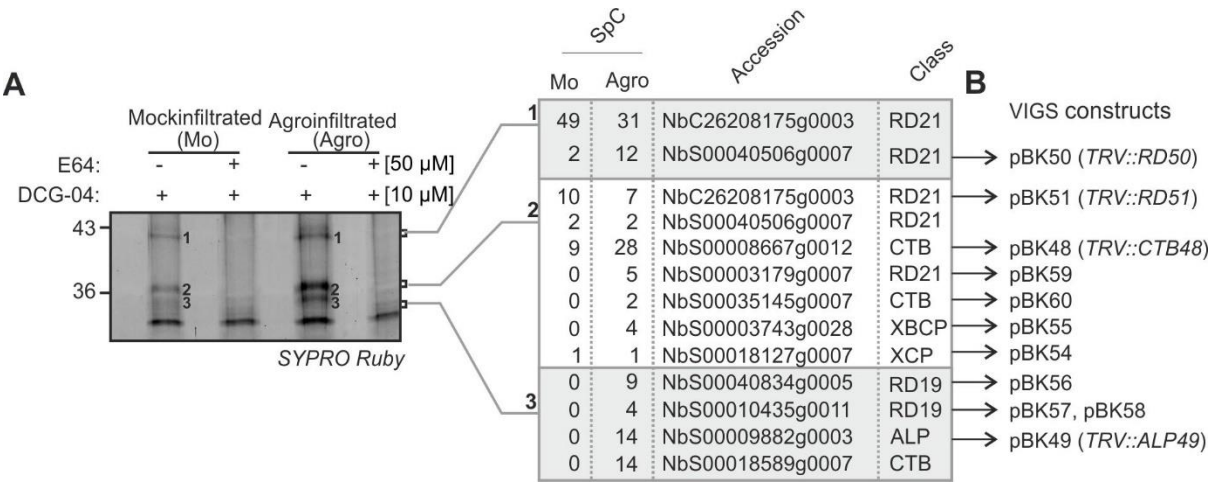

Figure 7.1 Identification of active PLCPs from apoplast of agroinfiltrated *N. benthamiana*

(A) Identification of the DCG04-labeled PLCPs. *N. benthamiana* leaves were infiltrated with the Agrobacterium strain (GV3101:pMP90) carrying p19 expressing plasmid or with water (Mock). Apoplastic fluids were collected from these plants at 4 dpi and large scale labeling was performed by incubating 30 ml of apoplastic fluids with 10 µM DCG-04 at pH 5.0. Biotinylated proteins were purified, separated on protein gels and visualized by fluorescent scanning of SYPRO Ruby-stained protein gels. Bands were excised, treated with trypsin and the peptides were identified by ion trap mass spectrometry. Proteins identified were selected and the spectral counts (SpC) are summarized. (B) Binary TRV constructs for silencing *PLCP* gene expression.

7.2.2 Silencing of *PLCPs* using virus-induced gene silencing (VIGS)

Transcript levels of the different *PLCP* genes were suppressed using virus-induced gene silencing (VIGS) (Lu et al., 2003). Eleven different TRV constructs were created to silence the *PLCP* genes (Figure. 7.1B). The constructs carried a 300-350 bp fragment from the respective *PLCP* gene cloned into the pTRV2 vector (Senthil-Kumar and Mysore, 2014). The fragments for the *PLCP* gene silencing were designed using the VIGS tool available in the solgenomics website (Fernandez-Pozo et al., 2015). VIGS was performed with *N. benthamiana* plants by infiltrating the agrobacterium strains carrying the TRV constructs for *PLCP* gene silencing. During my PhD studies, agrobacterium strains carrying *TRV::CTB48*, *TRV::ALP49*, *TRV::RD50* and *TRV::RD51* were tested since these constructs were ready at that time. In these experiments, the agrobacterium strain carrying a fragment from the Green Fluorescent Protein (*GFP*) (*TRV::GFP*) gene was used as a negative control. Interestingly, notable phenotypes were observed in the plants which were silenced for certain *PLCP* genes (Figure. 7.2A).

TRV::CTB and *TRV::ALP* plants displayed severe growth phenotypes at 3 weeks post infiltration when compared to the *TRV::GFP* control plants (Figure. 7.2A). The majority of the plants generated using these constructs died and their leaves appeared yellow in colour. The severe phenotype might be due the fact that the decreased levels of these PLCPs might have allowed the TRV virus to spread systemically. However, one out of three inoculated plants did suffer but did not die. Newly small green leaves could be observed appeared that were used for transient expression of the full length BGAL protein. By contrast *TRV::RD50* and *TRV::RD51* displayed stunted growth phenotypes at 3 weeks post infiltration when compared to the *TRV::GFP* control plants. These plants appeared shorter in height compared to the control plants.

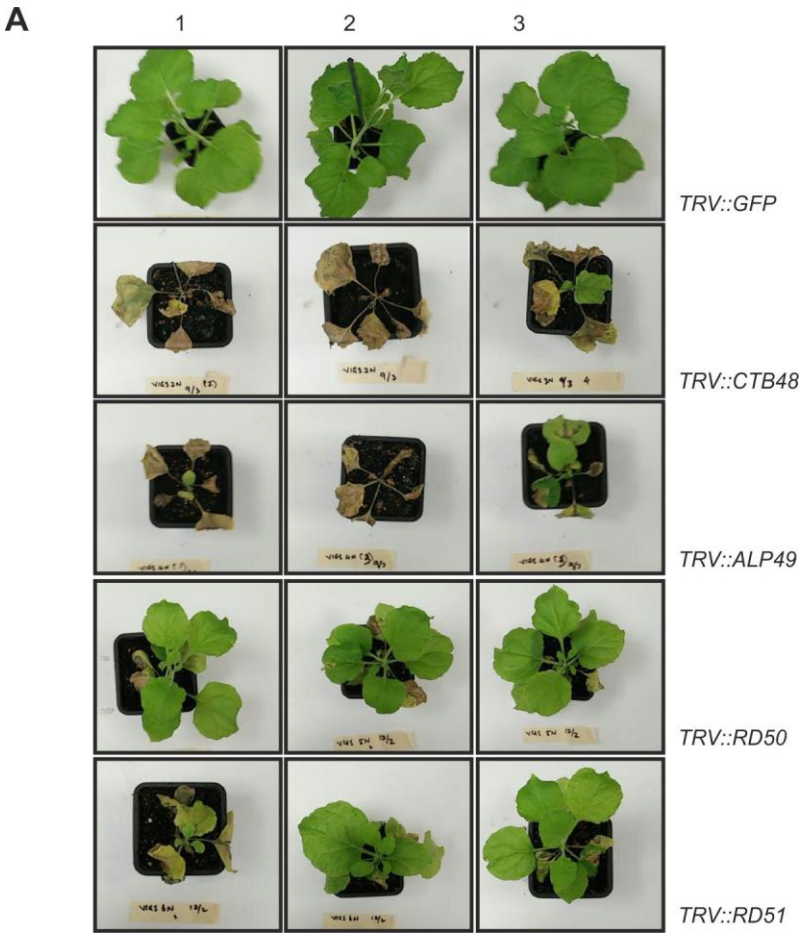

Figure 7.2 *TRV::CTB48* and *TRV::ALP49* plants display severe growth phenotype

Knock-down of *PLCP* gene expression using virus-induced gene silencing (VIGS). The different agrobacterium strains carrying the pBK48, pBK49, pBK50, pBK51 or the GFP control vector were mixed individually with the Agrobacterium strain carrying pTRV1 vector in 1:1 ratio. The mixed cultures having OD = 0.5 were infiltrated into leaves of 10 day old *N. benthamiana* plants and incubated at 23^0C degrees in the growth chamber. A three different representative plants from the *TRV:GFP* control and *TRV:PLCP* infiltrated *N. benthamiana* plants were photographed at 5 weeks after infiltration. These phenotypes were consistently observed in a second independent experiment.

7.2.3 Expression and detection of BGAL protein in the *PLCP* silenced plants

To transiently express the *BGAL* gene in *Nicotiana benthamiana* leaves, binary construct pBK26 was created carrying the cDNA of full length *BGAL* gene driven by the 35S promoter (Figure 7.3A). For this construct, the full length *BGAL* gene was cloned without signal peptide and terminator sequence into expression vector pRH509 which contained the signal peptide and the terminator sequences (Van der Hoorn et al., 2003). In addition, the cDNA of full length *BGAL* gene was cloned with a sequence encoding the strep-II tag at start of the BGAL open reading frame, behind a signal peptide encoded by the *PR1a* gene.

To validate if pBK26 expresses BGAL, the Agrobacterium strain carrying the construct pBK26 was infiltrated alone or together with the Agrobacterium strain carrying the p19 expressing plasmid into the leaves of *N. benthamiana*. P19 is a suppressor of gene silencing protein which is commonly used to overexpress the gene of interest in the leaves of *N. benthamiana* (Garabagi et al., 2012). Interestingly, the truncated BGAL protein was detected at 45 kDa in apoplastic fluids of agroinfiltrated plants (Figure 7.3B). This indicates that the full length BGAL protein is processed by proteases. However in the plants in which the BGAL is overexpressed using P19, also the full length BGAL protein was detected at 89.7 kDa (Figure 7.3B). In these plants, the full length BGAL protein might not have been completely processed because of overexpression. This result indicates that the *BGAL* gene can be expressed in the *Nicotiana benthamiana* leaves using the Agrobacterium carrying pBK26.

To investigate if any of the active PLCPs are involved in processing of BGAL, the full length *BGAL* gene was transiently expressed in VIGS plants generated using *TRV::PLCP* constructs. The Agrobacterium strain carrying the BGAL encoding construct pBK26 was infiltrated into the leaves of *TRV::PLCP* plants in the absence of P19 silencing inhibitor and the expressed BGAL protein was detected in leaf extracts from these plants using protein blotting and immuno-detection. Importantly, the full length BGAL protein at 89.7 kDa together with the truncated version at 45 kDa could be detected in the leaf extracts of *TRV::ALP49* or *TRV::RD50* plants (Figure. 7.4C). In *TRV::GFP*, *TRV::RD48* or *TRV::RD51* only the truncated BGAL protein could be detected (Figure. 7.3C). The same results were obtained in a second independent experiment performed with two biological replicates. In addition, the *TRV::PLCP* plants were agroinfiltrated using constructs expressing antibody 2F5 (Mandal et al., 2014), a receptor-like kinase of *Arabidopsis thaliana* RLK902 (PhD thesis, Dr. Joji grace Villamor) and a tomato protease RCR3 (PhD thesis, Dr. Selvakumari Ramasubramanian). Moreover, in *TRV::PLCP* plants, no effect on processing of these proteins was observed (data not shown). This result suggests that the PLCPs silenced in *TRV::ALP49* or *TRV::RD50* plants might be involved in processing of the BGAL protein present in the apoplast of *Nicotiana benthamiana* leaves.

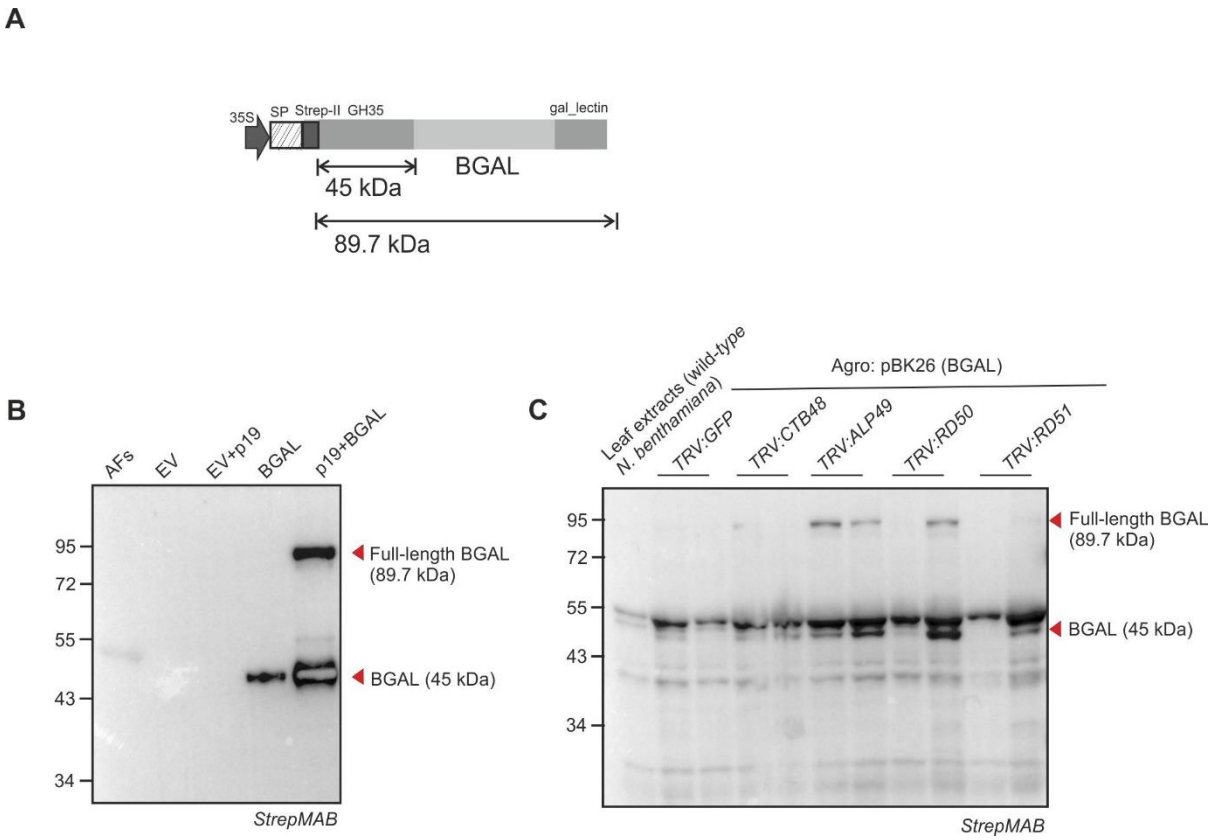

Figure 7.3 Expression and detection of BGAL in *PLCP* silenced plants

(A) Construct for the transcient expression of BGAL. pBK26 carries the full length *BGAL* gene cloned with strep-II tag at start of the GH35 domain driven by the 35S promoter in the pRH509 expression vector. (B) Expression and detection of BGAL in the apoplastic fluids. The construct pBK26 or the pRH509 (empty vector, EV) were transformed into Agrobacterium strain GV3101(PMP90) by electroporation. The transformed Agrobacterium strains were mixed the Agrobacterium strain carrying p19 expressing plasmid or only infiltration buffer in a 1:1 ratio. The mixed cultures having OD = 0.5 were infiltrated into leaves of 10 day-old *N. benthamiana* plants and incubated at 23^0C in the growth chamber. Apoplastic fluids were isolated from the plants at 4 dpi and the expressed BGAL protein was detected using anti-strep-II antibody after protein blotting. (C) Expression and detection of BGAL in *PLCP* silenced plants. The Agrobacterium carrying the construct pBK26 were infiltrated into leaves of 5-week old *N. benthamiana* plants silenced for different *PLCPs*. At 4 dpi, two the leaf discs were collected from the plants, ground in the gel loading buffer containing mercaptoethanol. The expressed BGAL was detected using the anti-strep-II antibody after protein blotting. The same results were obtained in a second independent experiment performed with two biological replicates.

7.3 Discussion

The activity of glycosidases is tightly regulated at the post-translational level. Cell wall proteome analysis suggested that glycosidases can be regulated by proteases (Minic et al., 2007). Consistent with this, we found that the labeled BGAL (NbS00024332g0007) is a truncated 45 kDa protein, which consists of only the GH35 catalytic domain. As a serendipity discovery we have observed that the two PLCPs, NbS00040506g0007 (RD50) and

NbS00009882g0003 (ALP49) which belong to the RD21 and ALP subfamilies respectively, might be involved in processing of the BGAL protein. There is a possibility that these two PLCPs might act together to process the apoplastic BGAL. Truncation of a lysosomal BGAL has also been observed in human cell cultures (Spoel et al., 2000). In this study, the C-terminal half is suggested to be removed in acidic environment by proteases to release a mature enzyme. Interestingly, a C-terminal truncation of a bacterial β-galactosidase resulted in an efficient transglycosidase (Jorgensen et al., 2001). Likewise the truncated BGAL in the plant apoplast might have acquired transglycosidase activity and may catalyse the transfer of galactose to acceptor molecules. In addition, the loss of the C-terminal half of the protein may also have altered the location of this enzyme in the apoplast. The role of proteolytic regulation of BGAL by these candidate PLCPs is therefore an interesting topic for further studies.

The *TRV::PLCP* constructs are designed in a way to specifically silence the respective apoplastic *PLCP* genes. However, the possibility for these constructs to silence any off-target *PLCPs* cannot be ignored. Hence the possible off-target silencing should also be investigated to ascertain the involvement of candidate PLCPs to process the BGAL protein. In addition, RT-PCR analysis should be also performed to verify the reduction of targeted transcripts.

7.4 References

Fernandez-Pozo, N., Menda, N., Edwards, J.D., Saha, S., Tecle, I.Y., Strickler, S.R., Bombarely, A., Fisher-York, T., Pujar, A., Foerster, H., et al. (2015). The Sol Genomics Network (SGN)--from genotype to phenotype to breeding. Nucleic Acids Res. *43*, D1036–D1041.

Garabagi, F., Gilbert, E., Loos, A., McLean, M.D., and Hall, J.C. (2012). Utility of the P19 suppressor of gene-silencing protein for production of therapeutic antibodies in Nicotiana expression hosts. Plant Biotechnol. J. *10*, 1118–1128.

Greenbaum, D., Medzihradszky, K.F., Burlingame, A., and Bogyo, M. (2000). Epoxide electrophiles as activity-dependent cysteine protease profiling and discovery tools. Chem. Biol. *7*, 569–581.

van der Hoorn, R.A.L., Leeuwenburgh, M.A., Bogyo, M., Joosten, M.H.A.J., and Peck, S.C. (2004). Activity profiling of Papain-Like cysteine proteases in plants. Plant Physiol. *135*, 1170–1178.

Jashni, M.K., Mehrabi, R., Collemare, J., Mesarich, C.H., Wit, D., and M, P.J.G. (2015). The battle in the apoplast: further insights into the roles of proteases and their inhibitors in plant–pathogen interactions. Front. Plant Sci. *6*.

Kapila, J., De Rycke, R., Van Montagu, M., and Angenon, G. (1997). An Agrobacterium-mediated transient gene expression system for intact leaves. Plant Sci. *122*, 101–108.

Lu, R., Martin-Hernandez, A.M., Peart, J.R., Malcuit, I., and Baulcombe, D.C. (2003). Virus-induced gene silencing in plants. Methods *30*, 296–303.

Mandal, M.K., Fischer, R., Schillberg, S., and Schiermeyer, A. (2014). Inhibition of protease activity by antisense RNA improves recombinant protein production in *Nicotiana tabacum* cv. Bright Yellow 2 (BY-2) suspension cells. Biotechnol. J. *9*, 1065–1073.

Matsumoto, K., Mizoue, K., Kitamura, K., Tse, W.C., Huber, C.P., and Ishida, T. (1999). Structural basis of inhibition of cysteine proteases by E-64 and its derivatives. Biopolymers *51*, 99–107.

Minic, Z., Jamet, E., Négroni, L., Arsene der Garabedian, P., Zivy, M., and Jouanin, L. (2007). A sub-proteome of *Arabidopsis thaliana* mature stems trapped on concanavalin A is enriched in cell wall glycoside hydrolases. J. Exp. Bot. *58*, 2503–2512.

Misas-Villamil, J.C., van der Hoorn, R.A.L., and Doehlemann, G. (2016). Papain-like cysteine proteases as hubs in plant immunity. New Phytol. *212*, 902–907.

Senthil-Kumar, M., and Mysore, K.S. (2014). Tobacco rattle virus–based virus-induced gene silencing in *Nicotiana benthamiana*. Nat. Protoc. *9*, 1549–1562.

Shabab, M., Shindo, T., Gu, C., Kaschani, F., Pansuriya, T., Chintha, R., Harzen, A., Colby, T., Kamoun, S., and Hoorn, R.A.L. van der (2008). Fungal effector protein AVR2 targets diversifying defense-related cys Proteases of tomato. Plant Cell *20*, 1169–1183.

Spoel, A. van der, Bonten, E., and d'Azzo, A. (2000). Processing of Lysosomal β-galactosidase the C-terminal precursor fragment is an essential domain of the mature enzyme. J.Biol.Chem.*275*, 10035-10040.

Van der Hoorn, R.A.L., Rivas, S., Wulff, B.B.H., Jones, J.D.G., and Joosten, M.H.A.J. (2003). Rapid migration in gel filtration of the Cf-4 and Cf-9 resistance proteins is an intrinsic property of Cf proteins and not because of their association with high-molecular-weight proteins. Plant J. *35*, 305–315.

Chapter 8: Product inhibition of plant glycosidases revealed by ABPP

8.1 Introduction

Monosaccharides or simple sugars such as glucose, galactose and xylose are released as a products during the hydrolytic action of glucosidases, galactosidases and xylosidases on their respective glycoside substrates. Several glycosidases exhibit a phenomenon called product inhibition (Gusakov et al., 1985). For example, cellulase is inhibited by its released glucose product at high concentrations (Hsieh et al., 2014). In most cases, the inhibition caused by the released monosaccharide is competitive (Olsen et al., 2016). This phenomenon is also exhibited by several other glycosidases like beta-glucosidase (Sørensen et al., 2013; Teugjas and Väljamäe, 2013; Xiao et al., 2004), beta-xylosidase (Nieto-Domínguez et al., 2015) and beta-galactosidase (Hu et al., 2010). In this chapter, the effect of applying the monosaccharide products released by various glycosidases on labeling the plant glycosidases is investigated using activity-based protein profiling (ABPP) with JJB70. Nine different monosaccharides are applied to three different plant proteomes at high concentrations and the specific suppression of labeling is investigated using ABPP and mass spectrometry (MS).

8.2 Results

8.2.1. Galactose at high concentrations suppresses the labeling of beta-galactosidases in apoplastic fluids

In the Chapter 2, the active state of various glycosidases present in apoplastic fluids from *N. benthamiana* leaves were monitored using JJB probes. The signals from the Band 1 and 2 were assigned to two different beta-galactosidases, BGAL1 and BGAL2 (Figure 8.1A). Likewise, the signals from Bands 2 and 3 were assigned to different beta-xylosidases, BXLU1 – BXLU5 (Figure 8.3A). The glycosidase causing Band 5 is not known.

To investigate the effect of galactose on labeling the glycosidases, apoplastic fluids from *Nicotiana benthamiana* leaves were pre-incubated with increasing concentrations (0.05 mM to 200 mM) of galactose. The pre-incubated apoplastic fluids were subsequently incubated with JJB70 to label the active glycosidases. Importantly, 10 to 200 mM galactose suppressed the labeling of two signals at 95 and 45 kDa (Figure 8.1A) (Bands 1 and 4). At these high concentrations, the intensity of labeling of these proteins were drastically reduced compared to other signals (Figure 8.1B) (Bands 2, 3 and 5). Galactose at lower concentrations (0.05 mM - 1 mM) did not have this suppression effect on any of the labeled glycosidases. However at 0.05 mM - 1 mM galactose, a gradual increase in labeling of BGAL2 (Band 4, 45

kDa) could be observed (Figures 8.1A, 8.1B). This result demonstrates that galactose at high concentration can suppress the labeling of two different BGALs. In addition, galactose at low concentrations can promote labeling of certain glycosidases.

To add further strength for the claim that galactose can inhibit beta-galactosidase activities, enzymatic assays were performed. The *BGAL2* gene was transiently overexpressed in leaves of *N. benthamiana* using the Agrobacterium strain carrying the construct pBK26 (Chapter 7). At 4 dpi, the apoplastic fluids were collected and pre-incubated with increasing concentrations (0.05 - 200 mM) of galactose. The pre-incubated apoplastic fluids were subsequently incubated with 4-MUG beta-galactosidase substrate and the enzyme activity was monitored by detecting the fluorescence 4-MU generated over different time points. Importantly, BGAL activity was gradually decreased on increasing the concentration of galactose (0.05 - 1 mM) (Figure 8.1C). Also, at high galactose concentrations (10 - 200 mM), no BGAL activity could not be detected in apoplastic fluids (Figure 8.1C). This results confirm that inhibits the activities of beta-galactosidases in apoplastic fluids.

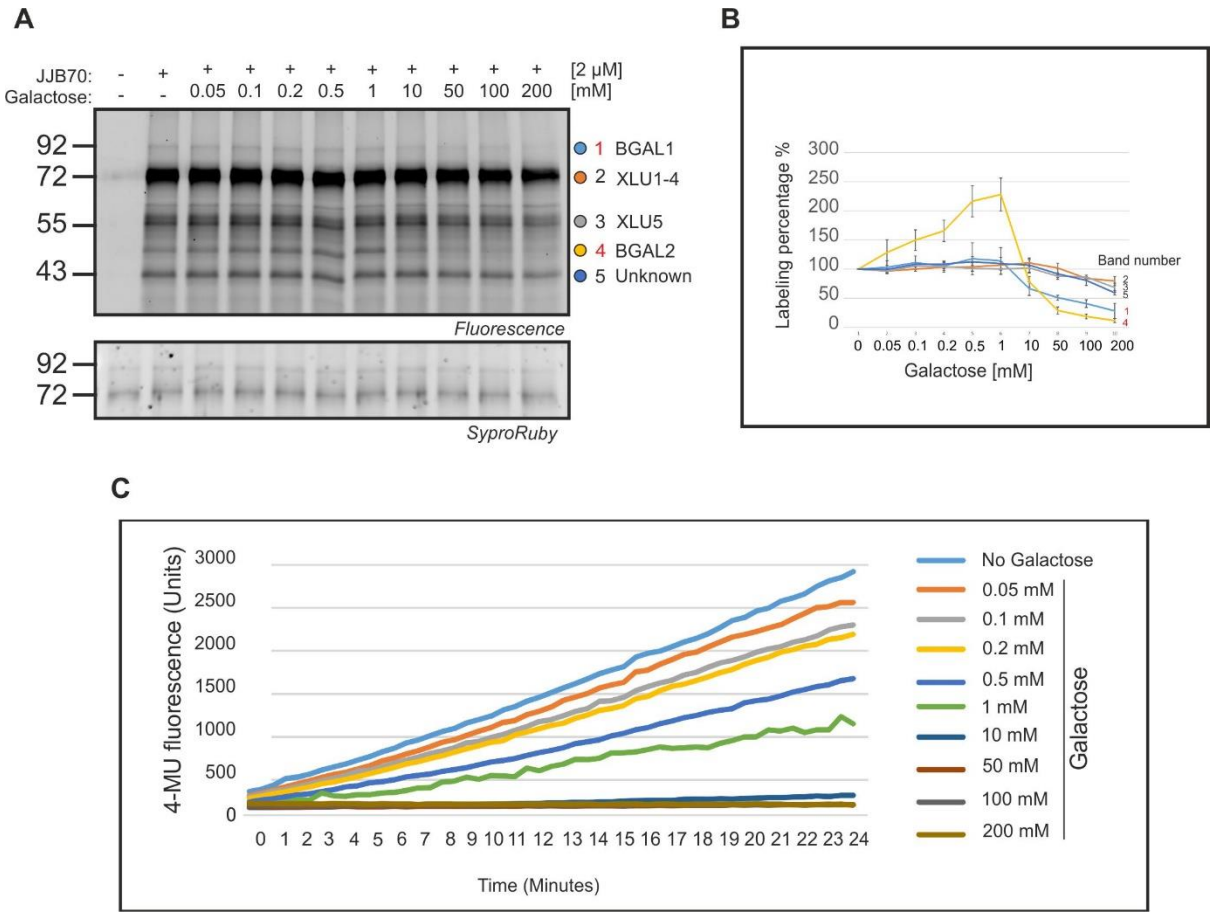

Figure 8.1 Galactose at high concentrations suppresses the labeling of active glycosidases in apoplastic fluids

(A) Competitive ABPP with increasing concentrations of galactose and apoplastic fluids. Apoplastic fluids were isolated from the leaves of *Nicotiana benthamiana* and pre-incubated with increasing concentrations of galactose (0.05 – 200 mM) at room temperature for 30 minutes. The pre-incubated apoplastic fluids were labeled with 2 µM JJB70 probe at pH 5.0 for one hour. Labeled proteins were detected by in-gel fluorescent scanning. The gel was subsequently stained with SYPRO Ruby to show equal loading of the sample. (B) Quantification of the fluorescent signals. Fluorescence of the signals was quantified using ImageQuant from three independent experiments. Labeling intensity was normalized to 0 mM galactose and expressed as a percentage. Error bars represent SEM of three independent experiments. (C) Enzymatic inhibition assay with different concentrations of galactose. Apoplastic fluids from leaves overexpressing the BGAL2 were pre-incubated with increasing concentrations of galactose (0.05 – 200 mM) at room temperature for 30 minutes. The pre-incubated apoplastic fluids were treated with the substrate 4-MUG at pH 5.0 and the enzymatic activity of BGAL was monitored over time with the excitation and emission wavelength of 360 nM and 460 nM respectively. The experiment was repeated three times with similar results.

8.2.2. Xylose at high concentrations suppresses the labeling of active glycosidases in apoplastic fluids

To investigate the effect of xylose on labeling of glycosidases, apoplastic fluids from *Nicotiana benthamiana* leaves were pre-incubated with increasing concentrations (0.05 - 200 mM) of xylose. The pre-incubated apoplastic fluids were subsequently incubated with JJB70 probe to label active glycosidases. Importantly, 10 - 200 mM xylose suppressed the labeling of three different signals at 75, 55 and 43 kDa (Figure 8.2A) (Band 2, Band 3 and Band 5), compared to other glycosidase signals (Figure 8.2B) (Band 1 and Band 5). However an increase in labeling of a two glycosidase band at 95 and 45 kDa was observed which might have been caused by increased probe availability for the labeling (Figure 8.2B). Interestingly similar to galactose, xylose at lower concentration range from 0.05 - 1 mM did not suppress labeling of glycosidases. This result demonstrate that the xylose only at high concentration range can suppress the labeling of five different beta-xylosidases BXLU1 – BXLU4 in the apoplastic fluids of *N. benthamiana* leaves and the signal 5 being suppressed by xylose might also be a beta-xylosidase.

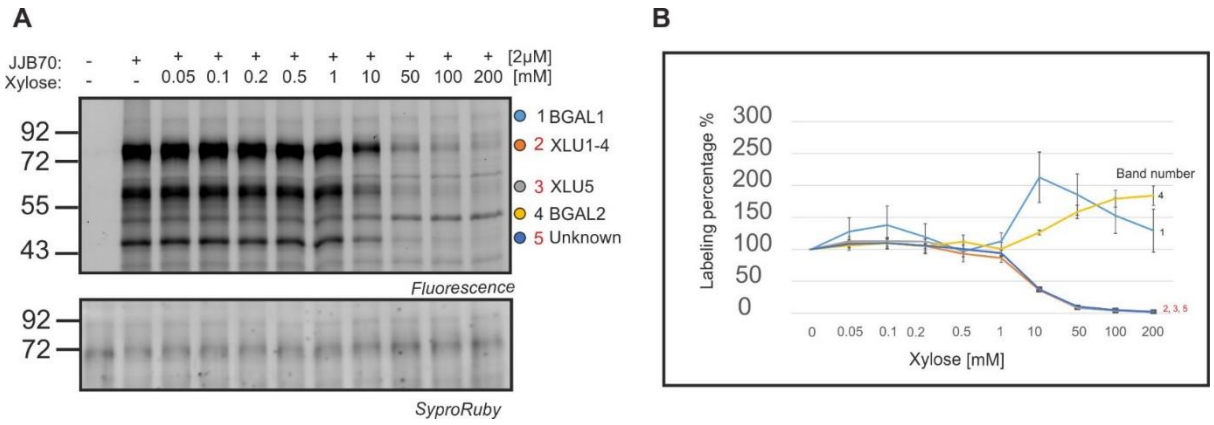

Figure 8.2 Xylose at high concentrations suppresses the labeling of active glycosidases in apoplastic fluids

(A) Competitive ABPP with increasing concentrations of xylose in apoplastic fluids. Apoplastic fluids were isolated from the leaves of *Nicotiana benthamiana* and pre-incubated with increasing concentrations of xylose (0.05 – 200 mM) at room temperature for 30 minutes. The pre-incubated apoplastic fluids were labeled with 2 µM JJB70 at pH 5.0 for one hour. Labeled proteins were detected by in-gel fluorescent scanning. The gel was subsequently stained with SYPRO Ruby to show the equal loading of the sample. (B) Quantification of suppressed protein signal. Fluorescence of the signals were quantified using ImageQuant from three independent experiments. Labeling intensity was normalized to the 0 mM xylose sample and expressed as a percentage. Error bars represent SEM of three independent experiments.

8.2.3. Specificity of glycosidase suppression at high monosaccharide concentrations

In previous experiments, we noticed that galactose and xylose at high concentrations suppress the labeling of different glycosidases. To investigate the specificity of glycosidase suppression caused by galactose and xylose, apoplastic fluids from *Nicotiana benthamiana* leaves were pre-incubated with nine different monosaccharides at 200 mM. The pre-incubated apoplastic fluids were subsequently incubated with JJB70 probe to label the active glycosidases. Interestingly, glycosidase bands 1 and 5 at 95 and 45 kDa, respectively, were specifically inhibited by galactose but not by other tested monosaccharides at 200 mM (Figure 8.3A & B). Likewise, glycosidase bands 2, 3 and 5 at 75, 55 and 43 kDa, respectively, were specifically inhibited by xylose but not by other tested monosaccharides at 200 mM (Figure 8.3A & B). These results demonstrate that glycosidases are specifically inhibited by their respective monosaccharide products at high concentrations in the apoplastic fluids of *N. benthamiana* leaves.

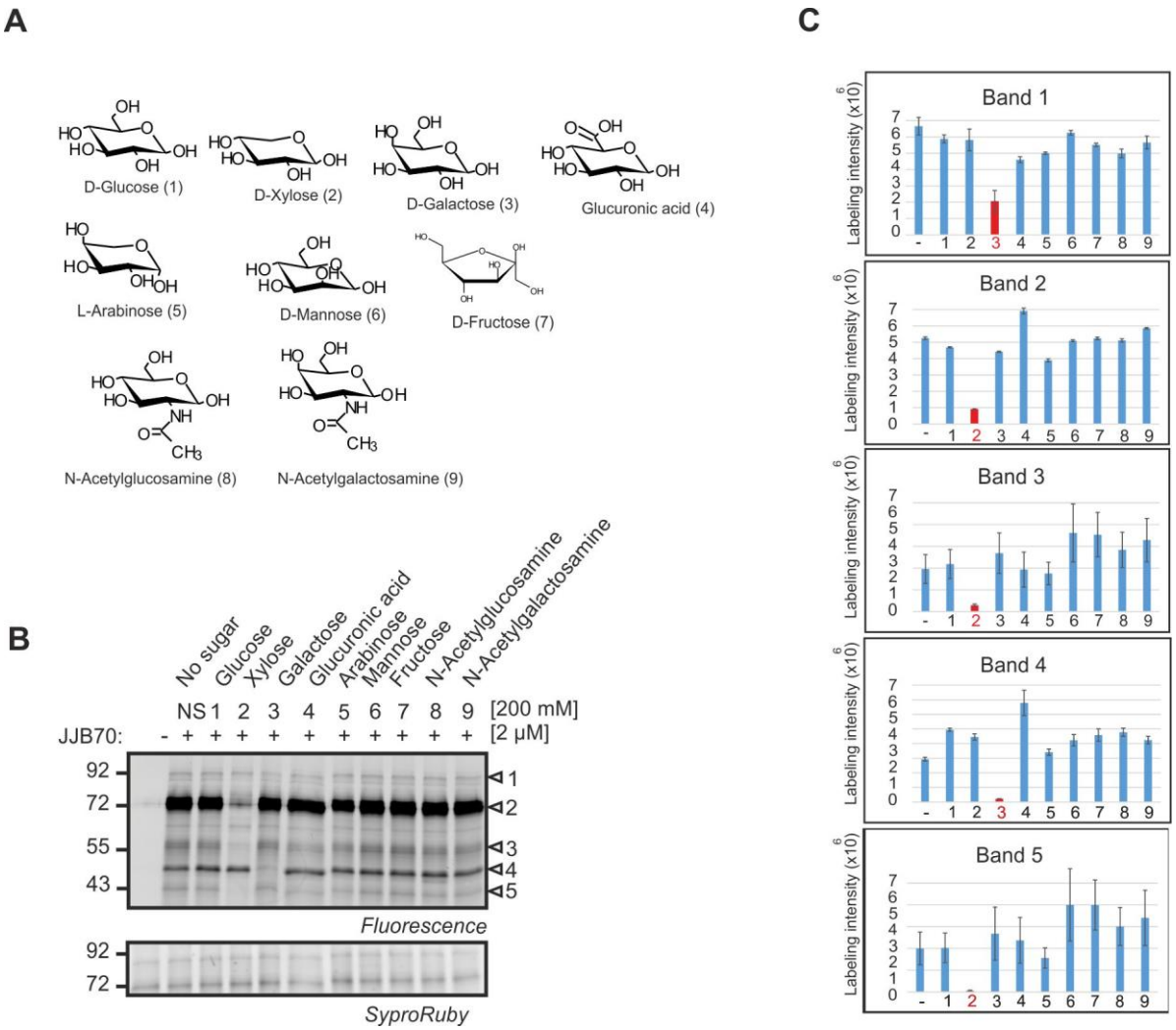

Figure 8.3 Specificity of glycosidase inhibition by monosaccharides

(A) Structures of nine different monosaccharides used for the competition assay. (B) Competitive ABPP with nine different sugars at high concentration in apoplastic fluids. Apoplastic fluids were isolated from leaves of *Nicotiana benthamiana* and pre-incubated with nine different sugars at 200 mM at pH 5.0 at room temperature for 30 minutes. The pre-incubated apoplastic fluids were labeled with 2 µM JJB70 for one hour. Labeled proteins were detected by in-gel fluorescent scanning. The gel was subsequently stained with SYPRO Ruby to show the equal loading of the sample. (C) Quantification of suppressed protein signal. Fluorescence of the signals were quantified using ImageQuant from three independent experiments and the average labeling intensities are represented. Error bars represent SEM of three independent experiments.

8.2.4. Application of the monosaccharide products to the Arabidopsis flower extracts

To test if suppression of labeling by monosaccharides can be used to annotate signals in glycosidase activity profiles, the flowers extracts from *Arabidopsis thaliana* plants were preincubated with nine different monosaccharides at 200 mM. Arabidopsis flowers show multiple signals (Figure 2.7) dominated by TGG1 and TGG2 myrosinases. We used the *tgg1-*

3/tgg2-1 mutant to remove the abundant TGG1 and TGG2 myrosinases and study the remaining glycosidases.

In the flower proteome of *tgg1-3/tgg2-1 A. thaliana* plants, JJB70 labeling causes 11 different signals at molecular weight range from 43 to 92 kDa. In the proteome pre-incubated with monosaccharides, suppression of three different protein bands were observed (Figure 8.4A & B). The protein bands 1 and 3 at 90 and 45 kDa, respectively, were specifically inhibited by 200 mM galactose but not by other tested monosaccharides (Figure 8.4A & B). Band 2 at 60 kDa was inhibited by 200 mM glucose, xylose and arabinose but not by other tested monosaccharides (Figure 8.4A & B).

To identify the glycosidases present in these three bands, large scale labeling was performed with flower extracts using JJB111. The labeled proteins were enriched on streptavidin beads, separated on a protein gel, stained with SYPRO Ruby and detected by fluorescent scanning. Protein bands 1-3 were excised, treated with trypsin, and the peptides were identified by ion-trap mass spectrometry. MS analysis showed that the 90 kDa signal consists of several glycosidases including two beta-galactosidases, BGAL6 and BGAL12 (Figure 8.4C). Likewise, the 60 kDa signal consists of several glycosidases such as beta-glucosidase, cellulase and a bifunctional beta-xylosidase/alphafuranosidase (Figure 8.4C). Moreover, the majority of the peptide spectra from the 45 kDa signal originates from beta-galactosidase BGAL8 (Figure 8.4C). Hence this confirms that bands 1 and 3 were inhibited by galactose contained two different beta-galactosidases. Likewise, band 2 was inhibited by glucose, xylose and arabinose contained the respective glycosidases: beta-glucosidase & cellulase and a beta-xylosidase/alpha-L-furanosidase. Therefore, in addition to xylose and galactose, we detected inhibitory effects of glucose and arabinose.

8.2.5. Application of the monosaccharide products to the wheat leaf extracts

To test if the suppression of labeling by monosaccharides could be also applicable to other proteomes, wheat leaf extracts were preincubated with nine different monosaccharides at 200 mM. The pre-incubated apoplastic fluids were subsequently labeled with JJB70. In wheat leaf extracts labeled with JJB70, three strong signals at the 72, 65 and 60 kDa and several weak signals above 72 kDa are detected (Figure 8.5A). In the proteome pre-incubated with monosaccharides, two signals were suppressed (Figure 8.5A & B). Band 1 at 72 kDa was inhibited by 200 mM glucose, xylose, galactose and arabinose but not by other tested monosaccharides (Figure 8.5A & B). The Band 2 at 65 kDa was suppressed by 200mM xylose but not by other tested monosaccharides (Figure 8.5A & B).

To identify the glycosidases present in these three bands, large scale labeling was performed with wheat leaf extracts using JJB111. The labeled proteins were enriched on

streptavidin beads, separated on a protein gel, stained with SYPRO Ruby and detected by fluorescent scanning. The protein bands 1 and 2 were excised, treated with trypsin, and the peptides were identified by ion-trap mass spectrometry. MS analysis revealed that the 72 kDa signal contains beta-glucosidase, beta-xylosidase, beta-galactosidase, cellulase, alphafuranosidase and several uncharacterized glycosidases belonging to the GH3 family (Figure 8.5C). Moreover, the 65 kDa signal contains beta-glucosidase, beta-galactosidase and several other uncharacterized glycosidases belonging to the GH3 family (Figure 8.5C). Hence similar to Arabidopsis flower proteome, we observed that band 1 was inhibited by monosaccharide products such as glucose, xylose, galactose and arabinose and contained beta-glucosidase & cellulase, beta-xylosidase, beta-galactosidase, and alpha-L-furanosidase. Unfortunately, no glycosidases with annotated beta-xylosidase activities were detected in band 2 even though it was inhibited by xylose. This might be due to the fact that the band 2 contained several glycosidases with unknown substrate specificities. Therefore, because this signal was suppressed by xylose any of the uncharacterized glycosidases detected in band 2 might have beta-xylosidase activity.

Taken together, these data indicate that a beta-glucosidase, beta-xylosidase, beta-galactosidase and alpha-furanosidase are specifically inhibited by their respective monosaccharide products at high concentrations in the flower proteome of Arabidopsis and leaf proteome of wheat and this method can be used to quickly annotate signals in a glycosidase activity profile.

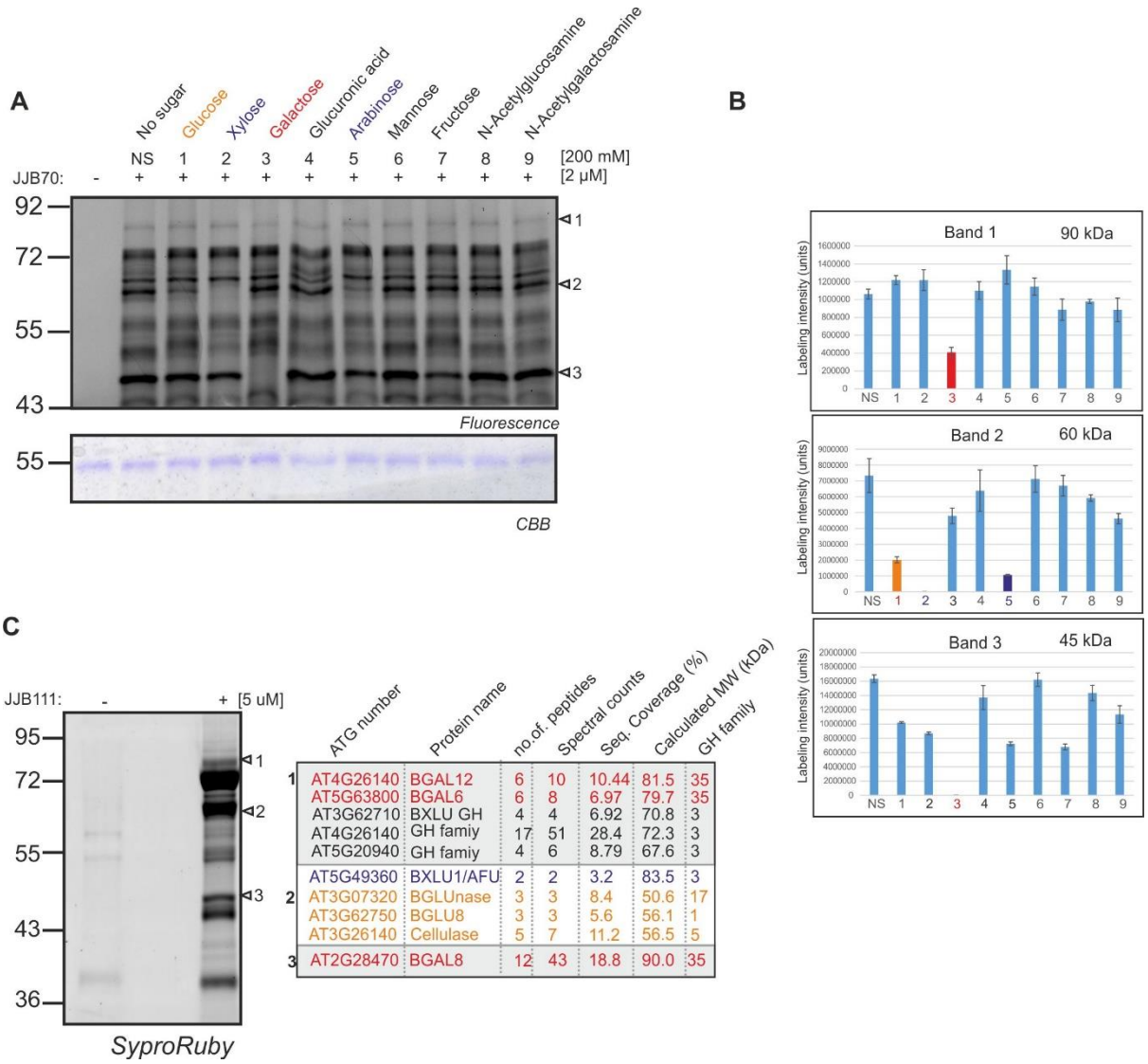

Figure 8.4 Monosaccharides suppress glycosidase labeling in flower extracts of *Arabidopsis thaliana*

(A) Competitive ABPP with nine different sugars at high concentration and flowers extracts of *tgg1-3/tgg2-1* Arabidopsis plants. Flower proteins from *tgg1-3/tgg2-1 Arabidopsis thaliana* plants were extracted in 50 mM MES buffer at pH 5.0 and pre-incubated individually with nine different sugars at 200 mM concentration at room temperature for 30 minutes. The pre-incubated apoplastic fluids were labeled with 2 µM JJB70 probe for one hour. Labeled proteins were detected by in-gel fluorescent scanning. The gel was subsequently stained with coomassie to show the equal loading of the sample. (B) Quantification of suppressed protein signal. Fluorescence of the signals were quantified using ImageQuant from three independent experiments and the average labeling intensities are represented. Error bars represent SEM of three independent experiments. (C) Identification of glycosidases from protein bands 1-3 labeled from JJB111 in flower extracts of *Arabidopsis thaliana*. Large scale labeling was performed by incubating Arabidopsis flower extracts with and without 5 µM JJB111 at pH 5.0. Biotinylated proteins were purified with streptavidin beads and separated on protein gels. Proteins were visualized by SYPRO Ruby staining and fluorescent scanning. Bands were excised, treated with trypsin and the peptides were identified by ion trap mass spectrometry. The glycosidases identified in protein bands 1-3 are represented. Beta-galactosidases are highlighted in red color, beta-xylosidase/alpha-furanosidase in blue and beta-glucosidase and cellulase in orange.

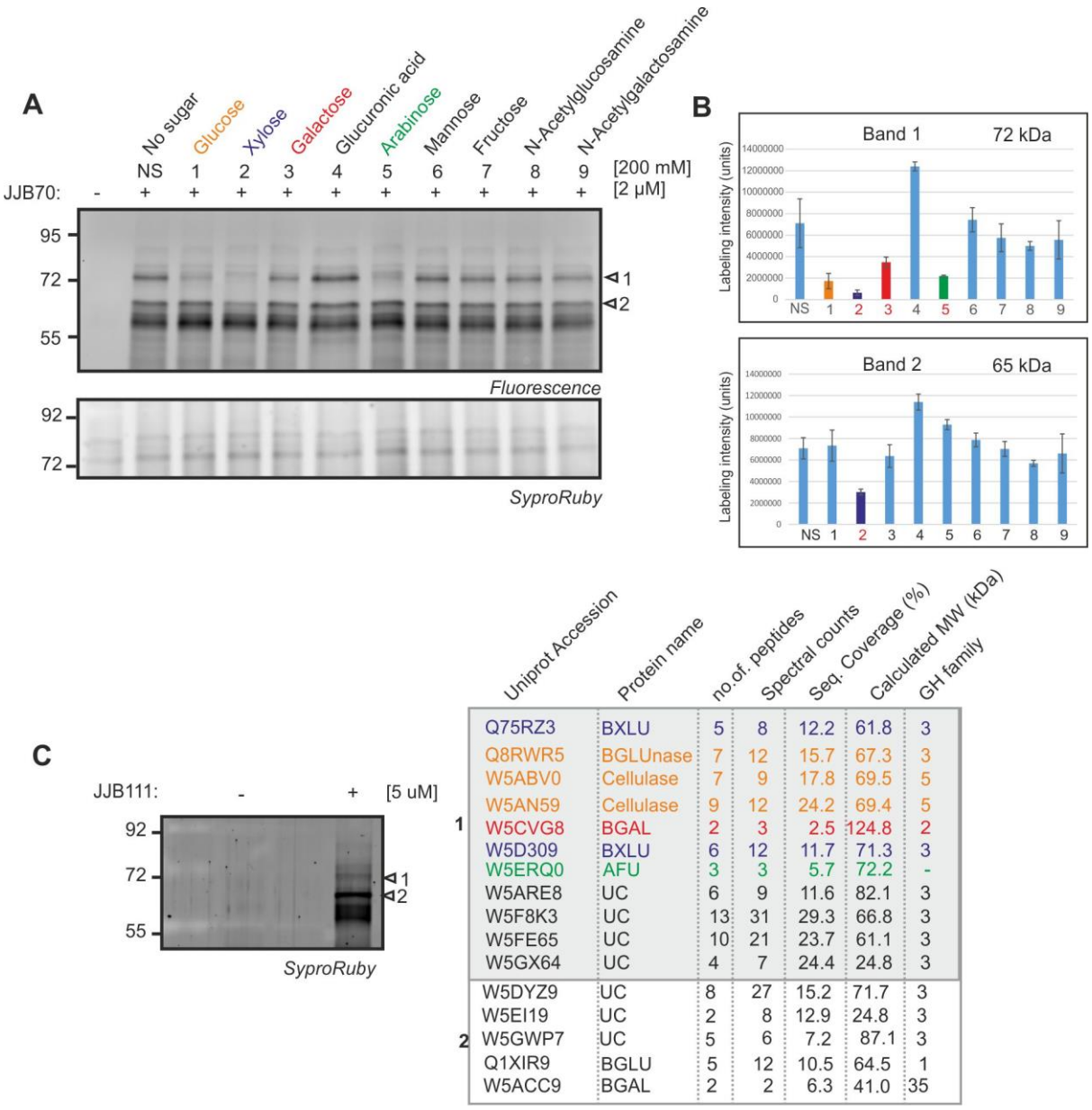

	Uniprot Accession	Protein name	no.of. peptides	Spectral counts	Seq. Coverage (%)	Calculated MW (kDa)	GH family
1	Q75RZ3	BXLU	5	8	12.2	61.8	3
	Q8RWR5	BGLUnase	7	12	15.7	67.3	3
	W5ABV0	Cellulase	7	9	17.8	69.5	5
	W5AN59	Cellulase	9	12	24.2	69.4	5
	W5CVG8	BGAL	2	3	2.5	124.8	2
	W5D309	BXLU	6	12	11.7	71.3	3
	W5ERQ0	AFU	3	3	5.7	72.2	-
	W5ARE8	UC	6	9	11.6	82.1	3
	W5F8K3	UC	13	31	29.3	66.8	3
	W5FE65	UC	10	21	23.7	61.1	3
	W5GX64	UC	4	7	24.4	24.8	3
2	W5DYZ9	UC	8	27	15.2	71.7	3
	W5EI19	UC	2	8	12.9	24.8	3
	W5GWP7	UC	5	6	7.2	87.1	3
	Q1XIR9	BGLU	5	12	10.5	64.5	1
	W5ACC9	BGAL	2	2	6.3	41.0	35

Figure 8.5 Monosaccharides suppress glycosidase labeling in wheat leaf extracts

(A) Competitive ABPP with nine different sugars at high concentration and wheat leaf extracts. Wheat leaf proteins were extracted in 50 mM MES buffer at pH 5.0 and pre-incubated individually with nine different sugars at 200 mM concentration at room temperature for 30 minutes. The pre-incubated apoplastic fluids were labeled with 2 µM JJB70 probe for one hour. Labeled proteins were detected by in-gel fluorescent scanning. The gel was subsequently stained with SYPRO Ruby to show the equal loading of the sample. (B) Quantification of suppressed protein signal. Fluorescence of the signals were quantified using ImageQuant from three independent experiments and the average labeling intensities are represented. Error bars represent SEM of three independent experiments. (C) Identification of glycosidases from protein band 1-2 labeled by JJB111 in wheat leaf extracts. Large scale labeling was performed by incubating wheat leaf extracts with and without 5 µM JJB111 at pH 5.0. Biotinylated proteins were purified with streptavidin beads and separated on protein gels. The proteins were visualized by SYPRO Ruby staining and fluorescent scanning. Bands were excised, treated with trypsin and the peptides were identified by ion trap mass spectrometry. Glycosidases identified in the protein bands 1-2 are shown. Beta-

galactosidases are highlighted in red, beta-xylosidase/alpha-furanosidase in blue and beta-glucosidase and cellulase in orange and alpha-L-furanosidase in green.

8.3 Discussion

In this study, the inhibitory actions of glucose, galactose, xylose and arabinose on labeling of beta-glucosidases, beta-galactosidases, beta-xylosidases and alpha-L-furanosidases, respectively, has been observed with the tested plant proteomes. Based on the MS data, the inhibitory effects caused by these monosaccharides are specific for the respective glycosidases. The approach of applying a high concentration of monosaccharides to plant proteomes can be used as a tool for quick functional classification of JJB-labeled glycosidases. By combing JJB70 profiling with the application of high concentrations of monosaccharides, the glycosidic activities such as beta-glucosidic, beta-galactosidic, beta-xylosidic and alpha-L-furanosidic activities exhibited by the active plant glycosidases can be assigned quickly. Presumably, this approach can be used to classify novel glycosidases for their glycosidic activities.

For several glycosidases, product inhibition can be used to quickly annotate signals in a typical glycosidase activity profile. However, no suppression was observed for several other glycosidases with the tested monosaccharides. In our assays, we have included all the possible monosaccharide products for glycosidases detected by the tested JJB probes (Chapter 2). Hence the non-suppressed glycosidases might not be sensitive for product inhibition. Furthermore, several glycosidases were inhibited by multiple sugars in the product inhibition assay. This might indicate that these glycosidases are sensitive for multiple sugars. For instance, cellulases inhibited by their product glucose and are also inhibited by mannose and galactose at higher concentrations (Hsieh et al., 2014). Interestingly, the intensity of labeling of some glycosidases increased upon addition of some monosaccharides to the plant proteomes. For example, galactose at lower concentration increased the intensity of labeling of both beta-galactosidases (BGALs) in the apoplastic fluids of *N. benthamiana*. Hence BGAL might be activated by galactose at low concentration. A similar phenomenon has been observed with a human beta-galactosidase where galactose increased the activity of the enzyme (Caciotti et al., 2009). Hence it is an interesting topic to study mechanisms of glycosidase activation by monosaccharides.

8.4 References

Caciotti, A., Donati, M.A., d'Azzo, A., Salvioli, R., Guerrini, R., Zammarchi, E., and Morrone, A. (2009). The potential action of galactose as a "chemical chaperone": Increase of beta-galactosidase activity in fibroblasts from an adult GM1-gangliosidosis patient. Eur. J. Paediatr. Neurol. *13*, 160–164.

Gusakov, A.V., Sinitsyn, A.P., Gerasimas, V.B., Savitskene, R.Y., and Steponavichus, Y.Y. (1985). A product inhibition study of cellulases from *Trichoderma longibrachiatum* using dyed cellulose. J. Biotechnol. *3*, 167–174.

Hsieh, C.C., Cannella, D., Jørgensen, H., Felby, C., and Thygesen, L.G. (2014). Cellulase inhibition by high Concentrations of monosaccharides. J. Agric. Food Chem. *62*, 3800–3805.

Hu, X., Robin, S., O'Connell, S., Walsh, G., and Wall, J.G. (2010). Engineering of a fungal beta-galactosidase to remove product inhibition by galactose. Appl. Microbiol. Biotechnol. *87*, 1773–1782.

Nieto-Domínguez, M., Eugenio, L.I. de, Barriuso, J., Prieto, A., Toro, B.F. de, Canales-Mayordomo, Á., and Martínez, M.J. (2015). Novel pH-stable glycoside hydrolase family 3 β-xylosidase from *Talaromyces amestolkiae*: an enzyme displaying regioselective transxylosylation. Appl. Environ. Microbiol. *81*, 6380–6392.

Olsen, J.P., Alasepp, K., Kari, J., Cruys-Bagger, N., Borch, K., and Westh, P. (2016). Mechanism of product inhibition for cellobiohydrolase Cel7A during hydrolysis of insoluble cellulose. Biotechnol. Bioeng. *113*, 1178–1186.

Sørensen, A., Lübeck, M., Lübeck, P.S., and Ahring, B.K. (2013). Fungal beta-glucosidases: a bottleneck in industrial use of lignocellulosic materials. Biomolecules *3*, 612–631.

Teugjas, H., and Väljamäe, P. (2013). Selecting β-glucosidases to support cellulases in cellulose saccharification. Biotechnol. Biofuels *6*, 105.

Xiao, Z., Zhang, X., Gregg, D.J., and Saddler, J.N. (2004). Effects of sugar inhibition on cellulases and beta-glucosidase during enzymatic hydrolysis of softwood substrates. Appl. Biochem. Biotechnol. *113-116*, 1115–1126.

Chapter 9: Two additional observations made during my PhD studies

9.1 Introduction

Two additional observations intrigued during my PhD research. First, two false positive blue colonies which I identified during the *in vivo* screening for BGAL inhibitor mutants (*Δbim*) (Figure 4.2). These mutants were deep blue in colour, which made me to think that I have obtained a BGAL inhibitor mutant (*Δbim*), but these blue mutants still produced the BGAL inhibitor when grown in minimal medium. This observation prompted me to further investigate the reason for their deep blue colour after the random mutagenesis using the *mini-tn5* transposons. Second, the commonly used antibiotics have unexpected inhibitory effects on plant beta-glycosidases. This effect was first observed when convolution ABPP was performed with the mannitol-glutamate medium containing kanamycin against the apoplastic fluids isolated from the leaves of *Nicotiana benthamiana*.

9.2 Results and Discussion

9.2.1 Increased glycosidase activities detected in the medium of *Pseudomonas syringae* mutants are due to an insertion of *mini-tn5* transposon in an ABC transporter

During random mutagenesis experiments to generate BGAL inhibitor mutants (Chapter 4), two independent mutants of *Pto*DC3000(*ΔHQ_lacZ*) appeared extremely blue on the X-gal containing mannitol-glutamate minimal medium (Figure 9.1A). Other random mutants and wild-type bacteria were white on the X-gal-containing mannitol glutamate minimal medium due to the production of the BGAL inhibitor (Figure 9.1A). The insertion site of the *mini-tn5* transposon was identified in these two blue strains using TAIL-PCR followed by sequencing the PCR products (Figure 9.1B). This revealed that both mutants had the *mini-tn5* transposon insertion in *PSPTO_1076* but at different locations. This suggests that the blue colour phenotype observed is associated with the loss of the *PSPTO_1076* gene product which encodes an O-antigen ABC transporter. Surprisingly, when the liquid cultures of these mutants were labelled with JJB70 probe, a large number of labelled proteins were observed in the minimal medium or rich LB medium inoculated with *ΔB6_topblue1* and *ΔB7_topblue2* mutants compared to *Pto*DC3000(*ΔHQ*) and *Pto*DC3000(*ΔHQ_lacZ*) (Figure 9.1D&E). Hence the blue deep colour of the *ΔB6_topblue1* and *ΔB7_topblue2* mutants is caused by the extracellular accumulation of a large number of glycosidases in the medium. These active glycosidases probably cleaved the X-gal substrate present in the medium causing the deep blue appearance. Hence it would be interesting to identify these active glycosidases using JJB111 labeling and pulldown. Furthermore, ABC transporters are important for import and export

essential nutrients in bacteria (Davidson et al., 2008). Here the absence of an ABC transporter has caused accumulation of extracellular glycosidases. The mechanism underlying this effect is not known. Nevertheless, to ascertain the involvement of the ABC transporter, gene complementation experiments should be performed with the *PSPTO_1076* gene.

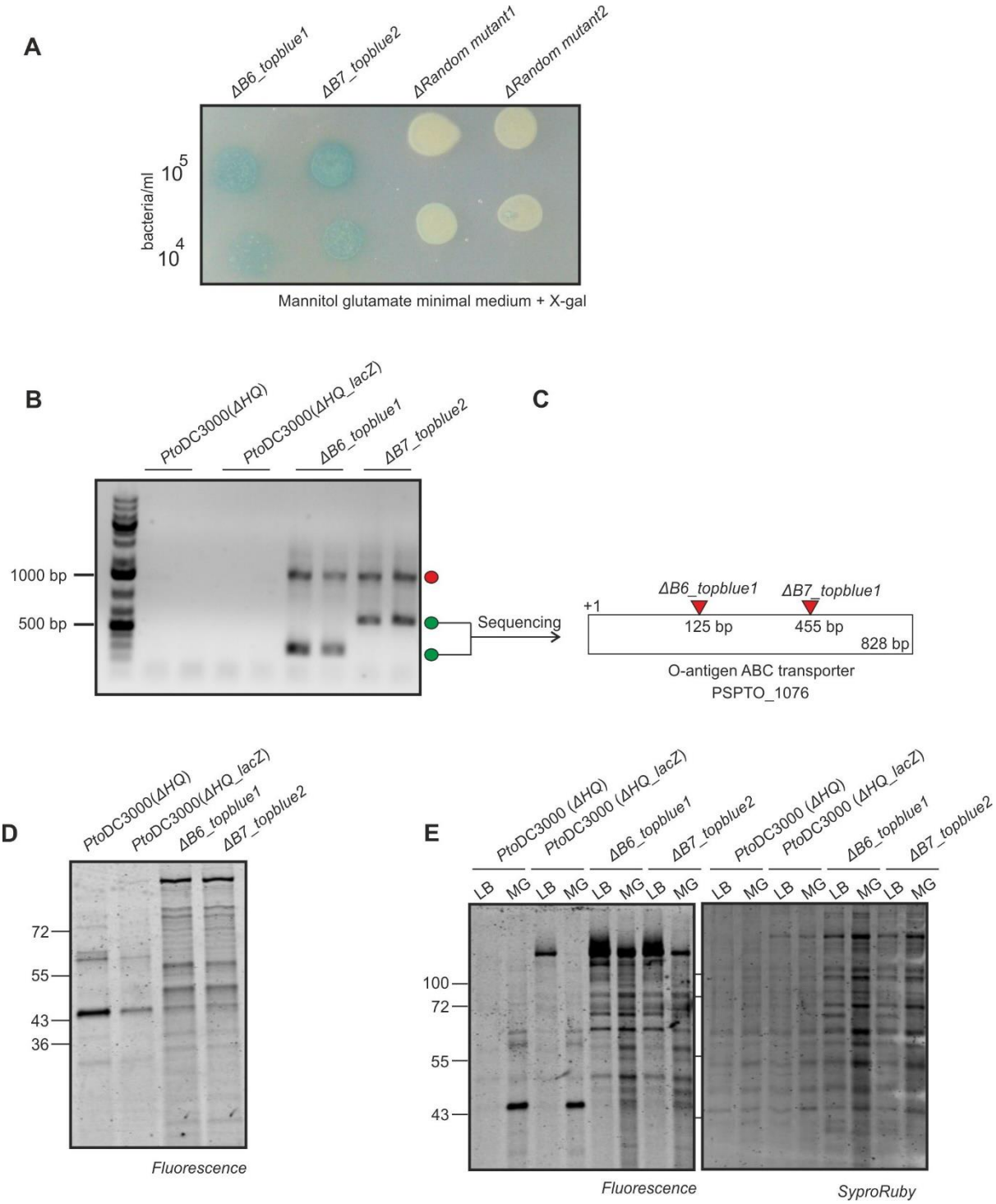

Figure 9.1 Increased glycosidase activities detected in the medium of *Pseudomonas syrinagae* mutants is transposon insertion in an ABC transporter

(A) Two blue coloured colonies obtained during the *in vivo* functional screening assay. The bacterial cultures *ΔB6_top blue1*, *ΔB7_top blue2*, *ΔRandom mutant1* and *ΔRandom mutant2* plated on X-gal containing mannitol-glutamate agar minimal medium at bacterial concentrations of 10^5 and 10^6 bacterial/ml. (B) Insertion site of *mini-tn5* transposons in *ΔB6_top blue1*, *ΔB7_top blue2*. TAIL PCR was performed with the genomic DNA of *ΔB6_top blue1*, *ΔB7_top blue2*, *ΔHQ_lacZ* and *ΔHQ* strains using arbitrary primers and transposon-specific primer pairs. The TAIL PCR products (highlighted in green) were sequenced using transposon-specific primers and contained the information about the insertion site. The band above 500 bp were also sequenced and were found to be unspecific PCR products with no insertion site information (red dot). (C) *ΔB6_top blue1*, *ΔB7_top blue2* had the *mini tn5* transposon inserted in *PSPTO_1076*, which encodes an ABC transporter. (D) Increased glycosidase activities in minimal medium of *ΔB6_top blue1* and *ΔB7_top blue2* mutants. The mutants obtained were inoculated at O.D=0.5 and grown in mannitol-glutamate medium. The overnight (16h) grown bacterial cultures were centrifuged and the mediums were labelled with JJB70 for one hour at pH 5.0. (E) Increased glycosidase activities in LB medium and minimal medium of *ΔB6_top blue1* and *ΔB7_top blue2* mutants. The mutants obtained were inoculated at O.D=0.5 and grown in LB or mannitol-glutamate medium. The overnight (16h) grown bacterial cultures were centrifuged and the mediums were labelled with JJB70 probe for one hour at pH 5.0.

9.2.2 Antibiotics inhibition of plant glycosidases revealed by ABPP

In the chapter 3, the *Pto*DC3000(*ΔHrcC*) mutant was used to investigate if the secretion of the BGAL inhibitor is dependent on the Type-III secretion system (Figure 3.5). During this investigation, convolution ABPP was performed with mannitol-glutamate minimal medium without any bacteria as a control. The control medium of *Pto*DC3000(*ΔHrcC*) inhibited the labelling of certain glycosidases (Lane 6, Figure 9.2A). Surprisingly this glycosidase inhibition was not observed with the medium of *Pto*DC3000(*ΔHQ*) (Figure 9.2A). This raised me an intriguing question how the control medium of *Pto*DC3000(*ΔHrcC*) can inhibit certain glycosidases but not the control medium of *Pto*DC3000(*ΔHQ*)? The only difference between these control mediums is that the control medium for *Pto*DC3000(*ΔHrcC*) contained kanamycin and the medium for *Pto*DC3000(*ΔHQ*) contained rifampicin. Hence I hypothesized that kanamycin might inhibit glycosidases.

To investigate if kanamycin and other antibiotics can inhibit glycosidases, competitive ABPP was performed with different commonly used antibiotics and apoplastic fluids isolated from *N. benthamiana* leaves. The chemical structures of seven different antibiotics used for competitive ABPP are shown (Figure 9.2B). Interestingly, of the tested different antibiotics, kanamycin, tetracycline and chloramphenicol inhibited different glycosidases in apoplastic fluids (Figure 9.2C)**.** Kanamycin suppressed two signals at 55 and 43 kDa, tetracycline suppressed a signal at 95 kDa and chloramphenicol suppressed two signals at 95 and 45 kDa (Figure 9.2C). Based on the MS data (Figure 2.8), the 95 kDa signal is caused by a beta-galactosidase (NbS00037566g0014) and 45 KDa is caused by a different beta-galactosidase (NbS00024332g0007). The 55 kDa signal is caused by a mixture of beta-D-glycosidases (Figure 2.8) and the identity of the 43 kDa signal is not known. Chloramphenicol seems to be

a potent beta-galactosidase inhibitor since both beta-galactosidase signals at 95 and 45 kDa are suppressed, whereas tetracycline is specific for the beta-galactosidase at 95 kDa. These data indicate that kanamycin, tetracycline and chloramphenicol can inhibit labeling of plant glycosidases. The structures of the antibiotics have some similarity to the inhibited glycosidases, but in case of tetracycline and chloramphenicol they lack galactose recognized by beta-galactosidases. Hence these antibiotics might exhibit non-competitive or uncompetitive mode of glycosidase inhibition. The mode of inhibition remains to be investigated by enzymatic assays. Kanamycin, tetracycline and chloramphenicol acts by binding to the large or small subunit of the ribosome and inhibit the protein synthesis process (Chopra and Roberts, 2001; Misumi et al., 1978; Siibak et al., 2009). To my knowledge the off-target inhibition of glycosidases by antibiotics has not been reported before.

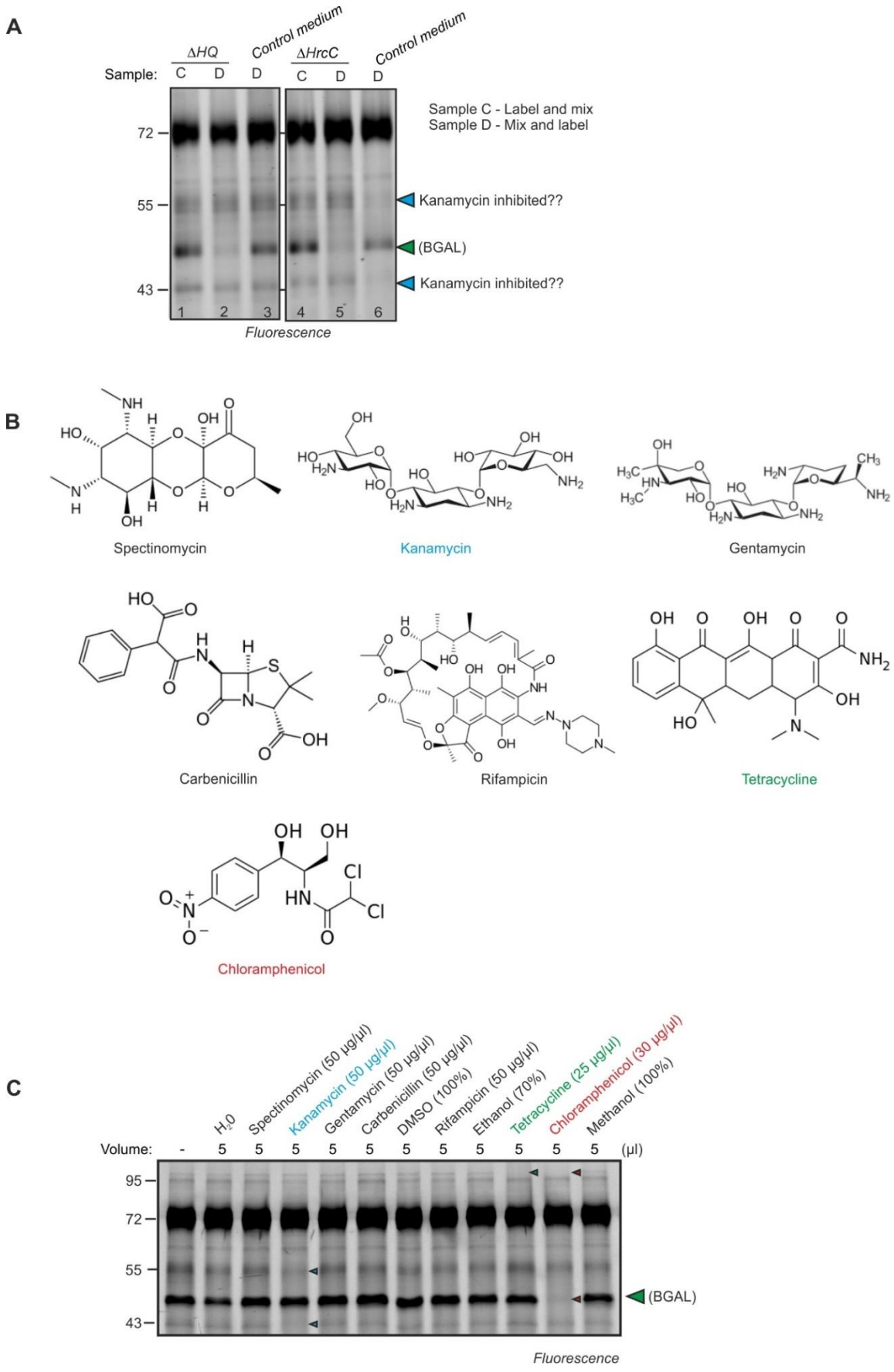

Figure 9.2 Antibiotics inhibition of plant glycosidases

(A) Convolution ABPP with the mannitol-glutamate minimal medium obtained from the *Pto*DC3000 (*ΔHQ*) and *Pto*DC3000(*ΔHrcC*). The *Pto*DC3000(*ΔHQ*) or *Pto*DC3000(*ΔHrcC*) strains were inoculated at O.D=0.5 and grown in the mannitol-glutamate medium. The overnight (16h) grown bacterial cultures were centrifuged and convolution ABPP was performed with the medium fractions against the apoplastic fluids of *N. benthamiana* leaves. (B) Structures of the used antibiotics. (C) Competitive ABPP with the commonly used antibiotics. Spectinomycin, kanamycin, gentamycin, carbenicillin were dissolved in water and filter-sterilized. Rifampicin was dissolved in DMSO. Tetracycline was dissolved in 70% ethanol and chloramphenicol in 100% methanol. 5 µl of antibiotics was preincubated with apoplastic fluids isolated of *N. benthamiana* leaves for 30 minutes and subsequently labelled with JJB70 at pH 5.0. The experiment was repeated once with same results.

9.3 References

Chopra, I., and Roberts, M. (2001). Tetracycline antibiotics: mode of action, applications, molecular biology and epidemiology of bacterial resistance. Microbiol. Mol. Biol. Rev. *65*, 232–260.

Davidson, A.L., Dassa, E., Orelle, C., and Chen, J. (2008). Structure, function and evolution of bacterial ATP-binding cassette systems. Microbiol. Mol. Biol. Rev. MMBR *72*, 317–364.

Misumi, M., Nishimura, T., Komai, T., and Tanaka, N. (1978). Interaction of kanamycin and related antibiotics with the large subunit of ribosomes and the inhibition of translocation. Biochem. Biophys. Res. Commun. *84*, 358–365.

Siibak, T., Peil, L., Xiong, L., Mankin, A., Remme, J., and Tenson, T. (2009). Erythromycin- and chloramphenicol-induced ribosomal assembly defects are secondary effects of protein synthesis inhibition. Antimicrob. Agents Chemother. *53*, 563–571.

Chapter 10: Future directions

During my PhD research, I established glycosidase activity profiling in plants has been established using activity-based probes based on cyclophellitol-aziridine. When these probes were applied to *N. benthamiana* plants infected with the bacterial pathogen *Pseudomonas syringae,* I discovered that the activity of a beta-galactosidase (BGAL) is suppressed during infection by a heat stable BGAL inhibitor produced by the pathogen. Crystallography revealed that this inhibitor is presumably a trihydroxy piperidine (THP). Pathogen growth assays has revealed that BGAL inhibitor mutants (*Δbim*) have reduced virulence. Furthermore, silencing of *BGAL* using virus-induced gene silencing increases bacterial growth, confirming the discovery of an important immune enzyme that is suppressed by a pathogenic bacteria.

In this chapter, I summarize the future prospects on the various research projects which I have been involved during my PhD studies.

10.1 Secretion system employed by *Pto*DC3000 to deliver the BGAL inhibitor

Pseudomonas syringae deploys Type-III secretory sytem to deliver effector proteins to manipulate the host systems during infections. In the Chapter 3, it was found that the secretion of the BGAL inhibitor into the host is independent of the Type-III secretory sytem. Hence it would be interesting to identify the secretion system employed by *Pto*DC3000 to deliver the BGAL inhibitor into the apoplast.

10.2 Unravelling the BGAL inhibitor production using genomics

In Chapter 3, it has been found that the *P. syringae* strains like NCPPB1106 , *Pto*DC3000 and *P.s.* pv *maculicola* KN91, *P.s.* pv*. glycinea* race-4 and *P.s.* pv. *pisi* race-6 can produce the BGAL inhibitor under minimal medium conditions. Other tested *P. syringae* pathovars like *syringae* B301D, *aesculi* 6617, *oryzae* I_6 and *avellanae* S92, *P.corrugata* 2445 and several field isolates of *P. syringae* pv. *tomato* did not produce the BGAL inhibitor. Hence performing comparative genomics experiments with *P. syringae* strains which can produce the BGAL inhibitor versus *P. syringae* strains which do not produce the inhibitor might provide insights in the genes involved in BGAL inhibitor production. Furthermore, ABPP experiments can be performed with plants infected with other microorganisms to test if BGAL inhibitor production is common to other plant pathogens.

10.3 Roles of HrpRS and GabT-1 in BGAL inhibitor production in *Pto*DC3000

In Chapter 4, it was found that HrpR and HrpS are required for BGAL inhibitor production in *Pto*DC3000. Hence, by performing comparative RNA sequencing of the *ΔhrpR/ΔhrpS* double mutant and the wild-type *Pto*DC3000, the genes regulated by *hrpRS* operon can be studied.

Similar studies have been performed using microarray technology (Lan et al., 2006). This information would be helpful for identifying the genes which are regulated by HrpR and HrpS to produce the BGAL inhibitor.

In the BGAL inhibitor mutant, *Δbim5* the *mini-tn5* transposon was inserted in the *gabT-1* gene. GabT-1 is a strong biosynthetic enzyme candidate for BGAL inhibitor production by *Pto*DC3000. GabT-1 from *Bacillus subtilis* MOR1 is involved in the production of 1-Deoxynojirimycin (DNJ), an imino sugar (Kang et al., 2011). Hence it is likely that GabT-1 is involved in the biosynthesis of trihydroxy piperidine (THP), an imino sugar produced by Pseudomonas during infections. Hence it would be interesting to ascertain the involvement of GabT-1 in producing the BGAL inhibitor by performing complementation experiments or by testing independent *ΔgabT-1* mutants.

10.4 Characterization of other BGAL inhibitor mutants (*Δbim*)

In Chapter 4, a total of 18 true BGAL inhibitor mutants have been obtained using the *in vivo* reporter based screening assay. Of these 18 mutants, only two mutants (*Δbim4* (*hrpRS*) and *Δbim5* (*gabT-1*)) have been characterized in detail. The remaining 16 *Δbim* can be characterized to gain insights into BGAL inhibitor production by *Pto*DC3000. Genome sequencing and TAIL-PCR can be performed to identify the insertion sites of the *mini-tn5* transposons and complementation experiments should be performed to ascertain the involvement of the identified gene in BGAL inhibitor production. Furthermore, GC-MS experiments can be performed with the other *Δbim* mutants to ensure if they do not produce trihydroxy piperidine (THP) in their minimal medium and to investigate the accumulation of intermediate metabolites.

10.5 Confirmation on the stereoisomeric form of THP produced by *Pto*DC3000

Several lines of evidence in the Chapter 5 indicate that the 3,4,5-trihydroxy piperidine (THP) is the BGAL inhibitor produced by *Pto*DC3000 during the infection of *N. benthamiana* and when grown in minimal medium. THP can exist in four different stereoisomeric forms. In this study, the co-crystal experiment performed with the semi-purified inhibitor from the *Pto*DC3000(*ΔHQ*) minimal medium sample indicated that the THP has its three hydroxyl groups oriented in same direction. Hence stereoisomer I (THP-MESO-I) is the likely stereoisomer produced by *Pto*DC3000(*ΔHQ*). However, stereoisomer III has moderate beta-galactosidase inhibitory activity with the tested glycosidases (Bernotas et al., 1990). To add further strength to the claim that THP-MESO-I is the actual BGAL inhibitor, the THP present in the apoplastic fluids during infection should be isolated as pure compound to perform 1D and 2D-NMR to determine the stereochemistry of the hydroxyl groups. Alternatively, inhibition

assays with a purified BGAL enzyme and the four stereoisomers of THP can be performed to determine their respective inhibition constants (Ki).

10.6 Does THP promote virulence?

In Chapter 6, several BGAL inhibitor mutants *(Δbim),* displayed reduced virulence on wild-type *N. benthamiana* leaves. These pathogen assays indicate that the THP might be a novel virulence molecule produced by *Pto*DC3000. To confirm that THP is associated with the virulence of *Pto*DC3000, the chemical complementation experiments by supplementing synthetic THP to BGAL inhibitor mutants can be performed. Chemical complementation can also be performed to determine if THP promotes virulence of other plant pathogens, and to test if galactostatin, a BGAL inhibitor can cause the same effects.

10.7 Active BGAL might have a functional role during plant-pathogen interactions

In Chapter 6, an increased growth of *Pto*DC3000(*ΔHQ*) was observed on *TRV:BGALa* plants generated using virus-induced gene silencing (VIGS). This indicates that BGAL might contribute to immunity in *N. benthamiana* plants. The pathogen assays can be also done with the BGAL-depleted plants generated using the amiRNA or CRISPR/Cas9 technologies to confirm the observed phenotype. Constructs for silencing BGAL using amiRNA have been transformed into *N. benthamiana* plants but BGAL depletion in these lines was found to be unstable. Similarly, for knocking out the *BGAL* gene using CRISPR/Cas9 constructs pBK13 and pBK14 have been transformed into *N. benthamiana* plants and stable transgenic plants are available for testing. Futhermore, pathogen growth assays can be performed using BGAL inhibitor mutants (*Δbim*) on the generated BGAL depleted plants to investigate if BGAL is the main target of the BGAL inhibitor produced by *Pto*DC3000. If BGAL is the main target for the inhibitor, the BGAL inhibitor mutants which displayed reduced growth on the wild-type *N. benthamiana* plants (Figure 6.2) will have growth levels similar to the parental *Pto*DC3000(*ΔHQ_lacZ*) strain on the BGAL depleted plants. Furthermore, pathogen growth assays can be performed with *Pto*DC3000 on *Arabidopsis thaliana* or *Solanum lycopersicum* (tomato) which are the *BGAL* gene. These assays would show if BGAL also contributes to immunity in other plant species.

10.8 References

Bernotas, R.C., Papandreou, G., Urbach, J., and Ganem, B. (1990). A new family of five-carbon iminoalditols which are potent glycosidase inhibitors. Tetrahedron Lett. *31*, 3393–3396.

Kang, K.-D., Cho, Y.S., Song, J.H., Park, Y.S., Lee, J.Y., Hwang, K.Y., Rhee, S.K., Chung, J.H., Kwon, O., and Seong, S.-I. (2011). Identification of the genes involved in 1-

deoxynojirimycin synthesis in *Bacillus subtilis* MORI 3K-85. J. Microbiol. Seoul Korea *49*, 431–440.

Lan, L., Deng, X., Zhou, J., and Tang, X. (2006). Genome-wide gene expression analysis of *Pseudomonas syringae* pv. *tomato* DC3000 reveals overlapping and distinct pathways regulated by hrpL and hrpRS. Mol. Plant-Microbe Interact. MPMI *19*, 976–987.

Chapter 11: Materials and methods

11.1 Biological Materials

Arabidopsis thaliana (ecotype Columbia, Col-0) were grown at 24°C (day)/20°C (night) in a growth chamber under a 12 h light regime. Leaves from rosettes of 4-week old Arabidopsis plants were used for the protein extraction. Cell cultures of *Arabidopsis thaliana* (ecotype Landsberg erecta) were grown and weekly subcultured in L9 liquid medium (4.41 g/l MS-Basal medium including nitsch vitamins (Duchefa M0256), 30 g/l sucrose, 5.4 µM α-naphthyleneacetic acid, 0.23 µM kinetin, adjusted to pH 5.6). *Nicotiana benthamiana* plants were grown at 23°C and 60% relative humidity under a 12 h light regime. 4-week old *N. benthamiana* plants were used for the apoplastic fluid isolation and infection assays. *Pseudomonas syringae* pv. *tomato* (*Pto*) strains: *Pto*DC3000(*WT)* and *Pto*DC3000(Δ*HQ*) were grown in LB medium containing rifamycin (50 µg/ml).

11.2 Sample preparation for labeling assays

Extracts for small scale labeling: Leaves of various plant species or different organs of Arabidopsis plants were homogenized with 500 µl of 50 mM MES buffer at pH 6.0 or 50 mM MOPS buffer at pH 7.5. For the pH course experiment, the leaves were homogenized in sterile water. Two leaf discs (1.5 cm, diameter) were taken from the leaves of different plant species and homogenized with 500 µl of 50 mM MOPS buffer at pH 7.5. After grinding the tissues in a 1.5 ml tube, the samples were centrifuged at 10000 g, 4ºC for 10 min to remove cell debris and the supernatant containing the soluble proteins was used for labeling.

Extracts for large scale labeling: 2 grams of Arabidopsis rosette leaves were frozen with liquid nitrogen and ground with mortar and pestle. 5 ml of extraction buffer (50mM MES buffer at pH 6.0, 0.1% Triton (X-100) and 10 % glycerol) were added to the leaf powder, vortexed and centrifuged at 4000 rpm, 4ºC for 30 minutes to remove cell debris. The supernatant containing the soluble proteins were used for large scale labeling. *Apoplastic fluid isolation*: The apoplastic fluids were isolated by vacuum-infiltration and centrifugation (Hong and Van der Hoorn, 2014; Joosten, 2012). In brief, the leaves were submerged in ice-cold sterile water and vacuum was applied. The water was infiltrated into intercellular spaces of leaves by slowly releasing the vacuum. The leaves were then dried shortly and centrifuged at 3000 rpm, 4ºC for 15 min. Protease inhibitor cocktail solution (cOmplete Protease Inhibitor Tablets, Roche Applied Sciences) was added to the isolated apoplastic fluids at 4X final concentration.

Infection with P.syringae: Strains of *Pseudomonas syringae* pv. *tomato* DC3000 were grown overnight in 10 ml NYG liquid medium containing rifamycin (50 µg/ml) and gentamicin (50 µg/ml), centrifuged and resuspended with sterile water. The resuspended solution was diluted to 10^6 bacteria/ml with sterile water. The infiltration was performed on leaves of *N. benthamiana* plant using a 1 ml needleless syringe and the infiltrated regions were maked on the leaves. Sterile water was infiltrated into the leaves as mock control. At two days post infiltration (2dpi), the infiltrated regions were excised from the leaves and apoplastic fluids were isolated from an equal number of excised regions. The protease inhibitor cocktail solution (cOmplete Protease Inhibitor Tablets, Roche Applied Sciences) was added at 4X final concentration and the apoplastic fluid was used for labeling assays.

Fractionation of infected apoplastic proteomes: Apoplastic fluids isolated from *Pto*DC3000(Δ*HQ*) treated samples were concentrated using vivaspin 500 spin colums with 3000 Da MWCO filter (Sartorius Stedim Biotech) by centrifuging at 10000 g, 4ºC for 60 min. The concentrate (>3 kDa) and filtrate (<3 kDa) were normalized to equal starting volumes and used for mixing and labeling assays.

11.3 Labeling assays with JJB probes

Labeling plant extracts: Leaf or organ extracts containing ~1.0-1.5 mg/ml total soluble proteins were pre-incubated with 50 µM KY371 or DMSO for 30 minutes at pH 6.0 or 7.5. These extracts were incubated with 2 µM JJB70 or JJB111 for 1h at room temperature in the dark in 50 µl total volume. Equal volumes of DMSO were added for the no-probe-control. For the pH course experiment, Arabidopsis leaf extracts were incubated with suitable pH buffers (50 mM sodium acetate buffer for pH 4.0, 50 mM MES buffer for pH 5.0-6.5, 50 mM MOPS buffer for pH 7.0-7.5, Tris buffer for pH 8-10) and 2 µM JJB70 in the dark for 1h at room temperature in 50 µl total volume.

Peptide-N-Glycosidase F (PNGaseF) treatment of labeled proteins: 10 µl of JJB70 or DMSO incubated extracts were treated with 1.5 µl of 10X glycoprotein denaturing buffer (New England BioLabs) and heated at 100 ºC for 10 min. The denatured proteins were treated with 3 µl of H_2O, 2 µl of 10% NP-40, 2 µl of 10X G7 buffer (New England BioLabs), 1.5 µl PNGaseF (New England BioLabs) or H_2O and incubated at 37 ºC for 1h.

Labeling apoplastic fluids: Apoplastic fluids were pre-incubated with or without 50 µM KY371 for 30 minutes at pH 5.0 with 50 mM MES buffer. These apoplastic fluids were incubated with or without 2 µM JJB70 in the dark for 1h at room temperature for labeling in 50 µl total reaction volume. For pH course experiment, apoplastic fluids were incubated with suitable pH buffer (50 mM sodium acetate buffer for pH 4.0, 50 mM MES buffer for pH 5.0-

6.5, 50 mM MOPS buffer for pH 7.0-7.5, Tris buffer for pH 8-10) and 2 µM JJB70 in the dark for 1h at room temperature in 50 µl total volume.

Analysis of labeled proteins: The labeling reactions were stopped by adding gel loading buffer containing β-mercaptoethanol at 1X final concentration and heating at 95 ºC for 10 minutes, unless indicated otherwise. The labeled proteins were separated on 12% protein gels at 200 volts for 1h. The JJB70-labeled proteins were detected in the protein gels with the Typhoon FLA 9000 scanner (GE Healthcare Life Sciences) using excitation wavelength at 472 nm and BPG1 filter (GE Healthcare Life Sciences). The fluorescence of the labeled proteins was quantified using ImageQuant (GE Healthcare Life Sciences). JJB111-labeled proteomes were transferred from the protein gels onto PVDF membranes, incubated with streptavidin HRP (ultra sensitive, Sigma) and detected using chemiluminescent substrates (SuperSignal West Chemiluminescent substrates, Thermo Scientific).

In vivo labeling of Arabidopsis cell cultures: 500 µl of an Arabidopsis cell cultures was transferred to a 12-well tissue culture plate. The medium was removed from the cell culture, replaced by 500 µl fresh L9 medium and kept shaking gently for 30 minutes before labeling. The cell cultures were preincubated with or without 50 µM KY371 for 30 minutes under gentle shaking. The cell culture was labeled by adding 2 µM JJB70 under gentle shaking for 1h. After labeling, the medium from the cell culture was removed and precipitated with 1 ml of 100% ice-cold acetone. 20 µl of 1X gel loading buffer (containing β-mercaptoethanol) was added to the precipitated proteins and the sample was heated at 95 ºC for 10 minutes. The labeled cells were ground with 50 µl of 4X gel loading buffer (containing β-mercaptoethanol) and the sample heated at 95 ºC for 10 minutes. For Control 1 (Ctr1): 500 µl washed and unlabeled cells were homogenized with 1 µl of 1 mM JJB70 for 30s and heated at 95 ºC for 10 minutes in the presence of 50 µl of 4X gel loading buffer (containing β-mercaptoethanol). For Control 2 (Ctr2), washed and unlabeled cells were homogenized with 50 µl of 4X gel loading buffer containing 2 µM JJB70 and β-mercaptoethanol. The labeled proteins were analyzed as explained above.

Large-scale labeling and affinity purification: 2 ml of leaf extracts containing ~2.0 mg/ml total leaf proteins were incubated with 5 µM JJB111 at room temperature for 1h. For labeling apoplastic fluids, 10 ml apoplastic fluids were incubated with 5 µM JJB111 at room temperature for 1h. Labeling was stopped by precipitating the total proteins by chloroform/methanol precipitation method (Wessel and Flügge, 1984). In brief, four volumes of ice-cold methanol, one volume of ice cold chloroform and three volumes of water were added. The samples were vortexed and centrifuged at 4000 rpm, 4ºC for 30 minutes. The precipitated proteins were dissolved in 2 ml of 1.2% SDS dissolved in 1X PBS solution (SDS/PBS) by sonication for 4-5s and heating at 95 ºC for 10 minutes. This solution was diluted to 0.2% SDS/PBS by adding 10 ml of 1X PBS solution. The resulting solution was

incubated with 100 µl of pre-equilibrated streptavidin beads (High capacity streptavidin beads, Thermo scientific) for 1h at room temperature. The beads containing the labeled proteins were isolated by centrifuging at 1400 g for 3 minutes. These beads were washed successively three times with 5 ml of 1.2% SDS/PBS solution, thrice with 5 ml of 1.0% SDS/PBS solution and thrice with 10 ml 1X PBS buffer. The final wash was with 10 ml water. The captured proteins were eluted by boiling the beads at 95 ºC in 30 µl of 4X gel loading buffer. The eluted proteins were separated on 12% protein gels at 200 volts for one hour and the protein gels were stained overnight with SYPRO Ruby (Life technologies). The proteins were detected by scanning the gels at excitation wavelength of 473 nm with LPG filter in Typhoon FLA 9000 scanner (GE Healthcare Life Sciences).

11.4 Identification of labeled proteins

In-gel digestion and MS: Bands were excised by hand and treated with trypsin as described elsewhere (Shevchenko et al., 2006). Digests were separated on a Thermo/Proxeon Easy nLC II in a two-column configuration (precolumn 3cm x 100um, 5um C18AQ medium, analytical column 10cm x 75 um, 3 um C18AQ) coupled to an LTQ-Velos ion trap (Thermo Scientific). Peptides were separated over a 35 minute gradient running from 5% - 32% ACN/H_2O with 0.1% formic acid. MS/MS spectra were acquired on multiply-charged precursors with m/z between 400 and 1600 Daltons using a Top20 method for with active exclusion for 30 seconds in a window from 0.2 Da below to 1.5 Da above the precursor mass. The resulting RAW files were de-noised and converted into mgf format using MS Convert from the Proteowizard 2.1 package (http://www.proteowizard.org/) accepting only the 6 strongest peaks per 100 Da window.

Database searching: The Nicotiana/Pseudomonas sequence database was based on the SOL genomics network (solgenomics.net) *Nicotiana benthamiana protein database* v0.4.4 (76379 sequences) to which 5619 Pseudomonas DC3000 sequences were added (Buell et al., 2003). The Arabidopsis database was based on TAIR10 (35384 sequences). 1095 common artifact sequences were added to both databases and both were then reversed and concatenated to provide decoys for false discovery rate (FDR) calculation. MS/MS spectra were searched against the described databases using MASCOT 2.4 (matrixscience.com) permitting JJB111 (735.386 Da) as an additional variable modification of Asp and Glu residues in the searches. For both searches, a Mascot score of 38 represents a 95% certainty cut-off.

Other Mascot parameters were: Precursor mass tolerance 0.4 Da, fragment mass tolerance 0.5 Da, 1 C13 permitted, one tryptic miscleavage, fixed modifications–carbamidomethyl (C), Variable modifications–oxidation (Met).

11.5 Bioinformatics

Glycosyl hydrolase (GH) family classification: GH family classification of identified glycosidases in the Arabidopsis leaf proteome was based on the annotations done for the genome of *Arabidopsis thaliana* in the CAZY database (Lombard et al., 2014). GH family classification of identified glycosidases in the secreted leaf proteome of *N. benthamiana* was made by submitting protein sequences to the PFAM database (Punta et al., 2012).

Phylogenetic tree construction: Protein sequences of 258 retaining glycosidases in the genome of Arabidopsis were retrieved from TAIR database (Lamesch et al., 2012). The protein sequences of AT4G33850 and A_IG002N01.5 were not available in the TAIR database hence they were retrieved from the National centre for Biotechnology Information (NCBI) (http://www.ncbi.nlm.nih.gov/). The sequences were aligned with ClustalX2 (Larkin et al., 2007). The pairwise alignment gap opening penalty 30 and gap extension penalty 0.75 was used, while for multiple alignment gap opening penalty 15 and gap extension penalty 0.3 was used. The alignment files were saved in PHYLIP format and R script has been implemented to constructing the tree (Charif and Lobry, 2007; Paradis et al., 2004). The Neighbor-Joining algorithm was used for tree construction from the calculated distance matrix in the program.

Arabidopsis thaliana leaf proteome analysis: The spectral counts (Qty spectra) of all 260 retaining glycosidases detected in the juvenile leaves of Arabidopsis were retrieved from pep2pro database (Hirsch-Hoffmann et al., 2012).

11.6 In-solution digestion of apoplastic fluids for proteome analysis

DTT (ThermoFischer, R0861) reducing agent was added at 5 mM final concentration to 500 µl of apoplastic fluids from *Nicotiana benthamiana* (isolated from 16 leaf discs) and the sample was incubated for 30 minutes at room temperature. IAM reagent was added at 20 mM final concentration to the reduced apoplastic fluids and the sample was incubated for 30 min at room temperature. Then the apoplastic fluids were aliquoted equally in two different eppendorf tubes and chloroform-methanol precipitation was performed. The precipitated proteins were dissolved in 100 µl of 6M Urea, vortexed well and 600 µl of milli-Q water was added. 2 µl of trypsin/lysC (Promega, cat.no. V5071) mix was added at final concentration of 0.4 µg and the sample was incubated at 37^{o}C for 18 hours. The trypsin digestion was stopped by adding 1 % formic acid and the digested peptides were purified using the sep-paK C18 columns.

11.7 Detection of inhibitors in the *Pto*DC3000(*ΔHQ*) sample by convolution ABPP

Two diiferent samples: sample C and sample D were prepared for the convolution ABPP. For sample C: The apoplastic fluids isolated from *Pto*DC3000(Δ*HQ*) and the mock treated samples were first labeled individually with JJB70 for one hour at pH 5.0. After stopping the labeling

reaction the labeled proteomes were mixed together in equal volumes. For sample D: Equal volumes of apoplastic fluids isolated from the *Pto*DC3000(Δ*HQ*) and the mock treated samples were first mixed together, preincubated for 30 minutes and then labeled with JJB70 one hour at pH 5.0. The labeling reaction was stopped by adding gel loading buffer and heating at 95 ºC. The sample C and sample D were separated on 12% protein gels at 200 volts for one hour. The JJB70-labeled proteins were detected in the protein gels with the Typhoon FLA 9500 scanner (GE Healthcare Life Sciences) using excitation wavelength at 472 nm and BPG1 filter (GE Healthcare Life Sciences).

11.8 Minimal medium assay to detect the BGAL inhibitor

The *Pto*DC3000(Δ*WT*) or *Pto*DC3000(Δ*HQ*) strains were grown in LB medium. The overnight grown bacterial cultures was centrifuged and resuspened in 5 ml of mannitol-glutamate minimal medium (Bronstein et al., 2008). The resuspened culture was centrifuged again and the supernantant was removed. The bacterial pellet was diluted to OD=0.5/ml using mannitol-glutamate minimal medium. The 2 ml of the resuspened bacteria was grown at 23^0C in a loose cap bacterial culture tubes. After 16 hours, the cultures were centrifued and convolution ABPP was performed with supernant against the apoplastic fluids isolated of *N. benthamiana* leaves using JJB70.

11.9 *In vivo* reporter-based functional assay to detect the BGAL inhibitor

The pHRP308 plasmid containing the *lacZ* reporter gene was transformed into *Pto*DC3000(*WT*) or *Pto*DC3000(*ΔHQ*) by electroporation. The transformed bacterial strains *Pto*DC3000(*WT_lacZ*) or *Pto*DC3000(*ΔHQ_lacZ*) were selected on the LB medium which contains X-gal (0.1mg/ml, Thermo scientific, cat.no. R0941), IPTG (0.1mM final concentration, Thermo scientific, cat.no. R1171), 12.5 µg/µl rifampicin and 12.5 µg/µl gentamycin antibiotics. The transformed blue colony was selected and grown in LB liquid medium. The overnight grown cultures were centrifuged and diluted to 10^6 bacteria/ml with LB medium or mannitol-glutamate minimal medium.100 µl of respective diluted bacterial cultures were plated either onto X-gal and IPTG containing LB medium or X-gal and IPTG containing mannitol-glutamate minimal medium with contains 12.5 µg/µl rifampicin and 12.5 µg/µl gentamycin antibiotics and incubated at 28^0C for 36 hours.

11.10 Random mutagenesis of *Pto*DC3000(*ΔHQ_lacZ*) to generate BGAL inhibitor mutants (*Δbim*)

The recipient strain (*Pto*DC3000(*ΔHQ_lacZ*)), the donor strain (*E.coli* (*mini-tn5*-km2)) and the helper strain (*E.coli* (pRK2013)) were grown in LB medium. The overnight grown cultures were centrifuged and washed once with LB medium without any antibiotics. The recipient strain

*Pto*DC3000(*ΔHQ_lacZ*) was diluted to O.D = 0.5 using LB medium without antibiotics. The donor and the helper strains were resuspened in 1 ml of LB medium without antibiotics. Tri-parental mating was performed by mixing 700 µl of *Pto*DC3000(*ΔHQ_lacZ*), 300 µl of *E.coli* (*mini-tn5*-km2) and 100 µl of *E.coli* (pRK2013). The mixed cultures were centrifuged and resuspened in 100ul of LB medium without antibiotics. The conjugation mix was plated on the LB Agar medium and incubated at 28^0C. After 6 hours, the conjugation mix was re-suspended in 1 ml mannitol-glutamate minimal medium and 100 µl of the suspension was plated onto mannitol-glutamate minimal medium containing 0.1mg/ml X-gal, 0.1mM IPTG, 12.5 µg/µl rifampicin, 12.5 µg/µl gentamycin and 12.5 µg/µl kanamycin antibiotics and plates were incubated at 28^0C for 36 hours.

11.11 Identification of the insertion site of *mini-tn5* transposons

Thermal asymmetric interlaced polymerase chain reaction (TAIL PCR) was performed to identify the insertion site of *mini-tn5* transposons. The single bacterial colony from the BGAL inhibitor mutants was dissolved in 50 µl water. 1st Round PCR was performed with 5 µl diluted bacteria in 20 µl standard PCR reaction which contains one unit Taq polymerase (NEB, M0273), 2.5 mM $MgCl_2$, 0.5 µM of 1st arbitrary primer (5'-GGCCACGCGTCGACTAGTACNNNNNNNNNGAACG-3') and 0.5 µM of 1st transposon specific primer (5'-GTGACAAGTGTTGGCCATGG-3'). The thermo cycler condition was followed for the 1st round PCR: 95^0C for 3 minutes, followed by cycles of 94^0C for 30 seconds, X^0C for 30 seconds and 72^0C for 3 minutes. The initial value of X was started from 62^0C and lowered to 54^0C in successive cycles by 1^0C. Further 30 cycles with annealing temperature at 54^0C were performed with final extension of 72^0C for 3 minutes. The 1st round PCR product was diluted with water in the ratio of 1:50 and 5 µl of diluted PCR product was used for the next round PCR reaction. 2nd round PCR was performed in a 50 µl standard PCR reaction which contains one unit Taq polymerase (NEB, M0273), 2.5 mM $MgCl_2$, 0.5 µM of 2nd arbitrary primer (5'- GGCCACGCGTCGACTAGTAC-3') and 0.5 µM of 2nd transposon specific primer (5'- CGTATGTTGCATCACCTTCACC-3'). The round PCR was performed with standard thermo cycler conditions with annealing temperature of 55^0C. The PCR products were eluted from the 2% agarose gel using Qiagen gel extraction kit and sent for sequencing using the sequencing primer (5'-GGACAACTCCAGTGAAAAGTTC-3').

11.12 Colony PCR to confirm the insertion of *Δbim4* and *Δbim5*

Colony PCR was performed with the single colony derived from the *Δbim4* or *Δbim5* mutants. The single bacterial colony from the BGAL inhibitor mutants were resuspened in 50 µl water and 5 µl of diluted bacteria was added to 20 µl standard PCR reaction which contains one unit

of Taq polymerase (NEB, M0273), 2.5 mM $MgCl_2$, 0.5 µM of forward primer (*hrpRS*) (5'-CTGGAGGCCTCTATGTAGCC-3') and 0.5 µM of reverse primer (*mini-tn5*) (5'-GCGTCAGCAACCAGTTATCC-3') for *Δbim4* and 0.5 µM of forward primer (*gabT-1*) (5'-GAGGTGAAGAACACCGCTTT-3') and 0.5 µM of reverse primer (*mini-tn5*) (5'-GCGTCAGCAACCAGTTATCC-3') for *Δbim5* mutants. The PCR products were cleaned up using the Qiagen gel extraction kit and sent for sequencing. The PCR products were sequenced using the sequencing forward primer (*hrpRS*) (5'-CGTTGACCACACCGAATAAC-3') and forward primer (*gabT-1*) (5'- CCAGGTAGGGCTGATAGGAC-3').

11.13 Chloroform-methanol precipitation to enrich for the BGAL inhibitor

4 ml of mannitol-glutamate minimal medium or 10 ml of the apoplastic fluids from the *Pto*DC3000(Δ*HQ*) samples were subjected to chloroform-methanol precipitation by adding equal volumes of metabolite isolation buffer containing chloroform-methanol-water in the ratio 1: 2.5:1. The upper hydrophilic phase (methanol/ water) and the lower hydrophobic phase (chloroform) were collected and freeze-dried separately using a lyophilizer. The freeze dried fractions were dissolved in 150 µl water and concentrated using ultrafiltration spin colums. The <3 kDa (filtrate) fractions were collected, heated at 95ºC for 5 min and competitive ABPP was performed with the apoplastic fluids isolated of *N. benthamiana* leaves using JJB70.

11.14 Cation-exchange chromatography to enrich for the BGAL inhibitor

Large scale chloroform-methanol precipitation was performed with 40 ml of mannitol glutamate medium or 50 ml of *Pto*DC3000(Δ*HQ*) apoplastic fluid. Samples were subjected to chloroform-methanol precipitation by adding equal volumes of metabolite isolation buffer containing chloroform-methanol-water in the ratio 1:2.5:1. The upper hydrophilic phase (methanol/water) was collected and freeze-dried using a lyophilizer. The freeze dried hydrophilic phase (methanol/water) was dissolved in 50 ml of water, acidified to pH=3.5 using 1M HCL. The cation exchange columns were prepared using the dowex50WX2 resin (Sigma cat.no. 217441) by filling up to 15 cm in a glass column. The resins were washed three times with 20 ml of 2.5M HCL and three times with 20 ml of water. Next, the 50 ml acidified hydrophilic phase (methanol/water) sample was added to the prepared dowex50WX2 resin column. The flow-through was collected and labelled as Fraction A. The column was washed with 200 ml water and the water-wash fraction was labelled as Fraction B. The cation-exchange columns were eluted using 200 ml of 2.5M ammonium hydroxide (NH_4OH) and the eluate was labelled as Fraction C. The fraction A, B and C were freeze-dried using a lyophilizer. The freeze-dried fractions were dissolved in 200 µl water and competitive ABPP was performed with the apoplastic fluids isolated of *N. benthamiana* leaves using JJB70.

11.15 Gel-filtration chromatography to purify the BGAL inhibitor

Large scale chloroform-methanol precipitation was performed with 2 litres of *Pto*DC3000(Δ*HQ*) grown mannitol glutamate medium. The upper hydrophilic phase (methanol/water) was collected and freeze-dried using a lyophilizer. The freeze dried hydrophilic phase (methanol/water) was dissolved in 50 ml of water, acidified using 1N HCL and the cation exchange chromatography was performed as mentioned in section 7.12.

Preparation of gel-filtration column: 30 g of sephadex LH-20 gel-filtration material (GE healthcare, 56-1190-97AD) was treated with in 200 ml of methanol:water (9:1) mixture for 3 hours. The material was packed into a 15 cm glass column without any air bubbles using a hand pump. The packed material was washed twice with 50 ml methanol:water (9:1) mixture. The freeze dried NH_4OH eluate after cation exchange chromatography was dissolved in 1 ml of methanol:water (9:1) mixture and loaded on to the prepared gel-filtration column. The molecules were separated using methanol:water (9:1) mixture as running buffer and 15 ml volume for each fraction was collected 14 fractions in total. Each fraction was freeze-dried using a lyophilizer. The freeze-dried fractions were dissolved in 100 µl water and competitive ABPP was performed with the apoplastic fluids isolated of *N. benthamiana* leaves using JJB70.

11.16 Derivatization of samples for chromatography mass spectrometry (GC-MS)

250 µl of the NH_4OH eluate from the *Pto*DC3000(Δ*HQ*) mannitol glutamate medium or the *Pto*DC3000(Δ*HQ*) apoplastic fluid samples were freeze-dried using a lyophilizer. The dried compound was dissolved in 70 µl of methoxyamine hydrochloride mixture (20 mg of methoxyamine hydrochloride (Sigma, cat.no. 226904) dissolved in 1 ml of 100% pure pyridine) and incubated at 37^0C for 2 hours. The samples were silylated by adding 100 µl of 97% pure *N*-Trimethylsilyl-*N*-methyl trifluoroacetamide (MSTFA) (Sigma, cat.no. 394866) and incubated at 60^0C for 2 hours.

15 µl of 100 mM of synthetic THP (MESO) was dried using speedvac concentrator. The dried compound was dissolved in 35 µl of methoxyamine hydrochloride mixture (20 mg of methoxyamine hydrochloride (Sigma, cat.no. 226904) dissolved in 1 ml of 100% pure pyridine) and incubated at 37^0C for 2 hours. The samples were silylated by adding 70 µl of 97% pure *N*-Trimethylsilyl-*N*-methyl trifluoroacetamide (MSTFA) (Sigma, cat.no. 394866) and incubated at 60^0C for 2 hours.

11.17 Virus-induced gene silencing (VIGS)

The DNA fragments for silencing the *BGAL* and *PLCP* gene expression in *Nicotiana benthamiana* plants were commercially synthesized (Biomatik) and obtained in a *pBluescript*

(pBS) cloning vector. The synthesised fragments contained restrictions sites (EcoRI and BamH1) for cloning to the binary vector. The respective fragments were cloned into TRV2 binary vector using EcoR1 and BamH1 restriction sites. The cloned VIGS constructs were verified using the forward primer (pTRV2F) (5'- GTTACTCAAGGAAGCACGATGAGC-3') and reverse primer (pTRV2R) (5'-GTCGAGAATGTCAATCTCGTAGG-3'). The different Agrobacterium strains carrying the different TRV constructs for silencing the *BGAL* or *PLCP* gene expression were mixed individually with the Agrobacterium strain carrying pTRV1 vector in a 1:1 ratio and incubated in the dark for 2 hours in presence of acetosyringone. The mixed cultures were diluted to OD=0.5 and infiltrated into leaves of 10 day old *N. benthamiana* plants and incubated at 23^0C degrees in the growth chamber.

11.18 Pathogen growth assay

N. benthamiana leaves were infiltrated with *Pto*DC3000(∆*HQ*) or BGAL inhibitor mutants at $2X10^5$ bacteria/ml or OD = 0.0002. The three leaf discs of one cm were isolated from the *N. benthamiana* plants at different time points, surface sterilized with 15% hydrogen peroxide and ground in 1ml water. The samples were then serially diluted with water, plated onto LB medium and incubated at 28^0C. After 36 hours, the colony forming units (CFU) were counted.

11.19 amiRNA construct for *BGAL* gene silencing

The 75 bp oligonucleotides for *BGAL* gene silencing were designed using the web server http://p-sams.carringtonlab.org/. The oligonucleotide annealing reaction was performed in 50 µl reaction in the presence of oligo annealing buffer (60 mM Tris-HCl (pH 7.5), 500 mM NaCl, 60 mM MgCl2, 10 mM DTT), 4 µM of forward oligonucleotide (5'-TGTATAGAATTTCCACTGTTTCCTAATGATGATCACATTCGTTATCTATTTTTTTAGGAAA CAGGGGAAATTCTA-3') and 4 µM of reverse oligonucleotide (5' AATGTAGAATTTCCCCTGTTTCCTAAAAAAATAGATAACGAATGTGATCATCATTAGGAA ACAGTGGAAATTCTA-3'). The annealing reaction was performed at 94°C for 5 minutes and then cooled down to 20°C at 0.05ºC/sec cycle. The annealed oligonucleotides were diluted to 0.15 µM final concentration and cloned to the *pMDC123SB-AtMIR390a-B/c* vector (Carbonell et al., 2014) using BsaI restriction site, which results in *amiRNA:BGAL* binary vector. The construct *amiRNA:BGAL* was transformed into *N. benthamiana* plants by Agrobacterium mediated transformation.

11.20 RT-PCR analysis of *amiRNA:BGAL* plants

100 mg of leaf tissues were ground in liquid nitrogen and the total RNA was extracted using 1 mL TRIzol Reagent (Invitrogen) and RNeasy kit (Qiagen). The total RNA from the samples

was diluted using the DEPC treated water. The first strand cDNA synthesis were performed using SuperScript™ II Reverse Transcriptase kit (Invitrogen). The obtained cDNA was diluted 20X using the DEPC treated water. Standard PCR reaction was performed with the diluted cDNA template in a 50 µl reaction, which contains one unit Taq polymerase (NEB, M0273), 2.5 mM $MgCl_2$, 0.5 µM of forward primer (*BGAL*) (5'- CGCATCCTTGTCAGGTTGGA -3') and 0.5 µM of reverse primer (*BGAL*) (5'- TGGCCAAGTGATTCCACATGA -3') for *BGAL* gene and 0.5 µM of forward primer (*F-box*) (5'- GGCACTCACAAACGTCTATTTC -3') and 0.5 µM of reverse primer (*F-box*) (5'- ACCTGGGAGGCATCCTGCTTAT -3') for *F-box* gene. The PCR products were separated on a 1.5% Agarose gel and imaged using the Gene snap fluorescence imager.

11.21 Expression and detection of BGAL protein in the *PLCP* silenced plants

The full length *BGAL* gene without its signal peptide was commercially synthesized and obtained in a pBluescript (pBS) cloning vector (Biomatik). The synthesised full length *BGAL* gene contained a strep-II tag at the start of the gene and restrictions sites (XhoI, SalI and BamH1) for cloning to the binary vector. The full length gene was cloned into the pRH509 binary vector using the SalI and BamH1 restriction sites, which resulted in the binary vector pBK26. The binary construct pBK26 was transformed into Agrobacterium strain GV3101 (PMP90) by electroporation. The transformed Agrobacterium strains were mixed the Agrobacterium strain carrying p19 expressing plasmid or only infiltration buffer in 1:1 ratio and incubated in the dark for 2 hours in presence of acetosyringone. The mixed cultures having OD = 0.5 were infiltrated into leaves of 4 weeks old *N. benthamiana* plants and incubated at 23^0C degrees in the growth chamber.

The apoplastic fluid was isolated from the *N. benthamiana* plants at 4 dpi and the proteins were precipitated by adding equal volume of 100% acetone. The precipitated proteins were dissolved in 50 µl of gel loading buffer containing β-mercaptoethanol at 2X final concentration and heated at 95 ºC for 10 minutes. The proteins were separated on 12% protein gels at 200 volts for one hour and were transferred from the protein gels onto PVDF membranes, incubated with anti-strep-tag II antibody (IBA life sciences, cat.no.2-1509-001) and detected using chemiluminescent substrates (SuperSignal West Chemiluminescent substrates, Thermo Scientific).

11.22 Large-scale labeling and affinity purification of DCG04-labeled proteins

30 ml of apoplastic fluids from the *N. benthamiana* plants were incubated with 10 µM DCG-04 at room temperature for 4h at pH 5.0. Labeling was stopped by precipitating the total proteins by chloroform/methanol precipitation method. The labelled proteins were enriched and analysed as mentioned in the section 11.3.

11.23 Competitive ABPP with monosaccharides and the apoplastic fluids

The nine different monosaccharides such as D-glucose, D-galactose, D-xylose, D-Glucuronic acid, L-Arabinose, D-Mannose, D-fructose, N-acetyl glucosamine and N-acetyl galactosamine were dissolved at 1M final concentration in 1X MES buffer at pH 5.0. The 1M *D*-Glucuronic acid solution was further adjusted to pH 5.0 using 1M NaOH. The apoplastic fluids from the N. benthamiana leaves were pre-incubated with or without the monosaccharides at 200 µM final concentration for 30 minutes at room temperature. The pre-incubated apoplastic fluids were labelled with JJB70 for one hour at pH 5.0. The labelled proteins were analysed as mentioned in the section 11.3.

11.24 Competitive ABPP with antibiotics and the apoplastic fluids

The antibiotics such as spectinomycin, kanamycin, gentamycin, carbenicillin were dissolved in water at 50 µg/µl final concentrations and and filter-sterilized. The rifampicin was dissolved in DMSO at 50 µg/µl final concentration. The tetracycline was dissolved in 70% ethanol at 25 µg/µl final concentration and the chloramphenicol is dissolved in 100% methanol at 30 µg/µl final concentration. The apoplastic fluids from the N. benthamiana leaves were pre-incubated with or without 5 µl of the diluted antibiotics for 30 minutes at room temperature. The pre-incubated apoplastic fluids were labelled with JJB70 for one hour at pH 5.0. The labelled proteins were analysed as mentioned in the section 11.3.

11.25 References

Bronstein, P.A., Filiatrault, M.J., Myers, C.R., Rutzke, M., Schneider, D.J., and Cartinhour, S.W. (2008). Global transcriptional responses of *Pseudomonas syringae* DC3000 to changes in iron bioavailability in vitro. BMC Microbiol.

Carbonell, A., Takeda, A., Fahlgren, N., Johnson, S.C., Cuperus, J.T., and Carrington, J.C. (2014). New generation of artificial microRNA and synthetic trans-acting small interfering RNA vectors for efficient gene silencing in Arabidopsis. Plant Physiol. pp.113.234989.

Charif, D., and Lobry, J.R. (2007). SeqinR 1.0-2: A Contributed package to the R project for statistical computing devoted to biological sequences retrieval and analysis. In structural approaches to sequence evolution, D.U. Bastolla, P.D.M. Porto, D.H.E. Roman, and D.M. Vendruscolo, eds. (Springer Berlin Heidelberg), pp. 207–232.

Hirsch-Hoffmann, M., Gruissem, W., and Baerenfaller, K. (2012). pep2pro: the high-throughput proteomics data processing, analysis, and visualization tool. Front. Plant Sci. *3*, 123.

Lamesch, P., Berardini, T.Z., Li, D., Swarbreck, D., Wilks, C., Sasidharan, R., Muller, R., Dreher, K., Alexander, D.L., Garcia-Hernandez, M., et al. (2012). The Arabidopsis Information Resource (TAIR): improved gene annotation and new tools. Nucleic Acids Res. *40*, D1202–D1210.

Lombard, V., Golaconda Ramulu, H., Drula, E., Coutinho, P.M., and Henrissat, B. (2014). The carbohydrate-active enzymes database (CAZy) in 2013. Nucleic Acids Res. *42*, D490–D495.

Paradis, E., Claude, J., and Strimmer, K. (2004). APE: Analyses of phylogenetics and evolution in R language. Bioinformatics *20*, 289–290.

Punta, M., Coggill, P.C., Eberhardt, R.Y., Mistry, J., Tate, J., Boursnell, C., Pang, N., Forslund, K., Ceric, G., Clements, J., et al. (2012). The Pfam protein families database. Nucleic Acids Res. *40*, D290–D301.

Shevchenko, A., Tomas, H., Havlis, J., Olsen, J.V., and Mann, M. (2006). In-gel digestion for mass spectrometric characterization of proteins and proteomes. Nat. Protoc. *1*, 2856–2860.

Wessel, D., and Flügge, U.I. (1984). A method for the quantitative recovery of protein in dilute solution in the presence of detergents and lipids. Anal. Biochem. *138*, 141–143.

Supplementary information

Probe Synthesis

All reagents were of a commercial grade and were used as received unless stated otherwise. Cyclophellitol-aziridine probes were synthesized as depicted in **Scheme 1**. The intermediate **9** was prepared from D-xylose over 7 steps (Hansen et al., 2005). Selective transformation of primary alcohol in **9** using tricloroacetonitrile in anhydrous CH_2Cl_2 followed by iodocyclisation to obtain stereocontrolled compound **10**. The imidate part of **10** was hydrolyzed by concentrated hydrochloride, and the aziridine ring compound **11** was formed after nucleophilic displacement of the iodine in base solution. The benzyl groups were removed via Birch reduction followed by Amberlite H^+ and Amberlite NH_4^+ cation-exchange work-up and the resulting aziridine intermediate **12** was acylated with activated 8-azidooctanoic acid 13 (David et al., 2003) by 2-ethoxy-1–ethoxycarbonyl-1,2-dihydroquinoline (EEDQ) (Vicik et al., 2006) to yield azidocyclophellitol aziridine (Kallemeijn et al., 2012)**.** The azidocyclophellitol aziridine was converted to target probes JJB70 and JJB111 by conjugating green BODIPY-alkkyne **14** and biotin-alkyne **15**, respectively, via the copper(I) catalyzed click reaction (Wang et al., 2003). Dichloromethane (DCM), tetrafuran (THF) and N,N-dimethylformamide (DMF) were stored over molecular sieves 4 Å, which were flamed dried *in vacuo* before use. All reactions were performed under argon unless stated otherwise. Solvents used for flash chromatography were of pro analysis quality. Reactions were monitored by TLC analysis using Merck aluminum sheets pre - coated with silica gel 60 with detection by UV - absorption (254 nm) and by spraying with a solution of $(NH_4)_6Mo_7O_{24}\cdot H_2O$ (25 g/L) and $(NH_4)_4Ce(SO_4)_4\cdot H_2O$ (10 g/L) in 10% sulfuric acid followed by charring at ~150˚C or by spraying with 20% sulphuric in ethanol followed by charring at ~150 ˚C. Column chromatography was performed using either Baker - or Screening Device silica gel 60 (0.04-0.063mm) in the indicated solvents. ^1H NMR and ^{13}C NMR spectra were recorded on a Bruker DMX-600 (600/150 MHz) and a Bruker AV-400 (400/100 MHz) spectrometer in the given solvent. Chemical shifts are given in ppm relative to the chloroform residual solvent peak or tetramethylsilane (TMS) as internal standard. Coupling constants are given in Hz. All given ^{13}C spectra are proton decoupled. High resolution mass spectra were recorded with a LTQ Orbitrap (Thermo Finnigan). FT- IR- spectra were recorded on a Shimadzu FTIR-83000 spectrometer. LC/MS analysis was performed on a Jasco HPLC-system (detection simultaneously at 214nm and 254nm) equipped with buffers A: H_2O, B: acetonitrile (MeCN) and C: 10% 0.5M NH_4OAc, and coupled to a Perkin Elmer Sciex API 165 mass instrument. For reverse phase(RP)-HPLC purifications, 'Agilent Technologies 1200 Series' equipped with a semi-preparative 'gemini' C_{18} column(10×25mm) was used. The applied buffers were A: H_2O, B: MeCN.

JJB70 Synthesis

Azido-cyclophillitol aziridine compound (10mg, 0.029mmol, 1eq) was dissolved in DMF(1mL), green BODIPY-alkyne **14** (10.4mg, 0.031mmol, 1.1eq), $CuSO_4$(1M solution in H_2O) (20µL, 0.02mmol, 0.69eq) and sodium ascorbate (1M solution in H_2O) (23µL, 0.023mmol, 0.79eq) were added to the solution under argon atmosphere, and the mixture was stirred at room temperature for 2h. After the complete conversion to triazole derivative, the volatiles were removed under reduced pressure and crude product was purified by semi-preparative reversed HPLC (linear gradient: 45→48% B, 3CV, solutions used A: H_2O, B: acetonitrile) and the fractions were freeze-dried directly resulting orange powder product (6.53mg, 0.0097mmol, 33.3%). ^{1}H NMR (600 MHz, MeOD) δ 7.73 (s, 1H), 6.11 (s, 2H), 4.35 (t, J = 7.2Hz, 2H), 4.04 (dd, J = 10.2Hz, 4.2Hz, 1H), 3.69-3.66 (m, 2H), 3.19 (dd, J = 10.2Hz, 8.4Hz, 1H), 3.07(t, J = 10.2Hz, 1H), 3.02-2.99 (m, 3H), 2.78 (t, J = 7.2Hz, 2H), 2.71 (d, J = 6.0Hz, 1H), 2.66-2.43 (m, 8H), 2.37 (s, 6H), 1.99-1.94 (m, 1H), 1.92-1.94 (m, 4H), 1.67-1.60 (m, 2H), 1.59-1.54 (m, 2H), 1.36-1.23 (m, 6H). ^{13}C NMR (151MHz, MeOD) δ 199.49, 154.94, 148.53, 147.90, 142.20, 132.59, 123.39, 122.84, 122.62, 79.10, 73.42, 69.37, 63.58, 51.16, 45.27, 42.43, 41.03, 36.77, 32.23, 31.14, 30.81, 29.94, 29.62, 29.07, 27.17, 25.88, 25.81, 16.49, 14.44. LC/MS:R_t: 7.087 min; linear gradient 10→90% B in 15 min; ESI-MS: *m/z*=671.4($M+H^+$). HRMS: $(M+H)^+$ calcd for $C_{34}H_{57}N_8O_8$ 671.39044 found 671.39033.

JJB111 Synthesis

Azido-cyclophillitol aziridine compound (24mg, 0.07mmol, 1eq) was dissolved in DMF (2mL), biotin-ahx-alkyne **16** (27.6mg, 0.07mmol, 1eq), $CuSO_4$(100mM) (0.14mL, 0.014mmol, 0.2eq) and sodium ascorbate (100mM) (0.14mL, 0.014mmol, 0.2eq) was added to the solution under argon atmosphere, and the mixture was stirred at 80ºC overnight. The volatiles were removed under reduced pressure and crude product was purified by semi-preparative reversed HPLC (linear gradient: 20→40%, 3CV, solutions used A: H_2O, B: acetonitrile) and the fractions were freeze-dried directly yieldinging as white powder product (8.9mg, 0.012mmol, 17%)

^{1}H NMR (400 MHz, MeOD) δ 7.84 (s, 1H), 4.50 (dd, J = 8.0, 5.2 Hz, 1H), 4.43 (s, 2H), 4.37 (t, J= 6.8 Hz, 2H), 4.31 (dd, J= 8.0, 4.4 Hz, 1H), 4.06 (dd, J=10.0, 4.4 Hz, 1H), 3.72 - 3.65 (m, 2H), 3.24- 3.14 (m, 4H), 3.08 (t, J = 9.6 Hz, 1H), 3.03 (dd, J = 6.0, 3.2 Hz, 1H), 2.93 (dd, J = 12.8, 4.8Hz, 1H), 2.73 (d, J = 5.6, 1H), 2.71 (d, J = 12.0, 1H), 2.84 (t, J = 8.0, 2H), 2.25 - 2.18 (m, 4H), 2.02- 1.96 (m, 1H), 1.95- 1.86 (m, 2H), 1.79- 1.58 (m, 9H), 1.55 - 1.42 (m, 4H), 1.38 - 1.30 (m, 10H) ^{13}C NMR (101 MHz, MeOD) δ 188.52, 176.01, 175.97, 166.11, 146.26, 124.14, 79.09, 73.42, 69. 34, 63.55, 63.38, 61.62, 57.00, 51.29, 49.42, 45.26, 42.44, 41.06, 41.04, 40.18, 36.81, 36.74, 35.68, 31.17, 30.10, 29.95, 29.77, 29.64, 29.49, 27.52, 27.21, 26.91,

26.50, 25.88. LC/MS: R_t : 5.103min; linear gradient 00%→90% B in 15 min; ESI-MS: *m/z*=737.8($M+H^+$) FT- IR: v_{max}(neat)/cm^{-1}: 3297.8, 2931.5, 2362.8, 2341.9, 1684.3, 668.4 . HRMS: $(M+H)^+$ calcd for $C_{34}H_{57}N_8O_8$ 737.40146 found 737.40201.

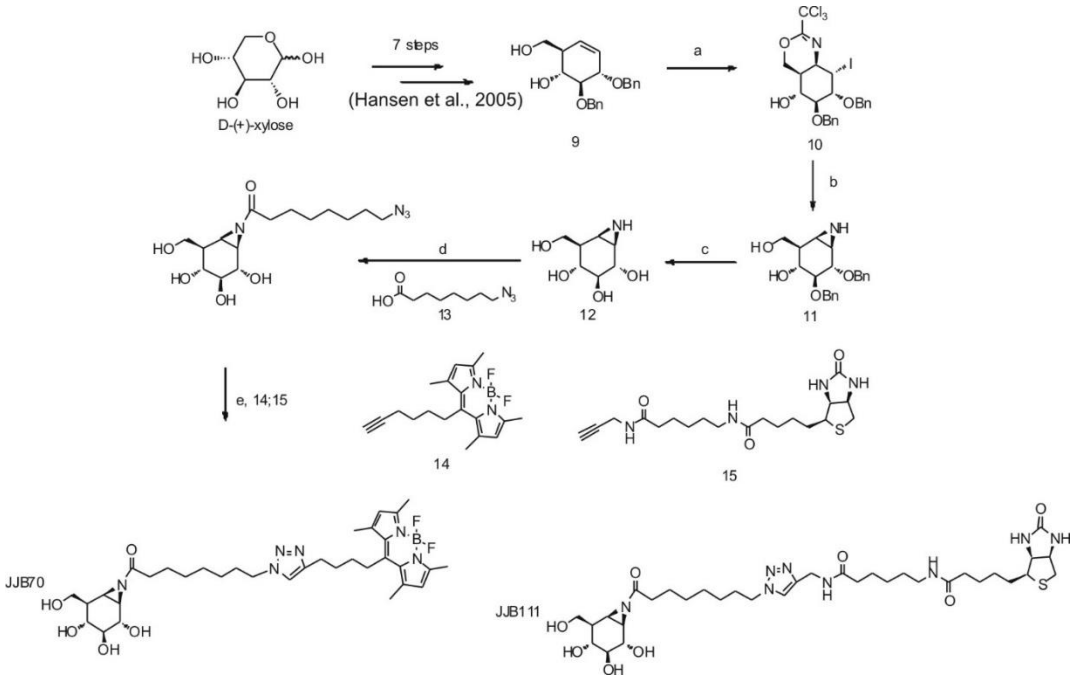

Scheme1. Synthesis of cyclophellitol-aziridine probes. Reagents and conditions: (a) i) CCl_3CN, DBU, CH_2Cl_2, 0ºC ; ii) H_2O, $NaHCO_3$, I_2 ; (b) i) 37% HCl, dioxane, 60ºC; ii) $NaHCO_3$, MeOH (over 4 steps 59%) ; (c) Li(s), NH_3, THF, -60ºC, 67% ; (d) 8- azidooctanoic acid 13, EEDQ, DMF, 57%; (e) $CuSO_4$, sodium ascorbate, DMF, 33%; 17%;

References

David, O., Meester, W.J.N., Bieraugel, H., Schoemaker, H.E., Hiemstra, H., and van Maarseveen, J.H. (2003). Intramolecular Staudinger ligation: A powerful ring-closure method to form medium-sized lactams. Angew Chem Int Edit **42:** 4373-4375.

Hansen, F.G., Bundgaard, E., and Madsen, R. (2005). A short synthesis of (+)-cyclophellitol. J Org Chem **70:** 10139-10142.

Kallemeijn, W.W., Li, K.Y., Witte, M.D., Marques, A.R.A., Aten, J., Scheij, S., Jiang, J.B., Willems, L.I., Voorn-Brouwer, T.M., van Roomen, C.P.A.A.*, et al.* (2012). Novel Activity-Based Probes for Broad-Spectrum Profiling of Retaining beta-Exoglucosidases In Situ and In Vivo. Angew Chem Int Edit **51:** 12529-12533.

Vicik, R., Busemann, M., Gelhaus, C., Stiefl, N., Scheiber, J., Schmitz, W., Schulz, F., Mladenovic, M., Engels, B., Leippe, M.*, et al.* (2006). Aziridide-based inhibitors of cathepsin L: Synthesis, inhibition activity, and docking studies. Chemmedchem **1:** 1126-1141.

Wang, Q., Chan, T.R., Hilgraf, R., Fokin, V.V., Sharpless, K.B., and Finn, M.G. (2003). Bioconjugation by copper(I)-catalyzed azide-alkyne [3+2] cycloaddition. Journal of the American Chemical Society **125:** 3192-3193.

Acknowledgements

‘Chance favours the prepared mind’ – Louis Pasteur

I take this as a great opportunity to thank everyone who helped me by during my PhD research period and prepared me for the next challenges in the academic research career. Without all your support and help I would not enjoyed doing science during my PhD research period.

First and foremost I would like to thank Prof. Dr. Renier van der Hoorn for his supervision, support, critical reading and correcting my thesis during my PhD program both at Cologne and Oxford. I thank Prof. Renier for allowing me to pursue several of my instinct ideas that generated during my PhD period. I also thank Prof. Renier for proving an opportunity to work with several academic visitors and students.

I would like to thank Prof. Dr. Dorothea Bartels for being my second supevisor during my PhD program. I also thank Prof. Bartels for her encourgement and support during my M.sc and PhD programs. I would like to thank Prof. Dr. Michael Gütschow (University of Bonn) and Prof. Dr. Erwin A. Galinski (University of Bonn) for kindly joining my Ph.D thesis committee.

I owe my gratitude to colleagues at the Plant Chemetics lab, MPIPZ, Cologne (2012-2013): Dr. Anja Hörger, Dr. Johana Misas-Villamil, Dr. Takayuki Shindo, Dr. Joji Grace Villamor, Dr. Mohammud Ilyas, Dr. Haibin Lu, Tram Ngoc Hong, Judit Kovács and Asif Emon Khan. You all have been a great support for me and helped me a lot during my various stages of PhD research period. All the constructive criticisms during the lab meetings and during all our scientific discussions shaped me and also channelized me to design my experiments in logical way.

I am particularly grateful to Department of Plant Sciences, Oxford, United Kingdom for hosting me as a recognized PhD student from February 2014 – March 2017. I owe my gratitude to all my colleagues at the Plant Chemetics lab, Oxford (2014 -2017) for their support and many golden times at Oxford. I would also like to thank David Miron, bachelor student, Somerville College for helping me during my final and crucial phase of PhD research. I really had a great research support from David during this period. I owe my gratitude to Sarah Rodgers for her support with organizing and ordering research materials and Ursula Pyzio for growing plants and offering help with cloning experiments. I also extend my thanks to Dosa Park, Oxford for

providing food and a place read to research articles. It is here most of my research ideas were generated.

My sincere thanks to Prof. Dr. Gail Preston, University of Oxford for helping and supporting me with numerous enchanting research ideas on various microbiology approaches. I would like to thank Dr. Anja Hörger for helping me a lot with basic research questions during my initial phase of PhD research both at Cologne and Oxford. I would like to thank Dr. Barney Geddes and Dr. Vinoy Ramachandran and for sharing their ideas during the Wednesday seminars. The advice and thoughts from you really helped me a lot to design my experiments. I owe my gratitude to Pedro Bota for his support with GC-MS experiments.

My sincere thanks to Prof. Dr. Hermen Overkleeft, Leiden Institute of Chemistry, The Netherlands for allowing me to work in his laboratory for two weeks to analyze the bacterial culture samples. This was my first research experience in a chemist lab and an exciting period during PhD. I extend my sincere thanks to Dr. Dimitri Filippov for helping me a lot during this project on BGAL inhibitor. Moments of solving the crystal structure of unknown compound by Dr. Dima which turned out to be mannitol which was present in the medium was an exciting experience. I also extend my thanks to Dr. Bobby Florea, Richard van den Berg, Nico Meeuwenoord and Hans van den Elst for helping me with the experiments and also analyzing my samples during the visit.

I would like to heartily thank Prof. Dr. Gideon Davis and Dr. Wendy Offen, University of York, UK for the collaboration on the BGAL inhibitor identification. The crystal structure of the discovered BGAL inhibitor has intrigued me very much. My sincere thanks to Dr. Wendy for her efforts in this project. I really enjoyed the inhibitor discovery process by solving the electron density structure with Dr. Wendy.

Last but not least I would like to thank my parents and my wife for their continuous support throughout my research period. Without all their support with moral values and I would not have survived and become strong during my final phase of PhD research period. My special thanks to my wife Mano for her patience and support especially during my stay at Oxford

Curriculum vitae

Personal Information

Name	:	Balakumaran Chandrasekar
Date of Birth	:	16 September 1987
Place of Birth	:	Virudhunagar, India
Nationality	:	Indian

Education

Programs	***Institutions***	***Year***	***Marks obtained***
Recognised PhD Student	Department of Plant Sciences, University of Oxford, United Kingdom (UK).	Feb 2014 - March 2017	0.7
Doctor of Philosophy (PhD)	Max Planck Institute for Plant Breeding Research, Cologne and University of Bonn, Germany.	April 2013 – March 2017	
Master of science (M.Sc) [Plant sciences]	University of Bonn, Germany.	2011 - 2013	1,5 (ECTS)
B.Tech [Biotechnology]	Department of Plant Molecular Biology and Biotechnology, Tamil Nadu Agricultural University, Coimbatore, India.	2007 - 2011	8.72 out of 10

Research experience:

1. Department of Plant Sciences, University of Oxford, UK and the Max Planck Institute for Plant Breeding Research, Cologne, Germany. April 2013 – March 2017: PhD student, under the guidance of Prof. Dr. Renier van der Hoorn and Prof. Dr. Dorothea Bartels, University of Bonn
Research topic: 'From glycosidase-activity profiling to inhibitor discovery in the plant pathogen *Pseudomonas syringae*'

2. Leiden Institute of Chemistry, Gorlaeus Laboratories, University of Leiden**,** the Netherlands. 8 June - 22 June 2015.
Student Visitor: Analytical techniques to identify an unknown small molecule inhibitor

3. Max Planck Institute for Plant Breeding Research, Cologne, Germany. Oct 2012 - Mar 2013.
Master thesis: 'Studies on hyperreactive cysteine containing proteins in *Arabidopsis* using electrophilic probes' – Under Dr. Renier van der Hoorn

4. Max Planck Institute for Plant Breeding Research, Cologne, Germany. 20 Feb - 06 April 2012.
Internship: 'Effect of calcium in labelling of *Arabidopsis* proteome with BHAcATP kinase probe' – Under Dr. Renier van der Hoorn

5. Centre for Plant Molecular biology (CPMB), Tamil Nadu Agricultural University, India. Nov 2010 - May 2011. *Bachelor thesis:* Isolation and splicing of cassava mosaic viral Genes for RNAi vector construction' – Under Prof. Dr. K.K.Kumar

6. The Leibniz Institute of Plant Genetics and Crop Plant Research (IPK), Gatersleben, Germany.
1 July - 30 Aug 2010.
Internship: 'Structural and Ultra structural analysis of Pollen embryogenesis in Barley' using Transmission Electron Microscope and Confocal Laser Scanning Microscope – Under Dr. Michael Melzer

Publications:

10. Kovacs J, Poór P, Kaschani F, Chandrasekar, B, Hong T, Misas-Villamil J, Xin B, Kaiser M, Overkleeft H, Tari I and Van Der Hoorn RAL (2017). Proteasome activity profiling uncovers alteration of catalytic β2 and β5 subunits of the stress-induced proteasome during salinity stress in tomato roots. *Front. Plant Sci.* **8**:107

9. Chandrasekar, B., Hong, T.N and Van der Hoorn, R.A.L. (2017). Inhibitor discovery by convolution Activity-Based Protein Profiling (ABPP) *Methods in Molecular Biology* 1491, 47-56.

8. Chandrasekar, B and Van der Hoorn, R.A.L. (2016). Beta galactosidases in Arabidopsis and tomato - a mini review. *Biochemical society transactions* 44(1), 150-158.

7. Daneri-Castro, S.N., Chandrasekar, B., Grosse-Holz, F.M., Van der Hoorn, R.A.L., Roberts, T.H. (2016). Activity-based protein profiling of hydrolytic enzymes induced by gibberellic acid in isolated aleurone layers of malting barley. *FEBS letters* 590 (17), 2956-62

6. Stiti, N., Chandrasekar, B., Strubl, L., Bartels, D and Van der Hoorn, R.A.L. (2016) Nicotinamide Cofactors Suppress Active-site Labeling of Aldehyde Dehydrogenases. *ACS Chemical Biology* 11 (6), 1578–1586.

5. Poret, M., Chandrasekar, B., Van der Hoorn, R.A.L and Avice, J.C. (2016). Characterization of senescence-associated protease activities involved in the efficient protein remobilization during leaf senescence of winter oilseed rape. *Plant Science* 246, 139-53.

4. Lu, H., Chandrasekar, B., Oeljeklaus, J., Misas-Villamil, J.C., Wang, Z., Shindo, T., Bogyo, M., Kaiser, M., and Van der Hoorn, R.A.L. (2015). Subfamily-specific fluorescent probes for cys proteases display dynamic Protease activities during seed germination. *Plant Physiol*. pp.114.254466.

3. Chandrasekar, B., Colby, T., Emon, A.E.K., Jiang, J., Hong, T.N., Villamor, J.G., Harzen, A., Overkleeft, H.S., and Van der Hoorn, R.A.L. (2014). Broad-range glycosidase activity profiling. *Mol. Cell. Proteomics 13*, 2787–2800. **(*Highlighted in Oxford Biochemical society Journal, Phenotype, 24th issue, Trinity term, 2016*)**

2. Ulker, B., Hommelsheim, C.M., Berson, T., Thomas, S., Chandrasekar, B., Olcay, A.C., Berendzen K.W., Frantzeskakis, L. (2012) Reevaluation of the reliability and usefulness of the somatic homologous recombination reporter lines. *Plant Cell* 24: 4314-4323.

1. Vichangal, P.S.K., Raja, K., Natarajan, S., Srinivasan, N., and Chandrasekar, B (2011) Molecular Docking Study on the anti-inflammatory effect of Osthol and its derivatives towards human p38alpha MAP kinase *International Journal of Bioinformatics* 4: 1-9

Talks/posters presentation at the International Conferences:

- Poster at the Gordon Research Conference (GRC) Waterville Valley, USA. 20-25 July 2016
- Oral talk at the Oxford Congress on Plant Sciences, University of Oxford. 23 July 2015
- Oral talk at the COST meeting on 'Chemical Proteomics', Uni. of. Oxford. 12-14 Apr 2015
- Oral talk at the 'Carbohydrate Recognition and Inhibition' meeting, Norwich. 21 Nov 2014
- Poster at the Gordon Research Conference on PMB, USA. 20 - 25 July 2014.
- Oral talk at the Oxford's Science day, University of Oxford. 10 July 2014
- Oral talk at AGRI-net Conference on Plant Chemical Biology, Syngenta, UK.16 May 2014
- Oral talk at the COST CM1004 meeting, Berlin, Germany. 9 April 2013.

Place : Bonn, Germany
Date : 13.03.2017 Balakumaran Chandrasekar

Declaration

Ich versichere, dass ich diese Arbeit selbstständig verfasst, keine anderen Quellen und Hilfsmittel als die angegebenen benutzt und die Stellen der Arbeit, die anderen Werken dem Wortlaut oder Sinn nach entnommen sind, kenntlich gemacht habe.

Diese Arbeit hat in dieser oder ähnlicher Form keiner anderen Prüfungsbehörde vorgelegen.

Place : Bonn, Germany
Date : 13.03.2017 Balakumaran Chandrasekar